# NATIONAL ADVISORY COMMITTEE FOR AERONAUTICS

TECHNICAL NOTE 3944

AN INTEGRAL SOLUTION TO THE FLAT-PLATE LAMINAR
BOUNDARY-LAYER FLOW EXISTING INSIDE AND AFTER EXPANSION
WAVES AND AFTER SHOCK WAVES MOVING INTO QUIESCENT FLUID
WITH PARTICULAR APPLICATION TO THE

COMPLETE SHOCK-TUBE FLOW

By Robert L. Trimpi and Nathaniel B. Cohen

Langley Aeronautical Laboratory Langley Field, Va.



Washington
June 1957

## TABLE OF CONTENTS

	Page
<u>SUMMARY</u>	. 1
<u>INTRODUCTION</u>	. 1
SYMBOLS	. 4
THEORY	. 10
DIFFERENTIAL EQUATIONS	. 10
Equations	13
Assumption of Constant Wall Enthalpy	
and Enthalpy	15 20
EQUATIONS	
Solutions for the Boundary-Layer Parameters Across Discontinuities in the Force-Stream Flow	52
TRANSFORMATION TO AND EVALUATION OF PERTINENT PARAMETERS IN THE PHYSICAL FLOW	56
Inversion From Transformed Coordinates to the Corresponding Physical Flow Coordinates	. 56
Transformation of Velocity and Temperature Profiles to the Physical Plane	58 60
RESULTS AND DISCUSSION  SHOCK SOLUTIONS  EXPANSION-FAN SOLUTION  DISCONTINUITY SOLUTIONS  At Trailing Edge of Expansion Fan  At the Contact Surface in a Shock Tube  DISCUSSION OF CHARACTERISTICS SYSTEM  The Characteristic Plot for the Shock Tube  Location of \$\xi_W^*\$ by the "Anchor Point" Method  Physical Significance of the Critical Characteristics  Momentum and Energy Shocks	63 63 66 74 74 76 77 78 79 80
Methods for Extending Present Results	82

		Page
THE COMPLETE SOLUTION FOR THE BOUNDARY LAYER IN A SHOCK TUBE FOR $\gamma=1.4$ , $R_{\in}=R_{\infty}$ , AND $\lambda \leqq 20$		83
APPROXIMATE SOLUTIONS FOR THE BOUNDARY LAYER IN A SHOCK TUBE USING ONLY ONE FLUID		85
Negative-Shock Approximation for the Expansion Fan and Region $\zeta$ Modified Negative-Shock Approximation		86 86
APPROXIMATE SOLUTION FOR THE BOUNDARY LAYER IN A SHOCK TUBE USING TWO DIFFERENT FLUIDS		91
CONCLUDING REMARKS		96
APPENDIX A - EXPRESSIONS FOR VARIOUS FUNCTIONS IN A CENTERED EXPANSION WAVE MOVING INTO FLUID AT REST		98
APPENDIX B - DERIVATION OF REDUCED BOUNDARY-LAYER EQUATIONS FO	<u>R</u>	100
APPENDIX C - TRANSFORMATION OF REDUCED DIFFERENTIAL EQUATIONS  CONICAL COORDINATE SYSTEM		108
APPENDIX D - DERIVATION OF VELOCITY AND ENTHALPY BOUNDARY-LAYE POWER-SERIES COEFFICIENTS, FORM PARAMETERS, AND DISSIPATION	R	
FUNCTIONS  POWER-SERIES COEFFICIENTS  VELOCITY FORM PARAMETERS  LOCAL ENTHALPY FORM PARAMETERS  TOTAL ENTHALPY FORM PARAMETERS  DISSIPATION FUNCTION		112 113 114 120 121
APPENDIX E - DERIVATION OF COMPLETE BOUNDARY-LAYER EQUATIONS F TWO-DIMENSIONAL UNSTEADY FLOW		122
APPENDIX F - DERIVATION OF INTEGRAL RELATIONSHIPS AT A DISCONTINUITY IN THE OUTER FREE-STREAM FLOW		127
REFERENCES		130
		132
ETGIRES		133

#### NATIONAL ADVISORY COMMITTEE FOR AERONAUTICS

### TECHNICAL NOTE 3944

AN INTEGRAL SOLUTION TO THE FLAT-PLATE LAMINAR

BOUNDARY-LAYER FLOW EXISTING INSIDE AND AFTER EXPANSION

WAVES AND AFTER SHOCK WAVES MOVING INTO QUIESCENT FLUID

WITH PARTICULAR APPLICATION TO THE

COMPLETE SHOCK-TUBE FLOW

By Robert L. Trimpi and Nathaniel B. Cohen

#### SUMMARY

A solution to the unsteady two-dimensional laminar boundary-layer flow inside centered expansion waves and behind both centered expansion waves and shock waves is obtained by utilizing an extension of the Karmán-Pohlhausen method. The Prandtl unsteady-boundary-layer equations are integrated normal to the surface bounding the flow and are transformed into a conical coordinate system. The resulting hyperbolic differential equations are integrated in closed form for flow behind shock waves and by numerical methods for the flow inside or following expansion waves. An integral technique is applied at the discontinuities existing at the trailing edge of the expansion fan and at contact discontinuities (entropy discontinuities) so that the characteristic solution may proceed across these discontinuities.

The solution to the two-dimensional unsteady laminar boundary layer existing at all points in an air-air shock tube is obtained by this method. A much shorter approximate method of solution is devised and is found to agree favorably with this method. This approximate method is used to predict the flow in hydrogen-air and helium-air shock tubes. Plots of wall heat-transfer rate and skin friction in air-air, helium-air, and hydrogen-air shock tubes are presented.

#### INTRODUCTION

Impetus to the study of time-dependent boundary layers has arisen because of the increased importance of the flows initiated along the ground and over buildings by the detonation of nuclear devices and of the air flow over missiles in hypersonic flight. The time-dependent

nature of the nuclear-shock-initiated flows is obvious; whereas hypersonic missile flight presents two less obvious problems, one of which is direct and the other, indirect. The direct problem arises because of the time-wise variation of the differences between conditions of the outer potential flow at the edge of the boundary layer and of the missile skin as the missile encounters rapidly varying ambient conditions during its flight. To date, because of the relative rapidity with which the fluid boundary layer is able to adjust to changes, the direct problem has been treated as a quasi-steady one; that is, for given wall and local conditions at a time in a time-dependent flow, the boundary layer is equivalent to that in a steady flow for the same stream and wall conditions. The main apparent difficulty in this approach is the prediction and simulation of the correct wall conditions since they are in turn dependent on the time history of the boundary layer.

The indirect problem arises from the use of shock tubes as a means of experimentally simulating the very high stagnation temperatures encountered in missile flight for purposes of obtaining data regarding heat transfer, skin friction, ionization, dissociation, and so forth. Correct interpretation of shock-tube test results requires a knowledge of the timedependent flow inherent therein. The perfect-fluid flow in a conventional (constant-area) shock tube is well known and is depicted in figure 1. At time  $t = 0^+$ , the diaphragm which originally separated the high-pressure or driver gas (state ε) from the low-pressure gas (state ∞) is instantaneously destroyed and the resultant pressure inequality is adjusted by the mechanism of: (1) a centered expansion wave or expansion fan (that is, one which originates at a single point in distance and time) progressing into region  $\epsilon$  and isentropically accelerating the fluid to state  $\ell$ following the wave; and (2) a shock wave progressing into region ∞ and accelerating the fluid to state  $\sigma$  behind it. (See fig. 1(c).) The regions  $\zeta$  and  $\sigma$ , composed of the fluid originally in regions  $\epsilon$  and  $\infty$ . respectively, are separated theoretically by a contact surface (entropy discontinuity) across which pressure and velocity are constant and the temperature and density are generally different. Hypersonic simulation testing is usually done in region  $\sigma$  where the stagnation temperature is highest. The pressure ratios across the expansion fan and shock wave are dependent only on the fluid in states  $\epsilon$  and  $\infty$ . Detailed discussion on the theoretical performance of the conventional shock tube, as well as modifications such as increasing the area of the high-pressure chamber to increase the shock strength or adding a nozzle to obtain hypersonic flow, may be found in references 1 to 6.

However, experiments have shown that, instead of regions  $\sigma$  and  $\zeta$  being regions of constant pressure and velocity as predicted by inviscid theory and as desired for testing, the outer inviscid flow in these regions is time dependent; and furthermore, it is found that the shock wave attenuates as it progresses down the tube. (See refs. 2 and 6 to 10.) These variations are attributable both to imperfect-gas effects and to boundary-layer effects. Several investigations have been undertaken to predict the

NACA TN 3944

magnitude of the wall shear and heat transfer. In addition, attenuation theories based on these wall effects have been advanced in references 6, 7, 9, and 11.

The laminar boundary-layer problems in region  $\sigma$  behind the shock have been treated in references 6, 12, 13, and 14. Reference 6 first presented the solution to this flow by solving the boundary-layer problem, in a coordinate system fixed to the moving shock wave, of a semi-infinite treadmill (that is, the Blasius problem with nonzero wall velocity). Solutions were obtained for the complete Prandtl boundary-layer equations on an analog computer and for the integrated momentum equation alone by simple computations (which, unfortunately, contained a numerical error). In references 12 and 13 the equations of reference 6 were solved to a higher degree of accuracy on a digital computer and, in addition, velocity and temperature profiles were determined. The momentum equation was also solved in closed form by an integral method by using a fourth-order series for the velocity profile. Another integral solution obtained by using the Rayleigh velocity profile for the momentum equation and then applying Crocco's relation between temperature and shear was used in reference 14. The wall shear and heat-transfer results of these references agree very well.

The situation in regard to the laminar boundary layer for the flow inside the expansion fan and in region ( has not been as favorable. Prior to the concurrent studies of the present report and the companion paper (ref. 15), the flow in these regions was handled by rather rough approximations. In reference 7, the expansion wave was assumed to be shrunk to zero thickness and region ( was allowed to exist from the leading edge of the wave to the contact discontinuity. The unsteady boundary layer was then assumed to be equal to that of a steady flow which had the same free-stream values of velocity, density, and viscosity, and which had traveled for the same time adjacent to a solid bounding surface. References 11 and 13 also followed the procedure of shrinking the fan to zero width but computed the boundary layer from the modified Blasius (nonzero-wall-velocity) solutions. Both solutions result in conditions physically unacceptable near the leading edge of the fan since they predict infinite wall shear and heat transfer at points where the velocity and temperature potential approaches zero. It is also evident that serious errors are introduced away from the leading edge for expansion-fan pressure ratios not near unity because an appreciable region of varying pressure and velocity has been replaced by a region of constant properties. Thus a correct solution to the boundary-layer problem outside of region  $\sigma$  is missing. The filling of this gap and the determination of the boundary layer throughout the shock tube by a common method was the primary purpose of the present report. Corner effects arising at the juncture of two walls or effects of opposite walls of the shock tube are neglected, and the boundary layer is treated as a two-dimensional unsteady flow over an infinite flat surface. The unqualified term "shock tube" will be used

in the remainder of this report to designate a shock tube in which these effects are considered to be negligible.

The theoretical investigation reported herein was conducted at the Langley gas dynamics laboratory. The time-dependent boundary-layer characteristic system developed in this paper for conical potential flows (appropriate to shock tubes and nuclear shocks) is a special case of a general characteristic system applicable to the study of any time-dependent laminar boundary-layer flow.

#### SYMBOLS

An	coefficients in dimensionless velocity-profile power series
a	speed of sound
$B_n$	coefficients in dimensionless local enthalpy-profile power series
b	ratio of thicknesses of velocity boundary layer and local enthalpy boundary layer in transformed plane, $\frac{\Delta}{\triangledown}$
$C_n$	coefficients in dimensionless total enthalpy-profile power series
$C_{\overline{W}}$	constant of proportionality relating absolute viscosity to temperature, $\frac{\mu}{\mu_1}  \frac{T_1}{T} = \left( \frac{T_w}{T_1} \right)^{1/2}  \frac{T_1  +  S}{T_w  +  S}$
С	ratio of thicknesses of velocity boundary layer and total enthalpy boundary layer in transformed plane, $\stackrel{\triangle}{\Box}$
c <sub>f</sub>	local skin-friction coefficient, $\frac{\tau_{\text{W}}}{\frac{1}{2} \rho_{\text{W}} u_{\text{L}}^2}$
$c_{ m h}$	local heat-transfer coefficient, $\frac{q_W}{\frac{1}{N} \rho_W u_1 h_1}^*$

 $N_{Pr}$ 

2

coefficient of specific heat at constant pressure Cp coefficient of specific heat at constant volume CV particle time derivative,  $\frac{\partial}{\partial t} + u \frac{\partial}{\partial x} + v \frac{\partial}{\partial v}$ functions of § functions of  $\xi,\eta$  defined in equations (E9) functions of boundary-layer shape total enthalpy,  $h + \frac{u^2}{2}$ Η H\* total enthalpy difference, H - Hw local enthalpy,  $\int_{0}^{T} \mathbf{c}_{p}(T) dT$ h h\* local enthalpy difference, h - hw  $I = \int_0^1 \left| 1 - \left( \frac{u}{u_1} \right)^3 \right| d\alpha$ states on opposite sides of free-stream discontinuity i,j k thermal conductivity distance normal to wall,  $L \gg \delta$ L

distance free-stream particle has traversed since

acceleration from zero velocity by moving wave

Μ

Mach number

Npr

Prandtl number,  $\frac{\mu c_p}{k}$ 

n

integer denoting exponent in profile power series or point in solution

0

arbitrary location of characteristic boundary condition

р

local pressure

$$Q = \frac{\psi^2}{\nu_{\epsilon} t}$$

q

heat-transfer rate normal to free-stream direction,

$$-k \frac{\partial x}{\partial x}$$

q̂€

local heat-transfer parameter,  $\frac{q_{\rm w}}{\rho_{\rm e} a_{\rm e}^2 \sqrt{\frac{\nu_{\rm e}}{t}}}$ 

R

Reynolds number,  $\frac{u_{l}l}{v_{w}}$ 

Ŕ

rate of streamwise growth of mixing region

r

recovery factor

S

Sutherland constant for viscosity-temperature relation

S

state at shock wave

Т

absolute temperature

t

time

11

velocity component along x-axis

$$u^* = u - V^*$$

velocity of free-stream discontinuity in x-direction velocity component along y-axis

$$W = \frac{\phi^2}{v_c t}$$

W

x

state at wall or bounding surface

coordinate parallel to surface bounding flow

$$Y = \int_{0}^{y} \frac{\rho}{\rho_{\epsilon}} dy$$

v

coordinate normal to surface bounding flow

$$Z = \frac{\theta^2}{\nu_{\epsilon} t}$$

α

transformed normal coordinate for velocity profile,

$$\frac{1}{\triangle} \int_{O}^{y} \frac{\rho}{\rho_{\varepsilon}} dy$$

β

transformed normal coordinate for local enthalpy

profile, 
$$\frac{1}{\nabla} \int_0^y \frac{\rho}{\rho_{\varepsilon}} dy$$

Γ

local enthalpy shape parameter, B2

 $\gamma$ 

ratio of specific heats,  $\frac{c_p}{c_v}$ 

$$\Delta = \int_0^{\delta_u} \frac{\rho}{\rho_{\epsilon}} \, dy$$

$$\nabla = \int_0^{\delta_h} \frac{\rho}{\rho_{\epsilon}} \, \mathrm{d}y$$

$$\Box = \int_0^{\delta_{\mathbf{H}}} \frac{\rho}{\rho_{\epsilon}} \, \mathrm{d}y$$

 $\delta$  value of y at edge of boundary layer, largest value of  $\delta_H,~\delta_h,~\text{or}~\delta_u$ 

 $\delta_{H}$  value of y at edge of total enthalpy boundary layer

 $\delta_{\text{h}}$  value of y at edge of local enthalpy boundary layer

 $\delta_{\mathrm{u}}$  value of y at edge of velocity boundary layer

 $\left(\frac{\delta t}{\delta \xi}\right)_+$  slopes of positive and negative characteristics in  $\xi$ , t plane

 $\frac{\left(\frac{\delta}{\delta \xi}\right)_{\pm}}{\text{istics in } \xi, t \text{ plane, } \left(\frac{\partial}{\partial \xi}\right)_{\pm} + \left(\frac{\delta t}{\delta \xi}\right)_{\pm} \left(\frac{\partial}{\partial t}\right)_{\xi}$ 

$$\delta^* = \int_0^\infty \left( 1 - \frac{u}{u_1} \right) \frac{\rho}{\rho_{\epsilon}} \, dy$$

$$\nabla^* = \int_0^\infty \left( 1 - \frac{h^*}{h_1^*} \right) \frac{\rho}{\rho_{\epsilon}} dy$$

$$\Box^* = \int_0^\infty \left( 1 - \frac{H^*}{H_1^*} \right) \frac{\rho}{\rho_{\epsilon}} dy$$

general reference state; for shock-tube case denotes undisturbed high-pressure region

ζ constant free-stream region behind expansion wave

$$\eta = \frac{Y}{\sqrt{v_{\epsilon}t}}$$

 $\in$ 

$$\theta = \int_0^\infty \left( 1 - \frac{u}{u_1} \right) \frac{u}{u_1} \frac{\rho}{\rho_{\epsilon}} dy$$

λ velocity shape parameter, -2A<sub>2</sub>

 $\mu$  absolute viscosity

 $\nu$  kinematic viscosity,  $\frac{\mu}{\rho}$ 

 $\frac{x}{a_{\epsilon}t}$  conical parameter,  $\frac{x}{a_{\epsilon}t}$ 

 $\xi_{\text{te}}$  value of  $\xi$  at trailing edge of expansion wave

 $\xi_{\rm d}$  value of  $\xi$  at entropy discontinuity

 $\xi_W^*, \xi_Z^*$  values of  $\xi$  at limits of forward integration along characteristic lines for energy and momentum equations

 $\xi_{7.s}$  values of  $\xi$  at location of Z-shock

 $\rho$  density

σ constant free-stream region behind shock wave

 $\tau$  shear stress,  $\mu \left( \frac{\partial u}{\partial y} \right)$ 

 $\hat{\tau}_{\varepsilon}$  local skin-friction parameter,  $\frac{\tau_{W}}{\rho_{\varepsilon}a_{\varepsilon}\sqrt{\frac{\nu_{\varepsilon}}{t}}}$ 

$$\Phi = \int_0^\infty \nu \left(\frac{\partial \mathbf{u}}{\partial \mathbf{y}}\right)^2 \frac{\rho}{\rho_{\epsilon}} \, d\mathbf{y}$$

$$\emptyset = \int_0^\infty \left( 1 - \frac{h^*}{h_1^*} \right) \frac{u}{u_1} \frac{\rho}{\rho_{\epsilon}} dy$$

 $\chi$  interval in numerical integration procedure,  $\,\xi_{\,n+1}$  -  $\xi_{\,n}$ 

¥ stream function

$$\psi = \int_{0}^{\infty} \left( 1 - \frac{H^*}{H_1^*} \right) \frac{u}{u_1} \frac{\rho}{\rho_{\epsilon}} dy$$

 $\Omega$  total enthalpy shape parameter,  $C_2$ 

 $\omega$  transformed normal coordinate for total enthalpy

profile, 
$$\frac{1}{\Box} \int_0^y \frac{\rho}{\rho_{\epsilon}} dy$$

 $_{\infty}$  quiescent state into which shock wave advances

l local free-stream state

Subscripts not specifically designated otherwise denote evaluation at the appropriate state or location.

Superscripts or subscripts + or - denote waves moving in the positive or negative x-direction.

A bar under a symbol denotes nondimensionalization by appropriate quantity in reference state  $\epsilon$ ; that is,  $\underline{u}_1 = \frac{u_1}{a_{\epsilon}}$ ,  $\underline{\rho} = \frac{\rho}{\rho_{\epsilon}}$ , and so forth.

#### THEORY

# DERIVATION OF GENERAL FORM OF THE REDUCED HYPERBOLIC DIFFERENTIAL EQUATIONS

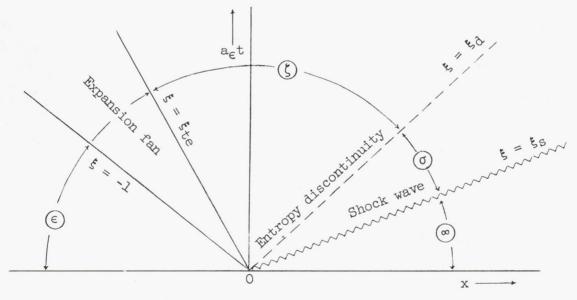
Discussion of Validity of Prandtl Boundary-Layer Equations

Since all the theoretical equations employed to describe the boundary-layer flow are based on the Prandtl boundary-layer assumptions, the validity of these assumptions must be considered further with regard to the unsteady expansion-wave and shock-wave flows to be treated in this paper. The point of origin of the wave (x = t = 0), representing, for example, the burst of a shock-tube diaphragm, is a singular point and must be excluded from the region of validity of the solution.

NACA TN 3944

The boundary layer in the vicinity of the shock wave, since it represents a discontinuity in the outer flow, also may be considered from a coordinate system fixed to the wave itself (that is, the coordinate system of refs. 6, 12, and 14). The problem is then equivalent to that of the semi-infinite flat plate with a nonzero wall velocity in steady flow, the leading edge of the plate analogous to the shock in unsteady flow being a singularity. The Blasius-type solution for this problem is valid everywhere except very near this singularity. Thus, in the unsteady flow problem, the present solution, as well as those given in references 6 and 12, is valid everywhere except very near the shock wave.

The ideal flow generated by centered expansion fans and shock waves is conical in a distance-time sense; that is, it is a function only of the ratio x/t. Consequently, such flows are easily handled in a  $\xi$ ,t coordinate system where  $\xi = \frac{x}{a_{\xi}t}$ . The accompanying sketch shows the significant values of  $\xi$  for the shock-tube flow of figure l(c).



Three regions in the expansion fan must be investigated with regard to the validity of the Prandtl boundary-layer assumptions. The area near the leading edge of the expansion fan represents a region of low velocity that increases from a value of zero at the leading edge ( $\xi = -1$ ). This situation appears analogous to that in the region near a stagnation point in steady flow; the Prandtl boundary-layer equations are thus assumed, as has been found in steady flow, to give results that are valid near the leading edge of the expansion fan. For an expansion fan having a finite ratio of leading-edge pressure to trailing-edge pressure, across the trailing edge of the expansion fan there is a discontinuity in the derivatives of the theoretical inviscid flow. At this point the theoretical inviscid-flow derivatives change discontinuously from a finite value ahead of the trailing

edge to a zero value behind the trailing edge although the theoretical inviscid flow itself is continuous. An analysis of the one-dimensional time-dependent equations of motion at such a discontinuity shows that the viscosity and thermal-conductivity terms are small compared with the inertia and energy terms; hence, laminar diffusion is negligible. Consequently, it will be assumed that, although the Prandtl boundary-layer equations are invalid across such a discontinuity where the second derivatives are nonexistent or infinite, the equations are valid on each side of the discontinuity. A matching procedure based on the conservation of momentum and energy will then be used to bridge the trailing-edge discontinuity.

Reference 16 has shown in regard to slip flow that the discriminating parameter, the square of the local Mach number divided by the local Reynolds number, is required to be of the order of unity or lower for the theory of continuous viscous flow to be valid. In the region of the fan where \xi\$

approaches  $\frac{2}{\gamma - 1}$ , pressure, density, and temperature approach values of

zero (see appendix A), slip-flow conditions are encountered, and the boundary-layer assumptions are violated. The approximate values (based on a perfect gas,  $\gamma = 1.4$  and  $a_{\rm c} = 1,117$  ft/sec) of this parameter for

various ratios of trailing-edge pressure to leading-edge pressure  $\frac{p_{te}}{p_{\varepsilon}}$ 

for values of  $p_{\varepsilon}$  of 1 atmosphere and 70 atmospheres are given in the following table. Also shown are the values of  $\xi$  and of the pressure ratio across the shock in an air-air shock tube corresponding to the value of  $\frac{p_{te}}{p_{\varepsilon}}$ .

₽€				
$\frac{p_{te}}{p_{e}}$	$\left(\frac{{\rm M_1}^2 \nu_1}{{\rm u_1}}\right)_{\rm te}$ for values of ${\rm p_{\varepsilon}}$ of -		ربعه	Shock-pressure ratio
	l atmosphere	70 atmospheres		
6.25 × 10 <sup>-4</sup>		1.2 × 10 <sup>-6</sup>	2.9	20
$7.5 \times 10^{-6}$	1.5 × 10 <sup>-3</sup>	2.1 × 10 <sup>-5</sup>	3.9	30
≈ 0	3.4 × 10 <sup>-1</sup>	4.9 × 10 <sup>-3</sup>	4.7	40
≈ 0	3.4 × 10 <sup>5</sup>	4.9 × 10 <sup>3</sup>	5 <b>-</b>	44

An inspection of the table shows that, based on the criteria  $\frac{M_1^2 v_1}{u_1} \gtrsim O(1)$ 

for slip flow, the slip-flow regime occupies only a limited region for extremely strong expansion waves.

#### Outline of Derivation Procedures

Since the development of the characteristic differential equations governing the unsteady-flow boundary layer is rather lengthy, a brief outline of the procedure followed will be presented before proceeding with the detailed development. The principal steps are as follows:

- (1) The Prandtl boundary-layer equations with velocity and both local and stagnation enthalpy as dependent variables are integrated in the x,y,t system from y=0 to  $y=\infty$  to obtain integral partial differential equations. These partial differential equations are then transformed to a conical coordinate system  $\xi$ ,y,t.
  - (2) The wall enthalpy is assumed to be constant.
- (3) The velocity and enthalpy profiles are expressed as a power series in transformed normal ordinates  $\alpha$ ,  $\beta$ , and  $\omega$ . Appropriate boundary conditions at the wall and free stream are applied to these series. The parameters  $\frac{\theta}{\Delta}$ ,  $\frac{\phi}{\nabla}$ , and so forth are evaluated in terms of  $\lambda$ ,  $\Gamma$ ,  $\Omega$ , b, c, and arbitrary constants.
- (4) Primary dependent variables Z, W, or Q are introduced and the derivatives of  $\lambda$ ,  $\Gamma$ ,  $\Omega$ , b, and c are evaluated. Substitution of these quantities into the partial differential equations results in pairs of characteristic equations for Z and W or Z and Q.

#### Derivation of Reduced Partial Differential Equations

The Prandtl boundary-layer equations for the two-dimensional time-dependent motion of a fluid over a flat plate are integrated over y in the x,y,t system (coordinate system fixed to the surface of the plate). The resulting partial differential equations obtained are then transformed to a conical coordinate system  $\xi$ ,y,t. In this transformation it is assumed that all the outer inviscid-flow functions are functions only of the conical parameter  $\xi = \frac{x}{a_{\varepsilon}t}$ . This assumption is valid for an analysis

of flows initiated by centered expansion waves or shock waves moving into quiescent fluid.

The qualification was also introduced in the determination of the final form of the equations that the nondimensional velocity and enthalpy profiles could be expressed as a Pohlhausen power series in a suitable variable which would be chosen to account for the density variation through the boundary layer.

(1)

The following equations are the resultant reduced partial differential equations in the conical coordinate system. (See appendixes B and C for details.) Because of their extreme length, they are written in abbreviated form here and may be found in their entirety in appendix C (eqs. (Cl1), (Cl4), (Cl5), and (Cl6)).

$$\frac{\partial \theta^{2}}{\partial \xi} \left( 1 - \frac{\xi}{\underline{u}_{1}} \frac{\delta *}{\theta} \right) + 2\theta^{2} \left( \frac{2}{\underline{u}_{1}} \frac{d\underline{u}_{1}}{d\xi} + \dots \right) + \frac{\delta *}{\theta} \frac{t}{\underline{u}_{1}} \frac{\partial \theta^{2}}{\partial t} = 2 \frac{\nu_{W}}{\underline{u}_{1}} \left( \frac{\rho_{W}}{\rho_{\varepsilon}} \right)^{2} \left( \frac{d}{d\alpha} \frac{\underline{u}_{1}}{\rho_{\varepsilon}} \right) + \frac{\delta}{\theta} \frac{d}{d\alpha}$$

$$\frac{\nabla^*}{\oint} \frac{t}{\underline{u}_1} \frac{\partial \phi^2}{\partial t} = 2 \frac{\nu_w}{\underline{u}_1} \left( \frac{\rho_w}{\rho_{\epsilon}} \right)^2 \frac{1}{N_{\text{Pr,w}}} \left( \frac{d \frac{h^*}{h_1^*}}{d\beta} \right)_w \frac{\phi}{\nabla} t - \frac{2t\phi}{\underline{u}_1 h_1^*} \Phi$$
 (2)

$$\frac{\partial \theta^{2}}{\partial \xi} \left( 1 - \frac{\xi}{\underline{u}_{1}} \frac{\delta *}{\theta} \right) + 2\theta^{2} \left( \frac{2}{\underline{u}_{1}} \frac{d\underline{u}_{1}}{d\xi} + \cdot \cdot \cdot \right) + \frac{\delta *}{\theta} \frac{t}{\underline{u}_{1}} \frac{\partial \theta^{2}}{\partial t} = 2 \frac{\nu_{W}}{\underline{u}_{1}} \left( \frac{\rho_{W}}{\rho_{\varepsilon}} \right)^{2} \left( \frac{d}{d\alpha} \frac{\underline{u}_{1}}{d\alpha} \right)_{W} \frac{\theta}{\Delta} t$$
(3)

$$\frac{\partial \psi^2}{\partial \xi} \left( \!\!\! \begin{array}{c} \!\!\! 1 - \frac{\xi}{\underline{u}_1} \frac{\square^{\bigstar}}{\psi} \end{array} \!\!\! \right) + 2 \psi^2 \left( \!\!\! \frac{1}{\underline{u}_1} \, \frac{d\underline{u}_1}{d\xi} + \dots + \frac{t}{H_1^{\bigstar}} \, \frac{\partial H_W}{\partial t} + \dots + \frac{\xi}{H_1^{\bigstar}} \, \frac{\partial H_W}{\partial \xi} + \dots \right) + \frac{1}{2} \left( \!\!\! \frac{\partial H_W}{\partial \xi} + \frac{\partial H_W}{\partial \xi} + \dots + \frac{1}{2} \frac{\partial H_W}{\partial \xi} + \dots + \frac{1}{2} \frac{\partial H_W}{\partial \xi} + \dots \right) + \frac{1}{2} \left( \!\!\! \frac{\partial H_W}{\partial \xi} + \dots + \frac{1}{2} \frac{\partial H_W}{\partial \xi} + \dots$$

$$\frac{\square^*}{\Psi} \frac{t}{\underline{u}_1} \frac{\partial \psi^2}{\partial t} = 2 \frac{\nu_w}{\underline{u}_1} \left( \frac{\rho_w}{\rho_e} \right)^2 \frac{1}{N_{\text{Pr,w}}} \left( \frac{d \frac{H^*}{H_1^*}}{d\omega} \right)_w \frac{\psi}{\Box} t$$
 (4)

Equations (1) and (2) are the momentum and energy equations for  $u_1$ ,  $h_1$ ,  $\theta$ , and  $\phi$  as dependent variables and equations (3) and (4) are for  $u_1$ ,  $H_1$ ,  $\theta$ , and  $\psi$ . The terms  $\frac{\delta^*}{\theta}$  and  $\frac{\Delta}{\theta}$  are functions only of the parameter  $\lambda$ ;  $\frac{\nabla^*}{\phi}$  and  $\frac{\nabla}{\phi}$  are functions of  $\lambda$ ,  $\Gamma$ , and  $\theta$ ; and  $\frac{\Box^*}{\psi}$  and  $\frac{\Box}{\psi}$  are

functions of  $\lambda$ ,  $\Omega$ , and c. It should be noted that, although  $\lambda=-2A_2$  (similar to Pohlhausen),  $\Gamma$  and  $\Omega$  are defined as equivalent to  $B_2$  and  $C_2$  for the enthalpy power series.

# Assumption of Constant Wall Enthalpy

The first step toward the simplification of this system of equations is concerned with the partial derivatives of  $h_W$  or  $H_W$  with respect to  $\xi$  and t. If the solution is restricted to gas flows of short duration over solid boundaries having high values of conductivity and of heat capacity per unit volume, it may be assumed that the wall temperature departs only slightly from its initial value. (See ref. 13.) If this slight departure is neglected and the wall temperature is assumed to be constant, all derivatives of the wall enthalpy are zero and are eliminated from the equations. This elimination is employed to obtain a solution and, furthermore, for all cases except those in which an insulated wall was considered, it will be assumed that  $h_W = H_W = h_{\mathfrak{C}}$ .

Note should be taken of the fact that, as  $\xi$  approaches  $\frac{2}{\gamma-1}$  in the fan, all derivatives with respect to  $\xi$  of the outer flow also approach zero; thus, there is the possibility in this case that the wall derivative of enthalpy would be significant. As  $\xi$  approaches  $\frac{2}{\gamma-1}$ ,

however, the boundary condition of zero fluid velocity at the wall is also violated as the slip-flow region is encountered and, since the equations and boundary conditions themselves are no longer valid in this region, the lack of consideration of the wall enthalpy derivative is not considered to be significant.

# Introduction of Power-Series Profiles for

# Velocity and Enthalpy

A transformation to a nondimensional "incompressible" ordinate normal to the surface is next introduced to eliminate the density terms arising in the integrals for  $\frac{\theta}{\Delta}$ ,  $\frac{\delta^*}{\Delta}$ ,  $\frac{\phi}{\nabla}$ ,  $\frac{\nabla^*}{\nabla}$ , and so forth. A power series in

this nondimensional ordinate is to be used to define the velocity and enthalpy profiles. Since boundary conditions applicable at infinity in the physical plane are to be applied at a finite distance in the transformed (incompressible) plane, the assumption is made that at a finite distance  $\delta$  in the physical plane the boundary conditions at infinity also apply. This distance  $\delta$  is the conventional boundary-layer thickness of either the velocity or enthalpy boundary layers. The nondimensional ordinates for velocity, local enthalpy, and total enthalpy are  $\alpha$ ,  $\beta$ , and  $\omega$  which are defined by the following relations:

$$\alpha = \frac{1}{\Delta} \int_{0}^{y} \frac{\rho}{\rho_{\epsilon}} dy$$

$$\Delta = \int_{0}^{\delta_{u}} \frac{\rho}{\rho_{\epsilon}} dy$$
(5)

$$\beta = \frac{1}{\nabla} \int_{0}^{y} \frac{\rho}{\rho_{\epsilon}} dy$$

$$\nabla = \int_{0}^{\delta h} \frac{\rho}{\rho_{\epsilon}} dy$$
(6)

$$\omega = \frac{1}{\Box} \int_{0}^{y} \frac{\rho}{\rho_{\epsilon}} dy$$

$$\Box = \int_{0}^{\delta_{H}} \frac{\rho}{\rho_{\epsilon}} dy$$
(7)

In equations (5) to (7) the values of  $\delta$  are not necessarily equal and, in fact, for the method of solution of this paper they are allowed to vary arbitrarily. An alternate procedure, often employed in steady flow, requires the various  $\delta$  values to be equal; such a procedure appears to be unduly restrictive and, consequently, is rejected. Thus in the present analysis, the ratio of the  $\delta$  values is one of the results of the solution and not one of the boundary conditions enforced. Kalikhman (ref. 17) was one of the first to adopt this procedure for  $\delta_{\rm u}$  and  $\delta_{\rm h}$ .

The expansion series for the various nondimensional profiles are now assumed to be represented adequately by either a five- or six-term series as shown in the following relations:

$$\frac{u}{u_1} = A_0 + A_1\alpha + A_2\alpha^2 + A_3\alpha^3 + A_4\alpha^4 + A_5\alpha^5$$
 (8)

$$\frac{h - h_W}{h_1 - h_W} = \frac{h^*}{h_1^*} = B_0 + B_1 \beta + B_2 \beta^2 + B_3 \beta^3 + B_4 \beta^4 + B_5 \beta^5$$
 (9)

$$\frac{H - H_W}{H_1 - H_W} = \frac{H^*}{H_1^*} = C_O + C_1\omega + C_2\omega^2 + C_3\omega^3 + C_4\omega^4 + C_5\omega^5$$
 (10)

The boundary conditions to be satisfied for the velocity profile are as follows:

Five-term series:

$$A_5 = 0 \tag{11}$$

For  $\alpha = 0$ ,

$$\frac{u}{u_1} = 0 \tag{12}$$

and for  $\alpha = 1$ ,

$$\frac{u}{u_1} = 1 \tag{13}$$

$$\frac{\mathrm{d} \frac{\mathrm{u}}{\mathrm{u}_{1}}}{\mathrm{d}\alpha} = 0 \tag{14}$$

$$\frac{d^2 \frac{u}{u_1}}{d\alpha^2} = \text{Constant (zero except for one special case)}$$
 (15)

For  $\alpha = 0$ ,

$$\left[\frac{\partial}{\partial y}\left(\mu \frac{\partial u}{\partial y}\right)\right]_{W} = \frac{\partial p}{\partial x} = -\rho_{\perp} \frac{Du_{\perp}}{Dt}$$
(16)

Six-term series:

For  $\alpha = 0$ ,

$$\frac{u}{u_1} = 0 \tag{17}$$

and for  $\alpha = 1$ ,

$$\frac{u}{u_1} = 1 \tag{18}$$

$$\frac{d \frac{u}{u_1}}{d\alpha} = 0 \tag{19}$$

$$\frac{\mathrm{d}^2 \frac{\mathrm{u}}{\mathrm{u}_1}}{\mathrm{d}\alpha^2} = 0 \tag{20}$$

$$\frac{d^3 \frac{u}{u_1}}{d\alpha^3} = \text{Constant (and later determined to be zero)}$$
 (21)

For  $\alpha = 0$ ,

$$\left[ \frac{\partial \lambda}{\partial u} \left( h \frac{\partial \lambda}{\partial u} \right) \right]^{M} = \frac{\partial x}{\partial b} = -b^{T} \frac{Df}{Du^{T}}$$
(55)

Similar boundary conditions are to be satisfied for the enthalpy profiles with appropriate energy equations in place of equations (16) and (22). The reason for the assumption of a constant value (which may be other than zero) for the highest derivative of velocity or enthalpy at the outer edge of the boundary layer is discussed in the consideration of the solution at the leading edge of the expansion fan.

The system of equations (11) to (15) or (17) to (21) may be solved to yield all the A values in terms of  $A_2$  and the constant of equation (15) or (21). (See appendix D.) The term  $A_2$  may, in turn, be expressed by an evaluation of equation (16) as follows:

$$-\rho_{\perp} \frac{Du_{\perp}}{Dt} = \left[ \frac{\partial}{\partial y} \left( \mu \frac{\partial y}{\partial y} \right) \right]_{w} = u_{\perp} \left( \frac{\partial \alpha}{\partial y} \right)_{w} \frac{\partial}{\partial \alpha} \left( \mu \frac{\partial \alpha}{\partial y} \frac{\partial \alpha}{\partial x} \frac{\partial \alpha}{\partial x} \right)_{\alpha=0}$$
(23)

But

$$\frac{\partial \alpha}{\partial y} = \frac{1}{\Delta} \frac{\rho}{\rho_E} \tag{24}$$

and

$$\frac{\rho\mu}{\rho_{w}\mu_{w}} = 1 \tag{25}$$

(for a given value of x,t from the assumption of the Chapman-Rubesin viscosity-temperature relation (ref. 18). A combination of equations (23), (24), and (25) results in

$$-\left(\frac{\partial^{2} \frac{\mathbf{u}}{\mathbf{u}_{1}}}{\partial \alpha^{2}}\right)_{\alpha=0} = \frac{\rho_{\epsilon}}{\rho_{w}} \frac{\rho_{1}}{\rho_{w}} \frac{1}{\underline{u}_{1}} \frac{D\underline{u}_{1}}{Dt} \frac{\mu_{\epsilon}}{\mu_{w}} \left(\frac{\Delta}{\theta}\right)^{2} \frac{\theta^{2}}{\nu_{\epsilon}}$$
(26)

Evaluating the left-hand side of equation (26) by differentiating equation (8) and evaluating the right-hand side by substituting the relation for  $\frac{D\underline{u}_{1}}{Dt}$  (eq. (C6)) and the definition of  $\xi$  yields

$$\lambda = -2A_2 = \frac{\rho_{\epsilon}}{\rho_{w}} \frac{\rho_{l}}{\rho_{w}} \frac{\mu_{\epsilon}}{\mu_{w}} \frac{\underline{u}_{l} - \xi}{\underline{u}_{l}} \frac{d\underline{u}_{l}}{d\xi} \left(\frac{\Delta}{\theta}\right)^2 \frac{\theta^2}{\nu_{\epsilon}t}$$
 (27)

A similar procedure for evaluating the energy equations (eqs. (B4) and (B5)) at the wall yields:

$$\Gamma = B_{2} = -\frac{N_{Pr}}{b^{2}} \frac{h_{1}}{h_{1}^{*}} \frac{\gamma - 1}{2} M_{1}^{2} \left[ A_{1}^{2} - \frac{\xi \frac{dp_{1}}{d\xi}}{(\underline{u}_{1} - \xi)\rho_{1}u_{1}} \frac{du_{1}}{d\xi} \right]$$
(28)

$$\Omega = C_2 = \frac{1}{c^2} \frac{u_1^2}{2H_1^*} \left[ (1 - N_{Pr}) A_1^2 + \frac{N_{Pr} \xi \frac{dp_1}{d\xi}}{(\underline{u}_1 - \xi) \rho_1 u_1 \frac{du_1}{d\xi}} \lambda \right]$$
(29)

The integrals required by the definitions of  $\theta = \int_0^\infty \frac{u}{u_1} \left(1 - \frac{u}{u_1}\right) \frac{\rho}{\rho_{\epsilon}} dy$ 

 $\delta \bm{*} = \int_0^\infty \left(1 - \frac{u}{u_1}\right) \frac{\rho}{\rho_\epsilon} \; dy, \; \text{and so forth are evaluated in appendix D and the} \\ \text{various relations for the shape parameters are expressed in the following form:}$ 

$$\frac{\theta}{\Delta} = \frac{\theta}{\Delta}(\lambda)$$

$$\frac{\delta^*}{\Delta} = \frac{\delta^*}{\Delta}(\lambda)$$

$$\frac{\phi}{\nabla} = \frac{\phi}{\nabla}(\lambda, \Gamma, b)$$

$$\frac{\nabla^*}{\nabla} = \frac{\nabla^*}{\nabla}(\Gamma)$$

$$\frac{\psi}{\Box} = \frac{\psi}{\Box}(\lambda, \Omega, c)$$

$$\frac{\psi}{\Box} = \frac{\psi}{\Box}(\Omega)$$
(30)

Transformation of Equations to Reduced Hyperbolic Form

New dependent variables, Z, W, and Q, are now introduced in recognition of the fact that, in laminar-diffusion problems, the diffusion distance (boundary-layer thickness) is proportional to the square root of the product of the kinematic viscosity and the time since diffusion began. These primary dependent variables are defined as follows:

$$Z(\xi,t) = \frac{\theta^2}{\nu_{\epsilon}t}$$
 (31a)

$$W(\xi,t) = \frac{\phi^2}{\nu_{\epsilon}t} \tag{31b}$$

$$Q(\xi,t) = \frac{\psi^2}{\nu_{\epsilon}t}$$
 (31c)

Substitution of equations (31) into equations (1) to (4) results in the following sets of simultaneous equations:

$$\begin{split} &\frac{\partial Z}{\partial \xi} \left( 1 - \frac{\xi}{\underline{u}_{1}} \frac{\delta^{*}}{\theta} \right) + 2Z \left\{ \frac{1}{2\underline{u}_{1}} \frac{\delta^{*}}{\theta} + \frac{1}{\underline{u}_{1}} \frac{d\underline{u}_{1}}{d\xi} \left[ 2 + \frac{\underline{u}_{1} - \xi}{\underline{u}_{1}} \left( \frac{\delta^{*}}{\theta} - \frac{h_{1}^{*}}{h_{1}} \frac{1}{b} \frac{\nabla^{*}}{\nabla} \frac{\Delta}{\theta} \right) \right] + \\ &\frac{1}{\underline{u}_{1}} \frac{d}{d\lambda} \left[ t \left( \frac{\partial \lambda}{\partial t} \right) - \xi \left( \frac{\partial \lambda}{\partial \xi} \right) \right] \right\} + \frac{1}{\underline{u}_{1}} \frac{\delta^{*}}{\theta} t \frac{\partial Z}{\partial t} = \frac{2}{\underline{u}_{1}} \frac{\nu_{w}}{\nu_{e}} \left( \frac{\rho_{w}}{\rho_{e}} \right)^{2} A_{1} \frac{\theta}{\Delta} \end{split}$$
(52)
$$\frac{\partial W}{\partial \xi} \left( 1 - \frac{\xi}{\underline{u}_{1}} \frac{\nabla^{*}}{\emptyset} \right) + 2W \left\{ \frac{1}{2\underline{u}_{1}} \frac{\nabla^{*}}{\emptyset} + \frac{1}{\underline{u}_{1}} \frac{d\underline{u}_{1}}{d\xi} + \frac{1}{h_{1}^{*}} \frac{dh_{1}}{d\xi} - \frac{1}{\rho_{1}h_{1}} \frac{d\underline{p}_{1}}{d\xi} + \frac{\xi}{\rho_{1}^{*}} \frac{d\underline{p}_{1}}{d\xi} + \frac{\xi}{\rho_{1}^{*}} \frac{d\underline{p}_{1}}{d\xi} - \frac{1}{\rho_{1}h_{1}} \frac{d\underline{p}_{1}}{d\xi} + \frac{\xi}{\rho_{1}^{*}} \frac{d\underline{p}_{1}}{d\xi} - \frac{1}{\rho_{1}^{*}} \frac{d\underline{p}_{1}}{d\xi} - \frac{1}{\rho_{1}^{*}} \frac{d\underline{p}_{1}}{d\xi} + \frac{\xi}{\rho_{1}^{*}} \frac{d\underline{p}_{1}}{d\xi} - \frac{1}{\rho_{1}^{*}} \frac{d\underline{p}_{1}}{d\xi} + \frac{1}{\rho_{1}^{*}} \frac{d\underline{p}_{1}}{d\xi} - \frac{1}{\rho_{1}^{*}} \frac{d\underline{p}_{1}}{d\xi} - \frac{1}{\rho_{1}^{*}} \frac{d\underline{p}_{1}}{d\xi} + \frac{1}{\rho_{1}^{*}} \frac{d\underline{p}_{1}}{d\xi} - \frac{1}{\rho_{1}^{*}} \frac{d\underline{p$$

(35)

$$\frac{\partial Z}{\partial \xi} \left( 1 - \frac{\xi}{\underline{u}_{1}} \frac{\delta^{*}}{\theta} \right) + 2Z \left\{ \frac{1}{2\underline{u}_{1}} \frac{\delta^{*}}{\theta} + \frac{1}{\underline{u}_{1}} \frac{d\underline{u}_{1}}{d\xi} \right[ 2 + \frac{(\underline{u}_{1} - \xi)}{\underline{u}_{1}} \frac{\underline{u}_{1}^{2}}{2} + \underline{H}_{1} \frac{\delta^{*}}{\theta} - \underline{H}_{1}^{*} \frac{1}{c} \frac{\Box^{*}}{\theta} \frac{\Delta}{\theta} \right] + \frac{1}{2\underline{u}_{1}} \frac{\delta^{*}}{d\xi} \left[ t \left( \frac{\partial \lambda}{\partial \xi} \right) - \xi \left( \frac{\partial \lambda}{\partial \xi} \right) \right] \right\} + \frac{1}{\underline{u}_{1}} \frac{\delta^{*}}{\theta} t \left( \frac{\partial Z}{\partial t} \right) = \frac{2}{\underline{u}_{1}} \frac{\nu_{w}}{\nu_{c}} \left( \frac{\rho_{w}}{\rho_{c}} \right)^{2} \underline{A}_{1} \frac{\theta}{\Delta} \qquad (54)$$

$$\frac{\partial Q}{\partial \xi} \left( 1 - \frac{\xi}{\underline{u}_{1}} \frac{\delta^{*}}{\theta} \right) + 2Q \left\{ \frac{1}{2\underline{u}_{1}} \frac{\Box^{*}}{\psi} + \frac{1}{\underline{u}_{1}} \frac{d\underline{u}_{1}}{d\xi} + \frac{1}{\underline{H}_{1}^{*}} \frac{d\underline{H}_{1}}{d\xi} + \frac{\xi}{\underline{u}_{1}} \left( \frac{1}{\underline{u}_{1}^{*}} - \frac{1}{\underline{u}_{1}^{*}} \frac{d\underline{p}_{1}}{d\xi} - \frac{1}{\underline{u}_{1}^{*}} \frac{d\underline{u}_{1}}{d\xi} \right) - \frac{1}{\underline{u}_{1}} \frac{d\underline{u}_{1}}{d\xi} - \frac{1}{\underline{u}_{1}^{*}} \frac{1}{\underline{u}_{1}^{*}} \frac{d\underline{u}_{1}}{d\xi} - \frac{1}{\underline{u}_{1}^{*}} \frac{1}{\underline{u}_{1}^{*}} \frac{d\underline{u}_{1}}{d\xi} - \frac{1}{\underline{u}_{1}^{*}} \frac{d\underline{u}_{1}}{d\xi} - \frac{1}{\underline{u}_{1}^{*}} \frac{d\underline{u}_{1}}{d\xi} - \frac{1}{\underline{u}_{1}^{*}} \frac{d\underline{u}_{1}}{d\xi} \right) - \frac{1}{\underline{u}_{1}} \frac{d\underline{u}_{1}}{d\xi} - \frac{1}{\underline{u}_{1}^{*}} \frac{d\underline{u}_{1}^{*}}{d\xi} - \frac{1}{\underline{u}_{1}^{*}} \frac{d\underline{u}_{1}^{*}}{d\xi} - \frac{1}{\underline{u}_{$$

The partial derivatives of  $\lambda$ ,  $\Gamma$ , b,  $\Omega$ , and c may be eliminated in the following manner: Equations (27), (28), and (29) may be expressed in the functional form:

$$\lambda(\xi,t) = E_0(\xi) \left(\frac{\Delta}{\theta}\right)^2 Z(\xi,t)$$
 (36a)

$$\Gamma(\xi,t) = \frac{E_{1h}(\xi) A_{1}^{2}(\lambda) + E_{2h}(\xi) \lambda}{b^{2}(\xi,t)}$$
 (36b)

$$\Omega(\xi,t) = \frac{E_{LH}(\xi) A_L^2(\lambda) + E_{2H}(\xi) \lambda}{c^2(\xi,t)}$$
(36c)

where the E terms are functions of  $\xi$  alone, whereas the terms  $A_1$  and  $\frac{\theta}{\Delta}$  are functions of  $\lambda$  only.

Since the derivatives are to be expressed in terms of the derivatives of the primary dependent variables, Z, W, and Q, another equation relating these quantities is required for each pair. The relevant equations are the identities

$$\frac{Z}{W} = \frac{\frac{\theta^2}{\nu_{\epsilon^{t}}}}{\frac{\emptyset^2}{\nu_{\epsilon^{t}}}} = \frac{\left(\frac{\theta}{\Delta}\right)^2}{\left(\frac{\emptyset}{\nabla}\right)^2} b^2$$
(37a)

$$\frac{Z}{Q} = \frac{\frac{\theta^2}{\nu_{\epsilon}^{t}}}{\frac{\psi^2}{\nu_{\epsilon}^{t}}} = \frac{\left(\frac{\theta}{\Delta}\right)^2}{\left(\frac{\psi}{\Box}\right)^2} c^2$$
(37b)

Differentiation of equation (36a) immediately gives the values for the partial derivatives of  $\lambda$ :

$$\left(\frac{\partial \lambda}{\partial \xi}\right)_{t} = \frac{\lambda}{g_{1}} \left[\frac{1}{E_{0}} \frac{dE_{0}}{d\xi} + \frac{1}{Z} \left(\frac{\partial Z}{\partial \xi}\right)_{t}\right]$$
(38a)

$$\left(\frac{\partial \lambda}{\partial t}\right)_{\xi} = \frac{\lambda}{g_{1}} \frac{1}{Z} \left(\frac{\partial Z}{\partial t}\right)_{\xi}$$
 (38b)

and

$$g_{1} = 1 + 2 \frac{\lambda}{\frac{\theta}{\Delta}} \frac{d \frac{\theta}{\Delta}}{d \lambda} = 1 + 2 \frac{d \log_{e} \frac{\theta}{\Delta}}{d \log_{e} \lambda}$$
 (39)

Differentiation of equations (36b), (36c), (37a), and (37b) and solution of the resultant two simultaneous equations employing the expressions above for  $\frac{\partial \lambda}{\partial t}$  and  $\frac{\partial \lambda}{\partial \xi}$  give the following relations for the derivatives of  $\Gamma$  and b (or  $\Omega$  and c). The equations are written for  $\Gamma$  and b but are also applicable for  $\Omega$  and c by everywhere substituting the equivalent functional form of the H-system for that of the h-system (that is,  $\Omega$  for  $\Gamma$ , c for b,  $\Pi^*$  for  $\nabla^*$ ,  $E_{1H}$  for  $E_{1h}$ ,  $E_{2H}$  for  $E_{2h}$ ,  $E_{2H}$  for  $E_{2h}$ ,  $E_{2H}$  for  $E_{2h}$ ,  $E_{2H}$ 

$$\left(\frac{\partial \Gamma}{\partial \xi}\right)_{t} = \frac{\Gamma}{g_{2h}} \frac{1}{W} \left(\frac{\partial W}{\partial \xi}\right) + \frac{\Gamma}{g_{2h}} \frac{1}{g_{1}Z} \left(\frac{\partial Z}{\partial \xi}\right) \left[\frac{\lambda}{\Gamma b^{2}} g_{3h} \left(1 - \frac{\partial \log_{e} \frac{Q}{\nabla}}{\partial \log_{e} b}\right) - 2 \frac{\partial \log_{e} \frac{Q}{\nabla}}{\partial \log_{e} \lambda} - 1\right] + \frac{\Gamma}{g_{2h}} \left[\frac{\lambda}{\Gamma b^{2}} g_{3h} \left(1 - \frac{\partial \log_{e} \frac{Q}{\nabla}}{\partial \log_{e} b}\right) + 2 \frac{\partial \log_{e} \frac{Q}{\Delta}}{\partial \log_{e} \lambda} - 1\right] + \frac{\Gamma}{g_{2h}} \left[\frac{\lambda}{\Gamma b^{2}} g_{3h} \left(1 - \frac{\partial \log_{e} \frac{Q}{\nabla}}{\partial \log_{e} b}\right) + 2 \frac{\partial \log_{e} \frac{Q}{\Delta}}{\partial \log_{e} \lambda} - 1\right] + \frac{\Gamma}{g_{2h}} \left[\frac{\lambda}{\Gamma b^{2}} g_{3h} \left(1 - \frac{\partial \log_{e} \frac{Q}{\nabla}}{\partial \log_{e} b}\right) + 2 \frac{\partial \log_{e} \frac{Q}{\Delta}}{\partial \log_{e} \lambda} - 1\right] + \frac{\Gamma}{g_{2h}} \left[\frac{\lambda}{\Gamma b^{2}} g_{3h} \left(1 - \frac{\partial \log_{e} \frac{Q}{\nabla}}{\partial \log_{e} b}\right) + 2 \frac{\partial \log_{e} \frac{Q}{\Delta}}{\partial \log_{e} \lambda} - 1\right] + \frac{\Gamma}{g_{2h}} \left[\frac{\lambda}{\Gamma b^{2}} g_{3h} \left(1 - \frac{\partial \log_{e} \frac{Q}{\nabla}}{\partial \log_{e} b}\right) + 2 \frac{\partial \log_{e} \frac{Q}{\Delta}}{\partial \log_{e} \lambda} - 1\right] + \frac{\Gamma}{g_{2h}} \left[\frac{\lambda}{\Gamma b^{2}} g_{3h} \left(1 - \frac{\partial \log_{e} \frac{Q}{\nabla}}{\partial \log_{e} b}\right) + 2 \frac{\partial \log_{e} \frac{Q}{\Delta}}{\partial \log_{e} \lambda} - 1\right] + \frac{\Gamma}{g_{2h}} \left[\frac{\lambda}{\Gamma b^{2}} g_{3h} \left(1 - \frac{\partial \log_{e} \frac{Q}{\nabla}}{\partial \log_{e} b}\right) + 2 \frac{\partial \log_{e} \frac{Q}{\Delta}}{\partial \log_{e} \lambda} - 1\right] + \frac{\Gamma}{g_{2h}} \left[\frac{\lambda}{\Gamma b^{2}} g_{3h} \left(1 - \frac{\partial \log_{e} \frac{Q}{\nabla}}{\partial \log_{e} b}\right) + 2 \frac{\partial \log_{e} \frac{Q}{\Delta}}{\partial \log_{e} \lambda} - 1\right] + \frac{\Gamma}{g_{2h}} \left[\frac{\lambda}{\Gamma b^{2}} g_{3h} \left(1 - \frac{\partial \log_{e} \frac{Q}{\nabla}}{\partial \log_{e} b}\right) + 2 \frac{\partial \log_{e} \frac{Q}{\Delta}}{\partial \log_{e} \lambda} - 1\right] + \frac{\Gamma}{g_{2h}} \left[\frac{\lambda}{\Gamma b^{2}} g_{3h} \left(1 - \frac{\partial \log_{e} \frac{Q}{\nabla}}{\partial \log_{e} b}\right) + 2 \frac{\partial \log_{e} \frac{Q}{\Delta}}{\partial \log_{e} \lambda} - 1\right] + \frac{\Gamma}{g_{2h}} \left[\frac{\lambda}{\Gamma b^{2}} g_{3h} \left(1 - \frac{\partial \log_{e} \frac{Q}{\nabla}}{\partial \log_{e} b}\right) + 2 \frac{\partial \log_{e} \frac{Q}{\Delta}}{\partial \log_{e} \lambda} - 1\right] + \frac{\Gamma}{g_{2h}} \left[\frac{\lambda}{\Gamma b^{2}} g_{3h} \left(1 - \frac{\partial \log_{e} \frac{Q}{\Delta}}{\partial \log_{e} b}\right) + 2 \frac{\partial \log_{e} \frac{Q}{\Delta}}{\partial \log_{e} \lambda} - 1\right] + \frac{1}{g_{2h}} \left[\frac{\lambda}{\Gamma b^{2}} g_{3h} \left(1 - \frac{\partial \log_{e} \frac{Q}{\Delta}}{\partial \log_{e} b}\right) + 2 \frac{\partial \log_{e} \frac{Q}{\Delta}}{\partial \log_{e} \lambda} - 1\right] + \frac{1}{g_{2h}} \left[\frac{\lambda}{\Gamma b^{2}} g_{3h} \left(1 - \frac{\partial \log_{e} \frac{Q}{\Delta}}{\partial \log_{e} b}\right) + 2 \frac{\partial \log_{e} \frac{Q}{\Delta}}{\partial \log_{e} \lambda} - 1\right] + \frac{\partial \log_{e} \frac{Q}{\Delta}}{\partial \log_{e} \lambda} + \frac{\partial \log_{e} \frac{Q}{\Delta}}{\partial \log_{e} \lambda} - 1$$

$$\left(\frac{\partial \Gamma}{\partial t}\right)_{\xi} = \frac{\Gamma}{g_{2h}} \frac{1}{W} \left(\frac{\partial W}{\partial t}\right) + \frac{\Gamma}{g_{2h}} \frac{1}{g_{1}Z} \left(\frac{\partial Z}{\partial t}\right) \left[\frac{\lambda}{\Gamma b^{2}} g_{3h} \left(1 - \frac{\partial \log_{e} \frac{\phi}{\nabla}}{\partial \log_{e} b}\right) - 2 \frac{\partial \log_{e} \frac{\phi}{\nabla}}{\partial \log_{e} \lambda} - 1\right] \tag{40b}$$

$$\left(\frac{\partial b}{\partial \xi}\right)_{t} = -\frac{b}{2g_{2h}} \frac{1}{w} \left(\frac{\partial w}{\partial \xi}\right) + \frac{b}{2g_{2h}} \frac{1}{g_{1}^{Z}} \left(\frac{\partial z}{\partial \xi}\right) \left(1 + \frac{2\lambda}{\Gamma b^{2}} g_{3h} \frac{\partial \log_{e} \frac{\phi}{\nabla}}{\partial \log_{e} \Gamma} + 2 \frac{\partial \log_{e} \frac{\phi}{\nabla}}{\partial \log_{e} \lambda}\right) + \frac{b}{2g_{2h}} \frac{1}{g_{1}^{Z}} \left(\frac{\partial z}{\partial \xi}\right) \left(1 + \frac{2\lambda}{\Gamma b^{2}} g_{3h} \frac{\partial \log_{e} \frac{\phi}{\nabla}}{\partial \log_{e} \Gamma} + 2 \frac{\partial \log_{e} \frac{\phi}{\nabla}}{\partial \log_{e} \lambda}\right) + \frac{b}{2g_{2h}} \frac{1}{g_{1}^{Z}} \left(\frac{\partial z}{\partial \xi}\right) \left(1 + \frac{2\lambda}{\Gamma b^{2}} g_{3h} \frac{\partial \log_{e} \frac{\phi}{\nabla}}{\partial \log_{e} \Gamma} + 2 \frac{\partial \log_{e} \frac{\phi}{\nabla}}{\partial \log_{e} \lambda}\right) + \frac{b}{2g_{2h}} \frac{1}{g_{1}^{Z}} \left(\frac{\partial z}{\partial \xi}\right) \left(1 + \frac{2\lambda}{\Gamma b^{2}} g_{3h} \frac{\partial \log_{e} \frac{\phi}{\nabla}}{\partial \log_{e} \Gamma} + 2 \frac{\partial \log_{e} \frac{\phi}{\nabla}}{\partial \log_{e} \lambda}\right)$$

$$b \frac{g_{6h}}{g_{2h}} \frac{\partial \log_e \frac{\emptyset}{\nabla}}{\partial \log_e \Gamma} + \frac{b}{g_1 g_{2h}} \left( \frac{\lambda}{\Gamma b^2} g_{3h} \frac{\partial \log_e \frac{\emptyset}{\nabla}}{\partial \log_e \Gamma} - \frac{d \log_e \frac{\theta}{\Delta}}{d \log_e \lambda} + \frac{d \log_e \frac{\emptyset}{\Delta}}{d \log_e \lambda} + \frac{d \log_e \frac{\emptyset}{\Delta}}{d \log_e \lambda} \right)$$

$$\frac{\partial \log_{e} \sqrt[d]{1}}{\partial \log_{e} \lambda} \frac{dE_{0}}{d\xi}$$
(41a)

$$\left(\frac{\partial b}{\partial t}\right)_{\xi} = -\frac{b}{2g_{2h}} \frac{1}{w} \left(\frac{\partial w}{\partial t}\right) + \frac{b}{2g_{2h}} \frac{1}{g_{1}Z} \left(\frac{\partial Z}{\partial t}\right) \left(1 + \frac{2\lambda}{\Gamma b^{2}} g_{3h} \frac{\partial \log_{e} \frac{\cancel{Q}}{\nabla}}{\partial \log_{e} \Gamma} + 2 \frac{\partial \log_{e} \frac{\cancel{Q}}{\nabla}}{\partial \log_{e} \lambda}\right) \tag{41b}$$

where

$$g_{2h} = 1 - \frac{\partial \log_{e} \frac{\phi}{\nabla}}{\partial \log_{e} b} + 2 \frac{\partial \log_{e} \frac{\phi}{\nabla}}{\partial \log_{e} \Gamma}$$

$$g_{2H} = 1 - \frac{\partial \log_{e} \frac{\psi}{\Omega}}{\partial \log_{e} c} + 2 \frac{\partial \log_{e} \frac{\psi}{\Omega}}{\partial \log_{e} \Omega}$$
(42)

$$g_{3h} = E_{1h} \frac{dA_1^2}{d\lambda} + E_{2h}$$
 (43)

$$g_{6h} = \frac{1}{\Gamma b^2} \left( A_1^2 \frac{dE_{1h}}{d\xi} + \lambda \frac{dE_{2h}}{d\xi} \right) \tag{44}$$

Elimination of the derivatives of the secondary dependent variables produces the final form of the differential equations.

For local enthalpy:

$$\left[\underline{u_{1}} \frac{\theta}{\delta^{*}} - \frac{\xi}{g_{1}} \left(1 + 2 \frac{d \log_{e} \frac{\delta^{*}}{\Delta}}{d \log_{e} \lambda}\right)\right] \left(\frac{\partial Z}{\partial \xi}\right)_{t} + \left(1 + 2 \frac{d \log_{e} \frac{\delta^{*}}{\Delta}}{d \log_{e} \lambda}\right) \frac{t}{g_{1}} \left(\frac{\partial Z}{\partial t}\right)_{\xi} + 2 \left\{\frac{1}{2} + \frac{1}{2} + \frac{1}{2}$$

$$\frac{d\underline{u}_{1}}{d\xi} \left[ 2 \frac{\theta}{\delta^{*}} + \frac{\underline{u}_{1} - \xi}{\underline{u}_{1}} \left( 1 - \frac{h_{1}^{*}}{h_{1}} \frac{1}{b} \frac{\nabla^{*}}{\nabla} \frac{\Delta}{\delta^{*}} \right) \right] - \frac{1}{g_{1}} \frac{d \log_{e} \frac{\delta^{*}}{\theta}}{d \log_{e} \lambda} \frac{d \log_{e} E_{0}}{d \log_{e} \xi} \right\} Z = 0$$

$$2 \frac{\nu_{W}}{\nu_{\epsilon}} \left\langle \stackrel{\rho_{W}}{\rho_{\epsilon}} \right\rangle^{2} A_{L} \frac{\theta}{\Delta} \frac{\theta}{\delta^{*}}$$
 (45)

$$\left( \frac{y}{1} \frac{\phi}{\nabla^*} - \frac{g_{1h}}{g_{2h}} \frac{1}{\xi} \right) \left( \frac{\partial W}{\partial \xi} \right)_{\xi} + \frac{g_{4h}}{g_{2h}} \frac{1}{\xi} \left( \frac{\partial W}{\partial \xi} \right)_{\xi} - \frac{2}{g_{1}} g_{5h} \frac{W}{Z} \left[ \frac{\xi}{\partial \xi} \right]_{\xi} - \frac{1}{\xi} \left( \frac{\partial Z}{\partial \xi} \right)_{\xi} \right] + 2 \left( \frac{1}{2} + \left( \frac{d\underline{u}_{1}}{d\xi} + \frac{\underline{u}_{1}}{h_{1}^{*}} \frac{dh_{1}}{d\xi} - \frac{\underline{u}_{1}}{\rho_{1}h_{1}} \frac{d\underline{p}_{1}}{d\xi} \right) \frac{\phi}{\nabla^{*}} + \frac{\xi}{\rho_{1}h_{1}} \frac{d\underline{p}_{1}}{d\xi} - \frac{\xi}{h_{1}^{*}} \frac{d\underline{h}_{1}}{d\xi} - \frac{\xi}{h_{1}^{*}} \frac{d\underline{h}_{1}}{d\xi} \right) - \frac{\xi}{\rho_{1}} \frac{d\underline{p}_{1}}{d\xi} \left( \frac{\partial W}{\partial \xi} \right)_{\xi} - \frac{2}{g_{1}} \frac{g_{2h}}{g_{1}} \frac{d\underline{p}_{2h}}{g_{1}} \frac{d\underline{p}_{2h}}{g_{2h}} \frac{d\underline{p}_{2h}}{g_{1}} \frac{d\underline{p}_{2h}}{g_{2h}} \frac{d\underline{p}_{2h}}{$$

For total enthalpy:

$$\left[\underline{u_{1}} \frac{\theta}{\delta^{*}} - \frac{\xi}{g_{1}} \left(1 + 2 \frac{d \log_{e} \frac{\delta^{*}}{\Delta}}{d \log_{e} \lambda}\right)\right] \left(\frac{\partial Z}{\partial \xi}\right)_{t} + \left(1 + 2 \frac{d \log_{e} \frac{\delta^{*}}{\Delta}}{d \log_{e} \lambda}\right) \frac{t}{g_{1}} \left(\frac{\partial Z}{\partial t}\right)_{\xi} + \left(1 + 2 \frac{d \log_{e} \lambda}{d \log_{e} \lambda}\right) \frac{t}{g_{1}} \left(\frac{\partial Z}{\partial t}\right)_{\xi} + \left(1 + 2 \frac{d \log_{e} \lambda}{d \log_{e} \lambda}\right) \frac{t}{g_{1}} \left(\frac{\partial Z}{\partial t}\right)_{\xi} + \left(1 + 2 \frac{d \log_{e} \lambda}{d \log_{e} \lambda}\right) \frac{t}{g_{1}} \left(\frac{\partial Z}{\partial t}\right)_{\xi} + \left(1 + 2 \frac{d \log_{e} \lambda}{d \log_{e} \lambda}\right) \frac{t}{g_{1}} \left(\frac{\partial Z}{\partial t}\right)_{\xi} + \left(1 + 2 \frac{d \log_{e} \lambda}{d \log_{e} \lambda}\right) \frac{t}{g_{1}} \left(\frac{\partial Z}{\partial t}\right)_{\xi} + \left(1 + 2 \frac{d \log_{e} \lambda}{d \log_{e} \lambda}\right) \frac{t}{g_{1}} \left(\frac{\partial Z}{\partial t}\right)_{\xi} + \left(1 + 2 \frac{d \log_{e} \lambda}{d \log_{e} \lambda}\right) \frac{t}{g_{1}} \left(\frac{\partial Z}{\partial t}\right)_{\xi} + \left(1 + 2 \frac{d \log_{e} \lambda}{d \log_{e} \lambda}\right) \frac{t}{g_{1}} \left(\frac{\partial Z}{\partial t}\right)_{\xi} + \left(1 + 2 \frac{d \log_{e} \lambda}{d \log_{e} \lambda}\right) \frac{t}{g_{1}} \left(\frac{\partial Z}{\partial t}\right)_{\xi} + \left(1 + 2 \frac{d \log_{e} \lambda}{d \log_{e} \lambda}\right) \frac{t}{g_{1}} \left(\frac{\partial Z}{\partial t}\right)_{\xi} + \left(1 + 2 \frac{d \log_{e} \lambda}{d \log_{e} \lambda}\right) \frac{t}{g_{1}} \left(\frac{\partial Z}{\partial t}\right)_{\xi} + \left(1 + 2 \frac{d \log_{e} \lambda}{d \log_{e} \lambda}\right) \frac{t}{g_{1}} \left(\frac{\partial Z}{\partial t}\right)_{\xi} + \left(1 + 2 \frac{d \log_{e} \lambda}{d \log_{e} \lambda}\right) \frac{t}{g_{1}} \left(\frac{\partial Z}{\partial t}\right)_{\xi} + \left(1 + 2 \frac{d \log_{e} \lambda}{d \log_{e} \lambda}\right) \frac{t}{g_{1}} \left(\frac{\partial Z}{\partial t}\right)_{\xi} + \left(1 + 2 \frac{d \log_{e} \lambda}{d \log_{e} \lambda}\right) \frac{t}{g_{1}} \left(\frac{\partial Z}{\partial t}\right)_{\xi} + \left(1 + 2 \frac{d \log_{e} \lambda}{d \log_{e} \lambda}\right) \frac{t}{g_{1}} \left(\frac{\partial Z}{\partial t}\right)_{\xi} + \left(1 + 2 \frac{d \log_{e} \lambda}{d \log_{e} \lambda}\right) \frac{t}{g_{1}} \left(\frac{\partial Z}{\partial t}\right)_{\xi} + \left(1 + 2 \frac{d \log_{e} \lambda}{d \log_{e} \lambda}\right) \frac{t}{g_{1}} \left(\frac{\partial Z}{\partial t}\right)_{\xi} + \left(1 + 2 \frac{d \log_{e} \lambda}{d \log_{e} \lambda}\right) \frac{t}{g_{1}} \left(\frac{\partial Z}{\partial t}\right)_{\xi} + \left(1 + 2 \frac{d \log_{e} \lambda}{d \log_{e} \lambda}\right) \frac{t}{g_{1}} \left(\frac{\partial Z}{\partial t}\right)_{\xi} + \left(1 + 2 \frac{d \log_{e} \lambda}{d \log_{e} \lambda}\right) \frac{t}{g_{1}} \left(\frac{\partial Z}{\partial t}\right)_{\xi} + \left(1 + 2 \frac{d \log_{e} \lambda}{d \log_{e} \lambda}\right) \frac{t}{g_{1}} \left(\frac{\partial Z}{\partial t}\right)_{\xi} + \left(1 + 2 \frac{d \log_{e} \lambda}{d \log_{e} \lambda}\right) \frac{t}{g_{1}} \left(\frac{\partial Z}{\partial t}\right)_{\xi} + \left(1 + 2 \frac{d \log_{e} \lambda}{d \log_{e} \lambda}\right) \frac{t}{g_{1}} \left(\frac{\partial Z}{\partial t}\right)_{\xi} + \left(1 + 2 \frac{d \log_{e} \lambda}{d \log_{e} \lambda}\right) \frac{t}{g_{1}} \left(\frac{\partial Z}{\partial t}\right)_{\xi} + \left(1 + 2 \frac{d \log_{e} \lambda}{d \log_{e} \lambda}\right) \frac{t}{g_{1}} \left(\frac{\partial Z}{\partial t}\right)_{\xi} + \left(1 + 2 \frac{d \log_{e} \lambda}{d \log_{e} \lambda}\right) \frac{t}{g_{1}} \left(\frac{\partial Z}{\partial t}\right)_{\xi} + \left(1 + 2 \frac{d \log_{e} \lambda}{d \log_$$

$$2 \left[ \frac{1}{2} + \frac{d\underline{u}_{1}}{d\xi} \left( 2 + \frac{\underline{u}_{1} - \xi}{\underline{u}_{1}} \right) \frac{\underline{u_{1}}^{2} + \underline{H}_{1} \frac{\delta^{*}}{\theta} - \underline{H}_{1}^{*} \frac{1}{c} \frac{\underline{\square}^{*}}{\underline{\square}} \frac{\Delta}{\theta}}{\underline{H}_{1} - \frac{\underline{u}_{1}^{2}}{2}} \right] \frac{\theta}{\delta^{*}} - \frac{1}{2}$$

$$\frac{1}{g_{1}} \frac{d \log_{e} \frac{\delta^{*}}{\theta}}{d \log_{e} \lambda} \frac{d \log_{e} E_{0}}{d \log_{e} \xi} Z = 2 \frac{\nu_{W}}{\nu_{\varepsilon}} \left( \frac{\rho_{W}}{\rho_{\varepsilon}} \right)^{2} A_{1} \frac{\theta}{\Delta} \frac{\theta}{\delta^{*}}$$
(47)

$$\left( \underline{\underline{u}}_{1} \cdot \frac{\psi}{\square^{*}} - \frac{g_{1jH}}{g_{2H}} \cdot \xi \right) \left( \frac{\partial \underline{Q}}{\partial \xi} \right)_{t} + \frac{g_{1jH}}{g_{2H}} \cdot t \left( \frac{\partial \underline{Q}}{\partial t} \right)_{\xi} - \frac{2}{g_{1}} \cdot g_{5H} \cdot \frac{\underline{Q}}{2} \left[ \xi \left( \frac{\partial \underline{Z}}{\partial \xi} \right)_{t} - t \left( \frac{\partial \underline{Z}}{\partial t} \right)_{\xi} \right] + 2 \left( \underbrace{\frac{1}{2}}_{2} + \underbrace{\frac{d\underline{u}_{1}}{d\xi}} + \frac{\underline{u}_{1}}{d\xi} \cdot \frac{d\underline{u}_{1}}{d\xi} \right) \underbrace{\psi}_{\square^{*}} + \underbrace{\frac{\xi}{\rho_{1}} \cdot \frac{d\underline{u}_{1}}{d\xi}}_{\underline{H_{1}} - \underbrace{u_{1}^{2}}_{\underline{Q}}} - \underbrace{\frac{\xi}{H_{1}^{*}} \cdot \frac{d\underline{u}_{1}}{d\xi}}_{\underline{H_{1}} - \underbrace{u_{1}^{2}}_{\underline{Q}}} - \underbrace{\frac{d\underline{u}_{1}}{d\xi}}_{\underline{H_{1}} - \underbrace{u_{1}^{2}}_{\underline{Q}}} - \underbrace{\frac{d\underline{u}_{1}}{d\xi}}_{\underline{H_{1}} - \underbrace{u_{1}^{2}}_{\underline{Q}}}_{\underline{H_{1}} - \underbrace{u_{1}^{2}}_{\underline{Q}}} - \underbrace{\frac{d\underline{u}_{1}}{d\xi}}_{\underline{H_{1}} - \underbrace{u_{1}^{2}}_{\underline{Q}}}_{\underline{Q}} - \underbrace{\frac{d\underline{u}_{1}}{d\xi}}_{\underline{H_{1}} - \underbrace{u_{1}^{2}}_{\underline{Q}}}_{\underline{Q}} - \underbrace{\frac{d\underline{u}_{1}}{d\xi}}_{\underline{H_{1}} - \underbrace{u_{1}^{2}}_{\underline{Q}}}_{\underline{Q}} - \underbrace{\frac{d\underline{u}_{1}}{d\xi}}_{\underline{H_{1}} - \underbrace{u_{1}^{2}}_{\underline{Q}}}_{\underline{Q}} - \underbrace{\frac{d\underline{u}_{1}}{d\xi}}_{\underline{Q}} - \underbrace{\frac{d\underline{u}_{1}}{d\xi}}_{$$

$$\frac{\frac{u_1^2}{2}}{H_1 - \frac{u_1^2}{2}} \frac{\xi}{\rho_1} \frac{dp_1}{d\xi} \right) c \cdot \frac{\delta^*}{\Delta} \frac{\square}{\square^*} - \frac{1}{H_1^*} \frac{\frac{u_1^2}{2}}{H_1 - \frac{u_1^2}{2}} \frac{\xi}{\rho_1} \frac{dp_1}{d\xi} \cdot c \cdot \frac{\theta}{\Delta} \frac{\square}{\square^*} - \frac{1}{g_1} \frac{\partial \log_e \frac{\square^*}{\psi}}{\partial \log_e \lambda} \frac{d \log_e E_0}{d \log_e \xi} - \frac{1}{g_{2H}} \frac{\partial \log_e \frac{\square^*}{\psi}}{\partial \log_e \Omega} \left\{ \xi g_{6H} \left( 1 - \frac{\partial \log_e \frac{\psi}{\square}}{\partial \log_e C} \right) + \frac{1}{g_{2H}} \frac{\partial \log_e \frac{\square^*}{\psi}}{\partial \log_e \Omega} \right\}$$

$$\frac{1}{g_1} \frac{d \log_e g_0}{d \log_e g_0} \left[ \frac{\lambda}{g_2 g_3 H} \left( 1 - \frac{\partial \log_e \frac{\psi}{13}}{\partial \log_e c} \right) + 2 \frac{d \log_e \frac{\theta}{\Delta}}{d \log_e \lambda} - 2 \frac{\partial \log_e \frac{\psi}{13}}{\partial \log_e \lambda} \right] \right\} \\ - \frac{1}{g_{2H}} \frac{\partial \log_e \frac{J^*}{\psi}}{\partial \log_e c} \left[ g_{3H} \frac{\partial \log_e \frac{\psi}{13}}{\partial \log_e \Omega} + \frac{\partial \log_e \frac{W}{13}}{\partial \log_e \Omega} \right]$$

$$\frac{1}{g_{1}} \frac{d \log_{e} E_{0}}{d \log_{e} \xi} \left( \frac{\lambda}{\rho_{c}^{2}} g_{3H} \frac{\partial \log_{e} \frac{\psi}{\Box}}{\partial \log_{e} \Omega} - \frac{d \log_{e} \frac{\theta}{\Delta}}{d \log_{e} \lambda} + \frac{\partial \log_{e} \frac{\psi}{\Box}}{\partial \log_{e} \lambda} \right) \right] Q = 2 \frac{\nu_{w} \left( \rho_{w} \right)^{2} \frac{C_{1}}{\nu_{e}} \left( \rho_{e} \right)^{2} \frac{C_{1}}{N_{Pr}} \frac{\psi}{\Box} \frac{\psi}{\Box}$$

$$(48)$$

where

$$g_{4h} = 1 + 2 \frac{\partial \log_e \frac{\nabla^*}{\nabla}}{\partial \log_e \Gamma} - \frac{\partial \log_e \frac{\nabla^*}{\nabla}}{\partial \log_e b}$$
 (49)

$$g_{5h} = \frac{\partial \log_e \frac{\nabla^*}{\emptyset}}{\partial \log_e \lambda} + \frac{1}{g_{2h}} \frac{\partial \log_e \frac{\nabla^*}{\emptyset}}{\partial \log_e \Gamma} \left[ \frac{\lambda}{\Gamma b^2} g_{3h} \left( 1 - \frac{\partial \log_e \frac{\emptyset}{\nabla}}{\partial \log_e b} \right) - 2 \frac{\partial \log_e \frac{\emptyset}{\nabla}}{\partial \log_e \lambda} - 1 \right] + \frac{\partial \log_e \frac{\nabla^*}{\emptyset}}{\partial \log_e \lambda} + \frac{1}{g_{2h}} \frac{\partial \log_e \frac{\nabla^*}{\emptyset}}{\partial \log_e \Gamma} \left[ \frac{\lambda}{\Gamma b^2} g_{3h} \left( 1 - \frac{\partial \log_e \frac{\emptyset}{\nabla}}{\partial \log_e b} \right) - 2 \frac{\partial \log_e \frac{\emptyset}{\nabla}}{\partial \log_e \lambda} - 1 \right] + \frac{\partial \log_e \frac{\nabla^*}{\emptyset}}{\partial \log_e \lambda} + \frac{1}{g_{2h}} \frac{\partial \log_e \frac{\nabla^*}{\emptyset}}{\partial \log_e \Gamma} \left[ \frac{\lambda}{\Gamma b^2} g_{3h} \left( 1 - \frac{\partial \log_e \frac{\emptyset}{\nabla}}{\partial \log_e b} \right) - 2 \frac{\partial \log_e \frac{\emptyset}{\nabla}}{\partial \log_e \lambda} - 1 \right] + \frac{\partial \log_e \frac{\nabla^*}{\emptyset}}{\partial \log_e \lambda} + \frac{\partial \log_e \frac{\nabla^*}{\emptyset}}{\partial \log_e \lambda} + \frac{\partial \log_e \frac{\nabla^*}{\nabla}}{\partial \log_e \lambda} + \frac{\partial \log_e \lambda}{\partial \log_e \lambda} + \frac{\partial \log_e$$

$$\frac{1}{2g_{2h}} \frac{\partial \log_{e} \frac{\nabla^{*}}{\phi}}{\partial \log_{e} b} \left( 1 + \frac{2\lambda}{\Gamma b^{2}} g_{3h} \frac{\partial \log_{e} \frac{\phi}{\nabla}}{\partial \log_{e} \Gamma} + 2 \frac{\partial \log_{e} \frac{\phi}{\nabla}}{\partial \log_{e} \lambda} \right)$$
(50)

Equations (45) and (46) and equations (47) and (48) are sets of hyperbolic differential equations for which real characteristics exist. The slopes of the characteristic curves are given by the following expressions:

$$\left(\frac{\delta t}{\delta \xi}\right)_{\underline{}} = \frac{\left(1 + 2 \frac{d \log_{e} \frac{\delta *}{\Delta}}{d \log_{e} \lambda}\right) t}{\underbrace{u_{1} \frac{\theta}{\delta *} g_{1} - \left(1 + 2 \frac{d \log_{e} \frac{\delta *}{\Delta}}{d \log_{e} \lambda}\right) \xi}$$
(51)

$$\left(\frac{\delta t}{\delta \xi}\right)_{+} = \frac{g_{\downarrow h}t}{\underbrace{u}_{1} \underbrace{\phi}_{\nabla *} g_{2h} - g_{\downarrow h}\xi}$$
(52a)

for the h-method; and

$$\left(\frac{\delta t}{\delta \xi}\right)_{+} = \frac{g_{\downarrow H} t}{\underline{u}_{\perp} \frac{\psi}{\Box *} g_{2H} - g_{\downarrow H} \xi}$$
(52b)

for the H-method.

The flow field in the &,t plane is confined to the region

$$\xi_{S}^{-} = \frac{u_{S}^{-}}{a_{\varepsilon}} \le \xi \le \xi_{S}^{+} = \frac{u_{S}^{+}}{a_{\varepsilon}}$$
 (0 < t < \infty)

where the waves initiating the flow have velocities  $u_s^-$  and  $u_s^+$ . Subsequently, it will be shown that the boundary conditions are specified only along  $\xi = \xi_s^-$  and  $\xi = \xi_s^+$ ; thus, integration along the characteristic lines must originate at one or the other of these values of  $\xi$ . Furthermore, as the integration progresses, even though no boundary condition is specified at t=0 or  $\infty$ , time must be increasing for the mathematical solution to be compatible with the physical one in that an event preceding another in time may influence the latter but not viceversa. Thus, the requirement

$$\delta t = \left(\frac{\delta t}{\delta \xi}\right) \delta \xi > 0$$

determines the limiting value of  $\xi$  at which (in the absence of discontinuities) the integration from  $\xi = \xi_s^-$  or  $\xi = \xi_s^+$  must stop. If this limiting value of  $\xi$  is denoted by  $\xi^*$ ,  $\frac{\delta t}{\delta \xi}$  (from eqs. (51) and (52a) or (52b)) changes sign at values of  $\xi^*$  given by

$$\xi_{-}^* = \xi_{Z}^* = \underline{u}_1 \frac{\theta}{\delta^*} g_1 \left( 1 + 2 \frac{d \log_e \frac{\delta^*}{\Delta}}{d \log_e \lambda} \right)^{-1}$$
 (53)

$$\xi_{+}^{*} = \xi_{W}^{*} = \underline{u}_{1} \frac{\phi}{\nabla x} g_{2h} g_{4h}^{-1}$$
 (54a)

or

$$\xi_{+}^{*} = \xi_{0}^{*} = \underline{u}_{1} \frac{\psi}{\Pi^{*}} g_{2H}^{g_{1}} - 1$$
 (54b)

These values also denote the vanishing of the coefficient of the term  $\frac{\delta Z}{\delta \xi}$  or  $\frac{\delta W}{\delta \xi}$  in the differential equations. Singular behavior of

the solution of a differential equation at any point where the coefficient of the leading derivative in the differential equation vanishes is a common mathematical phenomenon.

#### METHOD OF SOLUTION FOR THE REDUCED HYPERBOLIC

#### DIFFERENTIAL EQUATIONS

#### Statement of Problem

The solution of the unsteady boundary-layer equations has been reduced to the problem outlined below. (The h-system alone will be discussed, since the H-system is in general similar to it. Where major differences between the two systems arise, these will be noted.)

If the following five equations are given:

- (1) First differential equation for Z (eq. (45))
- (2) Second differential equation for W (eq. (46))

(3) 
$$\lambda = \lambda \left[ \xi, Z(\xi, t) \right]$$
 (eq. (36a))

(4) 
$$\Gamma = \Gamma(\lambda, b, \xi)$$
 (eq. (36b))

(5) 
$$\frac{Z(\xi,t)}{W(\xi,t)} = \frac{Z}{W}(\Gamma,b,\lambda) \text{ (eq. (37a))}$$

determine the five dependent variables Z, W,  $\lambda$ ,  $\Gamma$ , and b. The solutions to this set of equations with appropriate boundary conditions for the cases of constant free-stream flow and of a free-stream flow varying in a manner prescribed by a centered expansion wave are treated in subsequent sections.

# Method for Centered Expansion Fan

Solution of the problem at the leading edge. The determination of the critical values of  $\lambda$  and Z at the leading edge of the expansion fan ( $\xi=-1$ ) may be achieved by consideration of only two (eqs. (36a) and (45)) of the five equations listed previously. The elimination of the other equations arises from the fact that, at  $\xi=-1$ , the flow is

essentially incompressible ( $M_1$  approaches 0); thus, the momentum equation is divorced from the energy equation.

Consider first the equation for  $\lambda$  with  $E_O$  expressed in terms of  $\xi$  by using the fact that  $T_W=T_\varepsilon$  and  $\mu_W=\mu_\varepsilon$ :

$$\lambda = \frac{Z}{1+\xi} \left( \frac{\frac{\gamma+1}{2}}{1-\frac{\gamma-1}{2}\xi} \right)^{\frac{3\gamma-1}{\gamma-1}} \left( \frac{\Delta}{\theta} \right)^{2}$$
 (55)

If the boundary condition is stipulated that  $\lambda$  be finite at  $\xi = -1$ , it is evident from equation (55) that the following relations must hold at  $\xi = -1$ :

$$Z(-1,t) = 0 (56a)$$

$$\left(\frac{\delta Z}{\delta \xi}\right)_{\xi=-1} = \left[\lambda \left(\frac{\theta}{\Delta}\right)^{2}\right]_{\xi=-1}$$
(56b)

since  $\frac{\partial}{\partial t}(1+\xi)=0$  and  $\frac{\delta}{\delta \xi}$  denotes the characteristic derivative; that is,

$$\left(\frac{\delta}{\delta \xi}\right)_{\pm} = \left(\frac{\partial}{\partial \xi}\right) + \left(\frac{\partial}{\partial t}\right) \left(\frac{\delta t}{\delta \xi}\right)_{\pm}$$
(57)

Now the momentum equation at  $\xi = -1$  reduces to

$$\frac{1}{g_{1}}\left(1+2\frac{d \log_{e} \frac{\delta^{*}}{\Delta}}{d \log_{e} \lambda}\right)\left(\frac{\delta Z}{\delta \xi}\right)_{-}+2\left[\frac{1}{\underline{u}_{1}}\frac{d\underline{u}_{1}}{d\xi}-\frac{1}{g_{1}}\frac{d \log_{e} \frac{\delta^{*}}{\theta}}{d \log_{e} \lambda}\left(\frac{d \log_{e} E_{0}}{d \log_{e} \xi}\right)_{\xi=-1}\right]Z=$$

$$2A_1 \frac{\theta}{\Lambda} \frac{\theta}{\delta^*}$$
 (58)

since the ratio

$$\lim_{\xi \to -1} \frac{h_1^*}{u_1 h_1} = - (\gamma - 1)$$

Equation (58) may be reduced through further limiting and combining processes to

$$\frac{1}{g_{1}}\left(1+2\frac{d \log_{e} \frac{\delta *}{\Delta}}{d \log_{e} \lambda}\right)\left(\frac{\delta Z}{\delta \xi}\right)_{-}+2\frac{d \underline{u}_{1}}{d \xi}\frac{\left(\frac{\delta Z}{\delta \xi}\right)_{-}}{\left(\frac{\delta \underline{u}_{1}}{\delta \xi}\right)}-\frac{2 \xi}{g_{1}}\frac{d \log_{e} \frac{\delta *}{\theta}}{d \log_{e} \lambda}\left(-\frac{Z}{1+\xi}+\frac{Z}{\xi}\right)$$

$$\frac{3\gamma - 1}{1 - \frac{\gamma - 1}{2} \xi} = 2A_{\perp} \frac{\theta}{\Delta} \frac{\theta}{\delta *}$$
 (59)

or

$$\frac{1}{g_{1}}\left(1+2\frac{d \log_{e} \frac{\delta^{*}}{\Delta}}{d \log_{e} \lambda}\right)\left(\frac{\delta Z}{\delta \xi}\right)_{-}+2\left(\frac{\delta Z}{\delta \xi}\right)_{-}-\frac{2}{g_{1}}\frac{d \log_{e} \frac{\delta^{*}}{\theta}}{d \log_{e} \lambda}\left(\frac{\delta Z}{\delta \xi}\right)_{-}=2A_{1}\frac{\theta}{\Delta}\frac{\theta}{\delta^{*}}$$

and finally to

$$3\left(\frac{\delta Z}{\delta \xi}\right)_{-} = 2A_{\perp}\left(\frac{\theta}{\Delta}\right)^{2} \frac{\Delta}{\delta *} \tag{60}$$

Equating the values of  $\left(\frac{\delta Z}{\delta \xi}\right)_{-}$  at  $\xi$  = -1 from equations (56b) and (60) yields

$$\lambda \left(\frac{\theta}{\Delta}\right)^2 = \frac{2}{3} A_1 \left(\frac{\theta}{\Delta}\right)^2 \frac{\Delta}{\delta^*}$$

or

$$\lambda = \frac{2}{3} A_1 \frac{\Delta}{\delta^*} \tag{61}$$

The initial value of  $\lambda$  at  $\xi=-1$  for all t must satisfy equation (61) regardless of the values of  $\Gamma$  and b.

If a five-term velocity profile is assumed, substitution of the values of Al and  $\frac{\delta^*}{\Delta}$  in terms of  $\lambda$  into equation (61) determines the equality

$$\frac{\lambda^{2}}{120} + \left[ -\frac{17}{90} + \frac{1}{40} \left( \frac{u}{u_{1}} \right)^{"}_{\alpha=1} \right] \lambda + \frac{1}{9} \left[ 12 + \left( \frac{u}{u_{1}} \right)^{"}_{\alpha=1} \right] = 0$$
 (62)

For  $\lambda$  to be real, the value of  $\left(\frac{u}{u_1}\right)_{\alpha=1}^{"} = \left(\frac{d^2 \frac{u}{u_1}}{d\alpha^2}\right)_{\alpha=1}^{\alpha}$  must be such that

$$\left[ -\frac{17}{90} + \frac{1}{40} \left( \frac{u}{u_1} \right)^{"} \right]^{2} - \frac{4}{1,080} \left[ 12 + \left( \frac{u}{u_1} \right)^{"} \right] \ge 0$$
 (63)

or

$$\left(\frac{u}{u_1}\right)^{n/2} - 21.037 \left(\frac{u}{u_1}\right)^n - 14.025 \ge 0$$
 (63a)

The minimum absolute value for  $\left(\frac{u}{u_1}\right)''$  is found (by using the equal sign in eq. (63a)) to be -0.647. A minimum value is desired since the velocity should approach the stream velocity asymptotically at the edge of the boundary layer. When this value of  $\left(\frac{u}{u_1}\right)''_{\alpha=1}$  is used with equation (62), the starting value of  $\lambda$  is found to be 12.3.

If this sequence is duplicated for the six-term velocity profile, the corresponding equations are:

$$\frac{\lambda^{2}}{240} - \left[\frac{1}{6} + \frac{1}{240} \left(\frac{u}{u_{1}}\right)^{***}\right] \lambda + \frac{1}{6} \left[10 - \frac{1}{6} \left(\frac{u}{u_{1}}\right)^{****}\right] = 0$$
 (64)

$$\left[\frac{1}{6} + \frac{1}{240} \left(\frac{u}{u_1}\right)^{11}\right]^2 - \frac{4}{1,440} \left[10 - \frac{1}{6} \left(\frac{u}{u_1}\right)^{11}\right] \ge 0$$
 (65)

or

$$\left(\frac{\mathbf{u}}{\mathbf{u}_{1}}\right)^{\mathbf{u}_{1}^{2}} + \frac{320}{3}\left(\frac{\mathbf{u}}{\mathbf{u}_{1}}\right)^{\mathbf{u}_{1}^{2}} \ge 0 \tag{65a}$$

The minimum value is  $\left(\frac{u}{u_1}\right)^{n_1} = 0$ , and the corresponding value for  $\lambda$  is 20.

When the energy equation was considered, the following equalities were employed at the leading edge:

(a) For the characteristic slopes (see eqs. (51) and (52a)):

$$\left(\frac{\delta t}{\delta \xi}\right)_{+} = \left(\frac{\delta t}{\delta \xi}\right)_{-} = -\frac{t}{\xi}$$
(66)

(b) For the characteristic derivatives:

$$\left(\frac{\delta}{\delta\xi}\right)_{+} = \frac{\partial}{\partial\xi} + \left(\frac{\delta t}{\delta\xi}\right)_{+} \frac{\partial}{\partial t} = \frac{\partial}{\partial\xi} + \left(\frac{\delta t}{\delta\xi}\right)_{-} \frac{\partial}{\partial t} = \left(\frac{\delta}{\delta\xi}\right)_{-}$$
(67a)

(c) For the Z-derivatives:

$$\left(\frac{\delta Z}{\delta \xi}\right)_{\pm} = \frac{\partial Z}{\partial \xi} \tag{67b}$$

since  $\left(\frac{\partial z}{\partial t}\right)_{\xi=-1}$  is zero.

Since

$$W = \frac{Z}{\left(\frac{\theta}{\Delta}\right)^2} \left(\sqrt[d]{\frac{1}{\nabla}} \frac{1}{b}\right)^2$$

(eq. (37a)) and Z=0, it is necessary for W=0 to keep b finite. The assumption of a finite b is a physically plausible restriction since it implies a finite ratio of the thermal thickness to the velocity thickness in the physical plane. The dominant terms in the energy equation at  $\xi=-1$  are:

$$-\frac{g_{\frac{1}{4}h}}{g_{2h}} \xi \left(\frac{\delta W}{\delta \xi}\right)_{+} - \frac{2g_{5h}}{g_{1}} \frac{W}{Z} \xi \left(\frac{\partial Z}{\partial \xi}\right)_{t} + 2W \left(-\frac{\xi}{h_{1}*} \frac{dh_{1}}{d\xi} - \frac{1}{g_{1}} \frac{d \log_{e} E_{0}}{d \log_{e} \xi} \left\{\frac{\partial \log_{e} \frac{\nabla^{*}}{\phi}}{\partial \log_{e} \lambda} + \frac{1}{g_{2h}} \frac{\partial \log_{e} \frac{\nabla^{*}}{\phi}}{\partial \log_{e} \lambda}\right\} + 2\frac{d \log_{e} \frac{\phi}{\Delta}}{d \log_{e} \lambda} - 2\frac{\partial \log_{e} \frac{\phi}{\Delta}}{\partial \log_{e} \lambda} + 2\frac{\partial \log_{e} \frac{\phi}{\Delta}}{\partial \log_{e} \lambda} +$$

$$\frac{1}{g_{2h}} \frac{\partial \log_{e} \frac{\nabla^{*}}{\emptyset}}{\partial \log_{e} b} \left( \frac{\lambda}{\Gamma b^{2}} g_{3h} \frac{\partial \log_{e} \frac{\emptyset}{\nabla}}{\partial \log_{e} \Gamma} - \frac{d \log_{e} \frac{\theta}{\Delta}}{d \log_{e} \lambda} + \frac{\partial \log_{e} \frac{\emptyset}{\nabla}}{\partial \log_{e} \lambda} \right) = 2 \left( \frac{\emptyset}{\nabla} \right)^{2} \frac{\nabla}{\nabla^{*}} \frac{B_{1}}{N_{Pr}} \tag{68}$$

Substitution of the values already known at  $\xi = -1$  and employment of L'Hospital's rule yields

$$\lim_{\xi \to -1} \left( \frac{\delta W}{\delta \xi} \right)_{+} = \frac{2}{3} \left( \frac{\phi}{\nabla} \right)^{2} \frac{\nabla}{\nabla^{*}} \frac{B_{1}}{N_{Pr}}$$
(69)

But

$$\lim_{\xi \to -1} \left( \frac{\emptyset}{\nabla} \right)^2 = \lim_{\xi \to -1} b^2 \left( \frac{\theta}{\Delta} \right)^2 \frac{W}{Z} = b^2 \left( \frac{\theta}{\Delta} \right)^2 \frac{\left( \frac{\delta W}{\delta \xi} \right)_+}{\left( \frac{\delta Z}{\delta \xi} \right)_-}$$
(70)

since 
$$\left(\frac{\delta}{\delta \xi}\right)_{+} = \left(\frac{\delta}{\delta \xi}\right)_{-}$$
 at  $\xi = -1$ , and

and

$$\lim_{\xi \to -1} \left( \frac{\delta Z}{\delta \xi} \right)_{-} = \lambda \left( \frac{\theta}{\Delta} \right)^{2} = \frac{2}{3} A_{1} \left( \frac{\theta}{\Delta} \right)^{2} \frac{\Delta}{\delta *}$$

Furthermore, in the limit  $\xi \rightarrow -1$ , equation (28) reduces to

$$\Gamma = -\frac{\lambda}{2} \frac{N_{Pr}}{b^2} = \frac{A_2 N_{Pr}}{b^2} \tag{71}$$

37

Combination of the preceding four equations gives

$$B_{\perp} \frac{\nabla}{\nabla *} = -3\Gamma \tag{72}$$

This equation is identical in form to equation (61),

$$A_1 \frac{\Delta}{8*} = \frac{3}{2} \lambda = -3A_2$$

since the relations between  $\frac{\nabla}{\nabla^*}$  and  $\frac{\triangle}{\delta^*}$  are identical when  $\Gamma$  is replaced by A2.

Therefore, the initial solutions for the energy equation are identical to those for the momentum equation when  $A_2$  is replaced by  $\Gamma$ ; that is, For five-term series:

$$\lambda = -2A_2 = 12.3$$

$$\Gamma = B_2 = -6.1$$
(73)

For six-term series:

$$\lambda = 20$$

$$\Gamma = -10$$
(74)

From equation (71) it is evident that the initial value of b is equal to the square root of the Prandtl number for all cases.

A like treatment of the total enthalpy method would result in initial values of  $\Omega=\Gamma$  and b=c. This result is expected because, at  $\xi=-1$ ,  $M_1=0$ ; thus,

$$\lim_{\xi \to -1} H_1^* = \lim_{\xi \to -1} h_1^*$$

Solution inside the expansion wave. It has been proven that Z, W,  $\lambda$ ,  $\Gamma$ , and b are constant at  $\xi$  = -1 for all values of t; that is,

$$\left(\frac{\partial Z}{\partial t}\right)_{\xi=-1} = 0$$
 and  $\left(\frac{\partial W}{\partial t}\right)_{\xi=-1} = 0$ . A solution having these same properties

of invariance with t at constant  $\xi$  will be employed for the flow away from the leading edge. Justification for this assumption is based on the similarity found in the complete Prandtl boundary-layer equations derived in appendix E. (See also ref. 15.) In the following paragraphs, it will be shown that, since the outer inviscid flow is a function only of  $\xi$ , then the boundary-layer profile form factors  $\lambda$ ,  $\Gamma$ , and b, as well as the primary dependent variables, Z and W, are functions only of the conical parameter  $\xi$ .

First, consider any unsteady two-dimensional compressible flow over a flat surface such that the outer potential flow is conical in the sense that it is a function only of the conical coordinate  $\xi=\frac{x}{a_{\varepsilon}t}$ . If a

dimensionless parameter 
$$\eta$$
 is defined as  $\eta = \frac{\displaystyle \int_0^{\mathbf{y}} \frac{\rho}{\rho_\varepsilon} \, \mathrm{d} y}{\sqrt{\nu_\varepsilon t}}$  and the Prandtl

boundary-layer equations are transformed from the x,y,t system to the  $\xi,\eta,t$  system, the following results are obtained. (This transformation is carried out in appendix E.) Both the boundary-layer differential equations (eqs. (Ell) and (El2)) and the boundary conditions (eq. (El3)) become explicitly independent of the time t provided that the wall temperature is a function of  $\xi$  only. Consequently, the solutions to the differential equations must also be independent of t in the  $\xi,\eta,t$  system; the parameters  $\xi$  and  $\eta$  are similarity parameters; and the solutions may be classed as similar. The velocity and static enthalpy profiles are then functions of only  $\xi$  and  $\eta$ :

$$\frac{u(\xi,\eta,t)}{a_{\epsilon}} = \frac{1}{a_{\epsilon}} \left( \frac{\partial \Psi}{\partial Y} \right)_{x,t} = \frac{\partial f(\xi,\eta)}{\partial \eta} = \frac{u(\xi,\eta)}{a_{\epsilon}}$$
 (75)

$$\frac{h}{h_{\epsilon}}(\xi,\eta,t) = g(\xi,\eta) = \frac{h(\xi,\eta)}{h_{\epsilon}}$$
 (76)

A combination of these two equations shows the stagnation enthalpy profile to be also of the same type; that is,

$$\frac{H(\xi,\eta,t)}{H_{\epsilon}} = \frac{h + \frac{u^2}{2}}{H_{\epsilon}} = \frac{H(\xi,\eta)}{H_{\epsilon}}$$
 (77)

Consider the velocity profile of the integral method (eq. 8) which may be written in the functional form:

$$\frac{u(\xi,\eta)}{u_1(\xi)} = \sum_{n=0}^{n} A_n(\lambda) \alpha^n$$
 (78)

The  $\alpha$  variable is eliminated from equation (78) by expressing  $\alpha$  as a function of  $\eta$  and  $\Delta$ . (The required expression is an immediate consequence of the definitions of  $\alpha$  and  $\eta$ .) Equation (78) then reduces to

$$\frac{u(\xi,\eta)}{u_1(\xi)} = \sum_{n=0}^{n} A_n(\lambda) \left(\frac{\nu_{\epsilon}t}{\Delta^2}\right)^{n/2} \eta^n$$
 (78a)

Equation (36a) is of the functional form:

$$\lambda = E_0(\xi) \frac{\Delta^2}{\nu_e t} \tag{79}$$

Substitution of equation (79) into the velocity-profile equation (78a) yields

$$\frac{u(\xi,\eta)}{u_{\perp}(\xi)} = \sum_{n=0}^{n} A_{n}(\lambda) \left[ \frac{E_{0}(\xi)}{\lambda} \right]^{n/2} \eta^{n}$$
(80)

According to equation (80), the velocity profiles of the integral method are functions of  $\xi$ ,  $\eta$ , and  $\lambda$ , whereas equation (75) shows the exact profile to be a function of only  $\xi$  and  $\eta$ . Consequently, in order to make the integral-method differential equations compatible with the exact differential equations, the boundary-layer profiles applicable to both sets of equations must exhibit the same similarity in respect to  $\xi$  and  $\eta$ . Thus, it is necessary that

$$\lambda = \lambda(\xi, \eta)$$

Finally, since  $\lambda$  is the velocity form factor at an arbitrary value of x and t (or  $\xi$  and t) and is independent of y, it is then necessary that  $\lambda \neq \lambda(\eta)$ . Consequently, the following conclusion is reached:

$$\lambda(\xi,\eta) = \lambda(\xi)$$

and

$$\lambda(\xi) = E_{O}(\xi) \left[ \frac{\theta}{\Delta}(\lambda) \right]^{2} \left( \frac{\theta^{2}}{\nu_{\epsilon}^{t}} \right) = E_{O}(\xi) \left[ \frac{\theta}{\Delta}(\lambda) \right]^{2} Z$$
 (81)

Since all the terms of equation (81) except the last one are known to be functions of  $\xi$  alone, it follows that the last term must also be a function of  $\xi$  only; that is,

$$\frac{\theta^{2}}{\nu_{\epsilon}t} = Z = Z(\xi)$$

$$\left(\frac{\partial Z}{\partial t}\right)_{\xi} = 0$$

$$\left(\frac{\partial Z}{\partial \xi}\right)_{t} = \frac{dZ}{d\xi} = \left(\frac{\delta Z}{\delta \xi}\right)_{\pm}$$
(82)

In an analogous manner it may be shown that  $W=W(\xi)$ ,  $\Gamma=\Gamma(\xi)$ , and  $b=b(\xi)$  for the integral-method differential equation to exhibit

the same type of similarity as the complete differential equation. Consequently, the solution employing  $\left(\frac{\partial Z}{\partial t}\right)_{\xi} = \left(\frac{\partial W}{\partial t}\right)_{\xi} = \left(\frac{\partial \lambda}{\partial t}\right)_{\xi} = \left(\frac{\partial \Gamma}{\partial \tau}\right)_{\xi} = \left(\frac{\partial \Gamma}{\partial t}\right)_{\xi} = \left(\frac{\partial \Gamma}{\partial t}\right)_{\xi} = \left(\frac{\partial \Gamma}{\partial \tau}\right)_{\xi} = \left(\frac{\partial \Gamma}{\partial t}\right)_{\xi} = \left(\frac{$ 

 $\left(\frac{\partial b}{\partial t}\right)_{\xi} = 0$  is justified for the conical expansion-fan flow region. Simi-

larly, it may be shown that the stagnation enthalpy variables  $\,\mathbb{Q},\,$   $\,\Omega,\,$  and  $\,$  are functions only of the conical coordinate  $\,\xi\,.$ 

Whether to employ five- or six-term power-series profiles and whether to use static or stagnation enthalpy methods was next determined. The reasoning leading to the conclusion to use the six-term profiles with the static enthalpy as a variable was as follows: Use of a five-term

profile necessitates the specification of  $\left(\frac{u}{u_1}\right)_{\alpha=1}^{"}$  and  $\left(\frac{h^*}{h_1^*}\right)_{\beta=1}^{"}$  as

negative at the edge of the boundary layer in order to satisfy the initial conditions. Any profiles resulting therefrom, regardless of the variation of the outer flow, must be limited unduly by the restriction:

$$\lim_{\alpha \to 1} \frac{u}{u_1} < 1.0$$

$$\lim_{\beta \to 1} \frac{h^*}{h_1^*} < 1.0$$

Consequently, the five-term profiles were eliminated for use inside the expansion wave. Numerical integration of any differential equation is difficult when the integrand becomes improper. In the integral method, nondimensionalization was accomplished through division by  $u_1$ ,  $h_1^*$ , or  $H_1^*$ . Consequently, when these quantities become zero, the integrand becomes improper. In the expansion fan, these singular points occur at the following locations:

At  $\xi = -1$ 

At  $\xi = -1$ 

$$h_1 * = 0$$

and at  $\xi = \pm 1$ 

$$H_1* = 0$$

The singularities at  $\xi = -1$  may be easily handled analytically. (See previous section.) However, the singularity in  $H_1*$  at  $\xi = 1$  would occur in the middle of a numerical or graphical procedure and would present a possible source of difficulty. For this reason, the static enthalpy system was chosen for the solution in spite of the fact that the stagnation enthalpy method has been more generally used in steady flow.

Although a graphical-isocline technique could have been employed, the following numerical method appeared to be more advantageous in regard to both time and accuracy. First, two additional variables  $\frac{\delta Z}{\delta \xi}$  and  $\frac{\delta W}{\delta \xi}$ 

were introduced and the required two auxiliary equations were obtained by assuming a Taylor expansion for Z or W in the neighborhood of the point  $\xi_n$ ; that is,

$$Z_{n\pm 1} = Z_n \pm X Z_n' + \frac{X^2}{2} Z_n'' \pm \frac{X^3}{6} Z_n''' + \frac{X^{1}}{2^{1}} Z_n^{iv} \pm \frac{X^5}{120} Z_n^{v} + \dots$$
 (83)

where the plus and minus signs indicate values ahead of or behind the nth point, X is the interval between adjacent points, and the superscripts on the Z terms express total derivatives with respect to  $\xi$ .

Differentiating equation (83) with respect to § yields

$$Z_{n\pm 1}^{\prime} = Z_{n}^{\prime} \pm XZ_{n}^{\prime\prime} + \frac{X^{2}}{2} Z_{n}^{\prime\prime\prime} \pm \frac{X^{3}}{6} Z_{n}^{iv} + \frac{X^{l_{1}}}{2^{l_{1}}} Z_{n}^{v} \pm \frac{X^{5}}{120} Z_{n}^{vi} + \dots$$
 (84)

Multiplication of equation (84) (positive signs) by  $\frac{X}{2}$  and subtracting the result from equation (83) (positive signs) give an equation applicable to the starting problem (that is, when the values are known only at one previous point):

$$Z_{n+1}^{\prime} = \frac{2}{x} (Z_{n+1} - Z_n) - Z_n^{\prime} + \frac{x^2}{6} Z_n^{\prime\prime\prime} + \dots$$
 (85)

Subtraction of equation (83) (alternating signs) from equation (83) (positive signs) and addition of equation (84) (positive signs) to equation (84) (alternating signs) yield

$$Z_{n+1} - Z_{n-1} = 2XZ_n' + \frac{1}{3}X^3Z_n''' + \frac{1}{60}X^5Z_n'' + \dots$$
 (86)

$$Z_{n+1}^{\prime} + Z_{n-1}^{\prime} = 2Z_{n}^{\prime} + \chi^{2}Z_{n}^{\prime\prime\prime} + \frac{1}{12}\chi^{4}Z_{n}^{iv} + \dots$$
 (87)

The term  $Z_n^{""}$  may be eliminated from equations (86) and (87) to yield

$$Z_{n+1}^{\prime} = \frac{3}{x} \left( Z_{n+1} - Z_{n-1} \right) - \left( 4 Z_{n}^{\prime} + Z_{n-1}^{\prime} \right) + \frac{1}{30} x^{4} Z_{n}^{\prime} + \dots$$
 (88)

which is applicable when the values are known at two previous points.

Equation (88) is a form of Milne's equation (ref. 19) but has been derived in a different manner to show its natural compatibility with and extension to equation (85). Equation (85) (and its W counterpart), the third derivative being neglected, was employed to evaluate the first point away from the leading edge of the fan and thereafter equation (88), the fifth derivative being neglected, was used.

The best sequence of computational steps found for obtaining the solution at the  $\,n+1\,$  point from the nth point was determined to be:

- (1) Estimate  $\lambda_{n+1} = \lambda_n + x \lambda_n'$ ;  $\lambda_n'$  obtained from equation (38a)
- (2) Solve equation (27) for  $Z_{n+1}$

- (3) Solve equation (85) or (88) for  $Z_{n+1}^{\prime} = \left(\frac{\delta Z}{\delta \xi}\right)_{n+1}$
- (4) Solve equation (45) for  $b_{n+1}$  by trial and error until the value of  $\left(\frac{\delta Z}{\delta \xi}\right)_{n+1}$  obtained equals that obtained in step 3
- (5) Compute  $W_{n+1}$  from equation (37a)
- (6) Solve equation corresponding to equation (85) or (88) for  $W_{n+1}^{!} = \left(\frac{\delta W}{\delta \xi}\right)_{n+1}$
- (7) Solve equation (46) for  $W_{n+1}^{!} = \left(\frac{\delta W}{\delta \xi}\right)_{n+1}$
- (8) Compare values of  $\left(\frac{\delta W}{\delta \xi}\right)_{n+1}$  from steps 6 and 7 and repeat procedure with new value of  $\lambda_{n+1}$  until the two values of  $\left(\frac{\delta W}{\delta \xi}\right)_{n+1}$  are in agreement.

Values of the interval X were selected as follows:

$$x = 0.02$$
  $(-1 \le \xi \le -0.90)$   
 $x = 0.04$   $(-0.88 \le \xi \le -0.80)$   
 $x = 0.10$   $(-0.70 \le \xi \le 1.00)$ 

The smaller values of X were used near  $\xi=-1$  because of the strong curvature of the functions  $\lambda$ , b, and  $\Gamma$  when plotted against  $\xi$ . These functions all had infinite slopes at  $\xi=-1$  (it may be shown that  $\frac{d\lambda}{d\xi} \propto (1+\xi)^{-1/2}$  in the region where  $\xi$  approaches -1.0) whereas Z and W had finite slopes with small second derivatives.

# Methods for Regions of Constant

## Outer Inviscid Flow

Simplification of the reduced hyperbolic differential equations for special case of constant outer flow. The general reduced hyperbolic differential equations of motion and energy in the conical \$,t coordinate system are greatly simplified for regions of constant free-stream velocity, pressure, density, viscosity, and so forth.

Equations (36a), (36b), (37a), (45), and (46) represent the final form of the most general set of equations in  $\xi$ , to coordinates in terms of local enthalpy; corresponding stagnation enthalpy equations are (36a), (36c), (37b), (47), and (48). For the special case of constant outer flow these equations may be written in the following form:

For local enthalpy:

$$\lambda = 0 \tag{89a}$$

$$\Gamma = -\frac{N_{Pr}}{b^2} \frac{h_1}{h_1^*} \frac{\gamma - 1}{2} M_1^2 A_1^2$$
 (89b)

$$\frac{Z}{W} = \frac{\left(\frac{\Theta}{\Delta}\right)^2}{\left(\frac{\phi}{\nabla}\right)^2} b^2 \tag{90}$$

$$\left(\underline{u}_{1} \frac{\theta}{\delta^{*}} - \xi\right) \left(\frac{\partial Z}{\partial \xi}\right)_{t} + t \left(\frac{\partial Z}{\partial t}\right)_{\xi} + Z = 2 \frac{\nu_{W}}{\nu_{\varepsilon}} \left(\frac{\rho_{W}}{\rho_{\varepsilon}}\right)^{2} A_{1} \frac{\theta}{\delta^{*}} \frac{\theta}{\Delta}$$
(91)

$$\left( \underbrace{\mathbf{u}_{1}}_{\mathbf{Z}} \frac{\mathbf{w}}{\mathbf{w}} - \underbrace{\mathbf{g}_{1h}}_{\mathbf{g}_{2h}} \mathbf{\xi} \right) \left( \underbrace{\frac{\partial \mathbf{w}}{\partial \mathbf{\xi}}}_{\mathbf{t}} + \underbrace{\mathbf{g}_{1h}}_{\mathbf{g}_{2h}} \mathbf{t} \left( \underbrace{\frac{\partial \mathbf{w}}{\partial \mathbf{t}}}_{\mathbf{t}} \right)_{\mathbf{\xi}} - \left( \mathbf{1} - \underbrace{\mathbf{g}_{1h}}_{\mathbf{g}_{2h}} \right) \underbrace{\mathbf{w}}_{\mathbf{z}} \left[ \mathbf{\xi} \left( \underbrace{\frac{\partial \mathbf{z}}{\partial \mathbf{\xi}}}_{\mathbf{t}} \right)_{\mathbf{t}} - \mathbf{t} \left( \underbrace{\frac{\partial \mathbf{z}}{\partial \mathbf{t}}}_{\mathbf{\xi}} \right)_{\mathbf{\xi}} \right] + \mathbf{w}$$

$$= 2 \frac{\nu_{\rm w}}{\nu_{\rm c}} \left( \frac{\rho_{\rm w}}{\rho_{\rm c}} \right)^2 \frac{\phi}{\nabla} \frac{\phi}{\nabla^*} \left[ \frac{B_{\rm l}}{N_{\rm Pr}} - \frac{\gamma - 1}{b} \underline{u}_{\rm l}^2 \frac{h_{\rm c}}{h_{\rm l}^*} \int_0^1 \left( \frac{d \underline{u}}{u_{\rm l}} \right)^2 d\alpha \right]$$
(92)

For stagnation enthalpy:

$$\lambda = 0 \tag{93a}$$

$$\Omega = \frac{1}{c^2} \frac{\mathbf{u_l}^2}{2\mathbf{H_l}^*} \left( 1 - \mathbf{N_{Pr}} \right) \mathbf{A_l}^2 \tag{93b}$$

$$\frac{Z}{Q} = \frac{\left(\frac{\Theta}{\Delta}\right)^2}{\left(\frac{\Psi}{\Box}\right)^2} c^2 \tag{94}$$

$$\left(\underline{u}_{1} \frac{\theta}{\delta^{*}} - \xi\right) \left(\frac{\partial Z}{\partial \xi}\right)_{t} + t \left(\frac{\partial Z}{\partial t}\right)_{\xi} + Z = 2 \frac{\nu_{W}}{\nu_{\epsilon}} \left(\frac{\rho_{W}}{\rho_{\epsilon}}\right)^{2} A_{1} \frac{\theta}{\Delta} \frac{\theta}{\delta^{*}}$$
(95)

$$\left(\underline{u}_{\text{l}} \xrightarrow{\underline{\psi}} - \frac{g_{\text{l}_{\text{H}}}}{g_{\text{2H}}} \, \xi\right) \left(\frac{\partial \underline{Q}}{\partial \xi}\right)_{\text{t}} \, + \, \frac{g_{\text{l}_{\text{H}}}}{g_{\text{2H}}} \, t \left(\frac{\partial \underline{Q}}{\partial t}\right)_{\xi} \, - \, \left(1 \, - \, \frac{g_{\text{l}_{\text{H}}}}{g_{\text{2H}}}\right) \underline{\underline{Q}} \left[\xi \left(\frac{\partial \underline{Z}}{\partial \xi}\right)_{\text{t}} \, - \, t \left(\frac{\partial \underline{Z}}{\partial t}\right)_{\xi}\right] \, + \, \underline{Q} \, \left(1 \, - \, \frac{g_{\text{l}_{\text{H}}}}{g_{\text{2H}}}\right) \underline{\underline{Q}} \left[\xi \left(\frac{\partial \underline{Z}}{\partial \xi}\right)_{\text{t}} \, - \, t \left(\frac{\partial \underline{Z}}{\partial t}\right)_{\xi}\right] \, + \, \underline{Q} \, \left(1 \, - \, \frac{g_{\text{l}_{\text{H}}}}{g_{\text{2H}}}\right) \underline{\underline{Q}} \left[\xi \left(\frac{\partial \underline{Z}}{\partial \xi}\right)_{\text{t}} \, - \, t \left(\frac{\partial \underline{Z}}{\partial t}\right)_{\xi}\right] \, + \, \underline{Q} \, \left(1 \, - \, \frac{g_{\text{l}_{\text{H}}}}{g_{\text{2H}}}\right) \underline{\underline{Q}} \left[\xi \left(\frac{\partial \underline{Z}}{\partial \xi}\right)_{\text{t}} \, - \, t \left(\frac{\partial \underline{Z}}{\partial t}\right)_{\xi}\right] \, + \, \underline{Q} \, \left(1 \, - \, \frac{g_{\text{l}_{\text{H}}}}{g_{\text{2H}}}\right) \underline{\underline{Q}} \left[\xi \left(\frac{\partial \underline{Z}}{\partial \xi}\right)_{\text{t}} \, - \, t \left(\frac{\partial \underline{Z}}{\partial t}\right)_{\xi}\right] \, + \, \underline{Q} \, \left(1 \, - \, \frac{g_{\text{l}_{\text{H}}}}{g_{\text{2H}}}\right) \underline{\underline{Q}} \left[\xi \left(\frac{\partial \underline{Z}}{\partial \xi}\right)_{\text{t}} \, - \, t \left(\frac{\partial \underline{Z}}{\partial t}\right)_{\xi}\right] \, + \, \underline{Q} \, \left(1 \, - \, \frac{g_{\text{l}_{\text{H}}}}{g_{\text{2H}}}\right) \underline{\underline{Q}} \left[\xi \left(\frac{\partial \underline{Z}}{\partial \xi}\right)_{\text{t}} \, - \, t \left(\frac{\partial \underline{Z}}{\partial t}\right)_{\xi}\right] \, + \, \underline{Q} \, \underline{Q} \, + \, \underline{Q} \, + \, \underline{Q} \, \underline{Q} \, + \, \underline{$$

$$= 2 \frac{\nu_{W}}{\nu_{\epsilon}} \left( \frac{\rho_{W}}{\rho_{\epsilon}} \right)^{2} \frac{C_{1}}{N_{Pr}} \frac{\psi}{\Box} \frac{\psi}{\Box^{*}}$$
(96)

The following additional relations stem from the requirement that all free-stream quantities are constant and have been incorporated in the preceding equations:

$$g_{1} = 1$$

$$g_{5h} = \frac{1}{2} \left( 1 - \frac{g_{4h}}{g_{2h}} \right)$$

$$g_{5H} = \frac{1}{2} \left( 1 - \frac{g_{4H}}{g_{2H}} \right)$$

$$g_{6h} = g_{6H} = 0$$
(97)

The momentum differential equations (91) and (95) in both systems are identical and are independent of the corresponding energy differential equations for the case of constant outer flow. In subsequent derivations for this case, the equations in terms of local and stagnation enthalpy will be carried simultaneously.

The slopes of the characteristic curves are:

For equations (91) and (95):

$$\left(\frac{\delta t}{\delta \xi}\right)_{-} = \frac{t}{\underline{u}_{1}} \frac{\theta}{\delta *} - \xi \tag{98}$$

For equation (92):

$$\left(\frac{\delta t}{\delta \xi}\right)_{+} = \frac{t}{\underline{u}_{1} \sqrt{\star} \frac{g_{2h}}{g_{hh}} - \xi} \tag{99}$$

For equation (96):

$$\left(\frac{\delta t}{\delta \xi}\right)_{+} = \frac{t}{\underbrace{u_{1}} \frac{\psi}{\Box *} \frac{g_{2H}}{g_{\mu_{H}}} - \xi}$$
(100)

If the characteristic derivative notation of equation (57) is used, the differential equation (91) or (95) may be rewritten to yield

$$\left(\frac{\delta Z}{\delta \xi}\right)_{-} + \frac{Z}{\underline{u}_{1}} \frac{\theta}{\delta^{*}} - \xi = \frac{2 \frac{\nu_{W}}{\nu_{\varepsilon}} \left(\frac{\rho_{W}}{\rho_{\varepsilon}}\right)^{2} A_{1} \frac{\theta}{\Delta} \frac{\theta}{\delta^{*}}}{\underline{u}_{1} \frac{\theta}{\delta^{*}} - \xi} \tag{101}$$

Since  $\lambda$ ,  $\frac{\theta}{\Delta}$ , and  $\frac{\theta}{\delta^*}$  as well as the free-stream flow quantities are all constant, this equation may be integrated in closed form along a line of slope  $\left(\frac{\delta t}{\delta \xi}\right)$ . After the general boundary condition that  $Z=Z_0$ 

at  $\xi = \xi_0$  is applied, the result is

$$Z - Z_{O} = 2 \frac{\nu_{W}}{\nu_{\epsilon}} \left( \frac{\rho_{W}}{\rho_{\epsilon}} \right)^{2} A_{\perp} \frac{\theta}{\Delta} \frac{\theta}{\delta^{*}} \frac{\xi - \xi_{O}}{\underline{u}_{\perp} \frac{\theta}{\delta^{*}} - \xi_{O}} + Z_{O} \frac{\xi_{O} - \xi}{\underline{u}_{\perp} \frac{\theta}{\delta^{*}} - \xi_{O}}$$
(102)

As yet, no restrictions have been made regarding the dependence of Z upon t. Thus, in theory,  $Z_{0}$  may be a function of t, and the energy equations may be developed accordingly. However, since the constant-outer-flow case is only a special case of the general conical-flow case discussed previously, the same arguments may be applied to show that Z, W, Q,  $\lambda$ ,  $\Gamma$ ,  $\Omega$ , b, and c are functions only of  $\xi$ . This restriction immediately limits  $Z_{0}$ ,  $W_{0}$ , and  $Q_{0}$  to constant values.

It should be noted that, although the time dependency has been eliminated in direct form from the equations of motion and energy, it is still present implicitly in Z, W, and Q. These equations still possess characteristics and integration must proceed along the characteristic lines given by equations (98) to (100).

In line with these arguments, equation (102) is differentiated directly; this differentiation yields

$$\frac{dZ}{d\xi} = \left(\frac{\delta Z}{\delta \xi}\right)_{\underline{t}} = \frac{2 \frac{\nu_{W}}{\nu_{\varepsilon}} \left(\frac{\rho_{W}}{\rho_{\varepsilon}}\right)^{2} A_{\underline{1}} \frac{\theta}{\Delta} \frac{\theta}{\delta^{*}} - Z_{\underline{0}}}{\underline{u}_{\underline{1}} \frac{\theta}{\delta^{*}} - \xi_{\underline{0}}} = Constant$$
 (103)

After equations (89b), (90), (102), and (103) are substituted into equation (92) and the terms are transposed, the following differential equation for local enthalpy results:

$$\left(\frac{\delta W}{\delta \xi}\right)_{+} = \frac{W}{Z} \frac{2 \frac{v_{w}(\rho_{w})^{2}}{v_{\varepsilon}(\rho_{\varepsilon})^{2}} A_{1} \frac{\theta}{\Delta} \frac{\theta}{\delta *} - Z_{0}}{u_{1} \frac{\theta}{\delta *} - \xi_{0}} - \frac{1}{\underline{u}_{1} \frac{\phi}{\nabla *} - \frac{g_{l_{1}h}}{g_{2h}} \xi} \left\{ \frac{W}{Z} \underline{u}_{1} \frac{\phi}{\nabla *} \frac{2 \frac{v_{w}(\rho_{w})^{2}}{v_{\varepsilon}(\rho_{\varepsilon})^{2}} A_{1} \frac{\theta}{\Delta} \frac{\theta}{\delta *} - Z_{0}}{\underline{u}_{1} \frac{\theta}{\delta *} - \xi_{0}} + \frac{W}{Z} \frac{\underline{u}_{1} \frac{\theta}{\delta *}}{\underline{u}_{1} \frac{\theta}{\delta *} - \xi_{0}} \right\} Z_{0} - 2 \frac{v_{w}(\rho_{w})^{2}}{v_{\varepsilon}(\rho_{\varepsilon})^{2}} A_{1} \frac{\theta}{\Delta} \frac{\xi_{0}}{\underline{u}_{1}} - \frac{\xi_{0}}{\delta *} - \frac{\xi_{0}}{\delta *}$$

Similar manipulations lead to the equation in terms of stagnation enthalpy from equation (96):

$$\left( \frac{\delta Q}{\delta \xi} \right)_{+} = \frac{Q}{Z} \frac{2 \frac{v_{w} \left( \rho_{w} \right)^{2}}{v_{e} \left( \rho_{e} \right)^{2}} A_{1} \frac{\theta}{\Delta} \frac{\theta}{\delta \pi} - Z_{0}}{\underline{u}_{1} \frac{\theta}{\delta \pi} - \xi_{0}} - \frac{1}{\underline{u}_{1} \frac{\psi}{\Box^{*}} - \frac{g_{hH}}{g_{2H}} \xi} \left\{ \frac{Q}{Z} \underline{u}_{1} \frac{\psi}{\Box^{*}} \frac{2 \frac{v_{w} \left( \rho_{w} \right)^{2}}{v_{e} \left( \rho_{e} \right)^{2}} A_{1} \frac{\theta}{\Delta} \frac{\theta}{\delta \pi} - Z_{0}}{\underline{u}_{1} \frac{\theta}{\delta \pi} - \xi_{0}} + \frac{Q}{Z} \frac{\underline{u}_{1} \frac{\theta}{\delta \pi}}{\underline{u}_{1} \frac{\theta}{\delta \pi} - \xi_{0}} \left[ Z_{0} - 2 \frac{v_{w} \left( \rho_{w} \right)^{2}}{v_{e} \left( \rho_{e} \right)^{2}} A_{1} \frac{\theta}{\Delta} \frac{\xi_{0}}{\underline{u}_{1}} - 2 \frac{v_{w} \left( \rho_{w} \right)^{2}}{v_{e} \left( \rho_{e} \right)^{2}} \frac{v_{w} \psi}{\underline{v}_{e} \left( \rho_{e} \right)^{2}}{\underline{u}_{1} \frac{\theta}{\delta \pi} - \xi_{0}} \right]$$

$$(105)$$

Equations (104) and (105) represent the alternate forms of the energy equations and, in general, must be solved by either a graphical-isocline or a numerical step-by-step procedure in conjunction with equations (102) and either (89b) and (90) or (93b) and (94).

Analytic solution for flows generated by waves of zero thickness .-The boundary layer behind zero-thickness waves advancing into a fluid at rest permits the introduction of the relations  $Z_0 = W_0 = Q_0 = 0$  at the wave location ( $\xi_0 = \xi_s$ ) in the preceding set of equations. The familiar shock wave of the shock-tube flow is such a wave. Another is the mathematical model of a "negative shock" which is defined as an isentropic expansion wave having finite pressure ratio and zero thickness, traveling with the speed of sound of the undisturbed fluid, and generating a flow behind it otherwise identical to that generated by an expansion wave of finite thickness and identical isentropic pressure ratio. Hereafter in this report, the unqualified use of the word "shock" or "shock wave" in reference to a potential-flow discontinuity will designate a shock wave satisfying the Rankine-Hugoniot equations. Solutions to the complete Prandtl boundary-layer equations for the shock may be found in references 6 and 12 and for the negative shock in reference 13. In these solutions the velocity and temperature profiles are similar everywhere in the region of flow (that is, the profiles change shape only by a stretching factor normal to the wall as time increases). The integral-solution counterpart to such a similarity throughout the field of flow is represented by the constancy of  $\lambda$ ,  $\Gamma$ ,  $\Omega$ , b, and c everywhere in the field.

The conditions  $Z_O=W_O=Q_O=0$  at  $\xi_O=\xi_S$  transform equations (102), (104), and (105) into the following equations:

$$Z = 2 \frac{\nu_{W}}{\nu_{\epsilon}} \left( \frac{\rho_{W}}{\rho_{\epsilon}} \right)^{2} A_{\perp} \frac{\theta}{\Delta} \frac{\theta}{\delta^{*}} \frac{\xi - \xi_{S}}{\underline{u}_{\perp} \frac{\theta}{\delta^{*}} - \xi_{S}}$$
 (106)

$$\left( \frac{\delta \tilde{w}}{\delta \xi} \right)_{+} = \frac{\tilde{w}}{Z} \frac{2 \frac{v_{w} \left( \rho_{w} \right)^{2}}{v_{\varepsilon} \left( \rho_{\varepsilon} \right)^{2}} A_{1} \frac{\theta}{\Delta} \frac{\theta}{\delta^{**}} - \frac{1}{u_{1}} \frac{\theta}{\nabla^{**}} - \frac{g_{hh}}{g_{2h}} \xi} \left\{ \frac{\tilde{w}}{Z} \ge \frac{v_{w} \left( \rho_{w} \right)^{2}}{v_{\varepsilon} \left( \rho_{\varepsilon} \right)^{2}} A_{1} \frac{\theta}{\delta^{**}} \frac{\theta}{u_{1}} \frac{\tilde{w}}{\nabla^{**}} \frac{\xi_{s}}{\delta^{**}} - 2 \frac{v_{w} \left( \rho_{w} \right)^{2}}{v_{\varepsilon} \left( \rho_{\varepsilon} \right)^{2}} \frac{\tilde{w}}{\nabla^{**}} \frac{B_{1}}{N_{Pr}} \left[ 1 + 2 \frac{\Gamma}{B_{1}} \frac{b}{A_{1}^{2}} \int_{0}^{1} \left( \frac{d}{u_{1}} \frac{u}{d\alpha} \right)^{2} d\alpha \right] \right\}$$

$$\left( \frac{\delta Q}{\delta \xi} \right)_{+} = \frac{Q}{Z} \frac{2 \frac{\nu_{w}}{\nu_{\varepsilon}} \left( \frac{\rho_{w}}{\rho_{\varepsilon}} \right)^{2} A_{\perp} \frac{\theta}{\Delta} \frac{\theta}{\delta *}}{\underline{\nu}_{\perp} \frac{\theta}{\Delta} *} - \frac{1}{\underline{\nu}_{\perp} \frac{\psi}{\Box *} - \frac{g_{4H}}{g_{2H}} \xi} \left[ \frac{Q}{Z} 2 \frac{\nu_{w}}{\nu_{\varepsilon}} \left( \frac{\rho_{w}}{\rho_{\varepsilon}} \right)^{2} A_{\perp} \frac{\theta}{\Delta} \frac{\theta}{\delta *} - \frac{\underline{\nu}_{\perp}}{2} \frac{\psi}{\nu_{\varepsilon}} - \frac{\nu_{w}}{\nu_{\varepsilon}} \left( \frac{\rho_{w}}{\rho_{\varepsilon}} \right)^{2} A_{\perp} \frac{\theta}{\Delta} \frac{\theta}{\delta *} - \frac{\underline{\nu}_{\perp}}{2} \frac{\psi}{\nu_{\varepsilon}} - \frac{\nu_{w}}{\nu_{\varepsilon}} \left( \frac{\rho_{w}}{\rho_{\varepsilon}} \right)^{2} \frac{\underline{\psi}}{\Box} \frac{\psi}{\Delta} \frac{C_{\perp}}{\Delta *} \right]$$

$$(108)$$

If the conditions of constancy of  $\lambda$ ,  $\Gamma$ ,  $\Omega$ , b, and c are now imposed,  $\frac{\theta}{\Delta}$ ,  $\frac{\delta^*}{\Delta}$ ,  $\frac{\phi}{\nabla}$ ,  $\frac{\nabla^*}{\nabla}$ ,  $\frac{\psi}{\Box}$ , and  $\frac{\Box^*}{\Box}$  must be constant. It must then follow from equations (90) and (94) that

$$\frac{Z}{W} = \frac{\left(\frac{\theta}{\Delta}\right)^2 b^2}{\left(\frac{\phi}{\nabla}\right)^2} = \text{Constant}$$
 (109a)

$$\frac{Z}{Q} = \frac{\left(\frac{\theta}{\Delta}\right)^2 c^2}{\left(\frac{\psi}{\Box}\right)^2} = Constant$$
 (109b)

Since Z is a linear function of  $\xi$ , the terms W and Q must also be linear functions of  $\xi$ , and their derivatives with respect to  $\xi$  are constant. Equations (107) and (108) indicate, however, that the derivatives of W and Q are functions of  $\xi$  unless the second terms on the right-hand side of the equations are identically zero. Equating these terms to zero in order to satisfy the similarity relationship produces

$$\frac{\phi}{\nabla} = \frac{\xi_{s}}{\underline{u}_{1}} \frac{\nabla *}{\nabla} + \frac{b^{2}}{A_{1}} \frac{B_{1}}{N_{Pr}} \left[ 1 + 2 \frac{\Gamma}{B_{1}} \frac{b}{A_{1}^{2}} \int_{0}^{1} \left( \frac{d}{u_{1}} \frac{\underline{u}}{u_{1}} \right)^{2} d\alpha \right] \left( \frac{\theta}{\Delta} - \frac{\xi_{s}}{\underline{u}_{1}} \frac{\delta *}{\Delta} \right)$$
(110)

$$\frac{\Psi}{\Box} = \frac{\xi_{s}}{\underline{u}_{l}} \frac{\Box^{*}}{\Box} + \frac{e^{2}}{A_{l}} \frac{C_{l}}{N_{Pr}} \left( \frac{\theta}{\Delta} - \frac{\xi_{s}}{\underline{u}_{l}} \frac{\delta^{*}}{\Delta} \right)$$
(111)

Equation (110) must be solved simultaneously with those for  $\frac{\phi}{\nabla}$ 

(eqs. (D15) and (D16)), 
$$\frac{\nabla^*}{\nabla}$$
 (eqs. (D9) and (D10)), and  $\Gamma$  (eq. (89b))

to determine the values of  $\Gamma$  and b that would be required to make W linear. (Similar relations apply for eq.(lll).) Elimination of the terms in the braces reduces equations (107) and (108) to

$$\left(\frac{\delta W}{\delta \xi}\right)_{+} = \frac{W}{Z} \frac{2 \frac{\nu_{W}}{\nu_{\varepsilon}} \left(\frac{\rho_{W}}{\rho_{\varepsilon}}\right)^{2} A_{\perp} \frac{\theta}{\Delta} \frac{\theta}{\delta^{*}}}{\underline{\nu}_{\perp} \frac{\theta}{\delta^{*}} - \xi_{s}}$$
(112)

$$\left(\frac{\delta Q}{\delta \xi}\right)_{+} = \frac{Q}{Z} \frac{2 \frac{\nu_{W}}{\nu_{\varepsilon}} \left(\frac{\rho_{W}}{\rho_{\varepsilon}}\right)^{2} A_{\perp} \frac{\theta}{\Delta} \frac{\theta}{\delta^{*}}}{\underline{u}_{\perp} \frac{\theta}{\delta^{*}} - \xi_{s}} \tag{113}$$

The terms W and Q then may be evaluated either directly from equations (109a) and (109b) or by application of the linear relation between these parameters and \$; that is,

$$W(\xi) = \left(\frac{\delta W}{\delta \xi}\right)_{+} (\xi - \xi_S)$$

$$Q(\xi) = \left(\frac{\delta Q}{\delta \xi}\right)_{+} (\xi - \xi_S)$$

Solutions to these equations may be found for any arbitrary specification of free-stream and wall conditions behind any free-stream flow discontinuity moving into a fluid at rest. The shock and negative shock are special cases of this general case in that the free-stream conditions are specified by the conservation laws.

Solutions for the Boundary-Layer Parameters Across

Discontinuities in the Force-Stream Flow

Assumption of finite discontinuities to replace mixing regions.—
In the free-stream flow generated by traveling shock or expansion waves moving into quiescent fluid, there are two general types of discontinuities which will be classified as either strong or weak. The strong discontinuity arises from a jump in any of the flow quantities such as velocity, temperature, density, or pressure. The shock itself and a contact surface (entropy discontinuity) are of this type. The weak type indicates a discontinuity in the first derivatives of a free-stream flow variable. The flows at the leading and trailing edge of any finite expansion wave exhibit this type of singularity in that the derivatives change discontinuously from a nonzero value inside the wave to a zero value outside of it.

In the following paragraphs, equations giving approximate "matching" solutions to the integrated conservation equations for the case of the weak discontinuity at the trailing edge of the expansion fan and for the case of the strong entropy discontinuity are presented. (The cases of the shock or expansion-fan leading edge are trivial.) It is to be noted that a line (zero-thickness) discontinuity is employed in both cases. Although the entropy discontinuity actually becomes a strong entropy gradient either because of laminar diffusion, in which case the width of the gradient zone grows parabolically with time (ref. 20), or because of turbulent mixing, this growth is ignored for the sake of simplicity since any growth that is nonlinear in time would eliminate the conical symmetry of the problem. The behavior of the adjusting region for the boundary layer at the trailing edge probably also would be parabolic in time, but this fact has not been proven to date. The solutions obtained under these zero-thickness assumptions would be only approximate but should give fairly good indications of the correct boundary-layer behavior in regions not immediately adjacent to the discontinuities.

Matching equations for trailing edge of expansion fan. The equations representing the conservation of mass, momentum, and energy entering and leaving the discontinuity over the range of y from zero to  $L(L \gg \delta)$  are derived in appendix F (eqs. (F8), (F9), and (F10)). The states i and j represent states on opposite sides of the discontinuity. Since in this case there is only a discontinuity in the derivative,  $u_i = u_j$ ;  $p_i = p_j$ ; and  $h_i = h_j$ ; and the equations take the form:

$$\left(1 - \frac{V^*}{u_1}\right) \frac{h_1^*}{h_1} \nabla_i^* - \delta_i^* = \left(1 - \frac{V^*}{u_1}\right) \frac{h_1^*}{h_1} \nabla_j^* - \delta_j^* \tag{114a}$$

$$\theta_{i} + \left(1 - \frac{2V^{*}}{u_{1}}\right)\delta_{i}^{*} - \left(1 - \frac{V^{*}}{u_{1}}\right)^{2} \frac{h_{1}^{*}}{h_{1}} \nabla_{i}^{*} = \theta_{j} + \left(1 - \frac{2V^{*}}{u_{1}}\right)\delta_{j}^{*} - \left(1 - \frac{2V^{*}}{u_{1}}\right)\delta_{j}^{*}$$

$$\left(1 - \frac{\mathbf{v}^*}{\mathbf{u}_1}\right)^2 \frac{\mathbf{h}_1^*}{\mathbf{h}_1} \nabla_{\mathbf{j}^*} \tag{114b}$$

$$\frac{h_{1}^{*}}{h_{1}}\frac{h_{1}}{u_{1}^{2}}\phi_{i} - \frac{3}{2}\frac{v^{*}}{u_{1}}\theta_{i} - \frac{1}{2}\left[\frac{3v^{*}}{u_{1}}\left(1 - \frac{v^{*}}{u_{1}}\right) - \frac{2h_{1}}{u_{1}^{2}}\right]\delta_{i}^{*} - \frac{h_{1}^{*}}{h_{1}}\left[\frac{h_{1}}{u_{1}^{2}} + \frac{1}{2}\left(1 - \frac{v^{*}}{u_{1}}\right)^{3}\right]\nabla_{i}^{*} + \frac{1}{2}\Delta_{i}I_{i} = \frac{h_{1}^{*}}{h_{1}}\frac{h_{1}}{u_{1}^{2}}\phi_{j} - \frac{3}{2}\frac{v^{*}}{u_{1}}\theta_{j} - \frac{3}{2}\frac{v^{*}}{$$

$$\frac{1}{2} \left[ \frac{3 \mathbf{V}^*}{\mathbf{u_1}} \left( \mathbf{1} - \frac{\mathbf{V}^*}{\mathbf{u_1}} \right) - \frac{2 \mathbf{h_1}}{\mathbf{u_1}^2} \right] \delta_j^* - \frac{\mathbf{h_1}^*}{\mathbf{h_1}} \left[ \frac{\mathbf{h_1}}{\mathbf{u_1}^2} + \frac{1}{2} \left( \mathbf{1} - \frac{\mathbf{V}^*}{\mathbf{u_1}} \right) \right] \nabla_j^* + \frac{1}{2} \Delta_j^* \mathbf{I}_j$$
(114c)

These equations may be rearranged to give

$$\frac{\theta_{i}}{\theta_{j}} = \frac{\left(\frac{\delta*}{\theta}\right)_{j} - \left(1 - \frac{V*}{u_{1}}\right)\frac{h_{1}*}{h_{1}}\left(\frac{\nabla*}{\nabla} \frac{1}{b} \frac{\Delta}{\theta}\right)_{j}}{\left(\frac{\delta*}{\theta}\right)_{i} - \left(1 - \frac{V*}{u_{1}}\right)\frac{h_{1}*}{h_{1}}\left(\frac{\nabla*}{\nabla} \frac{1}{b} \frac{\Delta}{\theta}\right)_{i}}$$
(115a)

$$\frac{\theta_{i}}{\theta_{j}} = \frac{1 + \left(1 - \frac{2V^{*}}{u_{1}}\right) \left(\frac{\delta^{*}}{\theta}\right)_{j} - \left(1 - \frac{V^{*}}{u_{1}}\right)^{2} \frac{h_{1}^{*}}{h_{1}} \left(\frac{\nabla^{*}}{\nabla} \frac{1}{b} \frac{\Delta}{\theta}\right)_{j}}{1 + \left(1 - \frac{2V^{*}}{u_{1}}\right) \left(\frac{\delta^{*}}{\theta}\right)_{i} - \left(1 - \frac{V^{*}}{u_{1}}\right)^{2} \frac{h_{1}^{*}}{h_{1}} \left(\frac{\nabla^{*}}{\nabla} \frac{1}{b} \frac{\Delta}{\theta}\right)_{i}} \tag{115b}$$

$$\frac{\theta_{\mathbf{i}}}{\theta_{\mathbf{j}}} = \frac{\frac{3}{2} \frac{\mathbf{v} *}{\mathbf{u}_{\mathbf{l}}} - \left[\frac{\mathbf{h}_{\mathbf{l}}}{\mathbf{u}_{\mathbf{l}}^{2}} - \frac{3}{2} \frac{\mathbf{v} *}{\mathbf{u}_{\mathbf{l}}} \left(\mathbf{l} - \frac{\mathbf{v} *}{\mathbf{u}_{\mathbf{l}}}\right)\right] \left(\frac{\delta *}{\theta}\right)_{\mathbf{j}} + \left\{\frac{1}{2} \left(\mathbf{l} - \frac{\mathbf{v} *}{\mathbf{u}_{\mathbf{l}}}\right)^{3} + \frac{\mathbf{h}_{\mathbf{l}}}{\mathbf{u}_{\mathbf{l}}^{2}} \left[\mathbf{l} - \left(\frac{\phi}{\nabla *}\right)_{\mathbf{j}}\right]\right\} \frac{\mathbf{h}_{\mathbf{l}} *}{\mathbf{h}_{\mathbf{l}}} \left(\frac{\nabla *}{\nabla} \frac{1}{\mathbf{b}} \frac{\Delta}{\theta}\right)_{\mathbf{j}} - \frac{1}{2} \left(\frac{\Delta}{\theta}\right)_{\mathbf{j}} \mathbf{I}_{\mathbf{j}}$$

$$\frac{3}{2} \frac{\mathbf{v} *}{\mathbf{u}_{\mathbf{l}}} - \left[\frac{\mathbf{h}_{\mathbf{l}}}{\mathbf{u}_{\mathbf{l}}^{2}} - \frac{3}{2} \frac{\mathbf{v} *}{\mathbf{u}_{\mathbf{l}}} \left(\mathbf{l} - \frac{\mathbf{v} *}{\mathbf{u}_{\mathbf{l}}}\right)\right] \left(\frac{\delta *}{\theta}\right)_{\mathbf{i}} + \left\{\frac{1}{2} \left(\mathbf{l} - \frac{\mathbf{v} *}{\mathbf{u}_{\mathbf{l}}}\right)^{3} + \frac{\mathbf{h}_{\mathbf{l}}}{\mathbf{u}_{\mathbf{l}}^{2}} \left[\mathbf{l} - \left(\frac{\phi}{\nabla *}\right)_{\mathbf{i}}\right]\right\} \frac{\mathbf{h}_{\mathbf{l}} *}{\mathbf{h}_{\mathbf{l}}} \left(\frac{\nabla *}{\nabla} \frac{1}{\mathbf{b}} \frac{\Delta}{\theta}\right)_{\mathbf{i}} - \frac{1}{2} \left(\frac{\Delta}{\theta}\right)_{\mathbf{j}} \mathbf{I}_{\mathbf{i}}$$

$$(11.5c)$$

NACA TN 3944

If i is the state inside the expansion fan, all the parameters of state i may be assumed to be known from the solution obtained by integrating from  $\xi=-1$  to that point ( $\xi_{te}<\xi_Z^*$  being assumed). The velocity of the discontinuity must coincide with the trailing edge; that is,  $V^*=(u-a)_{\underline{i}}.$  In addition, since at  $\underline{j}$  all free-stream derivatives are zero,  $\lambda_{\underline{j}}=0.$ 

Consequently, the problem becomes one of satisfying the three simultaneous equations (115) of the form  $\frac{\theta_{\dot{1}}}{\theta_{\dot{j}}} = f\left(b_{\dot{j}},\Gamma_{\dot{j}}\right)$  and equation (28) in the form  $\Gamma_{\dot{j}} = \Gamma_{\dot{j}}\left(b_{\dot{j}}\right)$ . This system is equivalent to three equations of the form  $\frac{\theta_{\dot{1}}}{\theta_{\dot{j}}} = f\left(b_{\dot{j}}\right)$ . Such a system with only the two unknowns  $\frac{\theta_{\dot{1}}}{\theta_{\dot{j}}}$  and  $b_{\dot{j}}$  is redundant and solutions would not in general be expected to exist.

In an effort to satisfy the basic equations of mass, momentum, and energy, another unknown variable  $\hat{R}$  was introduced. The assumption was made that, instead of the line discontinuity, the regions i and j would be separated by a mixing region of thickness equal to the product of time and  $\hat{R};$   $\hat{R}$  by definition is equal to the difference between the leading- and trailing-edge velocities of the mixing region. In this manner, the conical symmetry was retained and a finite mixing region was permitted. In addition, storage of mass, momentum, and energy as well as heat-transfer and wall-shear effects was permitted inside this zone. Evaluation of these influences was on the basis that the values in the zone were assumed to be equal to the average of the values at the extremities of the zone. The three simultaneous equations in the form  $\frac{\theta_{\dot{1}}}{\theta_{\dot{1}}} = f(\hat{R},b_{\dot{1}})$  were then solved. However, values of  $\hat{R}$  so obtained

located the mixing zone as extending from a point inside the expansion fan back to the trailing edge. Such a solution is not acceptable since it was assumed that  $\lambda_j=0$ . This solution may be interpreted as an indication that the physical boundary layer is influenced upstream of the trailing edge, since the propagation velocity for the disturbances is higher in the boundary layer than in the free stream. (That is,  $|-a_{\varepsilon}|>|u_1-a_1|$ .) In other words, pressure pulses would travel faster in the boundary layer; thus, it is logical to expect some type of disturbance inside the boundary layer ahead of the potential-flow trailing edge.

Finally, in order to obtain a usable approximation, the momentum and energy equations (115b) and (115c) were solved simultaneously whereas

the continuity equation (115a) was ignored except to provide a check on the magnitude of the error introduced. Such a procedure has been employed successfully for the momentum and continuity equations since Von Karmán's early work on transition, in which it was assumed that at the transition point the laminar and turbulent momentum thicknesses were equal, continuity being disregarded entirely (ref. 21). Comparison of the values of  $\frac{\theta_{\dot{1}}}{\theta_{\dot{2}}}$ , obtained by simultaneous solution for bj and  $\frac{\theta_{\dot{1}}}{\theta_{\dot{2}}}$  of equations (115b)

and (115c), with that obtained from the continuity equation (using the solution for b<sub>j</sub>) showed a maximum discrepancy under 2 percent. Thus, the neglect of the continuity equation does not appear to be significant in this case.

Matching equations for contact surface or entropy discontinuity.— The case of a strong discontinuity bounded on both sides by constant free-stream flow regions of the same fluid will be considered. The discontinuity propagates with a velocity  $V^* = u_1 = u_j$  and, in addition,  $p_i = p_j$ , and  $\lambda_i = \lambda_j = 0$ . Under these conditions, the matching equations (eqs. (F8), (F9), and (F10)) reduce to

$$\delta_{\mathbf{i}}^* = \delta_{\mathbf{j}}^* \tag{116}$$

$$\theta_{i} - \delta_{i}^{*} = \theta_{j} - \delta_{j}^{*} \tag{117}$$

$$\frac{h_{i}^{*}}{h_{i}} \frac{h_{i}}{u_{i}^{2}} \phi_{i} - \frac{3}{2} \theta_{i} + \frac{h_{i}}{u_{i}^{2}} \delta_{i}^{*} - \frac{h_{i}^{*}}{h_{i}} \frac{h_{i}}{u_{i}^{2}} \nabla_{i}^{*} + \frac{1}{2} \Delta_{i} I_{i} =$$

$$\frac{h_{j}^{*}}{h_{j}} \frac{h_{j}}{u_{j}^{2}} \phi_{j} - \frac{3}{2} \theta_{j} + \frac{h_{j}}{u_{j}^{2}} \delta_{j}^{*} - \frac{h_{j}^{*}}{h_{j}} \frac{h_{j}}{u_{j}^{2}} \nabla_{j}^{*} + \frac{1}{2} \Delta_{j} I_{j}$$
 (118)

Solution of the continuity and momentum equations (116) and (117) immediately gives

$$\theta_i = \theta_j$$

$$\delta_{i}^* = \delta_{j}^*$$

Since  $\lambda_i = \lambda_j = 0$ , the following relations must also hold:

$$\Delta_{\hat{\mathbf{l}}} = \left(\frac{\Delta}{\theta}\right)_{\hat{\mathbf{l}}} \theta_{\hat{\mathbf{l}}} = \Delta_{\hat{\mathbf{j}}} \tag{119a}$$

$$I_i = I_i(\lambda_i) = I_j \tag{119b}$$

Substitution of these equalities into the energy equation and rearrangement results in

$$\frac{1}{b_{j}} \left[ \left( \frac{\nabla^{*}}{\nabla} \right)_{j} - \left( \frac{\cancel{p}}{\nabla} \right)_{j} \right] = \frac{h_{i}^{*}}{h_{j}^{*}} \frac{1}{b_{i}} \left[ \left( \frac{\nabla^{*}}{\nabla} \right)_{i} - \left( \frac{\cancel{p}}{\nabla} \right)_{i} \right] + \left( \frac{\delta^{*}}{\Delta} \right) \left( 1 - \frac{h_{i}^{*}}{h_{j}^{*}} \right) = f(\xi_{te}) \quad (120)$$

This equation of functional form  $f(b,\Gamma)=$  Constant is reduced to the form f(b)= Constant by use of equation (28). The resultant equation cannot be solved in closed form but may be easily solved by trial and error.

### TRANSFORMATION TO AND EVALUATION OF PERTINENT PARAMETERS

### IN THE PHYSICAL FLOW

Inversion From Transformed Coordinates to the

Corresponding Physical Flow Coordinates

The inverse transformation from the  $\alpha$ ,  $\beta$ , or  $\omega$  normal coordinate system to the physical normal coordinate  $\gamma$  may be carried out when the profile functions are known. This transformation is first illustrated for the local enthalpy case.

The definition of  $\beta$  (eq. (6)) is inverted to

$$\frac{y}{\nabla} = \int_{0}^{\beta} \frac{\rho_{\epsilon}}{\rho} d\beta = \frac{p_{\epsilon}}{p_{1}} \int_{0}^{\beta} \frac{h}{h_{\epsilon}} d\beta \tag{121}$$

Substitution of the definition of  $h^*$  and  $h_l^*$  enables equation (121) to be written as

$$\frac{y}{\nabla} = \frac{p_{\epsilon}}{p_{1}} \int_{0}^{\beta} \left[ \frac{h_{w}}{h_{\epsilon}} + \frac{h_{1}^{*}}{h_{\epsilon}} \frac{h_{1}^{*}}{h_{1}^{*}} (\beta) \right] d\beta = \frac{p_{\epsilon}}{p_{1}} \left[ \frac{h_{w}}{h_{\epsilon}} \beta + \frac{h_{1}^{*}}{h_{\epsilon}} \int_{0}^{\beta} \frac{h_{1}^{*}}{h_{1}^{*}} d\beta \right]$$
(122)

The expression for  $\frac{y}{\nabla}$  may then be evaluated for any known distribution of  $\frac{h^*}{h_1^*}$  with  $\beta$ . Equation (122) is suitable for transformation from  $\beta$  to  $\frac{y}{\nabla}$ . Transformation of the velocity profile is accomplished by substituting the identity  $b\alpha = \beta$ . The expression  $\frac{y}{\nabla}$  is, in turn, related to a nondimensional similar normal ordinate  $\frac{y}{\sqrt{\nu_\epsilon t}}$  as follows:

$$\frac{y}{\sqrt{\nu_{\epsilon}t}} = \frac{y}{\nabla} \frac{\nabla}{\sqrt{\nu_{\epsilon}t}} = \frac{y}{\nabla} \frac{\sqrt{Z}}{b \frac{\theta}{\Delta}}$$
 (123)

Thus,

$$\frac{y}{\sqrt{\nu_{\epsilon}t}} = \frac{\sqrt{z}}{b} \frac{p_{\epsilon}}{\frac{\theta}{\Delta}} \frac{p_{\epsilon}}{p_{1}} \left( \frac{h_{w}}{h_{\epsilon}} \beta + \frac{h_{1}*}{h_{\epsilon}} \right) \int_{0}^{\beta} \frac{h^{*}}{h_{1}*} d\beta$$
(124a)

or

$$\frac{y}{\sqrt{\nu_{\epsilon}t}} = \frac{\sqrt{z}}{b} \frac{p_{\epsilon}}{\frac{\theta}{\Delta}} \left( \frac{h_{w}}{h_{\epsilon}} b\alpha + \frac{h_{1}^{*}}{h_{\epsilon}} \int_{0}^{b\alpha} \frac{h^{*}}{h_{1}^{*}} d\beta \right)$$
(124b)

Equations (124a) and (124b) are the inversion equations for the local enthalpy transformation from the  $\beta$ - and  $\alpha$ -plane to the physical-flow coordinate system.

Corresponding equations for the total enthalpy transformations are as follows. (The identity  $c\alpha=\omega$  is also employed.)

$$\frac{y}{\Box} = \frac{p_{\epsilon}}{p_{1}} \left[ \frac{H_{w}}{h_{\epsilon}} \omega + \frac{H_{1}*}{h_{\epsilon}} \int_{0}^{\omega} \frac{H^{*}}{H_{1}*} d\omega - \frac{u_{1}^{2}}{2h_{\epsilon}} \int_{0}^{\omega} \left( \frac{u}{u_{1}} \right)^{2} d\omega \right]$$

$$\frac{y}{\sqrt{v_{\epsilon}t}} = \frac{y}{\Box} \frac{\sqrt{z}}{c \frac{\theta}{\Delta}}$$

$$\frac{y}{\sqrt{\nu_{\epsilon}t}} = \frac{\sqrt{Z}}{c} \frac{p_{\epsilon}}{\frac{\theta}{\Lambda}} \left[ \frac{H_{w}}{h_{\epsilon}} \omega + \frac{H_{l}*}{h_{\epsilon}} \int_{0}^{\omega} \frac{H^{*}}{H_{l}*} d\omega - \frac{u_{l}^{2}}{2h_{\epsilon}} c \int_{0}^{\omega/c} \left( \frac{u}{u_{l}} \right)^{2} d\alpha \right]$$
(125a)

$$\frac{y}{\sqrt{\nu_{\epsilon}t}} = \frac{\sqrt{Z}}{c} \frac{p_{\epsilon}}{\frac{\theta}{\Delta}} \left[ \frac{H_{w}}{h_{\epsilon}} \cos + \frac{H_{1}*}{h_{\epsilon}} \int_{0}^{c\alpha} \frac{H^{*}}{H_{1}*} d\omega - \frac{u_{1}^{2}}{2h_{\epsilon}} c \int_{0}^{\alpha} \left( \frac{u}{u_{1}} \right)^{2} d\alpha \right]$$
(125b)

Transformation of Velocity and Temperature

Profiles to the Physical Plane

Since the profile series result in distributions of  $\frac{u}{u_1}$  and  $\frac{h^*}{h_1^*}$ 

or  $\frac{H^*}{H_1^*}$  in terms of  $\alpha$ ,  $\beta$ , or  $\omega$ , it is desirable to obtain profiles

nondimensionalized by an invariant reference state in terms of y,  $\xi$ , and t. In the previous section the inverse transformation of  $\alpha$ ,  $\beta$ , and  $\omega$  was shown to be of the form

$$\alpha = \alpha \left( \xi, \frac{y}{\sqrt{\nu_{\epsilon} t}} \right)$$

$$\beta = \beta \left( \xi, \frac{y}{\sqrt{\nu_{\epsilon} t}} \right)$$

$$\omega = \omega \left( \xi, \frac{y}{\sqrt{\nu_{\epsilon} t}} \right)$$
(126)

The combinations of equations (126) with equations (8), (9), and (10) produces the following equations for the profiles in the physical plane:

$$\frac{u}{a_{\epsilon}}(y,\xi,t) = \frac{u_{1}}{a_{\epsilon}}(\xi) \frac{u}{u_{1}}(\xi,\frac{y}{\sqrt{\nu_{\epsilon}t}}) = \frac{u_{1}}{a_{\epsilon}}(\xi) \frac{u}{u_{1}}(\xi,\alpha)$$
 (127a)

$$\frac{h}{h_{\epsilon}}(y,\xi,t) = 1 + \frac{h_{\underline{l}}^{*}}{h_{\epsilon}}(\xi) \frac{h^{*}}{h_{\underline{l}}^{*}}(\xi,\frac{y}{\sqrt{\nu_{\epsilon}t}}) = 1 + \frac{h_{\underline{l}}^{*}}{h_{\epsilon}}(\xi) \frac{h^{*}}{h_{\underline{l}}^{*}}(\xi,\beta) \quad (127b)$$

$$\frac{H}{H_{\epsilon}}(y,\xi,t) = 1 + \frac{H_{\underline{l}}^{*}}{H_{\epsilon}}(\xi) \frac{H^{*}}{H_{\underline{l}}^{*}}(\xi,\omega)$$
 (127c)

If  $\frac{H}{H_{\varepsilon}}$  is computed by the local enthalpy method, the following equation with values substituted from equations (127a) and (127b) rather than equation (127c) would apply:

$$\frac{H}{H_{\epsilon}}(y,\xi,t) = \frac{h}{h_{\epsilon}}(y,\xi,t) \frac{h_{\epsilon}}{H_{\epsilon}} + \frac{\gamma - 1}{2} \left[ \frac{u}{a_{\epsilon}}(y,\xi,t) \right]^{2} \frac{h_{\epsilon}}{H_{\epsilon}}$$
(128)

Evaluation of Wall-Shear and Heat-Transfer Coefficients

The expressions for the wall shear and heat transfer in basic form and in various coefficient forms are derived. In this section the designation a after an equation number denotes the local enthalpy method and b, the stagnation enthalpy method.

Consider first the wall shear:

$$\tau_{W} = \mu_{W} \left( \frac{\partial u}{\partial y} \right)_{W}$$

$$\tau_{W} = \mu_{W} u_{1} \left( \frac{d \frac{u}{u_{1}}}{d\alpha} \right)_{\alpha=0} \left( \frac{\partial \alpha}{\partial y} \right)_{W}$$

$$\tau_{W} = \mu_{W} u_{1} A_{1} \frac{\rho_{W}}{\rho_{\epsilon}} \frac{1}{\Delta}$$

$$\tau_{W} = \mu_{W} \frac{\rho_{W}}{\rho_{\epsilon}} u_{1} A_{1} \frac{\theta}{\Delta} \frac{1}{\sqrt{\nu_{\epsilon} t Z}}$$
(129)

A dimensionless shear function  $\hat{\tau}_{\epsilon}$  is introduced to eliminate the time dependency in equations (129) with the result that  $\hat{\tau}_{\epsilon} = \hat{\tau}_{\epsilon}(\xi)$  and

$$\hat{\tau}_{\epsilon} = \frac{\tau_{W}}{\rho_{\epsilon} a_{\epsilon} \sqrt{\frac{\nu_{\epsilon}}{t}}} = \frac{\rho_{W}}{\rho_{\epsilon}} \frac{\mu_{W}}{\mu_{\epsilon}} \frac{u_{\underline{1}}}{a_{\epsilon}} \frac{A_{\underline{1}} \frac{\theta}{\underline{\Delta}}}{\sqrt{Z}}$$
(130)

The rate of heat transfer from the wall to the fluid may be treated in a like manner:

$$q_{W} = -k_{W} \left(\frac{\partial T}{\partial y}\right)_{W} = -\frac{1}{N_{Pr}} \mu_{W} \frac{\rho_{W}}{\rho_{\epsilon}} h_{L}^{*} B_{L} \frac{\phi}{\nabla} \frac{1}{\sqrt{\nu_{\epsilon} tW}}$$
(131a)

$$q_{W} = -\frac{1}{N_{Pr}} \mu_{W} \frac{\rho_{W}}{\rho_{\epsilon}} H_{L}^{*}C_{L} \stackrel{\psi}{\square} \frac{1}{\sqrt{\nu_{\epsilon} tQ}}$$
 (131b)

$$\hat{q}_{\epsilon} = \frac{q_{w}}{\rho_{\epsilon} a_{\epsilon}^{2} \sqrt{\frac{\nu_{\epsilon}}{t}}} = -\frac{1}{(\gamma - 1)N_{Pr}} \frac{\rho_{w}}{\rho_{\epsilon}} \frac{\mu_{w}}{\mu_{\epsilon}} \frac{h_{1}^{*}}{h_{\epsilon}} \frac{B_{1} \frac{\phi}{\nabla}}{\sqrt{w}}$$
(132a)

$$\hat{q}_{\epsilon} = -\frac{1}{(\gamma - 1)N_{Pr}} \frac{\rho_{W}}{\rho_{\epsilon}} \frac{\mu_{W}}{\mu_{\epsilon}} \frac{H_{l}*}{h_{\epsilon}} \frac{C_{l}}{\sqrt{Q}}$$
(132b)

Analogy ratios for  $\, \hat{\mathfrak{q}}_{\epsilon} \,$  and  $\, \hat{\mathfrak{ au}}_{\epsilon} \,$  may be simply formed and are

$$\frac{\hat{q}_{\epsilon}}{\hat{\tau}_{\epsilon}} = -\frac{1}{N_{\text{Pr}}} \frac{h_{1}^{*}}{u_{1}a_{\epsilon}} b \frac{B_{1}}{A_{1}}$$
 (133a)

$$\frac{\hat{q}_{\epsilon}}{\hat{\tau}_{\epsilon}} = -\frac{1}{N_{Pr}} \frac{H_{l}^{*}}{u_{l}a_{\epsilon}} c \frac{C_{l}}{A_{l}}$$
(133b)

An alternate coefficient form which, although it is more easily comparable with results of others, is dependent on both  $\xi$ , t, and a flow length l may be expressed in terms of a Reynolds number based on flow length. The following definitions are used:

l length potential flow has traversed since acceleration from zero velocity by wave 
$$R = \frac{u_1 l}{v_w}$$

$$c_f = \frac{\tau_w}{\frac{1}{2} \rho_w u_1^2}$$

$$c_h = \frac{Np_r q_w}{\rho_w u_1 h_1 *}$$
(134)

Equations (134) are combined with equations (129) and (131) to determine

$$c_{f} \sqrt{R} = \frac{2A_{l} \frac{\theta}{\Delta}}{\sqrt{Z}} \sqrt{\frac{\rho_{w} \mu_{w}}{\rho_{e} \mu_{e}}} \frac{1}{u_{l}t}$$
 (135)

$$c_{h}\sqrt{R} = -\frac{B_{1}\sqrt{\frac{\phi}{\nabla}}}{\sqrt{W}}\sqrt{\frac{\rho_{w}\mu_{w}}{\rho_{\epsilon}\mu_{\epsilon}}}\frac{1}{u_{1}t}$$
(136a)

$$c_{h}\sqrt{R} = -\frac{c_{1}}{\sqrt{Q}} \frac{\Psi_{1}^{*}}{h_{1}^{*}} \sqrt{\frac{\rho_{w}\mu_{w}}{\rho_{\epsilon}\mu_{\epsilon}}} \frac{1}{u_{1}^{t}}$$
(136b)

The resultant analogy ratios are

$$\frac{c_{h}}{c_{f}} = -\frac{bB_{l}}{2A_{l}} \tag{137a}$$

$$\frac{c_{h}}{c_{f}} = -\frac{cC_{l}}{2A_{l}} \frac{H_{l}^{*}}{h_{l}^{*}}$$
 (137b)

These relations (eqs. (135) to (137)) are appropriate for the constant free-stream flow behind a zero-thickness wave, since for this condition l is given by

$$l = \frac{u_1}{u_1 - u_s} (x - u_s t)$$
 (138)

# RESULTS AND DISCUSSION

## SHOCK SOLUTIONS

Equations (106) to (113) for the local and stagnation enthalpy methods were solved for the flow behind a shock wave advancing into undisturbed fluid (region  $\infty$ ). Solutions were determined for the following conditions:

- (a) Five- and six-term series represented profiles of velocity and enthalpy
- (b) The highest order derivative was assumed to be zero at  $\,\alpha=\,1\,$  and  $\,\beta\,=\,1\,$
- (c) Prandtl numbers of 0.72 and 1.0
- (d) Wall temperature equal to the undisturbed fluid temperature and wall temperature equal to the recovery temperature.

Figures 2 to 4 present the results in coefficient form and show comparable results for the solution of reference 12. The potential flow is designated by the subscript  $\sigma$  and represents the shock-tube region appropriate to this case.

The coefficients are independent of the ratio of the specific heats  $\gamma$  when plotted against a function of the ratio  $u_s/u_\sigma$ . The choice of  $\frac{u_s}{u_s-u_\sigma}$  rather than  $\frac{u_s}{u_\sigma}$  as the abscissa was made in order to represent the entire range of shock strengths along a finite abscissa.

These solutions necessitated finding the values of b which satisfied the equations for the local enthalpy case (eqs. (ll0) and (Dl5) or (Dl6)) or the values of c which satisfied equations (lll), and the equations for  $\psi/\Box$  (analogous to eqs. (Dl5) or (Dl6)) when the stagnation enthalpy equations were used. These equations are polynomials of high order in b and c and, as a consequence, multiple roots were possible. Only two roots with real positive values of b or c were found for each case. One family of equations originated at the value b,c = 0 for the limiting weak wave and the values were much less than unity throughout the entire range; the other family originated at the value b,c =  $\sqrt{NPr}$  for the limiting weak wave and remained of order one for all waves. The latter family was chosen as the correct one after application of the argument that, on physical grounds, an infinite ratio of velocity to thermal-boundary-layer thickness is not acceptable.

64 NACA TN 3944

Because the momentum equation is independent of the energy equation when the outer inviscid flow is constant, skin friction is independent of  $N_{Pr}$  and is the same for both local and stagnation enthalpy representations. The terms  $c_f\sqrt{R}$  for the five- and six-term profile series (fig. (2)) agree well with the corresponding values of reference 12, the five-term solution being 3 to 4 percent lower and the six-term solution being only from 1 to 3 percent lower than the reference values. The coefficients are significantly different from the steady-flow values of  $c_f\sqrt{R}$  and  $c_h\sqrt{R};$  the unsteady-flow values are about two to three times as large. This difference arises because shock-initiated laminar boundary-layer flows are more closely related to the Rayleigh problem of the infinite plates. The flow behind the shock is equivalent to the Rayleigh flow for the limiting weak shock with a pressure ratio of 1.0 (ref. 12).

Heat-transfer parameters for the special case  $T_W=T_\infty$  defined by equations (134) are plotted in figure 3; results of the present solutions are compared with results of the analysis of reference 12. As in the case of skin friction, heat-transfer coefficients agree well throughout the range of shock strengths.

The recovery factor r is defined as

$$r = \frac{h_{aw} - h_{1}}{H_{1} - h_{1}} = \frac{H_{aw} - h_{1}}{H_{1} - h_{1}}$$
 (139)

where  $h_{aw}=H_{aw}$  is the enthalpy of an insulated wall  $(q_w=0)$ . The condition of zero heat transfer occurs when  $\left(\frac{\partial h}{\partial y}\right)_W=0$  which, in turn, requires that  $B_1$  or  $C_1=0$ . These latter will be zero when

$$\Gamma, \Omega = 6$$

$$\Gamma, \Omega = 10$$

$$(140)$$

for the five-term series and six-term series, respectively. Although in figure 4 the discrepancy between the recovery factors of the local enthalpy methods and those of reference 12 appears to be large, the recovery-temperature error itself is fairly small because the Mach number is limited to a maximum of 1.89. The following numerical example for air

(as a perfect gas) with  $T_{\infty}=520^{\circ}$  illustrates the fact. At a shock-pressure ratio of 3.0, the adiabatic wall temperature from reference 12 is 1,443° compared with the six-term local enthalpy result of 1,411°; and at a shock pressure ratio of 100, the temperature from reference 12 is 14,737° and that of the present analysis is 14,804°.

Insulated-wall solutions by the stagnation enthalpy method required recovery factors of unity for both five- and six-term profiles regardless of Prandtl number. Failure of this method is attributed to the low number of terms in the profile function. In the local enthalpy method for five- and six-term profiles, stagnation enthalpy profiles contain 9 and ll terms, respectively, because of their quadratic dependence upon velocity. Thus the stagnation enthalpy profiles may have a sufficient number of inflection points to yield zero heat transfer at a wall temperature other than that equal to the stream stagnation temperature. When five- and six-term stagnation enthalpy profiles are required, however, too few points of inflection are available to satisfy the boundary conditions and to give zero heat transfer at any wall temperature other than stream stag-

nation temperature. The result is the unique profile  $\frac{H}{H_1}(\omega)=1$ ,  $\delta_H=0$ , and  $c=\infty$ ; these values appear to be unacceptable for Prandtl numbers other than unity.

Figure 5 presents velocity profiles of the five- and six-term local enthalpy solutions for the present analysis computed at the location

 $\xi = \frac{u_{\sigma}}{a_{\varepsilon}}$  for a value of the parameter  $\frac{u_{s}}{u_{s} - u_{\sigma}}$  equal to 2.0. Local and

stagnation enthalpy profiles for the same case are given in figure 6. Shown also in these figures are the corresponding profiles evaluated from reference 12. The integral-method profiles are slightly fuller in the outer part of the boundary layer but are in close agreement near the wall, the six-term profiles giving slightly better correlation than the five-term profiles.

Solutions by the local enthalpy method with six-term profiles and vanishing stream derivatives were obtained for the flow behind a negative shock propagating into region  $\epsilon$ . Skin-friction and heat-transfer results,  $c_f\sqrt{R}$  and  $c_h\sqrt{R}$ , are plotted in figures 7 and 8 against \$te\$ which is an index of negative shock strength. The functions are evaluated for  $\gamma$  equal to 1.4 and 1.667 and Prandtl numbers of 0.72 and 1.0. As for the case of the shock wave, only the family of solutions with b near unity was considered.

Results of the analysis of reference 13 for  $\gamma=1.4$  and Prandtl number of 0.72 are also shown in figures 7 and 8(a). Good agreement with the corresponding case of the present solution is evident.

#### EXPANSION-FAN SOLUTION

The initial solutions to the hyperbolic differential equations for Z and W indicated immediately that there was no unique mathematical solution to the problem; instead, an infinite number of solutions were possible for the six-term profiles. The reason for this behavior lay in the fact that the starting value of  $\lambda=20$  ( $\Gamma=-10$ ) not only produced the fullest profile without exceeding a value of 1.0 for  $\frac{u}{u_1} \left(\frac{h^*}{h_1^*}\right)$  but

was also the maximum point on the curves of  $\lambda \left(\frac{\theta}{\Delta}\right)^2$  and  $A_1 \frac{\theta}{\Delta} \frac{\theta}{\delta^*}$ 

against  $\lambda$ . In the range where  $\xi$  approaches -1, the dominant terms (as has been shown previously for  $\xi$  = -1 in the discussion of the starting problem) in equations (45) and (46) contain these parameters; thus, it is possible to find solutions on either side of  $\lambda$  = 20. Similarly, for each  $\lambda$  in this region, branch solutions exist for  $\Gamma$  on either side of -10 corresponding to a b on each side of  $N_{Pr}^{1/2}$ . Furthermore, it was possible to change from one family (say  $\lambda$  < 20,  $\Gamma$  > -10, b >  $N_{Pr}^{1/2}$ ) to another ( $\lambda$  < 20,  $\Gamma$  < -10, b <  $N_{Pr}^{1/2}$ ) in succeeding steps, and the derivatives obtained for  $\frac{d\Gamma}{d\xi}$  and  $\frac{db}{d\xi}$  would permit

fairing of a smooth, although inflected, curve of  $\Gamma$  and b against  $\xi$ . Thus, from a single solution at the start (point for n=1) the possible solutions multiplied so that at the first step away from  $\xi=-1$  (that is, n=2) there were four solutions; at the second step, eight solutions; or at the nth step,  $2^n$  possible solutions.

The aforementioned mathematical phenomenon was eliminated on the basis of physical logic that such oscillating solutions were not compatible (at least in the region where \xi\$ approaches -1) with smooth monotonic variation in all the potential-flow quantities. However, there still remained the first four branches of the solution:

Branch I:

$$\lambda$$
 < 20; b >  $\sqrt{N_{Pr}}$ ;  $\Gamma$  > -10

Branch II:

$$\lambda < 20;$$
 b  $< \sqrt{N_{Pr}};$   $\Gamma < -10$ 

Branch III:

$$\lambda >$$
 20; b >  $\sqrt{N_{Pr}}$ ;  $\Gamma >$  -10

Branch IV:

$$\lambda > 20$$
; b <  $\sqrt{N_{Pr}}$ ;  $\Gamma < -10$ 

These four branches were computed and the results of their solutions are presented in figures 9 to 15. Also plotted in figures 14 and 15 are the results of a power-series solution to the complete Prandtl equations (ref. 15). This solution, obtained by expanding the velocity stream function and a corresponding temperature-distribution function in terms of powers of  $\xi + 1$ , contains terms up to  $(\xi + 1)^2$ , is exact at  $\xi = -1$ , and has a progressive error as  $\xi$  increases. Note should be taken that the series solution was not completed until after the integral solution in the expansion fan was finished; thus, a comparison with the series solution was not available in the early stages of computation.

An inspection of figures 9 to 15 reveals that, in the neighborhood of  $\xi = -1$ , the Z, W,  $\hat{\tau}_{\varepsilon}$ , and  $\hat{q}_{\varepsilon}$  curves of the integral solution are nearly coincidental in spite of the variation in the profile parameters  $\lambda$ ,  $\Gamma$ , and b. The values of  $\hat{\tau}_{\varepsilon}$  and  $\hat{q}_{\varepsilon}$  also agree closely with the solution of reference 15 in this region. This near-equivalence of wall shear and heat transfer, concurrent with different values of  $\lambda$ ,  $\Gamma$ , and b, is typical of integral solutions which are not concerned directly with the various profile shapes inside the boundary layer but instead are dependent on the integral of these profiles and their derivative at the wall.

As  $\xi$  becomes larger, branches II and IV first diverge from branches I and III; and the solutions to the former branches become unacceptable when b becomes zero at  $\xi \approx -0.52$  since this condition indicates an infinite ratio of  $\frac{\delta_h}{\delta_u}$  in the physical plane. Branches I and III agree with the series solution within 2 percent up to  $\xi = -0.5$  for  $\hat{\tau}_{\varepsilon}$  and within 5 percent up to  $\xi = -0.7$  for  $\hat{q}_{\varepsilon}$ .

Branch I solution does not continue past  $\xi=0.62$ . At this point  $\xi=\xi Z^*$  and further integration along the characteristic originating from  $\xi=-1$  is prohibited. Branch III solution was halted arbitrarily at  $\xi\approx 1.0$ , the point at which Z approaches O. For this solution  $\xi_Z^*>1.0$  so that further integration was possible but was discontinued

in view of difficulties (to be discussed in a future section) encountered in joining the solutions to a constant-pressure region.

Velocity and enthalpy profiles of the four branch solutions and the power-series solution are shown in figures 16 and 17 for values of  $\xi = -0.9$ , -0.7, and -0.5 (no solution for branches II and IV at  $\xi = -0.5$ ). All solutions agree very well in regard to velocity profile (the overshoot in velocity in branch III at these values of  $\xi$  is almost negligible) and the agreement at  $\xi$  approaching -1 between the integral and the exact (that is, the power series as  $\xi$  approaches -1) is much better than that for the shock solutions. (Compare figs. 5 and 16.) Although the enthalpy profiles of branches I and III agree closely with each other and the series solution, those of branches II and IV indicate a different and very improbable behavior from the beginning. The profiles for branches II and IV show minimum values of h (maximum values of h\*/h<sub>1</sub>\*) to exist inside the boundary layer, and such a minimum does not appear to be physically logical since the convective derivative of free-stream temperature is always negative whereas the wall remains at a fixed temperature.

Of the two remaining branches, I and II, arguments could be advanced originally for the retention of both. For the case of  $\lambda <$  20 (branch I) consider the argument: Since the convective pressure gradient  $\frac{D\underline{p}_1}{D \log_e t}$ 

increases monotonically from a value of  $-\frac{2\gamma}{\gamma+1}$  at  $\xi=-1$  to a value of 0 at  $\xi=\frac{2}{\gamma-1}$  (value of  $\xi$  for  $\underline{p}_1=0$ ), from steady-flow analogy  $\lambda$  would be expected to decrease monotonically. For the case of  $\lambda>20$  (branch III), the following reasoning can be applied:

(a) If the solution were to be continued for an expansion fan of infinite pressure ratio  $\left(\underline{p}_1(\xi)=0,\ \xi=\frac{2}{\gamma-1}\right)$ , consider the expression relating  $\lambda$  with Z:

$$\lambda = \left(\frac{\Delta}{\theta}\right)^2 \frac{1}{1+\xi} \frac{Z}{\left(\frac{1-\frac{\gamma-1}{2}\xi}{\frac{\gamma+1}{2}}\right)^{\frac{3\gamma-1}{\gamma-1}}}$$

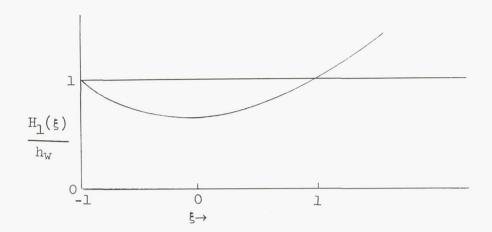
For  $\lambda$  to be finite at  $\xi=\frac{2}{\gamma-1}$  requires not only that Z is zero but also that all n derivatives  $\frac{d^nZ}{d\xi^n}$  for  $n\leq \frac{3\gamma-1}{\gamma-1}-1$  are zero. For  $\lambda$  to be zero would also require  $\frac{d^nZ}{d\xi^n}=0$  to be true for  $n\leq \frac{3\gamma-1}{\gamma-1}.$  These restrictions on  $\frac{d^nZ}{d\xi^n}$  are very rigid and a violation would not be unexpected; thus,  $\lambda=\infty$  (when  $\xi=\frac{2}{\gamma-1}$ ) is possible.

(b) From steady-flow experience, when a strong favorable pressure gradient is imposed on a flow in which the wall is hotter than the free stream, the local free-stream velocity is often exceeded inside the boundary layer (that is,  $\lambda > 20$ ).

The subsequent completion of the series solution indicated a preference for the case  $\lambda < 20$  since in the vicinity of  $\xi = -1$  the profile  $\frac{u}{u_1}$  never exceeds 1. (See fig. 16.) It should be noted, however, that, in the region  $\xi > -0.5$ , the profile of reference 15 shows a tendency to exceed 1.0. This value of  $\xi$  is such that the error arising in the series solution by neglecting  $0(1+\xi)^3$  is of the same order as the velocity overshoot.

In view of the foregoing arguments, the following policy was adopted: The branch of the solution for  $\lambda \leq 20$  is considered to be the correct and most accurate one. Results of this solution including pertinent derivatives may be found in table I. Results for both branches I and III will be presented in some cases of  $\hat{\tau}_{\varepsilon}$  and  $\hat{q}_{\varepsilon}$  since, as mentioned before, the integral method itself cannot distinguish the behavior inside the boundary layer.

From an inspection of figure 15, a maximum value of  $\hat{q}_{\varepsilon}$  is evident in both the integral and power-series solutions. Such a maximum was expected since the ratio of free-stream total enthalpy to wall enthalpy has an initial value of 1.0 at  $\xi=-1$ , decreases to  $\frac{2}{\gamma+1}$  at  $\xi=0$ , and increases thereafter so that it passes through 1.0 again at  $\xi=1$ . (See accompanying sketch.)



Since the difference in these enthalpies may be considered a measure of the influence of the local free-stream flow on heat transfer, the heat transfer to the fluid would be expected to increase from an initial value of zero to a positive maximum, return to zero, and finally become negative. The fact that the positive maximum at  $\xi = -0.6$  and the return to zero at  $\xi = 0.5$  for solution I occurred at lower values of  $\xi$  than the maximum and zero difference, respectively, in the stagnation enthalpies reflects the past history of the boundary-layer flow. Energy has been added to and stored in the boundary layer so that at a given value of  $\xi$  the total enthalpy distribution in the boundary layer is entirely different from that which would have existed if the local free-stream condition had been constant to that point. Similar behavior occurs for branch III.

A maximum also exists in the curve of the variation of  $\hat{\tau}_{\varepsilon}$  with  $\xi$  for the integral solutions (fig. 14). (It does not appear in the series solution since this effect requires consideration of terms of  $O(1+\xi)^3$  or higher.) A simple explanation for its occurrence in this particular range of  $\xi$  is not obvious although the existence of a maximum at some point in the expansion wave will be argued.

Although the computations have not been carried out to large values of  $\xi$  (and, as discussed previously, the no-slip conditions are violated), an idea of the behavior of  $\hat{\tau}_{\varepsilon}$  and  $\hat{q}_{\varepsilon}$  under the Prandtl boundary-layer assumptions can be obtained from physical considerations. For an infinite expansion-fan strength ( $\underline{p}_1$  = 0), the following conditions apply:

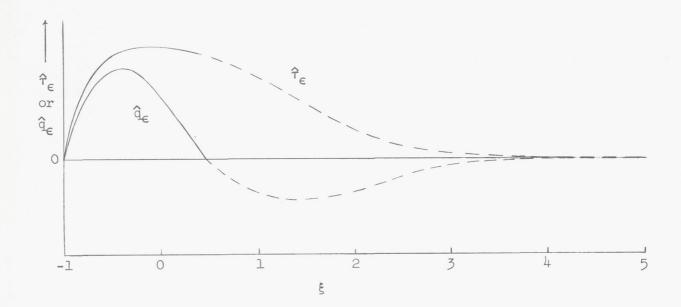
$$\underline{\mathbf{u}}_1 = \frac{2}{\gamma - 1}$$

$$\frac{H_{1}}{H_{W}} = \frac{h_{1}}{h_{W}} + \frac{\gamma - 1}{2} \underline{u}_{1}^{2} = 0 + \frac{2}{\gamma - 1}$$

V

Thus, although the free-stream density, pressure, and temperature have all become zero, the nondimensional free-stream velocity  $\underline{u}_1$  and stagnation enthalpy ratios  $\frac{\underline{H}_1}{H_W}$  are finite. If this situation is represented as an infinitely thick boundary layer separating a surface from a stream of finite velocity and total enthalpy, the wall shear and heat transfer would then become zero. The following sketch indicates the anticipated form of the curves for  $\hat{\tau}_{\varepsilon}$  and  $\hat{q}_{\varepsilon}$ , the solid lines denoting

computations and the dashed lines, possible extrapolations.



For the wall shear to approach zero as  $\xi$  approaches  $\frac{2}{\gamma-1}$  requires a maximum on the curve of the variation of  $\hat{\tau}_{\varepsilon}$  with  $\xi$ . Similarly, the curve for the variation of  $\hat{q}_{\varepsilon}$  with  $\xi$  must have both a maximum and minimum value.

Dimensionless velocity and enthalpy profiles inside the expansion fan for various values of  $\xi$  are shown in figures 18 and 19 for the branch I solution. One may note in figure 18 that the value of the dimensionless normal ordinate at the edge of the velocity boundary layer  $\left( \begin{array}{c} \underline{y} \\ \sqrt{\nu_\varepsilon t} \end{array} \right) \delta_u$  increases nearly linearly with  $\xi$  in the range -0.4  $\leq \xi \leq$  0.6. Since  $\frac{u_1}{a_\varepsilon} = \frac{2}{\gamma+1} (1+\xi) \quad \text{and} \quad \lambda \quad \text{does not change drastically, it is to}$ 

be expected that the slope of the velocity profile at the wall would be nearly constant in this range and hence result in an approximately constant skin-friction parameter. (See fig. 14.)

Although the value of  $\left(\frac{y}{\sqrt{\nu_{\varepsilon}t}}\right)_{\delta_h}$  is also approximately linear in

the same range, the wall heat transfer is not constant because: (a)  $\frac{h_1^*}{h_e}$ 

is not linear in  $\xi$ , and (b)  $\Gamma$  approaches and passes through the value 10. Condition (b) requires an inflected enthalpy profile and a resultant reversal of the sign of the heat transfer. (See curve for  $\xi=0.6$  in fig. 19.)

The behavior of the solutions at the leading edge of the expansion fan merits consideration. Consider the following limiting equations:

For six-term series:

$$\lim_{\xi \to -1} Z = \lim_{\xi \to -1} \lambda \left(\frac{\theta}{\Delta}\right)^{2} (\xi + 1) = \lim_{\xi \to -1} 0.1148(1 + \xi)$$

$$(141)$$

For six-term series:

$$\lim_{\xi \to -1} \hat{\tau}_{\varepsilon} = \lim_{\xi \to -1} \frac{\underline{u}_{1}}{\sqrt{\xi + 1}} \frac{A_{1}}{\sqrt{\lambda}} = \lim_{\xi \to -1} 1.118 \frac{\underline{u}_{1}}{\sqrt{1 + \xi}}$$
(142a)

For five-term series,  $\left(\frac{u}{u_1}\right)_{\alpha=1}^{"} = -0.647$ :

$$\lim_{\xi \to -1} \hat{\tau}_{\varepsilon} = \lim_{\xi \to -1} \frac{\underline{u}_{1}}{\sqrt{\xi + 1}} \frac{\underline{A}_{1}}{\sqrt{\lambda}} = \lim_{\xi \to -1} 1.125 \frac{\underline{u}_{1}}{\sqrt{1 + \xi}}$$
(142b)

Consider the same limiting equations for the case of a vanishingly weak positive or negative shock (that is,  $u_s \rightarrow \pm a_{\epsilon}$ ,  $u_l \rightarrow 0$ ):

For the six-term series:

$$\lim_{\substack{\xi_{S} \to \pm 1 \\ \xi \to \pm 1}} Z = 2A_{1} \frac{\theta}{\Delta} \frac{\theta}{\delta^{*}} \lim_{\substack{\xi_{S} \to \pm 1 \\ \xi \to \pm 1}} (\pm \xi_{S} \mp \xi) = 0.20406 \lim_{\substack{\xi_{S} \to \pm 1 \\ \xi \to \pm 1}} (\pm \xi_{S} \mp \xi)$$

$$\xi_{S} \to \pm 1$$

$$\xi \to \pm 1$$

$$(143)$$

For the six-term series:

$$\lim_{\substack{\xi_{S} \to \pm 1 \\ \xi \to \pm 1}} \hat{\tau}_{\varepsilon} = \lim_{\substack{\xi_{S} \to \pm 1 \\ \xi \to \pm 1}} \frac{\underline{u}_{1}}{\sqrt{\pm \xi_{S} \mp \xi}} \sqrt{\frac{A_{1}}{2}} \frac{\delta^{*}}{\Delta} = \lim_{\substack{\xi_{S} \to \pm 1 \\ \xi \to \pm 1}} \frac{0.559\underline{u}_{1}}{\sqrt{\pm \xi_{S} \mp \xi}}$$

$$\xi \to \pm 1 \qquad \qquad \xi_{S} \to \pm 1 \qquad \qquad (144a)$$

For the five-term series:

$$\lim_{\substack{\xi_{S} \to \pm 1}} \hat{\tau}_{\varepsilon} = \lim_{\substack{\xi_{S} \to \pm 1}} \frac{\underline{u}_{1}}{\sqrt{\pm \xi_{S} \mp \xi}} \sqrt{\frac{A_{1}}{2}} \frac{\delta^{*}}{\Delta} = \lim_{\substack{\xi_{S} \to \pm 1}} \frac{0.547\underline{u}_{1}}{\sqrt{\pm \xi_{S} \mp \xi}}$$

$$\xi \to \pm 1 \qquad \qquad \xi_{\to} \pm 1 \qquad \qquad \xi_{\to} \pm 1 \qquad \qquad (144b)$$

The ratios of the limiting values in the expansion fan to those in the shocks are then

For the six-term series:

$$\lim_{\xi \to -1} \frac{Z_{\text{exp}}}{Z_{\text{shock}}} = \frac{0.1148}{0.20406} = 0.5626 \tag{145}$$

For the six-term series:

$$\lim_{\xi \to -1} \frac{\left(\hat{\tau}_{\epsilon}\right)_{\text{exp}}}{\left(\hat{\tau}_{\epsilon}\right)_{\text{shock}}} = \frac{1.118}{0.559} = 2.000 \tag{146a}$$

For the five-term series:

$$\lim_{\xi \to -1} \frac{\left(\hat{\tau}_{\epsilon}\right)_{\text{exp}}}{\left(\hat{\tau}_{\epsilon}\right)_{\text{shock}}} = \frac{1.125}{0.547} = 2.06$$
 (146b)

Similar ratios may be found for W and  $\hat{\mathbf{q}}_{\epsilon}.$  The power-series solution, which is exact at  $\xi$  = -1, also yielded a ratio of  $\hat{\tau}_{\varepsilon}$  exactly twice the Rayleigh (vanishingly weak shock case) value. These results will be applied in a later section to obtain approximations to the integral solution for any gas.

#### DISCONTINUITY SOLUTIONS

# At Trailing Edge of Expansion Fan

Solutions to equations (114b) and (114c) for branches I and III obtained at the weak discontinuity arising at the trailing edge of the expansion fan are shown in figures 20 and 21. For type I solutions, the ratio  $\frac{\theta_{i}}{\theta_{i}}$  (the subscript i indicates conditions inside fan at trailing edge; the subscript j, conditions outside fan at trailing edge) was in the range  $1.05 \le \frac{\theta_i}{\theta_j} \le 1.12$  whereas  $\frac{\phi_i}{\phi_j}$  was in the interval  $0.93 \le \frac{\phi_i}{\phi_j} \le 1.10$ . For branch III, the ranges were  $0.56 \le \frac{\theta_i}{\theta_j} \le 1.12$  and  $0.98 \le \frac{\phi_i}{\phi_i} \le 2.2$ , respectively. As mentioned previously, the values

from the continuity equation (113) varied from those given in figure 20 by no more than 2 percent. For branch III and for values of  $\xi_{te} > 0.6$ , no solutions could be found with a physically acceptable value of b

(that is, O(1-10)). This inability to match the values at the trailing edge may be construed as a further argument against the use of branch III solutions.

Since 
$$\left(\frac{\theta_{i}}{\theta_{j}}\right)^{2} = \frac{Z_{i}}{Z_{j}}$$
 and  $\left(\frac{\phi_{i}}{\phi_{j}}\right)^{2} = \frac{W_{i}}{W_{j}}$ , the discontinuous change in  $Z$ 

and W at the trailing edge represents a Z-jump and a W-jump in the boundary-layer characteristic system. These jumps may be considered analogous to the change in values of the Prandtl-Busemann parameters ( $C_1$  and  $C_2$  of ref. 22) at a vortex sheet in the steady-flow characteristic system since there is a discontinuous variation without any intersection of characteristics of the same family. Of course, these Z- or W-jumps exist only mathematically, since in the physical flow viscous effects would diffuse the jumps into steep gradients with the peaks rounded off, a situation similar to that in the steady flow where the vortex sheet would undergo viscous diffusion.

In figure 21 are shown the ratios  $\frac{\left(\hat{\tau}_{\varepsilon}\right)_{i}}{\left(\hat{\tau}_{\varepsilon}\right)_{j}}$  and  $\frac{\left(\hat{q}_{\varepsilon}\right)_{i}}{\left(\hat{q}_{\varepsilon}\right)_{j}}$  of the shear

stress and heat transfer on opposite sides of the trailing-edge discontinuity. Both solutions exhibit  $\frac{\hat{\tau}_j}{\hat{\tau}_j} \ge 1.0$ , a relation which was expected

for a flow emerging from a region of favorable pressure gradient into one of zero gradient.

For weak expansion waves the trend of the heat transfer at the trailing-edge discontinuity is that which would be expected from Reynold's analogy in that the heat transfer decreases similarly to the skin friction. However, for values of  $\xi_{\text{tc}} > -0.2$ , the opposite occurs and the heat transfer in region  $\zeta$  at the trailing edge exceeds that inside the expansion fan. No obvious argument is apparent to justify this behavior.

Velocity and enthalpy profiles on opposite sides of the trailingedge discontinuity are shown in figures 22 and 23. Corresponding pairs of velocity and enthalpy profiles show only a slight deviation across the discontinuity.

The velocity profiles inside the fan are fuller near the wall than in the region  $\zeta$  because, as mentioned previously, the favorable pressure gradient is absent in  $\zeta$ . Since  $\frac{\theta_{\dot{1}}}{\theta_{\dot{j}}} \approx 1.0$  and the thicknesses of comparable pairs of velocity profiles are nearly equal, the adjustment

of the boundary layer at the trailing edge of the expansion fan is essentially a transfer of momentum from the inner part to the outer part of the boundary layer.

#### At the Contact Surface in a Shock Tube

Equation (120) was solved for various expansion- and shock-wave pressure ratios for the special case arising when the same gas is used in both the high-pressure and low-pressure chambers of a shock tube. These solutions indicated no change in shear stress across the discontinuity, and only a small decrease in the magnitude of the heat-transfer rate although W,  $\Gamma$ , and b show extreme discontinuities which, of course, would be rounded off by viscosity. At first glance this heattransfer result might appear to be incompatible with the physical flow since across the contact surface there is always a discontinuity in the free-stream stagnation enthalpy. For a recovery factor near 1.0, the heat-transfer rate might be expected to vary as the difference between the free-stream stagnation enthalpy and the wall enthalpy. (For example, when  $M_{f} = 1.0$ , this difference is  $-0.17h_{\epsilon}$  in region  $\zeta$  and  $0.5h_{\epsilon}$  in region  $\sigma$ ). However, on further inspection, it appears physically plausible to expect the heat transfer to change only slightly although the free stream changes markedly. As the outer contact surface progresses at freestream velocity, the colder fluid forming the outer part of the boundary layer just behind the contact surface overrides the hot fluid near the wall. Consequently, since the fluid adjacent to the wall originally came from region  $\sigma$  with a high stagnation enthalpy, it still possesses enough energy to maintain a large rate of heat transfer simultaneously to the wall and to the outer part of the boundary layer. The enthalpy and velocity profiles for the case  $M_{\xi} = 1.0$ ,  $\xi_{te} = 0$ ,  $\xi_{d} = 0.833$  in the region near the entropy discontinuity are shown in figures 24 to 26. These figures show the initial hot-fluid entrainment near the wall and the subsequent rapid readjustment as the energy of this fluid is given up to the wall and outer boundary layer until finally all identity with the previous flow in region  $\sigma$  is lost and the boundary layer behaves as one would expect if region ( had been the only influencing factor. Although the velocity boundary-layer thicknesses  $\left(\frac{y}{\sqrt{v_{\epsilon}t}}\right)$  at  $\frac{u}{u_{l}} = 1.0$  are approxi-

mately equal on both sides of the discontinuity (see fig. 24), the thermal

boundary-layer thickness immediately boundary-l

much larger thickness of the thermal layer in this region is justifiable on the physical basis that the temperature is forced to go first from  $T_W$  to a value near  $T_\sigma > T_W$  in the hot sublayer and then revert back to  $T_\zeta < T_W$  in the outer layer. (See figs. 25 and 26.) No such behavior is required for the velocity since  $u_\zeta = u_\sigma.$  Of course, because of the effect of mixing and diffusion, the discontinuity of zero thickness itself is a physical impossibility; thus, the profiles in the immediate neighborhood of the contact surface do not physically exist, although the trends exhibited are probably correct.

# DISCUSSION OF CHARACTERISTICS SYSTEM

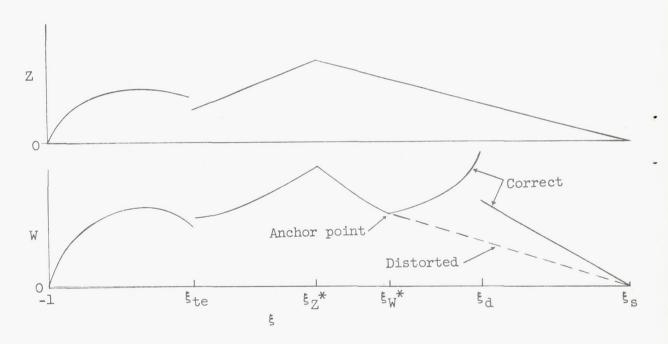
# The Characteristic Plot for the Shock Tube

Since the unifying influence on all the various particular solutions to the localized phenomena existing in the shock-tube flow (the effect of only one wall being considered) is the characteristic system, brief mention of a few significant factors will be made at this point. First, all solutions have been obtained in conical form in that everywhere Z, W,  $\lambda$ ,  $\Gamma$ , and b are functions only of  $\xi$ . Consequently, although the slopes of any characteristic curve are equal to the product of time t and a function of \$, the limiting lines dividing the integrations from  $\xi = -1$  and those from  $\xi = \xi_S$  are invariant with time. (See eqs. (53) and (54a).) A boundary-layer characteristic diagram for \$te = 0 is shown in figure 27 and may be considered typical of the diagrams for all  $\xi_{te} \leq 0.5$ . Free-stream flow characteristics and a particle path are also shown. The regions  $-1 \le \xi \le \xi_7$ \* and  $\xi_W$ \*  $\le \xi \le \xi_S$  emerge as two completely independent regions since no boundary-layer characteristic in one region was generated in the other. Only the region  $\xi_Z^* \subseteq \xi < \xi_W^*$ depends on both the expansion- and shock-wave strengths because characteristics which originated at  $\xi = -1$  and  $\xi = \xi_S$  cross this region.

From the characteristic theory, in the region of validity of the equations, there can be no discontinuity in the functions Z or W but there may be discontinuities in the derivatives of Z and W. At the location  $\xi = \xi_Z^*$ , there are discontinuities in both  $\left(\frac{\delta Z}{\delta \xi}\right)_+$  and  $\left(\frac{\delta W}{\delta \xi}\right)_+$ , whereas at the location  $\xi = \xi_W^*$  only  $\left(\frac{\delta W}{\delta \xi}\right)_-$  is discontinuous.

# Location of $\xi_W^*$ by the "Anchor Point" Method

The fortunate circumstance that Z is continuous across the entropy discontinuity (for the case of the same gas on both sides of the discontinuity) permits the analytical determination of both the location of  $\xi_W^*$  and values of W,  $\Gamma$ , and b along  $\xi_W^*$  (all of which would otherwise have to be obtained by numerical and graphical methods) and thus an "anchor point" is available toward which the graphical-isocline methods used for  $\xi_{te} \leq \xi \leq \xi_d$  must converge at  $\xi_W^*$ . The mathematical device employed to obtain this result is to shrink region  $\sigma$  to zero, to let region  $\zeta$  exist from  $\xi_{te}$  to  $\xi_s$ , and then to solve the resulting positive-shock equations. This distortion of the potential flow leaves Z completely unchanged from its distribution when  $\sigma$  is nonzero, since Z is still linear and continuous in the interval  $\xi_Z^* \leq \xi \leq \xi_s$ . (See accompanying sketch.)



Furthermore, the curve for the variation of W with  $\xi$  will remain unchanged in the interval  $\xi \leq \xi_W^*$  since the W-characteristics originate at  $\xi = -1$  and the Z-characteristics, although they originate at

V

 $\xi=\xi_{\rm S},$  carry the unchanged (correct) value of Z at each  $\xi$ . In the interval  $\xi>\xi_{\rm W}^*$ , the distribution of W is now both linear and continuous but does not represent the true distribution; however, at  $\xi=\xi_{\rm W}^*$ , the value of W is correct and can be computed analytically from its linear variation from O at  $\xi=\xi_{\rm S}.$  The terms  $\Gamma$  and b, which are constant for  $\xi_{\rm W}^* \le \xi \le \xi_{\rm S}$  in the distorted flow when region  $\sigma$  has zero width, are also the undisturbed values at  $\xi=\xi_{\rm W}^*.$ 

Physical Significance of the Critical Characteristics

The mathematical singularities  $\xi_Z^*$  and  $\xi_W^*$  of the characteristic integral solution have been found to be the limits of forward integration along a characteristic if the mathematical sequence of events is to follow the physical sequence. The further significance of these integral singularities in relation to singularities arising in the complete Prandtl boundary-layer equations and in the physical flow will be discussed in this section.

The complete unsteady Prandtl boundary-layer momentum and energy equations given in appendix E (eqs. (Ell) and (El2)) in the transformed coordinate system  $\xi, \eta, t$  contain the term  $\xi - \frac{\partial f}{\partial \eta}$  as a coefficient for  $\frac{\partial^2 f}{\partial \eta}$ ,  $\frac{\partial g}{\partial \xi}$ , and g. Consequently, singular behavior might be expected in the region where  $\xi$  approaches  $\frac{\partial f}{\partial \eta}$ .

Such singular points  $\left(\frac{u}{a_{\varepsilon}} = \frac{\partial f}{\partial \eta} = \frac{x}{a_{\varepsilon}t}\right)$  are roughly related to the

location in the boundary layer at time t of particles which were originally at x=0 and t=0. Now at x=0, t=0, when the flow was originated by the instantaneous formation of the expansion wave or shock wave or both, a singularity was propagated normal to the wall out to all values of y. This singularity coincided with the expansion wave (which at t=0 has zero thickness regardless of strength) or shock wave or both. In the case of the shock tube when both expansion waves and shock waves appear simultaneously with the diaphragm burst, the singularity is also concurrent with the position of the contact discontinuity at t=0.

The boundary-layer assumptions admit no diffusion in the streamwise direction so that this singularity is conveyed along with the boundary-layer flow and, at any time t, will appear at a value of

$$x = \int_0^t u(x,y,t) dt$$

Consequently, in the complete boundary-layer equations, the mathematical singularity at  $\xi=\frac{\partial f}{\partial \eta}$  may be assumed to have a correlation with the

physical location in the boundary layer of the generating singularity or contact discontinuity. In the shock-tube case the singularity reflects the separation within the boundary layer of the fluid accelerated by the shock from that set in motion by the expansion wave. The contact surface is analogous to the "critical characteristic" for the potential flow. The y-location of this singularity will vary from y=0 at x=0 to  $y=\delta$  at  $x=u_1t$ .

Since integral solutions are not affected by details of the flow inside the boundary layer but only take into account integrated average effects, the aforementioned singularity will also appear under averaged conditions. Instead of the singularity distribution, at various values of y for various values of  $\xi$ , which is found in the physical flow and in the complete Prandtl boundary-layer equations, the singularities are lumped together and appear for all values of  $y \le \delta$  at a particular  $\xi = \xi^*$ . The fact that the averaged location of the singularities in velocity and enthalpy do not coincide in the integral solution (that is,  $\xi_Z^* \ne \xi_W^*$ ) may be attributed to the fact that the velocity and enthalpy boundary layers are identical neither in profile shape nor in thickness. Thus the two critical characteristics represent different averaged positions of the same physical singularity.

Additional discussion of the appearance of singularities in the complete boundary-layer equations for the expansion fan may be found in reference 15. In reference 23 the case of a semi-infinite flat plate impulsively set in motion is treated, and the analogous problem of the relation between a similar singularity arising in the complete equations and that in the integral equations is examined.

#### Momentum and Energy Shocks

In any characteristics system, the merging of characteristic curves of the same family denotes the end of the continuous distribution of the dependent variables. For potential flow, the resultant discontinuous change is called a shock wave and this definition will also be applied to any discontinuous change in the boundary-layer parameters Z and W

resulting from the intersection of characteristics of the same family. Such a shock is formed by the Z-characteristics for expansion waves with values of  $\xi_{\text{te}} \geq 0.508$  because the slope of the characteristics originating from  $\xi = -1$  is greater than the slope of those originating from  $\xi = \xi_{\text{S}}$ . In figure 28 characteristic diagrams for the Z-characteristic family are sketched for the cases of

(a) 
$$\xi_{\text{te}} = -0.5 \ll 0.508$$

(b) 
$$\xi_{t,e} = 0.4 \rightarrow 0.508$$

(c) 
$$\xi_{te} = 0.508$$

(d) 
$$0.508 \le \xi_{te} \le 0.62$$

$$\xi_{t,e} = 0.55$$

(e) and (f) 
$$\xi_{te} = 1.00$$

The relative slopes of these sketches are distorted in order to indicate more clearly the convergence or divergence or both convergence and divergence of the characteristics. For values of  $\xi_{te} < 0.508$  (fig. 28(a)), there is no merging of the characteristics, although as  $\xi_{te} \rightarrow 0.508$ (fig. 28(b)) the heavy density of characteristic lines behind the expansion-fan trailing edge indicates a strong gradient. When  $\xi_{te} = 0.508$ (fig. 28(c)), the Z boundary-layer characteristic family in regions  $\zeta$ and  $\sigma$  has a slope equal to that of the upstream potential-flow characteristic (expansion-fan trailing edge) and all the Z-characteristic lines from  $\xi = -1$  are trapped at  $\xi_{te} = 0.508$  and extend to  $t = \infty$ along  $\xi_{te} = 0.508$ . This condition is the initial formation of the Z-shock due to the merging of the characteristics. For values of \$te between 0.508 and 0.62, the sketch (fig. 28(d)) is drawn for convenience with the Z-shock located concurrent with the expansion-fan trailing edge, but this location has not been established mathematically. The only mathematical restriction on the Z-shock location under this condition is that the slope of the shock must be between the slopes of the bounding characteristics.

# Methods for Extending Present Results

Since  $\lambda \geq 0$  in the fan, it can be proven for  $\xi_{\text{te}} > 0.508$  that any Z-characteristic entering the fan must be bent from its direction in region  $\zeta$  toward the trailing edge of the fan. Although computations in the expansion fan have not been extended past  $\xi = 0.62 = \xi_Z^*$  in the fan, two prime possibilities exist for flows with values at the trailing edge of  $\xi > 0.62$ . One is the shock-free flow diagramed in figure 28(e) in which the values of  $\xi$  for all the Z-characteristic lines approach  $\xi_Z^* = 0.62$  asymptotically. The other possibility, sketched in figure 28(f), shows a Z-shock which must be located at  $\xi \leq 0.62$  to permit characteristic intersection since the characteristics from  $\xi = -1$  cannot cross this line. Until the hyperbolic differential equations are solved for this region, the choice of one or the other of the flows would be purely speculative.

The method of procedure for solution where  $\xi_{\text{te}} > 0.62$  would be similar in many respects to that employed for determining the flow and shock location of a supersonic field about a cone (that is, integration backward toward the axis until certain conditions are satisfied on a ray from the origin of the conical system).

For the shock-free case, a possible procedure would be:

- (a) Assume a value of  $\left(\frac{\delta Z}{\delta \xi}\right)_{-}$  at  $\xi = 0.62$ .
- (b) Compute  $\left(\frac{\delta W}{\delta \xi}\right)_+$  at  $\xi = 0.62$ ; W and Z are equal to the value at  $\xi = 0.62$  obtained by integration from  $\xi = -1$ .
- (c) Integrate forward  $\begin{pmatrix} \delta \xi > 0 \\ \delta t > 0 \end{pmatrix}$  along  $\begin{pmatrix} \frac{\delta W}{\delta \xi} \end{pmatrix}_+$  and backward  $\begin{pmatrix} \delta \xi > 0 \\ \delta t < 0 \end{pmatrix}$  along  $\begin{pmatrix} \frac{\delta Z}{\delta \xi} \end{pmatrix}_-$  to obtain values of W and Z at various values of  $\xi$ .
- (d) By trial and error, find the value of  $\xi$  at which the trailing edge could be located in order to satisfy simultaneously equations (114b) and (114c) with the values of W and Z obtained in (c) and also the value of Z obtained by integrating forward from the corresponding shock to the trailing edge.

For the shock case the procedure would be slightly more complicated:

- (a) Assume a Z-shock location  $\xi_{\mathrm{ZS}}$
- (b) Solve simultaneously equations (114b) and (114c), with  $\frac{V}{a_c} = \xi_{ZS}$  for  $\lambda$ , b, and  $\theta$  on the positive side of  $\xi_{ZS}$
- (c), (d) Proceed as in (c) and (d) for shock-free case.

Two points of interest in regard to the preceding outline of procedure should be noted. First, it is not to be expected that every assumed slope at  $\xi=0.62$  or shock location  $\xi_{\rm ZS}$  would yield an eventual solution; in fact, one of the cases might be entirely eliminated and only a portion of the remaining case would be valid. Secondly, the possible difficulty which would be introduced if the W-characteristics either merged or reached their asymptotic value is not considered. By employing the anchor-point procedure to locate  $\xi_W^*$ , it was found that, for a shock tube employing air throughout, this difficulty arises at  $\xi_W^* = \xi_{\text{te}} = 2.25$ .

THE COMPLETE SOLUTION FOR THE BOUNDARY LAYER IN A SHOCK TUBE FOR  $\gamma=1.4$ ,  $R_{\rm c}=R_{\rm m}$ , AND  $\lambda \le 20$ 

Combination, on the basis of the boundary-layer characteristics system, of the component solutions described in the foregoing sections results in the general solution for the laminar boundary layer in a shock tube in the entire region affected by the shock or expansion wave. The solution for the case of  $\xi_{te}=0$  is illustrated in figures 29 to 32 by the solid lines. The dashed lines show possible smoothing or rounding off of the discontinuities. The trends shown by these figures are typical of the other values of  $\xi_{te}$ .

Since the solution for the flows inside the expansion fan and between the shock and entropy discontinuity have been discussed in detail, a brief discussion of the behavior only in the region  $\xi_{te} \leq \xi \leq \xi_d$  is presented. Here Z was computed analytically and W, by graphical integration. Figures 29 and 30 show Z to be linear and continuous in this range with a discontinuity in slope at  $\xi_Z^*$ ; whereas W is almost linear for  $\xi_{te} \leq \xi \leq \xi_W^*$  and then displays very strong curvature as  $\xi \to \xi_d$  because of the adjusting process required after the entropy discontinuity. The value of b changes very little for  $\xi_{te} < \xi < \xi_W^*$  and then becomes very small as W becomes large  $(\xi \to \xi_d)$ .

In the constant-pressure region between  $\xi_{te}$  and  $\xi_{Z}^{*}$ ,  $\hat{\tau}_{\varepsilon}$  and  $\hat{q}_{\varepsilon}$  decrease in a manner similar to the decrease found either in the flow over a semi-infinite flat plate or behind a shock or negative shock as the distance from the leading edge or shock increases. In fact, in regard to Z and  $\hat{\tau}_{\varepsilon}$ , the flow between  $\xi_{te}$  and  $\xi_{Z}^{*}$  is identical to that behind a negative shock of velocity  $\xi_{S} = \xi_{ZO}$  ( $\xi_{ZO}$  is the point in fig. 29 where linear extrapolation of the curve of the variation of Z with  $\xi$  intersects the Z-axis), the outer potential-flow conditions being identical to those in region  $\zeta$ .

The value of  $\hat{\tau}_{\varepsilon}$  reaches a minimum at  $\xi_Z^*$  and increases continuously and monotonically thereafter to a theoretically infinite value at the shock. On the other hand,  $\hat{q}_{\varepsilon}$  rises slightly from  $\xi_Z^*$  to  $\xi_W^*$  and then begins the rapid adjustment to the large negative values existing at the entropy discontinuity. The zero heat-transfer point appears in the interval between  $\xi_W^*$  and  $\xi_{d}$ . Between the entropy discontinuity and the shock, the value of  $\hat{q}_{\varepsilon}$  decreases continuously and monotonically to  $-\infty$ .

A composite diagram of the distribution of velocity and enthalpy in the boundary layer of the shock-tube flow is shown in figure 33 to complete the description of the entire boundary-layer flow for  $\xi_{te}=0$ . In parts (a) and (b) of figure 33, the profiles existing at the various values of  $\xi$  are plotted at that value of  $\xi$ , and in part (c) the extent and location of the various waves and regions are indicated. The profiles existing on both sides of the trailing-edge discontinuity are drawn. The enthalpy profiles existing on opposite sides of the entropy discontinuity have been illustrated previously in figure 25. The maximum boundary-layer thicknesses are located at the entropy discontinuity at any given time t and a second smaller maximum in velocity boundary-layer thickness is located at  $\xi_Z^*$ .

Complete distributions of  $\hat{\tau}_{\varepsilon}$  and  $\hat{q}_{\varepsilon}$  in the shock tube for various matched values of expansion- and shock-wave strength are plotted in figures 34 and 35. (Large-size working plots of figs. 34 and 35 are available on request from NACA Headquarters, Washington, D. C.) These curves, similar to those for  $\xi_{te}=0$  discussed previously, permit the evaluation of the wall shear and heat transfer at any point x,t or  $\xi$ ,t in a shock tube by using a single gas having  $\gamma=1.4$  and Npr = 0.72 for shock-pressure ratios up to approximately 5. The dashed line, representing the expansion-fan solution, is used for  $\xi \leq \xi_{te}$  and the solid lines, employed thereafter, are used for the constant-pressure regions  $\zeta$  and  $\sigma$ . These curves may be used in conjunction with the equations of reference 7 to predict waves generated by wall effects on an averaged basis (thick boundary Jayer).

layer.

If the method of reference ll (thin boundary layer) is used to predict the wave generation, it is necessary to determine the vertical velocity  $\mathbf{v}_\delta$  existing at the edge of the boundary layer. Integration of the continuity equation (eq. (B3)) from y=0 to  $y=\delta$  and application of the boundary condition  $\mathbf{v}_W=0$  results in the following expression for  $\mathbf{v}_\delta$ :

$$v_{\delta} \; \varrho_{\text{I}} \sqrt{\frac{t}{\nu_{\varepsilon} Z}} = - \frac{1}{2} \frac{h_{\text{I}} *}{h_{\text{I}}} \left( \!\!\! \frac{\nabla \!\!\! *}{\nabla} \; \frac{1}{b} \; \frac{\Delta}{\theta} \right) + \; \left( \!\!\! \left[ \!\! \left[ \!\!\! \left[ \!\! \left[ \!\!\! \left[ \!\!\! \left[ \!\! \left[ \!\!\! \left[ \!\!\! \left[ \!\!\! \left[ \!\!\! \left[ \!\!\! \left[ \!\! \left[ \!\!\! \left[ \!\!\! \left[ \!\! \left[ \!\!\! \left[ \!\!\! \left[ \!\!\! \left[ \!\! \left[ \right[ \right[ \right[ \right[ \right[ \right[ \left[ \!\! \left[ \right[ \right[ \right[ \right[ \right[ \right[ \right[ \left[ \right[ \left[ \right[ \right[ \right[ \right[ \right[ \right[ \right[ \right[ \left[ \right[ \right[ \right[ \right[ \right[ \right[ \right[ \right[ \right[ \left[ \right[ \right[ \right[ \right[ \right[$$

The nondimensional parameter  $v_\delta\sqrt{\frac{t}{\nu_\varepsilon}}$  is plotted as a function of  $\xi$  in figure 36 for the expansion fan in general and for particular values of expansion-fan strengths  $\xi_{te}=-0.6$ , 0, and 0.5. Also shown in this figure is the empirical curve  $v_\delta\sqrt{\frac{t}{\nu_\varepsilon}}=1.360\sqrt{1+\xi}$ . This curve gives a very close approximation to the computed results in the fan and would prove to be useful in the analytical integrations required if the method of reference 11 were to be extended to consider the expansion fan correctly. The rapid increase in  $v_\delta$  as  $\xi \to \xi_d$  is due to the rapid increase in boundary-layer thickness in this region because of the pres-

# APPROXIMATE SOLUTIONS FOR THE BOUNDARY LAYER IN A

ence of the hotter gas (low density) from of entrained in the boundary

#### SHOCK TUBE USING ONLY ONE FLUID

The complexity of the solutions to the reduced hyperbolic differential equations for the shock-tube flows is such that an approximate solution resulting in a large reduction in effort with only a small loss in accuracy would be most desirable. Such an approximate solution is described in this section. For purposes of discussion, the previous numerical and graphical solutions to the differential equations will be termed "correct" or "exact."

# Negative-Shock Approximation for the

#### Expansion Fan and Region (

The simplest approximation available is the replacement of the expansion fan by a negative shock. This substitution was first suggested in reference 7 and was also used as the basis for the computations of references ll and 13. In figures 29 to 32, which represent conditions in an air-air shock tube with  $\xi_{te}=0$ , the results obtained by the negative-shock assumption with both consideration and neglect of the critical characteristics are plotted for comparison with the correct integral solution. (Similar results are obtained for other values of  $\xi_{te}$ , the discrepancy between the negative-shock and correct solution increasing or decreasing as  $\xi_{te}$  increases or decreases.)

The skin-friction parameter  $\hat{\tau}_{\varepsilon}$  in the region  $\xi \geq \xi_Z^*$  does not depend upon the expansion when the critical characteristic is considered and is hence the same for both methods; this fact is also true for  $\hat{q}_{\varepsilon}$  in the region  $\xi \geq \xi_W^*$ . It is evident that the negative-shock distribution is a very poor approximation to the skin friction and heat transfer within the fan and that qualitative agreement exists only in the region  $\xi t \leq \xi_Z^*$ .

If it is assumed (by neglecting the critical characteristics) that the negative-shock solution is valid from the leading edge of the expansion fan all the way to the entropy discontinuity (refs. 7, ll, and 13), the distribution between  $\xi_Z^* \leq \xi \leq \xi_d$  is shown by the heavy extensions to the negative-shock curves. Neglect of the critical characteristics is tantamount to assuming that the flow generated by a negative shock which originated at time t=0 is equivalent to a flow generated by a negative shock of the same strength originating at  $t=-\infty$ .

#### Modified Negative-Shock Approximation

Inside expansion fan. In view of the failure of the simple negative-shock method to produce results that even qualitatively approximate the true expansion-fan results, a more refined method of approximating the expansion-fan solution with the negative shock as a basis was devised and applied to the entire shock-tube boundary layer. The relation between the true fan and the negative-shock wall-shear and heat-transfer functions for the vanishingly weak wave has been discussed and was found to be:

V

For  $\xi = \xi_{te} \rightarrow -1$ :

$$\frac{\left[\hat{\tau}_{\epsilon}(\xi)\right]_{Fan}}{\left[\hat{\tau}_{\epsilon}(\xi_{te})\right]_{Negative shock}} = 2.000$$

and

$$\frac{\left[\hat{q}_{\epsilon}(\xi)\right]_{\text{Fan}}}{\left[\hat{q}_{\epsilon}(\xi_{\text{te}})\right]_{\text{Negative shock}}} = 2.000$$

If these relations are assumed to be valid not only in the limit  $\xi \to -1$  but also throughout the entire expansion fan, the distribution of  $\hat{\tau}_{\varepsilon}$  and  $\hat{q}_{\varepsilon}$  may be approximated as follows: At a given value of  $\xi$  inside the expansion fan, let the value of  $\hat{\tau}_{\varepsilon}$  or  $\hat{q}_{\varepsilon}$  be twice the value (at this  $\xi$ ) obtained from the negative-shock solution for a constant potential flow identical to that existing at  $\xi$ .

The results of this approximation along with the correct expansionfan results are plotted in figures 37 and 38 for  $\gamma = 1.40$  and  $N_{Pr} = 0.72$ . The approximation for  $\,\hat{\tau}_{\varepsilon}\,$  is seen to have a negligible error for  $\,\xi<0\,$ and an error of only 13 percent at  $\xi = 0.5$  (approximately the critical characteristic for the negative shock). The approximation for  $\, \hat{q}_{\epsilon} \,$  diverges at lower values of  $\xi$ , reaches an error of 20 percent at  $\xi$  = -0.5, and increases thereafter. The reason for the relatively close agreement for  $\hat{ au}_{\epsilon}$  over a large range of  $\xi$  and the more rapid divergence of  $\hat{ au}_{\epsilon}$  lies in the fact that  $\,\,\hat{q}_{\varepsilon}\,\,$  is much more sensitive to the boundary-layer past history of varying values of H<sub>1</sub> at the edge of the boundary layer. fact, the approximate value of  $\hat{q}_{\epsilon}$  would not become zero until after  ${\rm H_1} > {\rm H_W}$  (r < 1) whereas the correct  $\hat{\rm q}_{\rm c}$  becomes zero at  $\xi \approx 0.5$  where  ${\rm H_1} < {\rm H_W}$  (r > 1). Therefore, in order to compensate for this effect, the approximate curve for the variation of  $\, \hat{q}_{\boldsymbol{\varepsilon}} \,$  with  $\, \boldsymbol{\xi} \,$  in the range  $-0.5 \le \xi \le 0.5$  is replaced by a straight line originating at the approximate value of  $\hat{q}_{\varepsilon}$  at  $\xi = -0.5$  and passing through zero at  $\xi = 0.5$ . The equation for  $H_1^*$  is

$$H_1 * = \frac{\gamma - 1}{\gamma + 1} (\xi^2 - 1) H_W$$

Consequently, the value of  $H_1^*$  passes through a minimum at  $\xi=0$  and becomes 0 at  $\xi=1$  irrespective of  $\gamma$ ; therefore, the linear approximation should be appropriate for other values of  $\gamma$ . The possible error introduced by the linear approximation for values of  $N_{Pr}$  other than 0.72 is not predictable.

In region  $\zeta$ .- In the limit of  $\xi \rightarrow -1$ , the relation

$$\frac{\left[Z(\xi)\right]_{\text{Fan}}}{\left[Z(\xi_{\text{te}})\right]_{\text{Negative shock}}} = 0.56 \approx \frac{1}{2}$$

for  $\xi=\xi_{te}\to -1$  was found to apply. It is now assumed that this relation is also applicable at the trailing edge of all finite expansion fans. In addition, at the trailing edge of the fan, the matching solution showed that the approximation  $\frac{Z_1}{Z_j}\approx 1.0$  was appropriate. Thus the value of Z on the  $\zeta$ -side of the trailing edge of the expansion fan may be closely approximated as

$$Z(\xi_{te})_{\zeta} = \frac{1}{2} \left[ Z(\xi_{te}) \right]_{Negative shock, \zeta}$$
 (-1 \le \xi \le 0.5) (147)

where the negative shock is that which produces conditions of region  $\zeta$  behind it. Figure 39 shows that this approximation compares closely with the correct values. The Z-distribution in the range  $\xi_{te} \leq \xi \leq \xi_{Z}$  is linear and may be computed from equation (102). The shear stress follows from equation (130) if a zero value for  $\lambda$  is used.

The heat-transfer parameter  $\hat{q}_{\varepsilon}$  for  $\xi_{te} \leq \xi \leq \xi_Z^*$  was computed from equation (133a) by using the values of  $\hat{\tau}_{\varepsilon}$  described previously and values of  $b(B_1)$  from the negative-shock solution. In this respect, it should be noted that the value of b in the correct solution changes only slightly in the interval  $\xi_{te} \leq \xi \leq \xi_W^*$  and, furthermore, the value of b for the corresponding negative shocks is a good approximation to the b-values in the region  $\xi$  for  $\xi < \xi_W^*$ .

The distribution of  $\hat{q}_{\varepsilon}$  for  $\xi_Z^* \leq \xi \leq \xi_W^*$  was assumed to be linear (correct solution was nearly linear, fig. 35) and the value of  $\hat{q}_{\varepsilon}(\xi_W^*)$  was computed by the anchor-point method. For the interval  $\xi_W^* \leq \xi \leq \xi_d$ , an inspection of the correct solution shows the following:

$$\frac{\mathrm{d}\hat{q}_{\epsilon}}{\mathrm{d}\xi} \approx 0$$

at  $\xi = \xi_W^*$ ,

$$\frac{\mathrm{d}\mathbf{\hat{q}_{\varepsilon}}}{\mathrm{d}\mathbf{\xi}} << -1$$

at  $\xi = \xi_d$ , and

$$(\hat{q}_{\epsilon})_{\zeta} \approx (\hat{q}_{\epsilon})_{\sigma}$$

at  $\xi = \xi_d$ .

Consequently, the following interpolation formula which gives  $\left(\frac{d\hat{q}_{\varepsilon}}{d\xi}\right)_{\xi_{W}^{*}} = 0, \quad \left(\frac{d\hat{q}_{\varepsilon}}{d\xi}\right)_{\xi_{d}} = -\infty, \text{ and } (\hat{q}_{\varepsilon})_{\zeta} = (\hat{q}_{\varepsilon})_{\sigma} \text{ at } \xi_{d} \text{ was used (the square-root term was used to make the slope a weak infinity at } \xi_{d}):$ 

$$\widehat{q}_{\epsilon}(\xi) = \widehat{q}_{\epsilon}(\xi_{W}^{*}) + \left\{ \left[ \widehat{q}_{\epsilon}(\xi_{d}) \right]_{\sigma} - \widehat{q}_{\epsilon}(\xi_{W}^{*}) \right\} \frac{\xi - \xi_{W}^{*}}{\xi_{d} - \xi_{W}^{*}} \left( 1 - \sqrt{\frac{\xi - \xi_{d}}{\xi_{W}^{*} - \xi_{d}}} \right) \quad (148)$$

The value of  $\left(\hat{q}_{\varepsilon}\right)_{\sigma}$  at  $\xi_{d}$  is known from the positive-shock solution.

Summary of modified solution. The refined approximate solution for the boundary layer in a shock tube when the same gas is used throughout is outlined as follows:

Inside fan:

$$\left[\hat{\tau}_{\epsilon}(\xi)\right]_{\text{Fan}} \approx 2\left[\hat{\tau}_{\epsilon}(\xi_{\text{te}})\right]_{\text{Negative shock, } \xi_{\text{te}}=\xi} \qquad (-1 \le \xi \le 0.5)$$

$$\left[\hat{q}_{\epsilon}(\xi)\right]_{\text{Fan}} \approx 2\left[\hat{q}_{\epsilon}(\xi_{\text{te}})\right]_{\text{Negative shock, }\xi_{\text{te}}=\xi}$$
 (-1 \le \xi \le \zeft \le -0.5)

$$\left[\hat{q}_{\epsilon}(\xi)\right]_{\text{Fan}} \approx 2(0.5 - \xi) \left[\hat{q}_{\epsilon}(\xi_{\text{te}})\right]_{\text{Negative shock, } \xi_{\text{te}}=-0.5}$$

$$(-0.5 \le \xi \le 0.5)$$

Region ζ:

(a) 
$$\xi = \xi_{te}$$
:  $Z(\xi_{te}) \approx \frac{1}{2} [Z(\xi_{te})]$  Negative shock,  $\xi_{te}$ 

- (b)  $\xi_{\text{te}} \leq \xi \leq \xi_{\text{Z}}^*$ : The value of Z is obtained from equation (102) by using  $\xi_{\text{te}}$  as the base point;  $\hat{\tau}_{\varepsilon}$  is obtained from equation (130); and  $\hat{q}_{\varepsilon}$  is obtained from equation (133a) by using values of b and  $B_{\text{l}}$  from the negative-shock solution.
- (c)  $\xi_Z^* \leq \xi \leq \xi_W^*$ : The value of Z is obtained from equation (102) by using  $\xi_d$  as the base point;  $\hat{\tau}_{\varepsilon}$  is obtained from equation (130) (Z and  $\hat{\tau}_{\varepsilon}$  are also exact values);  $\hat{q}_{\varepsilon}$  is linear; and the value of  $\hat{q}_{\varepsilon}(\xi_W^*)$  is obtained by the anchor-point method.
- (d)  $\xi_W^* \leq \xi \leq \xi_d$ : The values of Z and  $\hat{\tau}_\varepsilon$  are the same as those for condition (c) (these are exact values); and  $\hat{q}_\varepsilon$  is obtained from equation (148).

The results of this approximation for the shock-tube flow are compared with the correct solution for three expansion and shock strengths ( $\gamma=1.4$  and Npr = 0.72) in figures 40 and 41. In region  $\sigma$  the approximate and exact solutions are identical. The agreement between the approximate and exact methods is seen to be very favorable for the cases represented.

This approximate method is assumed to be applicable for Npr other than 0.72 and the approximate wall-shear and heat-transfer distributions have been computed for the case where the same gas exists in both  $\varepsilon$  and  $\infty$  with  $\gamma$  equal to 1.4 and Npr equal to unity. The appropriate shock and negative-shock results were utilized and heat-transfer results are shown in figure 42. The skin friction is identical to that for Npr = 0.72 for the preceding approximation since the constant potential-flow momentum equation is independent of Npr. However, in the exact solution  $\widehat{\tau}_{\varepsilon}$  depends on Npr in the fan through the pressure-gradient term in the momentum equation; this dependence would influence the entire region  $\xi \leq \xi_Z^*$ . This dependence is probably small and is neglected herein.

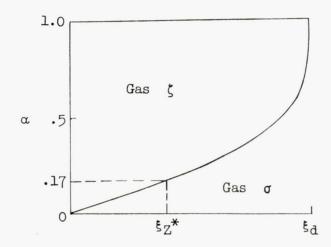
# APPROXIMATE SOLUTION FOR THE BOUNDARY LAYER IN A SHOCK TUBE USING TWO DIFFERENT FLUIDS

In order to obtain large shock-pressure ratios in constant-area shock tubes, it is common practice to use a gas with a high speed of sound as the driver gas in the high-pressure chamber. Hydrogen or helium are two such gases often employed. When various expansion-fan strengths for hydrogen or helium are matched to the appropriate values of shock strengths for air, the boundary-layer solutions of the resulting shock-tube flow in the regions  $\xi<0$  or  $\xi>\xi_{\rm d}$  may be determined by either the exact or the approximate methods described previously.

However, the region  $0 \le \xi \le \xi_d$  presents additional difficulty if an exact solution is to be found. This difficulty arises because the boundary layer in this region contains both gases which were initially ahead of and behind the diaphragm, the inner part of the boundary layer being comprised mainly of the gas that was originally in  $\sigma$  and vice versa. The relative distribution and concentration of these gases through the boundary layer will depend on many factors, one of which is diffusion normal to the wall. Instead of attempting to solve this problem exactly, the approximate method described in the following paragraphs was employed.

92 NACA TN 3944

First, it was assumed that the wall effects of the boundary layer in the region  $0 \le \xi \le \xi_Z^*$  were identical to those which would have existed if the boundary layer contained only the gas of region  $\zeta$ . This description of the boundary layer becomes more erroneous as  $\xi$  increases from zero, since the relative concentration of the gas  $\sigma$  will increase in the interval from  $\xi = 0$  to  $\xi_d$ . An approximation to the magnitude of the errors so introduced can be obtained from the following sketch in which the velocity profile for  $\lambda = 0$  is assumed to represent roughly the locus of the undiffused contact surface in the boundary layer between the diaphragm station and the entropy discontinuity.



At  $\xi_Z^*$   $\left(\frac{u}{u_1} = \frac{\theta}{\delta^*} = 0.404\right)$ , the contact surface inside the boundary layer is at a value of  $\alpha \approx 0.17$ ; thus, for  $\xi < \xi_Z^*$ , most of the boundary layer is comprised of gas  $\zeta$ .

The heat transfer and skin friction for  $0 \le \xi \le \xi Z^*$  can now be found from forward integration along the characteristics originating in  $\xi < 0$  or by the modified negative-shock approach discussed previously.

The next assumption was that across the contact surface the momentum deficiencies (that is,  $\int_0^\infty \rho \; \frac{u}{u_1} \left(1 - \frac{u}{u_1}\right) \mathrm{d}y$ ) of the boundary layer were

equal, a known fact for the case of the same gas on both sides of the discontinuity since  $\theta_{\rm i}=\theta_{\rm j}.$  This assumption appears to be reasonable because the velocity boundary layer in the vicinity of the entropy discontinuity is comprised almost entirely of the gas  $\sigma.$ 

Since the momentum thickness  $\theta$  as well as Z in region  $\sigma$  is usually computed by using values of  $\mu_W$  for the gas  $\sigma$ , the necessary general conversion factors are summarized here. In this section, subscripts denote the reference condition, and the conversion is based on the equivalence of the momentum deficiencies at any  $\xi$ .

$$\theta_{\epsilon} \rho_{\epsilon} = \int_{0}^{\infty} \rho \, \frac{u}{u_{1}} \left( 1 - \frac{u}{u_{1}} \right) dy = \theta_{\infty} \rho_{\infty}$$
 (149)

$$Z_{\epsilon} = \frac{\theta_{\epsilon}^{2}}{\nu_{\epsilon}t} = Z_{\infty} \frac{\rho_{\infty}\mu_{\infty}}{\rho_{\epsilon}\mu_{\epsilon}}$$
 (150)

Equations (149) and (150) would be used, for example, for a hydrogenair shock tube to evaluate Z in terms of hydrogen in state  $\epsilon$  from a known Z in terms of air in state  $\infty$ .

A linear variation is now assumed as the simplest approximation to the distribution for  $Z_{\varepsilon}$  and  $\rho_w \mu_w$  in the range  $\xi_Z^* \leq \xi \leq \xi_d$ ; thus

$$Z_{\epsilon}(\xi) = Z_{\epsilon}(\xi_{Z}^{*}) + \frac{\xi - \xi_{Z}^{*}}{\xi_{d} - \xi_{Z}^{*}} \left[ Z_{\epsilon}(\xi_{d}) - Z_{\epsilon}(\xi_{Z}^{*}) \right] \qquad (\xi_{Z}^{*} \leq \xi \leq \xi_{d}) \qquad (151)$$

where

$$Z_{\epsilon}(\xi_{d}) = Z_{\infty}(\xi_{d}) \frac{\rho_{\infty}\mu_{\infty}}{\rho_{\epsilon}\mu_{\epsilon}}$$

and

$$\rho_{W}(\xi) \ \mu_{W}(\xi) = \rho_{W}(\xi_{Z}^{*}) \ \mu_{W}(\xi_{Z}^{*}) + \frac{\xi - \xi_{Z}^{*}}{\xi_{d} - \xi_{Z}^{*}} \left[ \rho_{W}(\xi_{d}) \ \mu_{W}(\xi_{d}) - \rho_{W}(\xi_{Z}^{*}) \ \mu_{W}(\xi_{Z}^{*}) \right]$$

$$= \rho_{W}(\xi_{Z}^{*}) \ \mu_{\varepsilon} + \frac{\xi - \xi_{Z}^{*}}{\xi_{d} - \xi_{Z}^{*}} \left[ \rho_{W}(\xi_{d}) \ \mu_{\infty} - \rho_{W}(\xi_{Z}^{*}) \ \mu_{\varepsilon} \right] \qquad (\xi_{Z}^{*} \leq \xi \leq \xi_{d}) \qquad (152)$$

94 NACA TN 3944

since  $T_w = T_\varepsilon = T_\infty$  and since the boundary-layer gas at the wall was assumed to be  $\zeta$  at  $\xi Z^*$  and  $\sigma$  at  $\xi_d$ . The shear stress may then be evaluated from equations (130), (151), and (152) as

$$\frac{\hat{\tau}_{\varepsilon}(\xi)}{\hat{\tau}_{\varepsilon}(\xi_{Z}^{*})} = \frac{\rho_{w}(\xi) \ \mu_{w}(\xi)}{\rho_{w}(\xi_{Z}^{*}) \ \mu_{w}(\xi_{Z}^{*})} \sqrt{\frac{Z_{\varepsilon}(\xi_{Z}^{*})}{Z_{\varepsilon}(\xi)}} = \frac{1 + \frac{\xi - \xi_{Z}^{*}}{\xi_{d} - \xi_{Z}^{*}} \left[ \frac{\rho_{w}(\xi_{d}) \ \mu_{\infty}}{\rho_{w}(\xi_{Z}^{*}) \ \mu_{\varepsilon}} - 1 \right]}{\sqrt{1 + \frac{\xi - \xi_{Z}^{*}}{\xi_{d} - \xi_{Z}^{*}} \left[ \frac{Z_{\varepsilon}(\xi_{d})}{Z_{\varepsilon}(\xi_{Z}^{*})} - 1 \right]}}$$

$$(\xi_{Z}^{*} \leq \xi \leq \xi_{d})$$

$$(153)$$

For heat-transfer computations, the region  $\xi_Z^* \leq \xi \leq \xi_d$  is divided into two areas by the line  $\xi_W^*$ , its value having been determined from the value of b of the appropriate negative-shock solution. The anchorpoint method of the previous solutions is not applicable here because Ze is not unchanged in the interval  $\xi_Z^* \subseteq \xi \subseteq \xi_S$  when the region  $\sigma$  is shrunk to zero width. However, the values of b found in the other solutions from the negative-shock and anchor-point methods did not differ greatly; therefore, the value of  $\xi_W^*$  (which is a function of b) obtained by using b of the negative-shock solution should be a fair approximation. The value of  $\hat{q}_{\in}(\xi_{\mathbb{W}}^{*})$  is then determined from equations (133a) and (153) with the use of the negative-shock values of  $b(B_1)$ . Again, as in the single-gas approximation, a linear variation is used for  $\hat{q}_{\epsilon}$  in the interval  $\xi_Z^* \leq \xi \leq \xi_W^*$ , and the interpolation formula (eq. (148)) is applied in the interval  $\xi_W^* \leq \xi \leq \xi_d$ . The value of the heat transfer at the entropy discontinuity to be used in equation (148) is

$$\left[\hat{\mathbf{q}}_{\epsilon}(\boldsymbol{\xi}_{\mathrm{d}})\right]_{\sigma} = \left[\hat{\mathbf{q}}_{\infty}(\boldsymbol{\xi}_{\mathrm{d}})\right]_{\sigma} \left(\frac{\mathbf{a}_{\epsilon}}{\mathbf{a}_{\infty}}\right)^{2} \sqrt{\frac{\rho_{\epsilon}\mu_{\epsilon}}{\rho_{\infty}\mu_{\infty}}}$$
(154)

The summary of the modified solution for two different gases may be outlined as follows:

- (a)  $\xi < \xi_Z^*$  or  $\xi > \xi_d$ : The solution is the same as the corresponding solution for a single gas.
- (b)  $\xi_Z^* \leq \xi \leq \xi_W^*$ : The value of  $\xi_W^*$  is obtained from the negative-shock solution; the value of  $\hat{\tau}_{\epsilon}(\xi)$  is obtained from equation (153); the

NACA TN 3944

V

term  $\hat{q}_{\epsilon}(\xi)$  is linear from  $\hat{q}_{\epsilon}(\xi_Z^*)$  to  $\hat{q}_{\epsilon}(\xi_W^*)$ ; and the value of  $\hat{q}_{\epsilon}(\xi_W^*)$  is obtained from  $\hat{\tau}_{\epsilon}(\xi_W^*)$  and equation (133a).

(c)  $\xi_W^* \leq \xi \leq \xi_d$ : The value of  $\hat{\tau}_{\epsilon}(\xi)$  is obtained from equation (153); and the value of  $\hat{q}_{\epsilon}(\xi)$  is obtained from equation (148).

Wall-shear and heat-transfer distributions were obtained when an exact solution was unavailable by this approximate method for two gases for shock-tube flows using air ( $\gamma=1.40$  and Npr = 0.72) in the region  $\infty$  and hydrogen or helium in the region  $\epsilon$ . The properties of the hydrogen and helium employed, the viscosity being evaluated at room temperature, are indicated in the following table:

Gas	$\frac{\gamma_{\in}}{\gamma_{\infty}}$	$\frac{\left(N_{\rm Pr}\right)_{\epsilon}}{\left(N_{\rm Pr}\right)_{\infty}}$	$\frac{R_{\mathbf{\epsilon}}}{R_{\mathbf{\infty}}}$	<u>μ</u> <sub>€</sub>	<u>a</u> € a <sub>∞</sub>
Helium	1.190	1.000	7.236	1.082	2.935
Hydrogen	1.000	1.000	14.365	0.485	3.790

For the hydrogen-air combination, exact solutions are available for  $\xi>\xi_d$  and for  $\xi<0$  (since  $\gamma_{H_2}=\gamma_{air}$ ). The assumption that only gas  $\zeta$  comprised the boundary layer for  $0 \le \xi \le \xi_Z^*$  permitted the exact solution ( $\gamma=1.4$ ) to be extended to  $\xi_Z^*$  for this case. The approximate solution was used for  $\xi_Z^* \le \xi \le \xi_d$  for the hydrogenair combination and also for  $-1 \le \xi \le \xi_d$  for the helium-air combination.

The results of these computations are shown in figures 43 to 46 in which  $\xi_{te}$  is used as a cross-plotting parameter. (Large-size working plots of these figures are available on request from NACA Headquarters, Washington, D. C.) Distributions of  $\hat{q}_{\varepsilon}$  and  $\hat{\tau}_{\varepsilon}$  desired for a specific shock-pressure ratio may be obtained by interpolation from figures 43 to 46 and by use of the data from figure 47 which gives the values of  $\xi_{te}$  as a function of shock-pressure ratio for helium-air and hydrogenair shock tubes.

For helium,  $\xi_Z^* = \xi_{te}$  when  $\xi_{te} = 0.435$ ; this value of  $\xi_{te}$  corresponds to a shock-pressure ratio  $\frac{p_\sigma}{p_\omega} \approx 19$  for a helium-air shock tube. For hydrogen,  $\xi_Z^* = \xi_{te}$  when  $\xi_{te} = 0.508$ ; this value corresponds to a shock-pressure ratio  $\frac{p_\sigma}{p_\omega} \approx 40$  for a hydrogen-air shock tube.

#### CONCLUDING REMARKS

A solution to the unsteady laminar boundary-layer flow inside centered expansion waves and behind both centered expansion waves and shock waves has been obtained in this report.

- 1. The general method for obtaining these solutions may be summarized as follows:
- (a) The unsteady Prandtl boundary-layer equations are reduced by integration normal to the surface.
- (b) The velocity and temperature profiles are expanded in a power series.
  - (c) The wall temperature is assumed to be constant.
- (d) The reduced equations are transformed into hyperbolic equations in a conical coordinate system because the free-stream flow is conical.
- (e) The reduced hyperbolic equations are solved in closed form for the flow behind a shock and by numerical integration for the flow inside or behind the expansion fan. Multiple solutions were found inside the expansion fan and the correct one was selected by physical reasoning.
- (f) The integral technique is applied at the discontinuities existing at the trailing edge of the expansion fan and at a contact surface so that the characteristic solution may proceed across these discontinuities.
- 2. For the problem of the entire two-dimensional, nonstationary laminar boundary layer in a shock tube, the following solutions were obtained:
- (a) An "exact" solution for an air-air shock tube (for a ratio of specific heats of 1.4 and at a Prandtl number of 0.72) was obtained with the method described in the preceding paragraph. Inside weak expansion waves

waves and in the flow region bounded by the shock and contact discontinuity, solutions also exist to the complete Prandtl boundary-layer equations. The integral solution agreed extremely well with these solutions.

97

(b) Approximate solutions in closed form, employing zero-thickness expansion-fan results as a basis, for the following cases:

Air-air shock tube; Prandtl number of 0.72

Air-air shock tube; Prandtl number of 1.00

Helium-air shock tube; Prandtl number of 0.72

Hydrogen-air shock tube; Prandtl number of 0.72

The approximate (or modified negative shock) and "exact" solutions for air-air shock tube (Prandtl number of 0.72) exhibited very good agreement. The simple zero-width expansion-fan solutions gave very poor agreement.

- 3. Some of the more important features of the "exact" solution are:
- (a) The existence of zones of influence limiting the extent of forward integration along a characteristic. The solution of the present report was arbitrarily halted inside the expansion wave at the boundaries of one of these zones.
- (b) The existence of momentum and energy shocks or jumps inside the boundary layer.
- (c) The fact that skin friction and heat transfer inside the expansion wave near the leading edge was twice that for a corresponding zero-pressure-gradient potential (that is, Rayleigh) flow.
- 4. Note should be taken of the fact that the boundary-layer characteristic system in conical coordinates derived in this paper is only a special case of the universal compressible-boundary-layer characteristics system obtainable from the integrated form of the Prandtl equations. This universal boundary-layer characteristics system is applicable to unsteady compressible boundary layers in general and provides a powerful tool for the attack on the problem of wall effects in nonstationary flows.

Langley Aeronautical Laboratory,
National Advisory Committee for Aeronautics,
Langley Field, Va., January 30, 1957

#### APPENDIX A

# EXPRESSIONS FOR VARIOUS FUNCTIONS IN A CENTERED

# EXPANSION WAVE MOVING INTO FLUID AT REST

The wave is assumed to have the coordinates x=0, t=0 at its origin or center and to have a leading edge which advances into the region x<0 for t>0. The Riemann invariant (see, for example, ref. 24) prescribes the relation, valid everywhere in the wave, between  $\underline{u}_1$  and  $\underline{a}_1$  as follows:

$$\underline{u}_{1} + \frac{2}{\gamma - 1} \underline{a}_{1} = \frac{2}{\gamma - 1} \qquad \left(\underline{u}_{1} = \frac{\underline{u}_{1}}{\underline{a}_{\epsilon}}; \underline{a}_{1} = \frac{\underline{a}_{1}}{\underline{a}_{\epsilon}}\right) \tag{A1}$$

Since a characteristic (wave) moves with a speed equal to the algebraic difference of the speed of sound and fluid speed, a definite relation exists between x and t at a point dependent on the value of  $\underline{u}_1$  and  $\underline{a}_1$  at the point x,t.

$$x = \left(\underline{u}_{1} - \underline{a}_{1}\right) a_{\epsilon} t \tag{A2}$$

$$\xi = \frac{x}{a_{\epsilon}t} = \underline{u}_{1} - \underline{a}_{1} \tag{A3}$$

A combination of equations (Al) and (A3) results in the expressions for the conical form of  $\underline{u}_1$  and  $\underline{a}_1$ :

$$\underline{\mathbf{u}}_{1} = \frac{2}{\gamma + 1} \left( 1 + \xi \right) \tag{A4}$$

$$\underline{\mathbf{a}}_{1} = \frac{1 - \frac{\gamma - 1}{2} \, \xi}{\frac{\gamma + 1}{2}} \tag{A5}$$

The assumption of constant specific heat permits the expression of enthalpy in terms of speed of sound. Also, since the flow is isentropic, the pressure and density may be related to the speed of sound. The following equivalents are then obtained:

(A6)

$$M_{\perp} = \frac{1 + \xi}{1 - \frac{\gamma - 1}{2} \xi}$$

$$\frac{h_1}{h_{\epsilon}} = \underline{a}_1^2 = \frac{\left(1 - \frac{\gamma - 1}{2} \xi\right)^2}{\left(\frac{\gamma + 1}{2}\right)^2}$$

$$\underline{p}_{1} = \frac{p_{1}}{p_{\epsilon}} = \left(\underline{a}_{1}\right)^{\frac{2\gamma}{\gamma - 1}}$$

$$\underline{\rho}_{1} = \frac{\rho_{1}}{\rho_{\epsilon}} = \left(\underline{a}_{1}\right)^{\frac{2}{\gamma - 1}}$$

$$\frac{H_1}{H_{\epsilon}} = \frac{h_1}{h_{\epsilon}} + \frac{u_1^2}{2c_p T_{\epsilon}} = \frac{h_1}{h_{\epsilon}} + \frac{\gamma - 1}{2} \underline{u}_1^2 = \frac{2}{\gamma + 1} \left(1 + \frac{\gamma - 1}{2} \xi^2\right)$$

#### APPENDIX B

#### DERIVATION OF REDUCED BOUNDARY-LAYER EQUATIONS FOR

#### TWO-DIMENSIONAL UNSTEADY FLOW

The Navier-Stokes equations under the restriction of the Prandtl boundary-layer approximation may be written as

$$\frac{\partial u}{\partial t} + u \frac{\partial u}{\partial x} + v \frac{\partial u}{\partial y} = -\frac{1}{\rho} \frac{\partial p}{\partial x} + \frac{1}{\rho} \frac{\partial}{\partial y} \left( \mu \frac{\partial u}{\partial y} \right)$$
 (B1)

$$0 = -\frac{1}{\rho} \frac{\partial p}{\partial y}$$
 (B2)

$$\frac{\partial \rho}{\partial t} + \frac{\partial x}{\partial t} (\rho u) + \frac{\partial y}{\partial t} (\rho v) = 0$$
 (B3)

$$\frac{\partial h}{\partial t} + u \frac{\partial h}{\partial x} + v \frac{\partial h}{\partial y} + u \left( \frac{\partial u}{\partial t} + u \frac{\partial u}{\partial x} + v \frac{\partial u}{\partial y} \right) =$$

$$\frac{u}{\rho} \frac{\partial}{\partial y} \left( \mu \frac{\partial u}{\partial y} \right) + \frac{\mu}{\rho} \left( \frac{\partial u}{\partial y} \right)^2 + \frac{1}{\rho} \frac{\partial}{\partial y} \left( \frac{k}{c_p} \frac{\partial h}{\partial y} \right) + \frac{1}{\rho} \frac{\partial p}{\partial t}$$
(B4)

Equations (B1) and (B2) are the momentum equations in the x- and y-directions, equation (B3) is the continuity equation; and equation (B4) is a form of the energy equation that is desirable when the local enthalpy is to be a parameter of the solution. An alternate form of the energy equation employing the total enthalpy as a parameter is given by

$$\frac{\partial H}{\partial t} + u \frac{\partial H}{\partial x} + v \frac{\partial H}{\partial y} = \frac{1}{\rho} \frac{\partial}{\partial y} \left( \mu \frac{\partial H}{\partial y} \right) + \frac{1}{\rho} \frac{\partial}{\partial y} \left[ \frac{\mu}{N_{Pr}} (1 - N_{Pr}) \left( \frac{\partial H}{\partial y} - u \frac{\partial u}{\partial y} \right) \right] + \frac{1}{\rho} \frac{\partial p}{\partial t}$$
(B5)

An immediate consequence of equation (B2) is

$$p(x,y,t) = p(x,t) = p_1(x,t)$$
 (B6)

Combining equations (B6) and (B1) evaluated in the free stream yields:

$$\frac{\partial p}{\partial x} = \frac{\partial p_1}{\partial x} = -\rho_1 \left( \frac{\partial u_1}{\partial t} + u_1 \frac{\partial u_1}{\partial x} \right) = -\rho_1 \frac{Du_1}{Dt}$$
 (B7)

The technique of integrating each term from y=0 to  $y=\infty$  (see, for example, ref. 25 for steady-flow integral method) is then applied to equation (B1). The velocity component v is eliminated through substitution of the continuity equation (B3) and the following boundary conditions are employed:

At 
$$y = 0$$
 for all  $x,t$  
$$u = v = 0$$
 At  $y = \infty$  for all  $x,t$  
$$u = u_1$$
 At  $y = \infty$  for all  $x,t$  
$$\frac{\partial u}{\partial y} = 0$$

The following momentum equation results:

$$\frac{\partial}{\partial x} \int_{0}^{\infty} \left[ \frac{u}{u_{1}} - \left( \frac{u}{u_{1}} \right)^{2} \right] \frac{\rho}{\rho_{\varepsilon}} \, dy + \frac{2}{u_{1}} \frac{\partial u_{1}}{\partial x} \int_{0}^{\infty} \left[ \frac{u}{u_{1}} - \left( \frac{u}{u_{1}} \right)^{2} \right] \frac{\rho}{\rho_{\varepsilon}} \, dy + \left( \frac{1}{u_{1}} \frac{\partial u_{1}}{\partial x} + \frac{1}{u_{1}^{2}} \frac{\partial u_{1}}{\partial t} \right) \int_{0}^{\infty} \left[ \left( \frac{\rho_{1}}{\rho} - 1 \right) + \left( 1 - \frac{u}{u_{1}} \right) \right] \frac{\rho}{\rho_{\varepsilon}} \, dy + \left( \frac{1}{u_{1}} \frac{\partial}{\partial t} \right) \int_{0}^{\infty} \left( 1 - \frac{u}{u_{1}} \right) \frac{\rho}{\rho_{\varepsilon}} \, dy = \frac{\mu_{w}}{\rho_{\varepsilon} u_{1}^{2}} \left( \frac{\partial u}{\partial y} \right)_{w}$$
(B9)

Equation (B9) is then rewritten by substituting  $\theta$  and  $\delta^*$  into equation (B9):

$$\frac{\partial \theta}{\partial x} + \frac{2}{u_1} \frac{\partial u_1}{\partial x} \theta + \left(\frac{1}{u_1} \frac{\partial u_1}{\partial x} + \frac{1}{u_1^2} \frac{\partial u_1}{\partial t}\right) \left[\delta^* + \int_0^\infty \left(\frac{\rho_1}{\rho} - 1\right) \frac{\rho}{\rho_{\epsilon}} dy\right] + \frac{1}{u_1} \frac{\partial \delta^*}{\partial t} = \frac{\mu_W}{\rho_{\epsilon} u_1^2} \left(\frac{\partial u}{\partial y}\right)_W$$
(B10)

For a perfect gas with a constant specific heat, the integral term in equation (BlO) may be evaluated as follows:

$$\int_{0}^{\infty} \left(\frac{\rho_{\underline{1}}}{\rho} - 1\right) \frac{\rho}{\rho_{\underline{\epsilon}}} dy = \int_{0}^{\infty} \left(\frac{h}{h_{\underline{1}}} - 1\right) \frac{\rho}{\rho_{\underline{\epsilon}}} dy = -\frac{h_{\underline{1}}^{*}}{h_{\underline{1}}} \int_{0}^{\infty} \left(1 - \frac{h^{*}}{h_{\underline{1}}^{*}}\right) \frac{\rho}{\rho_{\underline{\epsilon}}} dy = -\frac{h_{\underline{1}}^{*}}{h_{\underline{1}}} \nabla^{*}$$
(B11)

or

$$\int_{0}^{\infty} \left(\frac{\rho_{1}}{\rho} - 1\right) \frac{\rho}{\rho_{\epsilon}} dy = \frac{1}{H_{1} - \frac{u_{1}^{2}}{2}} \left[ -H_{1}^{*} + \frac{u_{1}^{2}}{2} (\delta^{*} + \theta) \right]$$
 (Blla)

Substitution of (Bll) into (BlO) yields the momentum differential equation with x and t as the independent variables:

$$\frac{\partial \theta}{\partial x} + \frac{2}{u_1} \frac{\partial u_1}{\partial x} \theta + \frac{1}{u_1^2} \frac{Du_1}{Dt} \left( \delta * - \frac{h_1 *}{h_1} \nabla * \right) + \frac{1}{u_1} \frac{\partial \delta *}{\partial t} = \frac{\mu_W}{\rho_{\epsilon} u_1^2} \left( \frac{\partial u}{\partial y} \right)_W$$
 (B12)

or

$$\frac{\partial \theta}{\partial x} + \frac{2}{u_1} \frac{\partial u_1}{\partial x} \theta + \frac{1}{u_1^2} \frac{Du_1}{Dt} \left[ \delta^* + \frac{-H_1^* \Box^* + \frac{u_1^2}{2} (\delta^* + \theta)}{H_1 - \frac{u_1^2}{2}} \right] + \frac{1}{u_1} \frac{\partial \delta^*}{\partial t} = \frac{\mu_w}{\rho_{\epsilon} u_1^2} \left( \frac{\partial u}{\partial y} \right)_w$$
(B12a)

The energy equation (B4) in terms of local enthalpy is treated in a similar manner; again the continuity equation is used to eliminate  $\,v\,$  and the following free-stream equality is substituted:

$$\frac{DH_1}{Dt} = \frac{Dh_1}{Dt} + u_1 \frac{Du_1}{Dt} = \frac{1}{\rho_1} \frac{\partial p_1}{\partial t}$$
 (B13)

Appropriate boundary conditions for the local enthalpy are:

At y = 0 for all x,t

$$h = h_w$$

At  $y = \infty$  for all x,t

$$h = h_1$$

At  $y = \infty$  for all x,t

$$\frac{\partial h}{\partial v} = 0$$

The resulting equation for a perfect gas of constant specific heat is

$$\frac{\partial}{\partial x} \int_{0}^{\infty} \frac{u}{u_{1}} \left( 1 - \frac{h^{*}}{h_{1}^{*}} \right) \frac{\rho}{\rho_{\epsilon}} dy + \left( \frac{1}{u_{1}} \frac{\partial u_{1}}{\partial x} + \frac{1}{h_{1}^{*}} \frac{\partial h_{1}^{*}}{\partial x} - \frac{1}{\rho_{1}h_{1}} \frac{\partial p_{1}}{\partial x} \right) \times$$

$$\int_0^\infty \frac{u}{u_1} \left(1 - \frac{h^*}{h_1^*}\right) \frac{\rho}{\rho_\epsilon} \ \mathrm{d}y \ - \ \frac{1}{u_1} \left(\frac{1}{\rho_1 h_1} \ \frac{\partial p_1}{\partial t} \ - \ \frac{1}{h_1^*} \ \frac{\partial h_1^*}{\partial t}\right) \int_0^\infty \left(1 \ - \ \frac{h^*}{h_1^*}\right) \frac{\rho}{\rho_\epsilon} \ \mathrm{d}y \ - \frac{1}{u_1} \left(\frac{1}{\rho_1 h_1} \ \frac{\partial p_1}{\partial t} \ - \ \frac{1}{h_1^*} \ \frac{\partial h_1^*}{\partial t}\right) \int_0^\infty \left(1 \ - \ \frac{h^*}{h_1^*}\right) \frac{\rho}{\rho_\epsilon} \ \mathrm{d}y \ - \frac{1}{u_1} \left(\frac{1}{\rho_1 h_1} \ \frac{\partial p_1}{\partial t} \ - \ \frac{1}{h_1^*} \ \frac{\partial p_1}{\partial t} \ - \ \frac{1}{h_1^*} \ \frac{\partial h_1^*}{\partial t}\right) \int_0^\infty \left(1 \ - \ \frac{h^*}{h_1^*}\right) \frac{\rho}{\rho_\epsilon} \ \mathrm{d}y \ - \frac{1}{u_1} \left(\frac{1}{\rho_1 h_1} \ \frac{\partial p_1}{\partial t} \ - \ \frac{1}{h_1^*} \ \frac{\partial p_1}{\partial t} \ - \ \frac{1}{h_1^*} \ \frac{\partial h_1^*}{\partial t}\right) \int_0^\infty \left(1 \ - \ \frac{h^*}{h_1^*}\right) \frac{\rho}{\rho_\epsilon} \ \mathrm{d}y \ - \frac{1}{u_1} \left(\frac{1}{\rho_1 h_1} \ \frac{\partial p_1}{\partial t} \ - \ \frac{1}{h_1^*} \ \frac{\partial h_1^*}{\partial t}\right) \int_0^\infty \left(1 \ - \ \frac{h^*}{h_1^*}\right) \frac{\rho}{\rho_\epsilon} \ \mathrm{d}y \ - \frac{1}{u_1} \left(\frac{1}{\rho_1 h_1} \ \frac{\partial p_1}{\partial t} \ - \ \frac{1}{h_1^*} \ \frac{\partial p_1}{\partial t} \ - \ \frac{1}{h_1^*} \ \frac{\partial p_1}{\partial t}\right) \int_0^\infty \left(1 \ - \ \frac{h^*}{h_1^*}\right) \frac{\rho}{\rho_\epsilon} \ \mathrm{d}y \ - \frac{1}{u_1} \left(\frac{1}{\rho_1 h_1} \ \frac{\partial p_1}{\partial t} \ - \ \frac{1}{h_1^*} \ \frac{\partial p_1}{\partial t} \ - \ \frac{\partial p_1}{\partial t} \ - \ \frac{\partial p_1}{\partial t}\right) \int_0^\infty \left(1 \ - \ \frac{h^*}{h_1^*}\right) \frac{\rho}{\rho_\epsilon} \ \mathrm{d}y \ - \frac{1}{u_1} \left(\frac{1}{\rho_1 h_1} \ \frac{\partial p_1}{\partial t} \ - \ \frac{\partial p_1}{\partial t} \ -$$

$$\frac{1}{u_1h_1*}\left(\frac{\partial h_1}{\partial t} - \frac{1}{\rho_1}\frac{\partial p_1}{\partial t}\right)\int_0^\infty \left(1 - \frac{u}{u_1}\right)\frac{\rho}{\rho_\epsilon} \,\mathrm{d}y \, + \, \frac{1}{u_1}\frac{\partial}{\partial t}\int_0^\infty \left(1 - \frac{h^*}{h_1*}\right)\frac{\rho}{\rho_\epsilon} \,\mathrm{d}y \, = \, \frac{1}{u_1h_1*}\left(\frac{\partial h_1}{\partial t} - \frac{1}{\rho_1}\frac{\partial p_1}{\partial t}\right)\int_0^\infty \left(1 - \frac{u}{u_1}\right)\frac{\rho}{\rho_\epsilon} \,\mathrm{d}y \, + \, \frac{1}{u_1}\frac{\partial}{\partial t}\int_0^\infty \left(1 - \frac{h^*}{h_1*}\right)\frac{\rho}{\rho_\epsilon} \,\mathrm{d}y \, = \, \frac{1}{u_1h_1*}\left(\frac{\partial h_1}{\partial t} - \frac{1}{\rho_1}\frac{\partial p_1}{\partial t}\right)\int_0^\infty \left(1 - \frac{u}{u_1}\right)\frac{\rho}{\rho_\epsilon} \,\mathrm{d}y \, + \, \frac{1}{u_1}\frac{\partial}{\partial t}\int_0^\infty \left(1 - \frac{h^*}{h_1*}\right)\frac{\rho}{\rho_\epsilon} \,\mathrm{d}y \, = \, \frac{1}{u_1h_1*}\left(\frac{\partial h_1}{\partial t} - \frac{\partial h_1}{\partial t}\right)\frac{\partial h_1}{\partial t}$$

$$\frac{1}{\rho_{\epsilon} u_{1} h_{1}^{*}} \frac{k_{w}}{c_{p,w}} \left( \frac{\partial h}{\partial y} \right)_{w} - \frac{1}{u_{1} h_{1}^{*}} \int_{0}^{\infty} \frac{\mu}{\rho} \left( \frac{\partial u}{\partial y} \right)^{2} \frac{\rho}{\rho_{\epsilon}} dy$$
(B14)

The last term on the right-hand side of equation (B14), which represents the viscous dissipation, may be manipulated in the following manner. First, the Chapman-Rubesin relation (ref. 18) between viscosity and temperature

$$\frac{\mu}{\mu_{\perp}} = C_{W} \frac{T}{T_{\perp}}$$

$$C_{W} = \left(\frac{T_{W}}{T_{\perp}}\right)^{1/2} \frac{T_{\perp} + S}{T_{W} + S}$$
(B15)

is combined with the gas law and equation (B6) to give

$$\frac{\rho\mu}{\rho_{\rm W}\mu_{\rm W}} = 1.0 \tag{B16}$$

a relation valid across the boundary layer at arbitrary  $\,\mathbf{x}\,$  and  $\,\mathbf{t}\,.$  Also since

$$\alpha = \frac{1}{\Delta} \int_{0}^{y} \frac{\rho}{\rho_{\epsilon}} dy$$
 (B17)

and

$$\frac{\partial \alpha}{\partial y} = \frac{1}{\Delta} \frac{\rho}{\rho_{\epsilon}}$$
 (B18)

$$\frac{\partial u}{\partial y} = u_1 \frac{\partial \frac{u}{u_1}}{\partial \alpha} \frac{\partial \alpha}{\partial y} = \frac{u_1}{\Delta} \frac{\rho}{\rho_{\epsilon}} \frac{\partial \frac{u}{u_1}}{\partial \alpha}$$
(B19)

Therefore,

$$\Phi = \int_{0}^{\infty} \frac{\mu}{\rho} \left(\frac{\partial u}{\partial y}\right)^{2} \frac{\rho}{\rho_{\epsilon}} dy = \frac{u_{1}^{2}}{\Delta \rho_{\epsilon}^{2}} \int_{0}^{\infty} \rho \mu \left(\frac{\partial \frac{u}{u_{1}}}{\partial \alpha}\right)^{2} d\alpha = \frac{u_{1}^{2}}{\rho_{\epsilon}^{2}} \frac{\rho_{w} \mu_{w}}{\Delta} \int_{0}^{1} \left(\frac{\partial \frac{u}{u_{1}}}{\partial \alpha}\right)^{2} d\alpha$$
(B20)

since  $\frac{\partial \frac{u}{u_1}}{\partial \alpha} = 0$  for  $\alpha \ge 1.0$ . Equation (Bl4) is now rewritten to give the energy equation in terms of the local enthalpy with independent variables x and t:

$$\frac{\partial \phi}{\partial x} + \left(\frac{1}{u_1} \frac{\partial u_1}{\partial x} + \frac{1}{h_1 *} \frac{\partial h_1 *}{\partial x} - \frac{1}{\rho_1 h_1} \frac{\partial p_1}{\partial x}\right) \phi - \frac{1}{u_1} \left(\frac{1}{\rho_1 h_1} \frac{\partial p_1}{\partial t} - \frac{1}{h_1 *} \frac{\partial h_1 *}{\partial t}\right) \nabla^* - \frac{1}{u_1 h_1 *} \left(\frac{\partial h_1}{\partial t} - \frac{1}{\rho_1} \frac{\partial p_1}{\partial t}\right) \delta^* + \frac{1}{u_1} \frac{\partial \nabla^*}{\partial t} = \frac{1}{\rho_{\epsilon} u_1 h_1 *} \frac{k_w}{c_{p,w}} \left(\frac{\partial h}{\partial y}\right)_w - \frac{1}{u_1 h_1 *} \Phi$$
(B21)

Similar integrations are performed with equation (B5) by utilizing the following boundary conditions on total enthalpy:

At y = 0 for all x,t

$$H = H_W$$

At  $y = \infty$  for all x,t

$$H = H_1$$

At  $y = \infty$  for all x,t

$$\frac{\partial y}{\partial H} = 0$$

The following equations, which are the total enthalpy forms of the energy equation and are equivalent to equations (B14) and (B21) result:

$$\frac{\partial}{\partial x} \int_{0}^{\infty} \frac{u}{u_{1}} \left(1 - \frac{H^{*}}{H_{1}^{*}}\right) \frac{\rho}{\rho_{\epsilon}} dy + \left(\frac{1}{u_{1}} \frac{\partial u_{1}}{\partial x} + \frac{1}{H_{1}^{*}} \frac{\partial H_{1}^{*}}{\partial x}\right) \int_{0}^{\infty} \frac{u}{u_{1}} \left(1 - \frac{H^{*}}{H_{1}^{*}}\right) \frac{\rho}{\rho_{\epsilon}} dy + \frac{1}{u_{1}^{*}} \frac{\partial H_{1}^{*}}{\partial x} \int_{0}^{\infty} \left(1 - \frac{H^{*}}{H_{1}^{*}}\right) \frac{\rho}{\rho_{\epsilon}} dy + \frac{1}{H_{1}^{*}} \frac{\partial H_{1}}{\partial x} \int_{0}^{\infty} \left(1 - \frac{u}{u_{1}^{*}}\right) \frac{\rho}{\rho_{\epsilon}} dy + \frac{1}{u_{1}^{*}} \frac{\partial h_{1}^{*}}{\partial x} \int_{0}^{\infty} \left(1 - \frac{H^{*}}{H_{1}^{*}}\right) \frac{\rho}{\rho_{\epsilon}} dy + \frac{1}{u_{1}^{*}} \frac{\partial h_{1}^{*}}{\partial x} \int_{0}^{\infty} \left(1 - \frac{H^{*}}{H_{1}^{*}}\right) \frac{\rho}{\rho_{\epsilon}} dy = \frac{1}{u_{1}^{*}} \frac{h_{u}^{*}}{h_{1}^{*}} \frac{\partial h_{1}^{*}}{\partial x} \int_{0}^{\infty} \left(\frac{\partial h_{1}^{*}}{\rho_{\epsilon}} + \frac{1}{u_{1}^{*}} \frac{\partial h_{1}^{*}}{\partial x}\right) \int_{0}^{\infty} \left(1 - \frac{H^{*}}{H_{1}^{*}}\right) \frac{\rho}{\rho_{\epsilon}} dy = \frac{1}{u_{1}^{*}} \frac{h_{u}^{*}}{h_{1}^{*}} \frac{\partial h_{1}^{*}}{\partial x} \int_{0}^{\infty} \left(\frac{\partial h_{1}^{*}}{\rho_{\epsilon}} + \frac{1}{u_{1}^{*}} \frac{\partial h_{1}^{*}}{\partial x}\right) \int_{0}^{\infty} \left(1 - \frac{H^{*}}{H_{1}^{*}}\right) \frac{\rho}{\rho_{\epsilon}} dy = \frac{1}{u_{1}^{*}} \frac{h_{u}^{*}}{h_{1}^{*}} \frac{\partial h_{1}^{*}}{\partial x} \int_{0}^{\infty} \left(\frac{\partial h_{1}^{*}}{\rho_{\epsilon}} + \frac{1}{u_{1}^{*}} \frac{\partial h_{1}^{*}}{\partial x}\right) \int_{0}^{\infty} \left(1 - \frac{H^{*}}{h_{1}^{*}}\right) \frac{\rho}{\rho_{\epsilon}} dy + \frac{1}{u_{1}^{*}} \frac{\partial h_{1}^{*}}{\partial x} \int_{0}^{\infty} \left(1 - \frac{H^{*}}{h_{1}^{*}}\right) \frac{\rho}{\rho_{\epsilon}} dy + \frac{1}{u_{1}^{*}} \frac{\partial h_{1}^{*}}{\partial x} \int_{0}^{\infty} \left(1 - \frac{H^{*}}{h_{1}^{*}}\right) \frac{\rho}{\rho_{\epsilon}} dy + \frac{1}{u_{1}^{*}} \frac{\partial h_{1}^{*}}{\partial x} \int_{0}^{\infty} \left(1 - \frac{H^{*}}{h_{1}^{*}}\right) \frac{\rho}{\rho_{\epsilon}} dy + \frac{1}{u_{1}^{*}} \frac{\partial h_{1}^{*}}{\partial x} \int_{0}^{\infty} \left(1 - \frac{H^{*}}{h_{1}^{*}}\right) \frac{\rho}{\rho_{\epsilon}} dy + \frac{1}{u_{1}^{*}} \frac{\partial h_{1}^{*}}{\partial x} \int_{0}^{\infty} \left(1 - \frac{H^{*}}{h_{1}^{*}}\right) \frac{\rho}{\rho_{\epsilon}} dy + \frac{1}{u_{1}^{*}} \frac{\partial h_{1}^{*}}{\partial x} \int_{0}^{\infty} \left(1 - \frac{H^{*}}{h_{1}^{*}}\right) \frac{\rho}{\rho_{\epsilon}} dy + \frac{1}{u_{1}^{*}} \frac{\partial h_{1}^{*}}{\partial x} \int_{0}^{\infty} \left(1 - \frac{H^{*}}{h_{1}^{*}}\right) \frac{\partial h_{1}^{*}}{\partial x} \int_{0}^{\infty} \left(1 - \frac{H^{*}}{h_{1}^{*}$$

$$\frac{\partial \psi}{\partial x} + \left(\frac{1}{u_1} \frac{\partial u_1}{\partial x} + \frac{1}{H_1^*} \frac{\partial H_1^*}{\partial x}\right) \psi - \frac{1}{u_1} \left(\frac{1}{H_1} - \frac{u_1^2}{2} \frac{1}{\rho_1} \frac{\partial p_1}{\partial t} - \frac{1}{H_1^*} \frac{\partial H_1^*}{\partial t}\right) v + \frac{1}{u_1^*} \frac{1}{u_1^*} \left(\frac{\partial H_1}{\partial x} + \frac{u_1^2}{\partial x} + \frac{u_1^2}{H_1^*} \frac{\partial p_1}{\partial t}\right) \delta x + \frac{1}{u_1^*} \frac{u_1^2}{H_1^*} \frac{u_1^2}{H_1^*} \frac{\partial p_1}{\partial t} \theta + \frac{1}{u_1^*} \frac{\partial u_1^*}{\partial t} = \frac{1}{u_1^*} \frac{1}{u_1^*} \frac{u_1^2}{\partial t} \frac{\partial h_1}{\partial t} \theta + \frac{1}{u_1^*} \frac{\partial h_1}{\partial t} \theta + \frac{1}{u_1^*} \frac{\partial h_1}{\partial t} \theta + \frac{1}{u_1^*} \frac{\partial h_1^*}{\partial t} \theta +$$

The reduced partial differential equations in final form for  $\, x \,$  and  $\, t \,$  as independent variables are:

$$\frac{\partial \theta}{\partial x} + \left[ \frac{2}{u_1} \frac{\partial u_1}{\partial x} + \frac{1}{u_1^2} \frac{Du_1}{Dt} \left( \frac{\delta *}{\theta} - \frac{h_1^*}{h_1} \frac{1}{b} \frac{\nabla^*}{\nabla} \frac{\Delta}{\theta} \right) + \frac{1}{u_1} \frac{\partial \frac{\delta *}{\theta}}{\partial t} \right] \theta +$$

$$\frac{1}{u_1} \frac{\delta *}{\theta} \frac{\partial \theta}{\partial t} = \frac{\mu_w}{\rho_{\epsilon} u_1^2} \left( \frac{\partial u}{\partial y} \right)_w = \frac{\nu_w}{u_1} \left( \frac{\rho_w}{\rho_{\epsilon}} \right)^2 \left( \frac{\partial \frac{u}{u_1}}{\partial x} \right)_w \frac{\theta}{\Delta} \frac{1}{\theta}$$

$$\frac{\partial \phi}{\partial x} + \left[ \frac{1}{u_1} \frac{\partial u_1}{\partial x} + \frac{1}{h_1^*} \frac{\partial h_1^*}{\partial x} - \frac{1}{\rho_1 h_1} \frac{\partial p_1}{\partial x} - \frac{1}{u_1} \left( \frac{1}{\rho_1 h_1} \frac{\partial p_1}{\partial t} - \frac{1}{h_1^*} \frac{\partial h_1^*}{\partial t} \right) \frac{\nabla^*}{\phi} -$$

$$\frac{1}{u_1 h_1^*} \left( \frac{\partial h_1}{\partial t} - \frac{1}{\rho_1} \frac{\partial p_1}{\partial t} \right)_b \frac{\delta *}{\Delta} \frac{\nabla}{\phi} + \frac{1}{u_1} \frac{\partial \frac{\nabla^*}{\phi}}{\partial t} \right) \phi + \frac{1}{u_1} \frac{\nabla^*}{\phi} \frac{\partial \phi}{\partial t} =$$

$$\frac{1}{\rho_{\epsilon} u_1 h_1^*} \frac{k_w}{c_{p,w}} \left( \frac{\partial h}{\partial y} \right)_w - \frac{1}{u_1 h_1^*} \Phi = \frac{\nu_w}{u_1} \left( \frac{\rho_w}{\rho_{\epsilon}} \right)^2 \frac{1}{N_{Pr,w}} \left( \frac{\partial \frac{h^*}{h_1^*}}{\partial \beta} \right)_w \frac{\phi}{\nabla} \frac{1}{\phi} - \frac{1}{u_1 h_1^*} \Phi$$

$$(B24b)$$

$$\frac{\partial \theta}{\partial x} + \left[ \frac{2}{u_1} \frac{\partial u_1}{\partial x} + \frac{1}{u_1^2} \frac{\partial u_1}{\partial t} \left( \frac{u_1^2}{2} + H_1 \frac{\delta^*}{\theta} - H_1^* \frac{1}{c} \frac{\square^*}{\square^*} \frac{\Delta}{\theta} \right) + \frac{1}{u_1} \frac{\partial \frac{\delta^*}{\theta}}{\partial t} \theta + \frac{1}{u_1} \frac{\delta^*}{\theta} \frac{\partial \theta}{\partial t} = \frac{v_W}{u_1} \left( \frac{\rho_W}{\rho_E} \right)^2 \left( \frac{\partial \frac{u_1}{u_1}}{\partial x} \right)_W \frac{\theta}{\Delta} \frac{1}{\theta}$$

$$\frac{\partial \psi}{\partial x} + \left[ \frac{1}{u_1} \frac{\partial u_1}{\partial x} + \frac{1}{H_1^*} \frac{\partial H_1^*}{\partial x} - \frac{1}{u_1} \left( \frac{1}{H_1} - \frac{u_1^2}{2} \frac{1}{\rho_1} \frac{\partial p_1}{\partial t} - \frac{1}{H_1^*} \frac{\partial H_1^*}{\partial t} \right) \frac{\square^*}{\psi} + \frac{1}{u_1^2} \frac{\partial H_1^*}{\partial x} + \frac{u_1^2}{u_1^2} \frac{\partial p_1}{\partial t} c \frac{\theta}{\Delta} \frac{\square}{\psi} + \frac{1}{u_1} \frac{\partial \frac{\square^*}{\theta}}{\partial t} \right) c \frac{\delta^*}{\Delta} \frac{\square}{\psi} + \frac{1}{u_1} \frac{\square^*}{\psi} \frac{\partial \psi}{\partial t} = \frac{1}{u_1^2} \frac{u_1^2}{u_1^2} \frac{1}{\rho_1} \frac{\partial p_1}{\partial t} c \frac{\theta}{\Delta} \frac{\square}{\psi} + \frac{1}{u_1} \frac{\partial \frac{\square^*}{\theta}}{\partial t} \psi + \frac{1}{u_1} \frac{\square^*}{\psi} \frac{\partial \psi}{\partial t} = \frac{1}{\rho_1^2} \frac{u_1^2}{u_1^2} \frac{\partial p_1}{\partial t} c \frac{\theta}{\Delta} \frac{\square}{\psi} + \frac{1}{u_1} \frac{\partial \frac{\square^*}{\theta}}{\partial t} \psi + \frac{1}{u_1} \frac{\square^*}{\psi} \frac{\partial \psi}{\partial t} = \frac{1}{\rho_1^2} \frac{u_1^2}{u_1^2} \frac{\partial H_1}{\partial t} c \frac{\partial H_1}{\partial t} \frac{\partial H_1}{\partial t} c \frac{\partial H_1}{\partial t} \frac{\partial H_1}{$$

Equations (B24) are for  $u_1$ ,  $h_1$ ,  $\theta$ , and  $\phi$  as primary dependent variables whereas equations (B25) are for  $u_1$ ,  $H_1$ ,  $\theta$ , and  $\psi$  as primary dependent variables.

## APPENDIX C

## TRANSFORMATION OF REDUCED DIFFERENTIAL EQUATIONS

### TO CONICAL COORDINATE SYSTEM

The differential equations obtained in appendix B are to be transformed from the x,y,t system to a conical coordinate system  $\xi$ ,y,t where

$$\xi = \frac{x}{a_{\epsilon}t}$$

$$y = y$$

$$t = t$$
(C1)

This transformation is arbitrarily restricted to conical free-stream flows (that is, all free-stream quantities are functions of  $\xi$  alone) to reduce the complexity of the equations while still retaining the features that are necessary for application to flows generated by shock waves and centered expansion waves.

The following derivatives are equivalent:

$$\left(\frac{\partial}{\partial x}\right)_{t} = \left(\frac{\partial}{\partial \xi}\right)_{t} \left(\frac{\partial \xi}{\partial x}\right)_{t} = \frac{1}{a_{\epsilon}t} \left(\frac{\partial}{\partial \xi}\right)_{t} \tag{C2}$$

$$\left(\frac{\partial}{\partial t}\right)_{x} = \left(\frac{\partial}{\partial t}\right)_{\xi} + \left(\frac{\partial}{\partial \xi}\right)_{t} \left(\frac{\partial \xi}{\partial t}\right)_{x} = \left(\frac{\partial}{\partial t}\right)_{\xi} - \frac{\xi}{t} \left(\frac{\partial}{\partial \xi}\right)_{t}$$
(C3)

In particular, for any free-stream function  $f_1(x,t) = f_1(\xi)$ ,

$$\left(\frac{\partial f_{1}}{\partial x}\right)_{t} = \frac{1}{a_{\epsilon}t} \frac{df_{1}}{d\xi} \tag{C4}$$

$$\left(\frac{\partial f_1}{\partial t}\right)_{x} = -\frac{\xi}{t} \frac{df_1}{d\xi} \tag{C5}$$

and

$$\frac{Df_{\underline{1}}}{Dt} = \left(-\frac{\xi}{t} + \frac{u_{\underline{1}}}{a_{\varepsilon}t}\right) \frac{df_{\underline{1}}}{d\xi} = \left(\underline{u}_{\underline{1}} - \xi\right) \frac{1}{t} \frac{df_{\underline{1}}}{d\xi} \tag{C6}$$

It should be noted that  $h_1^*$  is not a free-stream function for  $h_W = h_W(\xi,t)$ ; thus the derivatives of  $h_1^*$  become

$$\left(\frac{\partial h_{\underline{1}}^{*}}{\partial x}\right)_{\underline{t}} = \frac{\partial}{\partial x}(h_{\underline{1}} - h_{\underline{w}}) = \frac{1}{a_{\underline{\epsilon}}t} \frac{\partial}{\partial \xi}(h_{\underline{1}} - h_{\underline{w}}) = \frac{1}{a_{\underline{\epsilon}}t} \left(\frac{dh_{\underline{1}}}{d\xi} - \frac{\partial h_{\underline{w}}}{\partial \xi}\right) \\
\left(\frac{\partial h_{\underline{1}}^{*}}{\partial t}\right)_{\underline{x}} = \frac{\partial}{\partial t}(h_{\underline{1}} - h_{\underline{w}}) - \frac{\xi}{t} \frac{\partial}{\partial \xi}(h_{\underline{1}} - h_{\underline{w}}) = -\frac{\partial h_{\underline{w}}}{\partial t} + \frac{\xi}{t} \frac{\partial h_{\underline{w}}}{\partial \xi} - \frac{\xi}{t} \frac{dh_{\underline{1}}}{d\xi} \right) \tag{C7}$$

Similar equations are applicable for H1\*.

Application of these equations to equation (B24a) results in the following relations:

$$\frac{\partial \theta}{\partial \xi} + \left[ \frac{2}{u_{1}} \frac{du_{1}}{d\xi} + \frac{a_{\epsilon}}{u_{1}^{2}} \left( \underline{u}_{1} - \xi \right) \frac{du_{1}}{d\xi} \left( \frac{\delta *}{\theta} - \frac{h_{1}*}{h_{1}} \frac{1}{b} \frac{\nabla *}{\nabla} \frac{\Delta}{\theta} \right) + \frac{a_{\epsilon}t}{u_{1}} \frac{\partial \frac{\delta *}{\theta}}{\partial t} - \frac{a_{\epsilon}\xi}{u_{1}} \frac{\partial \frac{\delta *}{\theta}}{\partial \xi} \right] \theta + \frac{a_{\epsilon}t}{u_{1}^{2}} \frac{\delta *}{\theta} \frac{\partial \theta}{\partial t} - \frac{a_{\epsilon}\xi}{u_{1}^{2}} \frac{\delta *}{\theta} \frac{\partial \theta}{\partial \xi} = \frac{v_{W}}{u_{1}} \left( \frac{\rho_{W}}{\rho_{\epsilon}} \right)^{2} \left( \frac{\partial \frac{u}{u_{1}}}{\partial \alpha} \right)_{W} \frac{\theta}{\Delta} \frac{a_{\epsilon}t}{\theta}$$
(C8)

or

$$\theta \frac{\partial \theta}{\partial \xi} \left( 1 - \frac{\xi}{\underline{u}_{1}} \frac{\delta *}{\theta} \right) + \theta^{2} \left\{ \frac{1}{\underline{u}_{1}} \frac{d\underline{u}_{1}}{d\xi} \left[ 2 + \left( \underline{u}_{1} - \xi \right) \frac{1}{\underline{u}_{1}} \left( \frac{\delta *}{\theta} - \frac{h_{1} *}{h_{1}} \frac{1}{b} \frac{\nabla *}{\nabla} \frac{\Delta}{\theta} \right) \right] + \frac{t}{\underline{u}_{1}} \frac{\partial \frac{\delta *}{\theta}}{\partial t} - \frac{\xi}{\underline{u}_{1}} \frac{\partial \frac{\delta *}{\theta}}{\partial \xi} \right\} + \frac{\delta *}{\theta} \frac{t\theta}{\underline{u}_{1}} \frac{\partial \theta}{\partial t} = \frac{\nu_{W}}{\underline{u}_{1}} \left( \frac{\rho_{W}}{\rho_{\varepsilon}} \right)^{2} \left( \frac{\partial \frac{\underline{u}}{u}}{\partial \alpha} \right)_{W} \frac{\theta}{\Delta} t$$
(C9)

In anticipation of a Pohlhausen power series for the velocity profile, let  $\frac{\delta^*}{\theta} = f(\lambda)$ . Derivatives of  $\frac{\delta^*}{\theta}$  may then be expressed as derivatives of  $\lambda$  as follows:

$$\left(\frac{\partial \frac{\delta^{*}}{\theta}}{\partial t}\right)_{\xi} = \frac{d \frac{\delta^{*}}{\theta}}{d\lambda} \left(\frac{\partial \lambda}{\partial t}\right)_{\xi}$$

$$\left(\frac{\partial \frac{\delta^{*}}{\theta}}{\partial \xi}\right)_{t} = \frac{d \frac{\delta^{*}}{\theta}}{d\lambda} \left(\frac{\partial \lambda}{\partial \xi}\right)_{t}$$
(C10)

Equations (C9) and (C10) are combined to give

$$\frac{\partial^{2}}{\partial \xi} \left( 1 - \frac{\xi}{\underline{u}_{1}} \frac{\delta *}{\theta} \right) + 2\theta^{2} \left\{ \frac{1}{\underline{u}_{1}} \frac{d\underline{u}_{1}}{d\xi} \left[ 2 + \frac{\underline{u}_{1} - \xi}{\underline{u}_{1}} \left( \frac{\delta *}{\theta} - \frac{h_{1}*}{h_{1}} \frac{1}{b} \frac{\nabla *}{\nabla} \frac{\Delta}{\theta} \right) \right] + \frac{1}{\underline{u}_{1}} \frac{d}{d\lambda} \left( t \frac{\partial \lambda}{\partial t} - \xi \frac{\partial \lambda}{\partial \xi} \right) \right\} + \frac{\delta *}{\theta} \frac{t}{\underline{u}_{1}} \frac{\partial^{2}}{\partial t} = 2 \frac{\nu_{w}}{\underline{u}_{1}} \left( \frac{\rho_{w}}{\rho_{\epsilon}} \right)^{2} \left( \frac{\partial}{\partial u} \frac{\underline{u}_{1}}{\partial \alpha} \right)_{w} \frac{\theta}{\Delta} t \tag{C11}$$

Substitution of equations (C1) to (C7) into equation (B24b) results in the following equation:

$$\frac{\partial \phi}{\partial \xi} + \left\{ \frac{1}{u_{1}} \frac{du_{1}}{d\xi} + \frac{1}{h_{1}} \left( \frac{dh_{1}}{d\xi} - \frac{\partial h_{w}}{\partial \xi} \right) - \frac{1}{\rho_{1}h_{1}} \frac{dp_{1}}{d\xi} - \frac{a_{\varepsilon}}{u_{1}} \left[ \frac{-\xi}{\rho_{1}h_{1}} \frac{dp_{1}}{d\xi} - \frac{\lambda}{\mu_{1}} \frac{dp_{1}}{d\xi} \right] \right\} - \frac{1}{h_{1}} \left( \frac{\partial h_{w}}{\partial \xi} - \frac{\partial h_{w}}{\partial \xi} - \frac{\lambda}{\mu_{1}} \frac{\partial h_{w}}{\partial \xi} - \frac{\lambda}{$$

In anticipation of a power-series representation of the local enthalpy, the restriction is introduced that  $\frac{\nabla^*}{\phi} = \frac{\nabla^*}{\phi}(\lambda,\Gamma,b)$ . The following equations which are parallel to equations (ClO) express the derivatives of  $\frac{\nabla^*}{\phi}$ :

$$\left(\frac{\partial \overset{\nabla^{*}}{\phi}}{\partial t}\right)_{\xi} = \frac{\partial \overset{\nabla^{*}}{\phi}}{\partial \lambda} \left(\frac{\partial \lambda}{\partial t}\right)_{\xi} + \frac{\partial \overset{\nabla^{*}}{\phi}}{\partial \Gamma} \left(\frac{\partial \Gamma}{\partial t}\right)_{\xi} + \frac{\partial \overset{\nabla^{*}}{\phi}}{\phi} \left(\frac{\partial b}{\partial t}\right)_{\xi}$$

$$\left(\frac{\partial \overset{\nabla^{*}}{\phi}}{\partial \xi}\right)_{t} = \frac{\partial \overset{\nabla^{*}}{\phi}}{\partial \lambda} \left(\frac{\partial \lambda}{\partial \xi}\right)_{t} + \frac{\partial \overset{\nabla^{*}}{\phi}}{\partial \Gamma} \left(\frac{\partial \Gamma}{\partial \xi}\right)_{t} + \frac{\partial \overset{\nabla^{*}}{\phi}}{\phi} \left(\frac{\partial b}{\partial \xi}\right)_{t}$$
(C13)

The combination of equations (C12) and (C13) gives

$$\frac{\partial \phi^{2}}{\partial \xi} \left( 1 - \frac{\xi}{\underline{u}_{1}} \frac{\nabla^{*}}{\phi} \right) + 2 \phi^{2} \left\{ \frac{1}{\underline{u}_{1}} \frac{d\underline{u}_{1}}{d\xi} + \frac{1}{\underline{h}_{1}^{*}} \left( \frac{d\underline{h}_{1}}{d\xi} - \frac{\partial \underline{h}_{W}}{\partial \xi} \right) - \frac{1}{\rho_{1}\underline{h}_{1}} \frac{d\underline{p}_{1}}{d\xi} + \frac{1}{\underline{u}_{1}} \left( \frac{\xi}{\rho_{1}\underline{h}_{1}} \frac{d\underline{p}_{1}}{d\xi} + \frac{1}{\underline{u}_{1}} \frac{\xi}{\rho_{1}\underline{h}_{1}} \frac{d\underline{p}_{1}}{d\xi} \right) + \frac{1}{\rho_{1}\underline{h}_{1}^{*}} \left( \frac{1}{\rho_{1}} \frac{d\underline{p}_{1}}{d\xi} - \frac{d\underline{h}_{1}}{d\xi} \right) b \frac{\delta^{*}}{\Delta} \frac{\nabla}{\phi} + \frac{1}{\underline{u}_{1}} \frac{\partial \nabla^{*}}{\partial \xi} \left( t \frac{\partial \underline{h}_{1}}{\partial \xi} - \xi \frac{\partial \underline{h}_{1}}{\partial \xi} \right) + \frac{1}{\underline{u}_{1}} \frac{\partial \nabla^{*}}{\partial \xi} \left( t \frac{\partial \underline{h}_{2}}{\partial \xi} - \xi \frac{\partial \underline{h}_{2}}{\partial \xi} \right) + \frac{1}{\underline{u}_{1}} \frac{\partial \nabla^{*}}{\partial \xi} \left( t \frac{\partial \underline{h}_{2}}{\partial \xi} - \xi \frac{\partial \underline{h}_{2}}{\partial \xi} \right) + \frac{1}{\underline{u}_{1}} \frac{\partial \nabla^{*}}{\partial \xi} \left( t \frac{\partial \underline{h}_{2}}{\partial \xi} - \xi \frac{\partial \underline{h}_{2}}{\partial \xi} \right) + \frac{1}{\underline{u}_{1}} \frac{\partial \nabla^{*}}{\partial \xi} \left( t \frac{\partial \underline{h}_{2}}{\partial \xi} - \xi \frac{\partial \underline{h}_{2}}{\partial \xi} \right) + \frac{1}{\underline{u}_{1}} \frac{\partial \nabla^{*}}{\partial \xi} \left( t \frac{\partial \underline{h}_{2}}{\partial \xi} - \xi \frac{\partial \underline{h}_{2}}{\partial \xi} \right) + \frac{1}{\underline{u}_{1}} \frac{\partial \nabla^{*}}{\partial \xi} \left( t \frac{\partial \underline{h}_{2}}{\partial \xi} - \xi \frac{\partial \underline{h}_{2}}{\partial \xi} \right) + \frac{1}{\underline{u}_{1}} \frac{\partial \nabla^{*}}{\partial \xi} \left( t \frac{\partial \underline{h}_{2}}{\partial \xi} - \xi \frac{\partial \underline{h}_{2}}{\partial \xi} \right) + \frac{1}{\underline{u}_{1}} \frac{\partial \nabla^{*}}{\partial \xi} \left( t \frac{\partial \underline{h}_{2}}{\partial \xi} - \xi \frac{\partial \underline{h}_{2}}{\partial \xi} \right) + \frac{1}{\underline{u}_{1}} \frac{\partial \nabla^{*}}{\partial \xi} \left( t \frac{\partial \underline{h}_{2}}{\partial \xi} - \xi \frac{\partial \underline{h}_{2}}{\partial \xi} \right) + \frac{1}{\underline{u}_{1}} \frac{\partial \nabla^{*}}{\partial \xi} \left( t \frac{\partial \underline{h}_{2}}{\partial \xi} - \xi \frac{\partial \underline{h}_{2}}{\partial \xi} \right) + \frac{1}{\underline{u}_{1}} \frac{\partial \nabla^{*}}{\partial \xi} \left( t \frac{\partial \underline{h}_{2}}{\partial \xi} - \xi \frac{\partial \underline{h}_{2}}{\partial \xi} \right) + \frac{1}{\underline{u}_{1}} \frac{\partial \nabla^{*}}{\partial \xi} \left( t \frac{\partial \underline{h}_{2}}{\partial \xi} - \xi \frac{\partial \underline{h}_{2}}{\partial \xi} \right) + \frac{1}{\underline{u}_{1}} \frac{\partial \nabla^{*}}{\partial \xi} \left( t \frac{\partial \underline{h}_{2}}{\partial \xi} - \xi \frac{\partial \underline{h}_{2}}{\partial \xi} \right) + \frac{1}{\underline{u}_{1}} \frac{\partial \nabla^{*}}{\partial \xi} \left( t \frac{\partial \underline{h}_{2}}{\partial \xi} - \xi \frac{\partial \underline{h}_{2}}{\partial \xi} \right) + \frac{1}{\underline{u}_{1}} \frac{\partial \nabla^{*}}{\partial \xi} \left( t \frac{\partial \underline{h}_{2}}{\partial \xi} - \xi \frac{\partial \underline{h}_{2}}{\partial \xi} \right) + \frac{1}{\underline{u}_{1}} \frac{\partial \nabla^{*}}{\partial \xi} \left( t \frac{\partial \underline{h}_{2}}{\partial \xi} - \xi \frac{\partial \underline{h}_{2}}{\partial \xi} \right) + \frac{1}{\underline{u}_{1}} \frac{\partial \nabla^{*}}{\partial \xi} \left( t \frac{\partial \underline{h}_{2}}{\partial \xi} - \xi \frac{\partial \underline{h}_{2}}{\partial \xi} \right) + \frac{1}{\underline{u}_{1}} \frac{\partial \nabla^{*}}{\partial \xi} \left( t \frac{\partial \underline{h}_{2}}{\partial \xi} - \xi \frac{\partial \underline{h}_{2}}{\partial \xi} \right) + \frac{1}{\underline{u}_{1}} \frac{\partial \nabla^{*}}{\partial \xi} \left( t \frac{\partial \underline{h}_{$$

In a similar manner, the conical partial differential equations in terms of  $\theta$  and  $\psi$  may be obtained from equations (B25) as

$$\frac{\partial\theta^{2}}{\partial\xi}\left(1-\frac{\xi}{\underline{u}_{1}}\frac{\delta^{*}}{\theta}\right)+2\theta^{2}\left[\frac{1}{\underline{u}_{1}}\frac{d\underline{u}_{1}}{d\xi}\left(2+\frac{\underline{u}_{1}-\xi}{\underline{u}_{1}}\frac{u_{1}^{2}}{2}+\underline{H}_{1}\frac{\delta^{*}}{\theta}-\underline{H}_{1}^{*}\frac{1}{c}\frac{\underline{u}^{*}}{\underline{u}}\frac{\Delta}{\theta}\right)+\frac{1}{2}\frac{\partial\theta^{2}}{\partial\xi}\left(1-\frac{\xi}{\underline{u}_{1}}\frac{\partial\lambda}{\partial\xi}\right)+\frac{1}{2}\frac{\delta^{*}}{\theta}+\frac{1}{2}\frac{\partial\theta^{2}}{\partial\xi$$

## APPENDIX D

## DERIVATION OF VELOCITY AND ENTHALPY BOUNDARY-LAYER

## POWER-SERIES COEFFICIENTS, FORM PARAMETERS,

### AND DISSIPATION FUNCTIONS

### POWER-SERIES COEFFICIENTS

The coefficients for the velocity-profile power series may be expressed in terms of  $A_2$  (coefficient of  $\alpha^2$ ) and the highest order free-stream derivative. The values of  $A_n$  are found by solving simultaneously equations (11) to (15) or (17) to (21) prescribing the boundary conditions on the profile together with the profile equation itself (eq. 8). This procedure yields:

For the five-term series  $\frac{u}{u_1}$ :

$$A_1 = 2 - \frac{1}{3} A_2 + \frac{1}{6} \left( \frac{u}{u_1} \right)_{\alpha=1}^{"}$$
 (Dla)

$$A_3 = -2 - A_2 - \frac{1}{2} \left( \frac{u}{u_1} \right)_{\alpha-1}^{\alpha}$$
 (Dlb)

$$Au_{1} = 1 + \frac{1}{3} A_{2} + \frac{1}{3} \left(\frac{u}{u_{1}}\right)^{"}_{\alpha=1}$$
 (Dlc)

For the six-term series  $\frac{u}{u_1}$ :

$$A_1 = \frac{5}{2} - \frac{1}{4} A_2 - \frac{1}{24} \left(\frac{u}{u_1}\right)_{\alpha=1}^{\alpha}$$
 (D2a)

$$A_3 = -5 - \frac{3}{2} A_2 + \frac{1}{4} \left( \frac{u}{u_1} \right)_{\alpha=1}^{11}$$
 (D2b)

$$A_{4} = 5 + A_{2} - \frac{1}{3} \left(\frac{u}{u_{1}}\right)_{\alpha=1}^{m}$$
 (D2c)

$$A_5 = -\frac{3}{2} - \frac{1}{4} A_2 + \frac{1}{8} \left( \frac{u}{u_1} \right)_{\alpha=1}^{\alpha=1}$$
 (D2d)

A prime over a symbol represents differentiation with respect to the argument of the function in question.

Local and stagnation enthalpy coefficients are obtained simply by replacing  ${\tt A}_n$  in the preceding equations by  ${\tt B}_n$  and  ${\tt C}_n,$  respectively. This substitution is permissible because the series expressions for local and stagnation enthalpy and the appropriate stream boundary conditions are identical in form to the corresponding velocity functions and boundary conditions.

#### VELOCITY FORM PARAMETERS

The displacement and momentum thicknesses are defined, respectively, by

$$\delta^{*} = \int_{0}^{\infty} \frac{\rho}{\rho_{\epsilon}} \left( 1 - \frac{u}{u_{1}} \right) dy$$

$$\theta = \int_{0}^{\infty} \frac{\rho}{\rho_{\epsilon}} \frac{u}{u_{1}} \left( 1 - \frac{u}{u_{1}} \right) dy$$
(D3)

After transformation to the incompressible normal coordinate  $\alpha$  through the use of equation (5) and introduction of the requirement that  $\frac{u}{u_1} = 1$  for  $\alpha \ge 1$ , the relations (D3) become

$$\delta^* = \Delta \int_0^1 \left( 1 - \frac{u}{u_1} \right) d\alpha \quad \text{or} \quad \frac{\delta^*}{\Delta} = \int_0^1 \left( 1 - \frac{u}{u_1} \right) d\alpha$$

$$\theta = \Delta \int_0^1 \frac{u}{u_1} \left( 1 - \frac{u}{u_1} \right) d\alpha \quad \text{or} \quad \frac{\theta}{\Delta} = \int_0^1 \frac{u}{u_1} \left( 1 - \frac{u}{u_1} \right) d\alpha$$

$$(D4)$$

Evaluation of these functions then requires substitution of the correct velocity-profile coefficients into the general relation for  $\frac{u}{u_1}$  (eq. (8))

and substituting the latter into equation (D4). Results of this calculation for the five- and six-term velocity profiles are:

For the five-term series  $\frac{u}{u_1}$ :

$$\frac{\delta^*}{\Delta} = \frac{3}{10} - \frac{\lambda}{120} - \frac{1}{40} \left(\frac{u}{u_1}\right)_{\alpha=1}^{"}$$
 (D5a)

$$\frac{\theta}{\Delta} = \frac{37}{315} - \frac{\lambda}{945} - \frac{\lambda^2}{9,072} - \frac{5\lambda \left(\frac{u}{u_1}\right)_{\alpha=1}^{"}}{9,072} - \frac{37}{3,780} \left(\frac{u}{u_1}\right)_{\alpha=1}^{"} - \frac{19}{22,680} \left[\left(\frac{u}{u_1}\right)_{\alpha=1}^{"}\right]^{2}$$
(D5b)

For the six-term series  $\frac{u}{u_1}$ :

$$\frac{\delta *}{\Delta} = \frac{1}{4} - \frac{\lambda}{240} + \frac{\left(\frac{u}{u_1}\right)_{\alpha=1}^{n}}{240}$$
 (D6a)

$$\frac{\theta}{\Delta}$$
 = 0.10101 - 0.00063131\(\lambda\) - 0.000031566\(\lambda^2\) + 0.0000526\(\lambda\limbda\ru\_1\right)\_{\alpha=1}^{\mathbf{i}''}\) +

0.0016835 
$$\left(\frac{u}{u_1}\right)_{\alpha=1}^{n}$$
 - 0.0000260  $\left[\left(\frac{u}{u_1}\right)_{\alpha=1}^{n}\right]^2$  (D6b)

The definition of  $\lambda = -2A_2$  has been utilized in these equations.

#### LOCAL ENTHALPY FORM PARAMETERS

The quantity  $\nabla^*$  is defined as

$$\nabla^* = \int_0^\infty \frac{\rho}{\rho_{\epsilon}} \left( 1 - \frac{h^*}{h_1^*} \right) dy \tag{D7}$$

After transformation to the incompressible normal coordinate  $\beta$  through the use of equation (6) and introduction of the boundary condition  $\frac{h^*}{h_1^*} = 1$  for  $\beta \ge 1$ , the expression becomes

$$\nabla^* = \nabla \int_0^1 \left( 1 - \frac{h^*}{h_1^*} \right) d\beta \quad \text{or} \quad \frac{\nabla^*}{\nabla} = \int_0^1 \left( 1 - \frac{h^*}{h_1^*} \right) d\beta \tag{D8}$$

The profile function of  $\beta$  (eq. (9)) and the coefficients appropriate to the term of the profile series are substituted into equation (D8) and the following expressions for  $\frac{\nabla^*}{\nabla}$  result:

For the five-term series  $\frac{h^*}{h_1^*}$ :

$$\frac{\nabla^*}{\nabla} = \frac{3}{10} + \frac{1}{60} \Gamma - \frac{1}{40} \left( \frac{h^*}{h_1^*} \right)_{\beta=1}^{"}$$
 (D9)

For the six-term series  $\frac{h^*}{h_1^*}$ :

$$\frac{\nabla^*}{\nabla} = \frac{1}{4} + \frac{1}{120} \Gamma + \frac{1}{240} \left( \frac{h^*}{h_1^*} \right)_{\beta=1}^{11}$$
 (D10)

The coefficient  $B_2$  has been replaced by its equivalent  $\Gamma$ .

Next to be considered is the quantity  $\phi$  which is defined by the relation

$$\emptyset = \int_{0}^{\infty} \frac{\rho}{\rho_{\epsilon}} \frac{u}{u_{1}} \left(1 - \frac{h^{*}}{h_{1}^{*}}\right) dy$$
 (D11)

The local enthalpy boundary condition that  $\frac{h^*}{h_1^*}=1$  for  $\beta \geq 1$  must be applied in conjunction with the velocity boundary condition  $\frac{u}{u_1}=1$  for  $\alpha \geq 1$ . It is apparent that the relative thickness of the velocity and thermal boundary layers must be considered in order to evaluate the integral. For the case where the enthalpy thickness is equal to or greater than the velocity thickness,  $\delta_h \geq \delta_u$ , the integral (D11) becomes:

$$\phi = \int_0^{\delta_u} \frac{\rho}{\rho_\epsilon} \frac{u}{u_1} \left( 1 - \frac{h^*}{h_1^*} \right) dy + \int_{\delta_u}^{\delta_h} \frac{\rho}{\rho_\epsilon} \left( 1 - \frac{h^*}{h_1^*} \right) dy$$

When this equation is transformed to the  $\beta$ -plane, it becomes

$$\phi = \nabla \int_{0}^{\beta(\delta_{\mathbf{u}})} \frac{\mathbf{u}}{\mathbf{u}_{1}} \left(1 - \frac{\mathbf{h}^{*}}{\mathbf{h}_{1}^{*}}\right) d\beta + \nabla \int_{\beta(\delta_{\mathbf{u}})}^{1} \left(1 - \frac{\mathbf{h}^{*}}{\mathbf{h}_{1}^{*}}\right) d\beta$$
 (D12)

The limit  $\beta(\delta_u)$  is evaluated from the relations (5) and (6), and the following equation results:

$$\beta(\delta_{\rm u}) = \frac{1}{\nabla} \int_{0}^{\delta_{\rm u}} \frac{\rho}{\rho_{\rm c}} \, \mathrm{d}y = \frac{\triangle}{\nabla} = b \tag{D13}$$

The quantity b is equal to  $\frac{\int_0^{\delta_u} \frac{\rho}{\rho_\varepsilon} \, \mathrm{d}y}{\int_0^{\delta_h} \frac{\rho}{\rho_\varepsilon} \, \mathrm{d}y}, \text{ and for } \delta_u \leqq \delta_h, \text{ b} \leqq 1.$ 

When the velocity thickness is considered to be equal to or greater than the enthalpy thickness ( $b \ge 1$ ), the integral (Dll) can be written as

$$\phi = \int_0^{\delta_h} \frac{\rho}{\rho_{\epsilon}} \frac{u}{u_1} \left(1 - \frac{h*}{h_1*}\right) dy$$

and is directly reduced to

$$\frac{\phi}{\nabla} = \int_{0}^{1} \frac{u}{u_{1}} \left( 1 - \frac{h^{*}}{h_{1}^{*}} \right) d\beta$$

since  $\left(1 - \frac{h^*}{h_1^*}\right) = 0$  for  $\beta \ge 1$ .

Thus, the integral relations for  $\frac{\emptyset}{\nabla}$  are dependent on whether the quantity b is less than or greater than unity. These integrals may be written

for  $b \le 1$ :

$$\frac{\phi}{\nabla} = \int_0^b \frac{u}{u_1} \left( 1 - \frac{h^*}{h_1^*} \right) d\beta + \int_b^1 \left( 1 - \frac{h^*}{h_1^*} \right) d\beta$$
 (D14a)

and for  $b \ge 1$ :

$$\frac{\phi}{\nabla} = \int_0^1 \frac{u}{u_1} \left( 1 - \frac{h^*}{h_1^*} \right) d\beta$$
 (D14b)

Application of the five- and six-term profile functions of  $\frac{u}{u_1}$  and  $\frac{h^*}{h_1^*}$  to equations (D14) yields

For  $b \le 1$ , five-term series:

$$\frac{\phi}{\nabla} = \frac{3}{10} - \frac{3}{10} b + \frac{2}{15} b^{2} - \frac{3}{140} b^{4} + \frac{1}{180} b^{5} + \lambda \left( \frac{b}{120} - \frac{b^{2}}{180} + \frac{b^{4}}{840} - \frac{b^{5}}{3,024} \right) + \lambda \left( \frac{h^{*}}{h_{1}^{*}} \right)_{\beta=1}^{"} \left( -\frac{b^{2}}{2,160} + \frac{b^{4}}{3,360} - \frac{b^{5}}{9,072} \right) + \left( \frac{h^{*}}{h_{1}^{*}} \right)_{\beta=1}^{"} \left( -\frac{1}{40} + \frac{b^{2}}{90} - \frac{3b^{4}}{560} + \frac{b^{5}}{540} \right) + \lambda \left( \frac{u}{u_{1}} \right)_{\alpha=1}^{"} \left( \frac{b}{40} - \frac{b^{2}}{45} + \frac{b^{4}}{140} - \frac{b^{5}}{432} \right) + \left( \frac{u}{u_{1}} \right)_{\alpha=1}^{"} \left( \frac{h^{*}}{h_{1}^{*}} \right)_{\beta=1}^{"} \left( -\frac{b^{2}}{540} + \frac{b^{4}}{560} - \frac{b^{5}}{1,296} \right) + \Gamma \left[ \frac{1}{60} - \frac{b^{2}}{45} + \frac{b^{3}}{42} - \frac{3b^{4}}{280} + \frac{b^{5}}{540} + \left( \frac{u}{u_{1}} \right)_{\alpha=1}^{"} \left( \frac{b^{2}}{270} - \frac{b^{3}}{168} + \frac{b^{4}}{280} - \frac{b^{5}}{1,296} \right) + \lambda \left( \frac{b^{2}}{1,080} - \frac{b^{3}}{840} + \frac{b^{4}}{1,680} - \frac{b^{5}}{9,072} \right) \right] \tag{D15a}$$

For  $b \ge 1$ , five-term series:

$$\frac{\phi}{\nabla} = \frac{2}{15} \frac{1}{b} - \frac{3}{140} \frac{1}{b^{3}} + \frac{1}{180} \frac{1}{b^{4}} + \lambda \left(\frac{1}{90} \frac{1}{b} - \frac{1}{84} \frac{1}{b^{2}} + \frac{3}{560} \frac{1}{b^{3}} - \frac{1}{1,080} \frac{1}{b^{4}}\right) + \lambda \left(\frac{h^{*}}{h_{1}^{*}}\right)^{"}_{\beta=1} \left(-\frac{1}{540} \frac{1}{b} + \frac{1}{356} \frac{1}{b^{2}} - \frac{1}{560} \frac{1}{b^{3}} + \frac{1}{2,592} \frac{1}{b^{4}}\right) + \left(\frac{h^{*}}{h_{1}^{*}}\right)^{"}_{\beta=1} \left(-\frac{1}{45} \frac{1}{b} + \frac{1}{140} \frac{1}{b^{3}} - \frac{1}{1432} \frac{1}{b^{4}}\right) + \left(\frac{u}{u_{1}}\right)^{"}_{\alpha=1} \left(\frac{1}{90} \frac{1}{b} - \frac{3}{560} \frac{1}{b^{3}} + \frac{1}{540} \frac{1}{b^{4}}\right) + \left(\frac{u}{u_{1}}\right)^{"}_{\alpha=1} \left(\frac{h^{*}}{h_{1}^{*}}\right)^{"}_{\beta=1} \left(-\frac{1}{540} \frac{1}{b} + \frac{1}{560} \frac{1}{b^{3}} - \frac{1}{1,296} \frac{1}{b^{4}}\right) + \Gamma\left[\frac{1}{90} \frac{1}{b} - \frac{1}{420} \frac{1}{b^{3}} + \frac{1}{840} \frac{1}{b^{2}} + \frac{1}{1,680} \frac{1}{b^{3}} - \frac{1}{1,680} \frac{1}{b^{3}} - \frac{1}{1,680} \frac{1}{b^{3}} - \frac{1}{1,680} \frac{1}{b^{3}}\right) + \lambda \left(\frac{1}{1,080} \frac{1}{b} - \frac{1}{840} \frac{1}{b^{2}} + \frac{1}{1,680} \frac{1}{b^{3}} - \frac{1}{1,680} \frac{1}{b^{3}} - \frac{1}{1,680} \frac{1}{b^{3}}\right)$$
(D15b)

For  $b \le 1$ , six-term series:

$$\frac{Q}{\nabla} = \frac{1}{4} - \frac{b}{4} + 0.1190477b^{2} - 0.0297619b^{4} + 0.0138889b^{5} - 0.0021644b^{6} + \left(\frac{u}{u_{1}}\right)_{\alpha=1}^{m} \left(-\frac{b}{240} + 0.0039682b^{2} - 0.0019841b^{4} + 0.0011574b^{5} - 0.0002164b^{6}\right) + \left(\frac{h^{*}}{h_{1}^{*}}\right)_{\beta=1}^{m} \left(\frac{1}{240} - 0.0019841b^{2} + 0.0014881b^{4} - 0.0009259b^{5} + 0.0001804b^{6}\right) + \left(\frac{u}{u_{1}}\right)_{\alpha=1}^{m} \left(\frac{h^{*}}{h_{1}^{*}}\right)_{\beta=1}^{m} \left(-0.000066136b^{2} + 0.000099206b^{4} - 0.000077161b^{5} + 0.00001804b^{6}\right) + \lambda \left(\frac{b}{240} - 0.0029762b^{2} + 0.0009921b^{4} - 0.0004960b^{5} + 0.0000812b^{6}\right) + \lambda \left(\frac{h^{*}}{h_{1}^{*}}\right)_{\beta=1}^{m} \left(0.00004960b^{2} - 0.00004961b^{4} + 0.00003307b^{5} - 0.0000677b^{6}\right) + \Gamma \left[\frac{1}{120} - 0.0119048b^{2} + 0.0148809b^{3} - 0.0089286b^{4} + 0.0027777b^{5} + 0.0003608b^{6} + \left(\frac{u}{u_{1}}\right)_{\alpha=1}^{m} \left(-0.0003968b^{2} + 0.0007440b^{3} - 0.0005952b^{4} + 0.0002315b^{5} - 0.0000361b^{6}\right) + \lambda \left(0.0002976b^{2} - 0.0004464b^{3} + 0.0002976b^{4} - 0.0000992b^{5} + 0.0000136b^{6}\right) \right]$$

$$(D16a)$$

For  $b \ge 1$ , six-term series:

$$\frac{0}{\sqrt{a}} = 0.1190477 \frac{1}{b} - 0.0297619 \frac{1}{b^{3}} + 0.0138889 \frac{1}{b^{4}} - 0.0021644 \frac{1}{b^{5}} + 0.0138889 \frac{1}{b^{4}} = 0.0021644 \frac{1}{b^{5}} + 0.0021644 \frac{1}{b^{5}} = 0.0021644 \frac{1}{b^{5$$

$$\left(\frac{u}{u_1}\right)_{\alpha=1}^{n}\left(-0.0019841\,\frac{1}{b}+0.0014881\,\frac{1}{b^3}-0.0009259\,\frac{1}{b^4}+0.0001804\,\frac{1}{b^5}\right)+$$

$$\left(\frac{h^*}{h_1^*}\right)_{\beta=1}^{***} \left(0.0039682 \, \frac{1}{b} - 0.0019841 \, \frac{1}{b^3} + 0.0011574 \, \frac{1}{b^4} - 0.0002164 \, \frac{1}{b^5}\right) + \\$$

$$\left(\frac{u}{u_1}\right)_{\alpha=1}^{m} \left(\frac{h^*}{h_1^*}\right)_{\beta=1}^{m} \left(-\frac{0.000066136}{b} + \frac{1}{b} + \frac{0.000099206}{b^{\frac{1}{3}}} - 0.000077161 + \frac{1}{b^{\frac{1}{4}}} + \frac{1}{b^{\frac{1}{4}$$

$$0.00001804 \frac{1}{b^{5}} + \lambda \left(0.0059524 \frac{1}{b} - 0.0074404 \frac{1}{b^{2}} + 0.0044643 \frac{1}{b^{3}} - 0.0044643 \frac{1}{b^{2}} \right)$$

$$0.0013889 \ \frac{1}{b^4} + 0.0001804 \ \frac{1}{b^5} \bigg) + \lambda \bigg(\frac{h*}{h_1*}\bigg)_{\beta=1}^{**} \bigg(0.00019841 \ \frac{1}{b} - 0.00037202 \ \frac{1}{b^2} +$$

0.00029762 
$$\frac{1}{b^3}$$
 - 0.00011574  $\frac{1}{b^4}$  + 0.00001803  $\frac{1}{b^5}$ ) +  $\Gamma$  0.0059523  $\frac{1}{b}$  -

$$0.0019842 \frac{1}{b^{3}} + 0.0009920 \frac{1}{b^{4}} - 0.0001623 \frac{1}{b^{5}} + \left(\frac{u}{u_{1}}\right)_{\alpha=1}^{10} \left(-0.0000992 \frac{1}{b} + \frac{1}{b^{2}}\right)$$

$$0.0000992 \ \frac{1}{b^{3}} - 0.0000661 \ \frac{1}{b^{4}} + 0.0000135 \ \frac{1}{b^{5}} \bigg) + \lambda \bigg( 0.0002976 \ \frac{1}{b} -$$

0.0004464 
$$\frac{1}{b^2}$$
 + 0.0002976  $\frac{1}{b^3}$  - 0.0000992  $\frac{1}{b^4}$  + 0.0000136  $\frac{1}{b^5}$ ) (D16b)

#### TOTAL ENTHALPY FORM PARAMETERS

The quantities  $\square$ \* and  $\Psi$  are defined, respectively, as

$$\Box * = \int_{0}^{\infty} \frac{\rho}{\rho_{\epsilon}} \left( 1 - \frac{H^{*}}{H_{1}^{*}} \right) dy$$
 (D17a)

$$\Psi = \int_{0}^{\infty} \frac{\rho}{\rho_{\epsilon}} \frac{u}{u_{1}} \left( 1 - \frac{H^{*}}{H_{1}^{*}} \right) dy$$
 (D17b)

These definitions are transformed to the  $\omega$ -plane through use of equation (7). Because of the similarity between corresponding relations for the total enthalpy and local enthalpy, the equations for  $\square */\square$  and  $\psi/\square$  are identical to those for the local enthalpy thickness equations (D9), (D10), (D15), and (D16) when  $\psi$ ,  $\square *$ ,  $\square$ , c, and  $\Omega$  are substituted for  $\emptyset$ ,  $\nabla *$ ,  $\nabla$ , b, and  $\Gamma$ , respectively, and the stream boundary conditions  $\left(\frac{h^*}{h_1^*}\right)^{"}_{\beta=1}$  and  $\left(\frac{h^*}{h_1^*}\right)^{"}_{\beta=1}$  are replaced by  $\left(\frac{H^*}{H_1^*}\right)^{"}_{\omega=1}$  and  $\left(\frac{H^*}{H_1^*}\right)^{"}_{\omega=1}$ .

#### DISSIPATION FUNCTION

The dissipation function  $\,\Phi\,$  is defined in appendix B and is given by

$$\Phi = \frac{u_1^2}{\rho_{\epsilon}^2} \frac{\rho_{\mathbf{w}} \mu_{\mathbf{w}}}{\Delta} \int_0^1 \left[ \frac{d\left(\frac{u}{u_1}\right)}{d\alpha} \right]^2 d\alpha$$

For the five- and six-term profiles, this integral is evaluated as: For the five-term series  $\frac{u}{u_1}$ :

$$\Phi = \frac{u_1^2}{\rho_{\epsilon}^2} \frac{\rho_{w} \mu_{w}}{\Delta} \left\{ \frac{52}{35} + \frac{4}{105} \lambda + \frac{1}{420} \lambda^2 - \frac{397}{1,260} \lambda \left( \frac{u}{u_1} \right)_{\alpha=1}^{n} + \frac{13}{105} \left( \frac{u}{u_1} \right)_{\alpha=1}^{n} + \frac{1}{105} \left[ \left( \frac{u}{u_1} \right)_{\alpha=1}^{n} \right]^2 \right\}$$
(D18)

For the six-term series  $\frac{u}{u_1}$ :

$$\Phi = \frac{u_1^2}{\rho_e^2} \frac{\rho_w \mu_w}{\Delta} \left\{ \frac{25}{14} + \frac{5}{168} \lambda - \frac{5}{168} \left( \frac{u}{u_1} \right)_{\alpha=1}^{11} + \frac{1}{1,008} \lambda^2 + \frac{1}{2,520} \left[ \left( \frac{u}{u_1} \right)_{\alpha=1}^{11} \right]^2 - \frac{1}{1,008} \lambda \left( \frac{u}{u_1} \right)_{\alpha=1}^{11} \right\}$$
(D19)

## APPENDIX E

## DERIVATION OF COMPLETE BOUNDARY-LAYER EQUATIONS

## FOR TWO-DIMENSIONAL UNSTEADY FLOW

The Prandtl boundary-layer equations (eqs. (B1) to (B4)) may be rewritten with the aid of equation (B6) in slightly different form as

$$\frac{\partial u}{\partial t} + u \frac{\partial u}{\partial x} + v \frac{\partial u}{\partial y} = -\frac{1}{\rho} \frac{\partial p_{\underline{1}}}{\partial x} + \frac{1}{\rho} \frac{\partial}{\partial y} \left( \mu \frac{\partial u}{\partial y} \right)$$
 (E1)

$$\frac{\partial f}{\partial v} + \frac{\partial x}{\partial (vn)} + \frac{\partial x}{\partial (vn)} = 0$$
 (E3)

$$\frac{\partial h}{\partial t} + u \frac{\partial h}{\partial x} + v \frac{\partial h}{\partial y} = \frac{1}{\rho} \left( \frac{\partial p_1}{\partial t} + u \frac{\partial p_1}{\partial x} \right) + \frac{1}{\rho} \frac{\partial}{\partial y} \left( \frac{c_p}{c_p} \frac{\partial h}{\partial y} \right) + \frac{\mu}{\rho} \left( \frac{\partial u}{\partial y} \right)^2$$
(E3)

The "incompressible" normal ordinate Y is now introduced together with a stream function  $\Psi$  which satisfies the equation of continuity (eq. (E2)). (A similar procedure was used in ref. 23.)

$$Y = \int_{0}^{y} \frac{1}{\rho_{\epsilon}} \rho(x, y, t) dy$$
 (E4)

$$u = \frac{\rho_{\epsilon}}{\rho} \left( \frac{\partial \Psi}{\partial y} \right)_{x,t}$$

$$v = -\frac{\rho_{\epsilon}}{\rho} \left[ \left( \frac{\partial \Psi}{\partial x} \right)_{y,t} + \left( \frac{\partial}{\partial t} \int_{0}^{y} \frac{\rho}{\rho_{\epsilon}} \, dy \right)_{x,y} \right]$$
(E5)

The relationships of the partial derivatives in the x,y,t system to those in the x,Y,t system are:

$$\left(\frac{\partial}{\partial x}\right)_{x,t} = \left(\frac{\partial}{\partial x}\right)_{x,t} + \left(\frac{\partial}{\partial y}\right)_{x,t} \left(\frac{\partial y}{\partial x}\right)_{x,t} + \left(\frac{\partial}{\partial y}\right)_{x,t} + \left(\frac{\partial}{\partial y}\right)_{x,t}$$

The stream function is then defined by

$$v = -\frac{\rho}{\rho \epsilon} \left[ \left( \frac{\partial x}{\partial y} \right)^{X,t} + \left( \frac{\partial y}{\partial y} \right)^{X,t} \left( \frac{\partial x}{\partial y} \right)^{X,t} + \left( \frac{\partial t}{\partial y} \right)^{X,y} \right]$$
(E6)

Transforming the equations of motion (eqs. (E1) and (E3)) to x,Y,t coordinates with the aid of the preceding equations, employing the Chapman-Rubesin viscosity-temperature relation (appendix B), and considering the Prandtl number and specific heat to be constant results in the following equations:

$$\frac{\partial^2 \Psi}{\partial Y \partial t} + \frac{\partial \Psi}{\partial Y} \frac{\partial^2 \Psi}{\partial X \partial Y} - \frac{\partial \Psi}{\partial X} \frac{\partial^2 \Psi}{\partial Y^2} = -\frac{1}{\rho} \frac{\partial p_1}{\partial X} + \frac{\rho_1 \mu_1}{\rho_e^2} C_W \frac{\partial^3 \Psi}{\partial Y^3}$$
 (E7a)

$$\frac{\partial F}{\partial r} + \frac{\partial F}{\partial r} \frac{\partial F}{\partial r} - \frac{\partial F}{\partial r} \frac{\partial F}{\partial r} = \frac{1}{2} \left( \frac{\partial F}{\partial r} + \frac{\partial F}{\partial r} \frac{\partial F}{\partial r} \right) + \frac{\partial F}{\partial r} \frac{\partial F}{\partial r} + \left( \frac{\partial F}{\partial r} \frac{\partial F}{\partial r} \right) + \left( \frac{\partial F}{\partial r} \frac{\partial F}{\partial r} \right)$$
(E.1p.)

The boundary conditions to be satisfied are then

$$\Psi(x,0,t) = 0$$

$$\left(\frac{\partial \Psi}{\partial Y}\right)_{Y=0} = 0$$

$$\left(\frac{\partial \Psi}{\partial Y}\right)_{Y\to\infty} = u_{1}(x,t)$$

$$h(x,0,t) = h_{w}$$

$$h(x,\infty,t) = h_{1}(x,t)$$
(E8)

For the case of either the shock wave or the rarefaction wave propagating into air at rest in a uniform channel, the free-stream quantities become functions only of the parameter  $\xi = \frac{x}{a_{\varepsilon}t}$ . The equations of motion may be written in similarity form by using this conical parameter. After introduction of the identities:

$$\Psi = \sqrt{\nu_{\epsilon}t} \ a_{\epsilon}f(\xi,\eta)$$

$$h = h_{\epsilon}g(\xi,\eta)$$

$$\xi = \frac{x}{a_{\epsilon}t}$$

$$\eta = \frac{Y}{\sqrt{\nu_{\epsilon}t}}$$

$$t = t$$
(E9)

the transformation equations from the x,Y,t coordinate system to the  $\xi,\eta,t$  coordinate system are

$$\left(\frac{\partial}{\partial t}\right)_{x,Y} = \left(\frac{\partial}{\partial \xi}\right)_{\eta,t} \left(\frac{\partial \xi}{\partial t}\right)_{x} + \left(\frac{\partial}{\partial \eta}\right)_{\xi,t} \left(\frac{\partial \eta}{\partial t}\right)_{Y} + \left(\frac{\partial}{\partial t}\right)_{\xi,\eta} = -\frac{\xi}{t} \left(\frac{\partial}{\partial \xi}\right)_{\eta,t} - \frac{1}{2} \frac{\eta}{t} \left(\frac{\partial}{\partial \eta}\right)_{\xi,t} + \left(\frac{\partial}{\partial t}\right)_{\xi,\eta}$$

$$\left(\frac{\partial}{\partial x}\right)_{t,Y} = \left(\frac{\partial}{\partial \xi}\right)_{\eta,t} \left(\frac{\partial \xi}{\partial x}\right)_{t} = \frac{1}{a_{\epsilon}t} \left(\frac{\partial}{\partial \xi}\right)_{\eta,t}$$

$$\left(\frac{\partial}{\partial Y}\right)_{x,t} = \left(\frac{\partial}{\partial \eta}\right)_{\xi,t} \left(\frac{\partial \eta}{\partial Y}\right)_{t} = \frac{1}{\sqrt{\nu_{\epsilon}t}} \left(\frac{\partial}{\partial \eta}\right)_{\xi,t}$$

$$\left(\frac{\partial}{\partial Y}\right)_{x,t} = \left(\frac{\partial}{\partial \eta}\right)_{\xi,t} \left(\frac{\partial \eta}{\partial Y}\right)_{t} = \frac{1}{\sqrt{\nu_{\epsilon}t}} \left(\frac{\partial}{\partial \eta}\right)_{\xi,t}$$
(E10)

Equations (E7a) and (E7b) are then transformed to the  $\xi,\eta,t$  coordinate system by using equations (E9) and (E10), the equation of state,  $p=\frac{\gamma-1}{\gamma}$   $\rho h$ , and so forth; the following equations result

$$\underline{\rho}_{\underline{1}}\underline{\mu}_{\underline{1}}C_{w}\frac{\partial^{3}\underline{f}}{\partial\eta^{3}} + \left(\frac{\eta}{2} + \frac{\partial \underline{f}}{\partial\xi}\right)\frac{\partial^{2}\underline{f}}{\partial\eta^{2}} + \left(\xi - \frac{\partial \underline{f}}{\partial\eta}\right)\frac{\partial^{2}\underline{f}}{\partial\eta\partial\xi} = \frac{1}{\gamma} g \frac{1}{\underline{p}_{\underline{1}}} \frac{d\underline{p}_{\underline{1}}}{d\xi} \tag{E11}$$

$$\underline{\rho}_{\underline{1}}\underline{\mu}_{\underline{1}}C_{w}\left[\frac{1}{N_{\mathrm{Pr}}}\frac{\partial^{2}\underline{g}}{\partial\eta^{2}} + (\gamma - 1)\left(\frac{\partial^{2}\underline{f}}{\partial\eta^{2}}\right)^{2}\right] + \left(\frac{\eta}{2} + \frac{\partial \underline{f}}{\partial\xi}\right)\frac{\partial \underline{g}}{\partial\eta} + \left(\xi - \frac{\partial \underline{f}}{\partial\eta}\right)\frac{\partial \underline{g}}{\partial\xi} = \frac{\gamma}{\gamma} \frac{1}{p_{\underline{1}}}\frac{d\underline{p}_{\underline{1}}}{d\xi}\left(\xi - \frac{\partial \underline{f}}{\partial\eta}\right)g \tag{E12}$$

with the boundary conditions

$$f(\xi,0) = 0$$

$$\left(\frac{\partial f}{\partial \eta}\right)_{\eta=0} = 0$$

$$\left(\frac{\partial f}{\partial \eta}\right)_{\eta\to\infty} = \frac{u_{\underline{1}}}{a_{\underline{\epsilon}}} = \underline{u}_{\underline{1}}(\xi)$$

$$g(\xi,0) = \frac{h_{\underline{W}}}{h_{\underline{\epsilon}}} = \underline{h}_{\underline{W}}$$

$$g(\xi,\infty) = \frac{h_{\underline{1}}}{h_{\underline{\epsilon}}} = \underline{h}_{\underline{1}}(\xi)$$
(E13)

## APPENDIX F

# DERIVATION OF INTEGRAL RELATIONSHIPS AT A DISCONTINUITY

## IN THE OUTER FREE-STREAM FLOW

In the outer inviscid flow, consider an arbitrary discontinuity which moves with a velocity  $V^{\star}$  relative to the wall. The mass flux through this discontinuity in an arbitrary distance L normal to the wall,  $L >\!\!> \delta$ , may be expressed in a coordinate system moving with a velocity  $V^{\star}$  as

(Mass flux)
$$(\rho_{\epsilon} a_{\epsilon})^{-1} = \int_{0}^{L} \underline{\rho} \underline{u}^* dy$$
 (F1)

The velocity relative to the discontinuity is  $\underline{u}^* = \underline{u} - \underline{V}^*$  and the bars denote nondimensionalization by the reference density and velocity  $(\rho_{\varepsilon}a_{\varepsilon})$ . Equation (F1) may be evaluated by substitution and use of the definitions of  $\delta^*$  and  $\nabla^*$  to give

$$(\text{Mass flux})(\rho_{\epsilon}a_{\epsilon})^{-1} = \left(\underline{u}_{1} - \underline{v}^{*}\right) \frac{h_{1}^{*}}{h_{1}} \nabla^{*} - \underline{u}_{1}\delta^{*} + \left(\underline{u}_{1} - \underline{v}^{*}\right)\underline{\rho}_{1} \int_{0}^{L} dy \quad (\text{F2})$$

The momentum flux may likewise be expressed as

(Momentum flux) 
$$\left(\rho_{\epsilon} a_{\epsilon}^{2}\right)^{-1} = \int_{0}^{L} \left(\rho \underline{u}^{*2} + \frac{p}{\rho_{\epsilon} a_{\epsilon}^{2}}\right) dy$$
 (F3)

$$(\text{Momentum flux}) \left( \rho_{\epsilon} a_{\epsilon}^{2} \right)^{-1} = \underline{u}_{1}^{2} \theta - \underline{u}_{1} \delta * \left( \underline{u}_{1} - 2\underline{v} * \right) + \left( \underline{u}_{1} - \underline{v} * \right)^{2} \frac{h_{1}^{*}}{h_{1}} \ \, \nabla * + \left( \underline{u}_{1} - \underline{v} * \right)^{2} \left($$

$$\int_{0}^{L} \left[ \rho_{1} \left( \underline{u}_{1} - \underline{v}^{*} \right)^{2} + \frac{p_{1}}{\rho_{\epsilon} a_{\epsilon}^{2}} \right] dy$$
 (F4)

In a similar manner the energy flux into the discontinuity may be evaluated as

(Energy flux) 
$$\left(\rho_{\epsilon} a_{\epsilon}^{3}\right)^{-1} = \int_{0}^{L} \underline{\rho u}^{*} \frac{h + \underline{u}^{*2}}{a_{\epsilon}^{2}} dy$$
 (F5)

$$(\text{Energy flux}) \left( \rho_{\epsilon} \mathbf{a}_{\epsilon}^{3} \right)^{-1} = -\frac{\mathbf{h}_{1}^{*}}{\mathbf{a}_{\epsilon}^{2}} \underline{\mathbf{u}}_{1} \phi + \frac{3}{2} \underline{\mathbf{u}}_{1}^{2} \underline{\mathbf{v}}^{*} \theta + \frac{\underline{\mathbf{u}}_{1}}{2} \left[ 3 \underline{\mathbf{v}}^{*} \left( \underline{\mathbf{u}}_{1} - \underline{\mathbf{v}}^{*} \right) - \frac{2\mathbf{h}_{1}}{\mathbf{a}_{\epsilon}^{2}} \right] \delta^{*} + \frac{\mathbf{h}_{1}^{*}}{\mathbf{h}_{1}} \left[ \frac{\underline{\mathbf{u}}_{1} \mathbf{h}_{1}}{\mathbf{a}_{\epsilon}^{2}} + \frac{\left( \underline{\mathbf{u}}_{1} - \underline{\mathbf{v}}^{*} \right)^{3}}{2} \right] \nabla^{*} - \frac{1}{2} \underline{\mathbf{u}}_{1}^{3} \Delta \mathbf{I} + \int_{0}^{\mathbf{L}} \underline{\mathbf{h}}_{1}^{2} \underline{\mathbf{h}}_{1}^{2} + \frac{\left( \underline{\mathbf{u}}_{1} - \underline{\mathbf{v}}^{*} \right)^{2}}{2} \left( \underline{\mathbf{u}}_{1} - \underline{\mathbf{v}}^{*} \right) d\mathbf{y}$$

$$(F6)$$

where

$$I = \int_{0}^{1} \left[ 1 - \left( \frac{u}{u_{1}} \right)^{3} \right] d\alpha = I(\lambda)$$
 (F7)

If the discontinuity is assumed to have zero thickness and to contain no sources or sinks, the entering flux must equal that leaving since heat transfer and wall shear have zero length in which to influence the flow. If the conditions on opposite sides of the discontinuity are denoted as states i and j, the following equalities must apply:

Mass:

$$u_{i}\left[\left(1-\frac{v^{*}}{u_{i}}\right)\frac{h_{i}^{*}}{h_{i}} \nabla_{i}^{*}-\delta_{i}^{*}\right] = u_{j}\left[\left(1-\frac{v^{*}}{u_{j}}\right)\frac{h_{j}^{*}}{h_{j}} \nabla_{j}^{*}-\delta_{j}^{*}\right] + \left[\rho_{j}u_{j}\left(1-\frac{v^{*}}{u_{j}}\right)-\rho_{i}u_{i}\left(1-\frac{v^{*}}{u_{i}}\right)\right]L \quad (F8)$$

Momentum:

$$u_{i}^{2} \left[\theta_{i} + \left(1 - \frac{2V^{*}}{u_{i}}\right) \delta_{i}^{*} - \left(1 - \frac{V^{*}}{u_{i}}\right)^{2} \frac{h_{i}^{*}}{h_{i}} \nabla_{i}^{*}\right] = u_{j}^{2} \left[\theta_{j} + \left(1 - \frac{2V^{*}}{u_{j}}\right) \delta_{j}^{*} - \left(1 - \frac{V^{*}}{u_{j}}\right)^{2} \frac{h_{j}^{*}}{h_{j}} \nabla_{j}^{*}\right] - \left\{\rho_{j}^{u}_{j}^{2} \left[\left(1 - \frac{V^{*}}{u_{j}}\right)^{2} + \frac{p_{j}^{2}}{\rho_{j}^{u}_{j}^{2}}\right] - \rho_{i}^{u}_{i}^{2} \left[\left(1 - \frac{V^{*}}{u_{i}}\right)^{2} + \frac{p_{i}^{2}}{\rho_{i}^{u}_{i}^{2}}\right]\right\} L$$
(F9)

Energy:

$$\begin{split} u_{i}^{3} & \left\{ \frac{h_{i}^{*}}{u_{i}^{2}} \, \phi_{i} - \frac{3}{2} \, \frac{v^{*}}{u_{i}} \, \theta_{i} - \frac{1}{2} \left[ \frac{3v^{*}}{u_{i}} \left( 1 - \frac{v^{*}}{u_{i}} \right) - \frac{2h_{i}}{u_{i}^{2}} \right] \delta_{i}^{*} - \frac{h_{i}^{*}}{h_{i}} \left[ \frac{h_{i}}{u_{i}^{2}} + \frac{1}{2} \left( 1 - \frac{v^{*}}{u_{i}} \right)^{3} \right] \nabla_{i}^{*} + \frac{1}{2} \Delta_{i} I_{i} \right\} \\ & = u_{j}^{3} \left\{ \frac{h_{j}^{*}}{u_{j}^{2}} \, \phi_{j} - \frac{3}{2} \, \frac{v^{*}}{u_{j}} \, \theta_{j} - \frac{1}{2} \left[ \frac{3v^{*}}{u_{j}} \left( 1 - \frac{v^{*}}{u_{j}} \right) - \frac{2h_{j}}{u_{j}^{2}} \right] \delta_{j}^{*} - \frac{h_{j}^{*}}{u_{j}^{2}} \left[ \frac{h_{j}}{u_{j}^{2}} + \frac{1}{2} \left( 1 - \frac{v^{*}}{u_{j}} \right)^{3} \right] \nabla_{j}^{*} + \frac{1}{2} \Delta_{j} I_{j} \right\} - \left\{ \rho_{j} u_{j}^{3} \left( 1 - \frac{v^{*}}{u_{j}} \right) \left[ \frac{h_{j}}{u_{j}^{2}} + \frac{1}{2} \left( 1 - \frac{v^{*}}{u_{j}} \right)^{2} \right] - \rho_{i} u_{i}^{3} \left( 1 - \frac{v^{*}}{u_{i}} \right) \left[ \frac{h_{i}}{u_{i}^{2}} + \frac{1}{2} \left( 1 - \frac{v^{*}}{u_{j}} \right)^{2} \right] \right\} L \tag{F10} \end{split}$$

### REFERENCES

- 1. Duff, Russell E.: The Use of Real Gases in a Shock Tube. Rep. 51-3, Project M720-4 (Contract No. N6-ONR-232, TO IV), Eng. Res. Inst., Univ. of Michigan, Mar. 1951.
- 2. Glass, I. I., Martin, W., and Patterson, G. N.: A Theoretical and Experimental Study of the Shock Tube. UTIA Rep. No. 2, Inst. of Aerophysics, Univ. of Toronto, Nov. 1953.
- 3. Hertzberg, A.: Shock Tubes for Hypersonic Flow. Rep. No. AF-702-A-1, Cornell Aero. Lab., Inc., May 1951.
- 4. Yoler, Y. A.: Hypersonic Shock Tube. Memo. No. 18 (Contract DA-04-495-Ord-19), GALCIT, July 19, 1954.
- 5. Resler, E. L., Lin, Shao-Chi, and Kantrowitz, Arthur: The Production of High Temperature Gases in Shock Tubes. Jour. Appl. Phys., vol. 23, no. 12, Dec. 1952, pp. 1390-1399.
- 6. Hollyer, Robert N., Jr.: A Study of Attenuation in the Shock Tube. Proj. M720-4 (Contract No. N6-ONR-232-TO IV), Univ. of Michigan Eng. Res. Inst., July 1, 1953.
- 7. Trimpi, Robert L., and Cohen, Nathaniel B.: A Theory for Predicting the Flow of Real Gases in Shock Tubes With Experimental Verification. NACA TN 3375, 1955.
- 8. Boyer, D. W.: Effects of Kinematic Viscosity and Wave Speed on Shock Wave Attenuation. UTIA Tech. Note No. 8, Inst. of Aerophysics, Univ. of Toronto, May 1956.
- 9. Donaldson, Coleman duP., and Sullivan, Roger D.: The Effect of Wall Friction on the Strength of Shock Waves in Tubes and Hydraulic Jumps in Channels. NACA TN 1942, 1949.
- 10. Emrich, R. J., and Curtis, C. W.: Attenuation in the Shock Tube. Jour. Appl. Phys., vol. 24, no. 3, Mar. 1953, pp. 360-363.
- 11. Mirels, Harold: Attenuation in a Shock Tube Due to Unsteady-Boundary-Layer Action. NACA TN 3278, 1956.
- 12. Mirels, Harold: Laminar Boundary Layer Behind Shock Advancing Into Stationary Fluid. NACA TN 3401, 1955.
- 13. Mirels, Harold: Boundary Layer Behind Shock or Thin Expansion Wave Moving Into Stationary Fluid. NACA TN 3712, 1956.

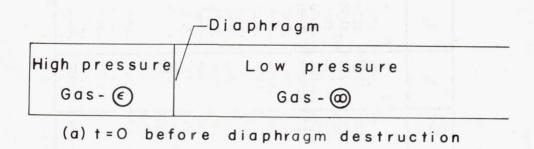
14. Rott, N., and Hartunian, R.: On the Heat Transfer to the Walls of a Shock Tube. Graduate School Aero. Eng., Cornell Univ. (Contract AF 33 (038)-21406), Nov. 1955.

- 15. Cohen, Nathaniel B.: A Power-Series Solution for the Unsteady Laminar Boundary-Layer Flow in an Expansion Wave of Finite Width Moving Through a Gas Initially at Rest. NACA TN 3943, 1957.
- 16. Von Kármán, Theodore: On the Foundations of High Speed Aerodynamics. Proc. First U. S. Nat. Cong. Appl. Mech. (Chicago, Ill., 1951), A.S.M.E., 1952, pp. 673-685.
- 17. Kalikhman, L. E.: Heat Transmission in the Boundary Layer. NACA TM 1229, 1949.
- 18. Chapman, Dean R., and Rubesin, Morris W.: Temperature and Velocity Profiles in the Compressible Laminar Boundary Layer With Arbitrary Distribution of Surface Temperature. Jour. Aero. Sci., vol. 16, no. 9, Sept. 1949, pp. 547-565.
- 19. Scarborough, James B.: Numerical Mathematical Analysis. The Johns Hopkins Press (Baltimore), 1930.
- 20. Hall, J. G.: The Transition Through a Contact Region. UTIA Rep. No. 26, Inst. of Aerophysics, Univ. of Toronto, Jan. 1954.
- 21. Von Kármán, Th.: Turbulance and Skin Friction. Jour. Aero. Sci., vol. 1, no. 1, Jan. 1934, pp. 1-20.
- 22. Ferri, Antonio: Elements of Aerodynamics of Supersonic Flows. The MacMillan Co., 1949.
- 23. Stewartson, K.: On the Impulsive Motion of a Flat Plate in a Viscous Fluid. Quart. Jour. Mech. and Appl. Math., vol. IV, pt. 2, June 1951, pp. 182-198.
- 24. Courant, R., and Friedrichs, K. O.: Supersonic Flow and Shock Waves. Pure & Appl. Math., vol. 1, Interscience Publishers, Inc. (New York), 1948.
- 25. Young, A. D.: Boundary Layers. Vol. I of Modern Developments in Fluid Dynamics High Speed Flow, L. Howarth, ed., The Clarendon Press (Oxford), 1953.

TABLE I. - RESULTS OF NUMERICAL INTEGRAL SOLUTION INSIDE EXPANSION FAN.

[BRANCH I; 
$$\gamma = 1.4$$
;  $N_{Pr} = 0.72$ .]

ţ	Z	W	λ	Г	ъ	<u>dZ</u> d <b>ξ</b>	<u>d₩</u> dţ	<u>dλ</u> d <b>ξ</b>	<u>dr</u> d <b>ţ</b>	db d <b>ξ</b>	÷̂∈	ĝ̃∈
-1.00 98 96 94 92 90 88 80 70 50 40 30 10 0 .10 .20 .40 .50 .60	0 .002225 .004309 .006260 .008081 .009779 .011356 .014171 .016560 .023269 .024117 .023808 .022679 .020965 .018949 .016764 .014562 .012449 .010499 .008754 .005930	0 .003760 .007337 .010755 .014015 .017134 .020106 .025658 .030698 .041321 .049392 .055258 .059201 .061468 .062274 .061854 .060390 .058069 .055091 .051632 .047857 .043930 .039966	20.000 18.675 18.087 17.662 17.278 16.949 16.633 15.559 14.410 13.369 12.402 11.482 10.612 9.762 8.971 8.210 7.490 6.817 6.196 5.631 5.124 4.674	-10.000 -7.907 -7.058 -6.433 -5.894 -5.429 -5.006 -4.256 -3.591 -2.148 890 .261 1.343 2.378 3.380 4.356 5.316 6.263 7.203 8.139 9.076 10.971	0.8485 .9038 .9220 .9335 .9427 .9493 .9544 .9661 .9689 .9643 .9553 .9428 .9282 .9112 .8936 .8749 .8558 .8749 .7658	0.1148 .1077 .1009 .0943 .0879 .0818 .0760 .0547 .0328 .0154 .0021 0076 0147 0189 0215 0222 0218 0205 0164 0164 0141	0.1926 .1832 .1748 .1670 .1593 .1521 .1454 .1322 .0928 .0692 .0486 .0306 .0150 .0016 0099 0194 0269 0366 0389 0398 0398	-% -36.11 -23.63 -20.30 -17.51 -16.17 -14.86 -13.37 -12.32 -10.86 -9.99 -9.43 -8.64 -8.17 -7.48 -7.48 -7.48 -7.551 -5.57 -4.70	52.34 35.48 28.67 24.74 22.13 20.14 17.58 13.32 11.96 11.12 10.55 10.17 9.88 9.67 9.43 9.37 9.35 9.45 9.56	.192 .726 .492 .383 .294 .229 .143 .080 014 071 136 160 172 185 190 194 193 197 154	0 .1305 .1829 .2219 .2538 .2811 .3051 .3457 .3794 .4434 .4888 .5220 .5465 .5645 .5777 .5870 .5935 .5977 .6001 .6008 .5999 .5974	0 .1513 .2091 .2498 .2814 .3070 .3280 .3602 .3826 .4108 .4131 .3990 .3739 .3413 .3036 .2626 .2195 .1754 .1309 .0864 .042400090430



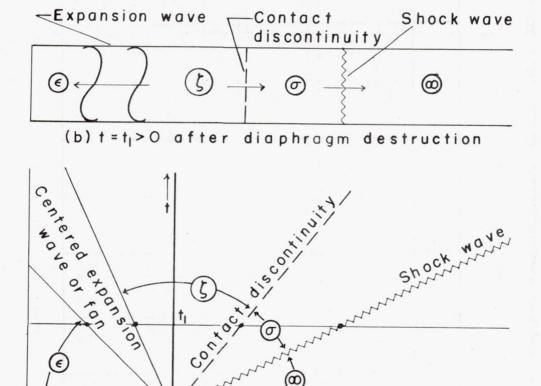


Figure 1.- Sketches showing various regions and waves existing in a constant-area shock tube before and after diaphragm destruction. Circled symbols indicate regions.

wave

diagram,

t ≥ 0

0

(c) Shock tube

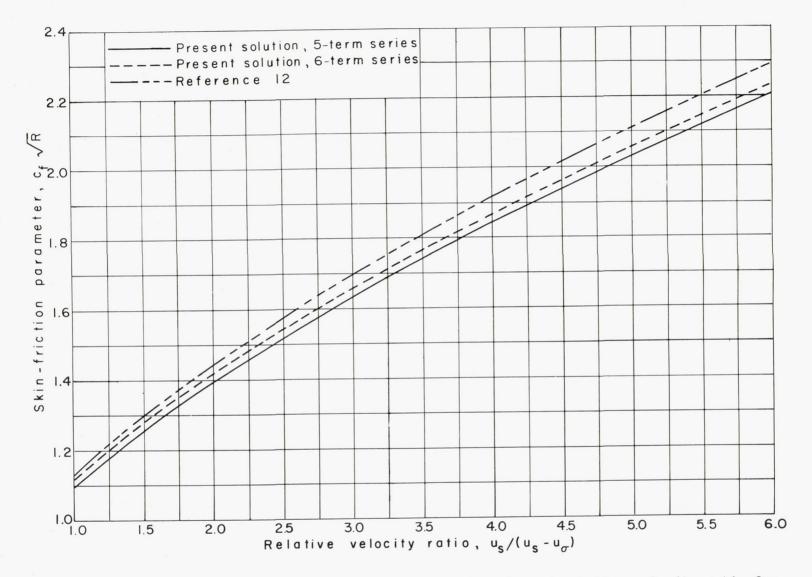


Figure 2.- Variation of skin-friction parameter as a function of relative velocity ratio for shock-initiated flows.

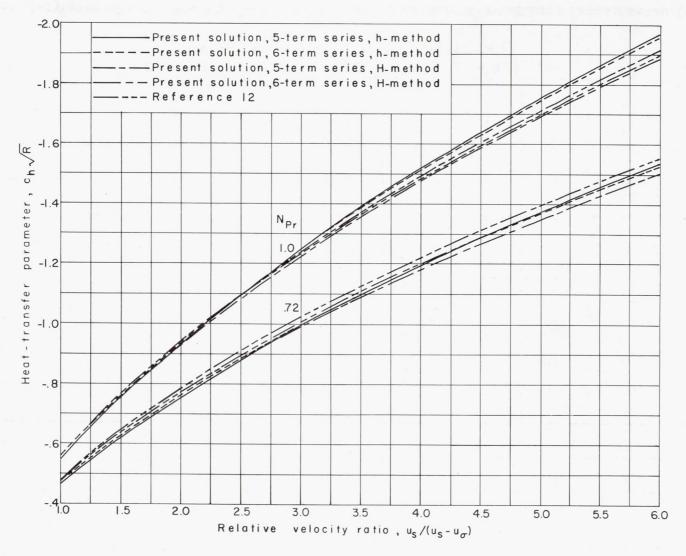


Figure 3.- Variation of heat-transfer parameter as a function of relative velocity ratio for shock-initiated flows.

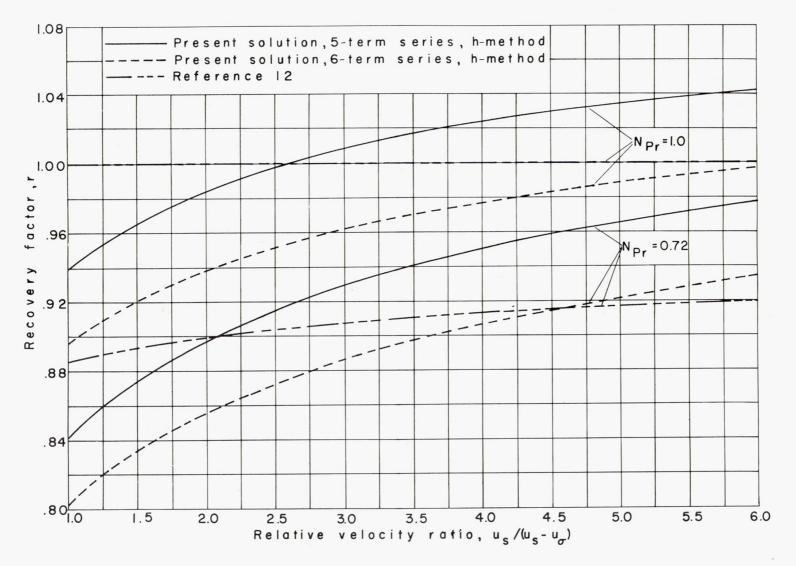


Figure 4.- Variation of recovery factor as a function of relative velocity ratio for shock-initiated flows.

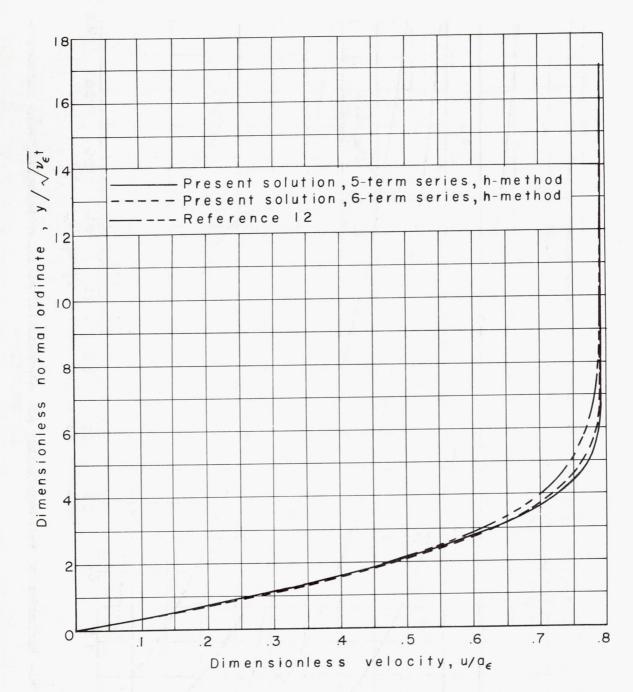


Figure 5.- Velocity profiles at  $\xi_d$  for shock-initiated flow of  $u_s/(u_s-u_\sigma)=2.0$ .

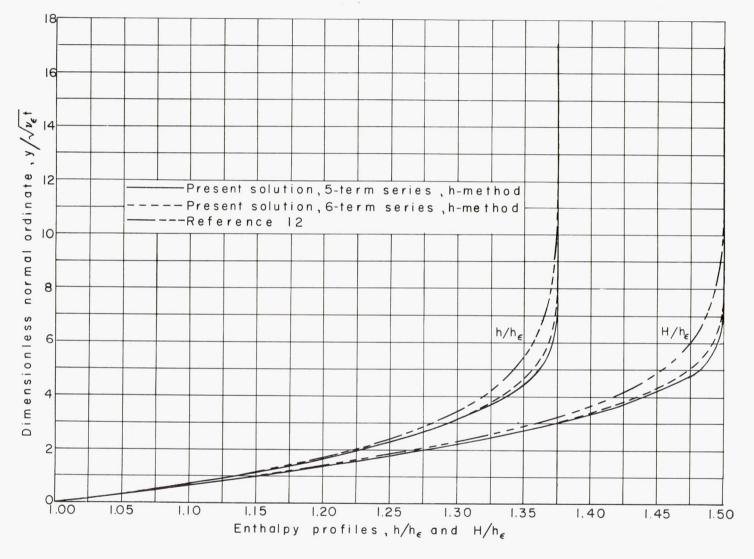


Figure 6.- Enthalpy profiles at  $\xi_d$  for shock-initiated flow of  $u_s/(u_s - u_\sigma) = 2.0$ .

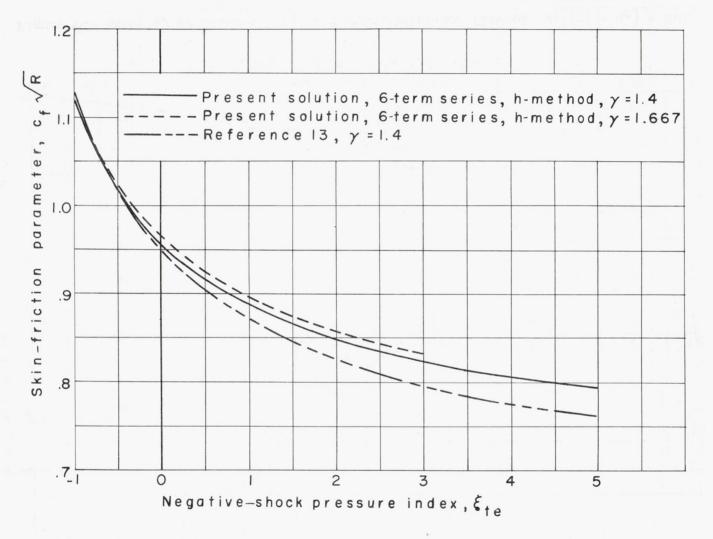


Figure 7.- Variation of skin-friction parameter as a function of negative-shock pressure index for negative-shock initiated flow.

$$\xi_{\text{te}} = \frac{2}{\gamma - 1} - \frac{\gamma + 1}{\gamma - 1} \left( \frac{p\zeta}{p_{\epsilon}} \right)^{\frac{\gamma - 1}{2\gamma}}$$
.

NACA TN 3944

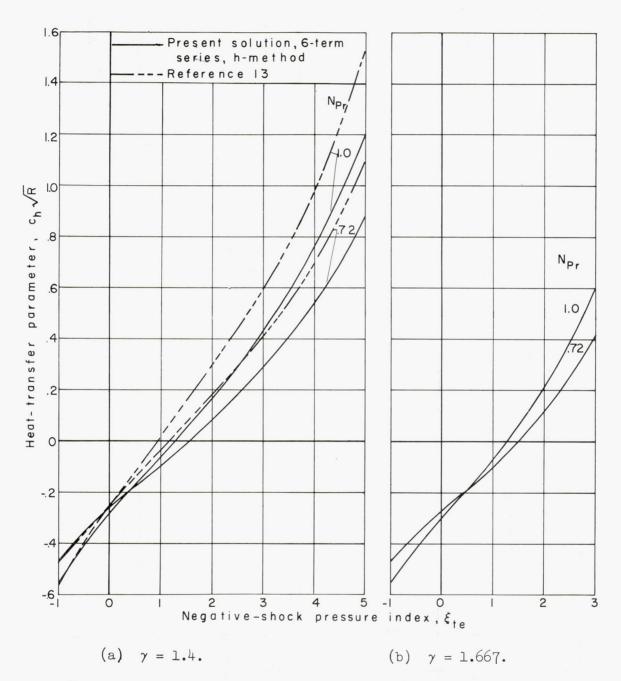


Figure 8.- Variation of heat-transfer parameter as a function of negativeshock pressure index for negative-shock initiated flow,  $\gamma\text{--}1$ 

$$\xi_{\text{te}} = \frac{2}{\gamma - 1} - \frac{\gamma + 1}{\gamma - 1} \left( \frac{p\zeta}{p_{\epsilon}} \right)^{\frac{\gamma - 1}{2\gamma}}.$$

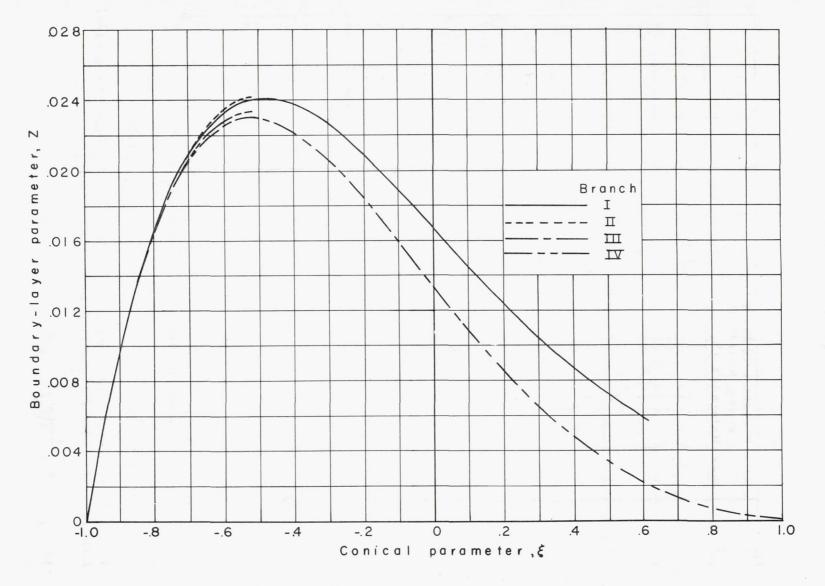


Figure 9.- Variation of  $\,\mathbf{Z}\,$  inside expansion fan.

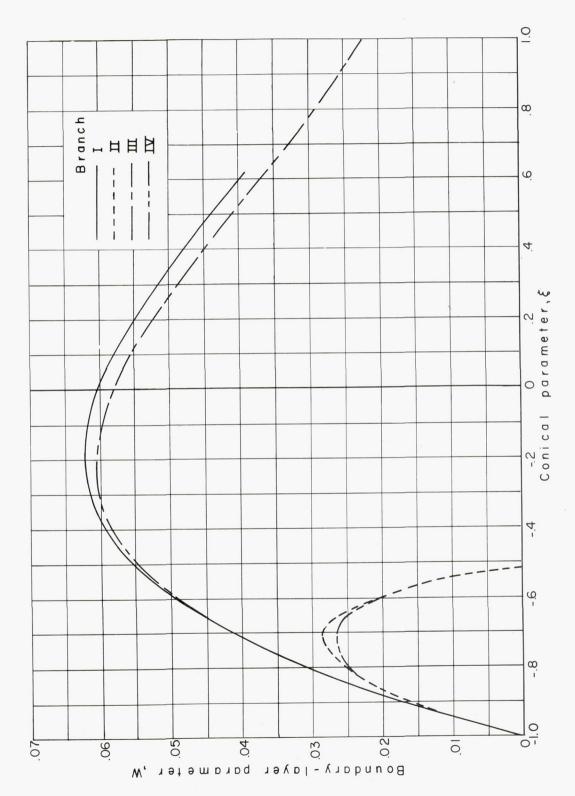


Figure 10.- Variation of W inside expansion fan.

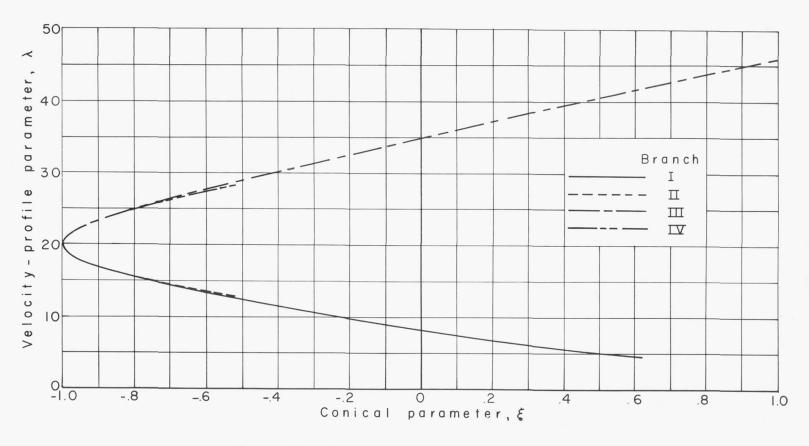


Figure 11.- Variation of  $\ \lambda \$  inside expansion fan.

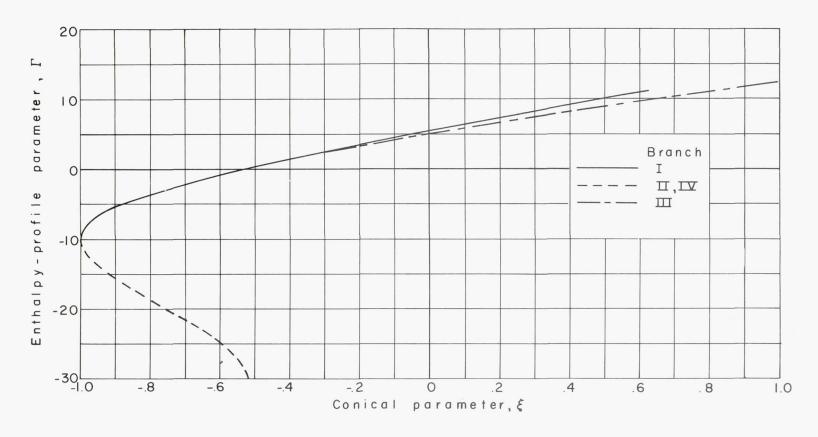


Figure 12.- Variation of  $\Gamma$  inside expansion fan.

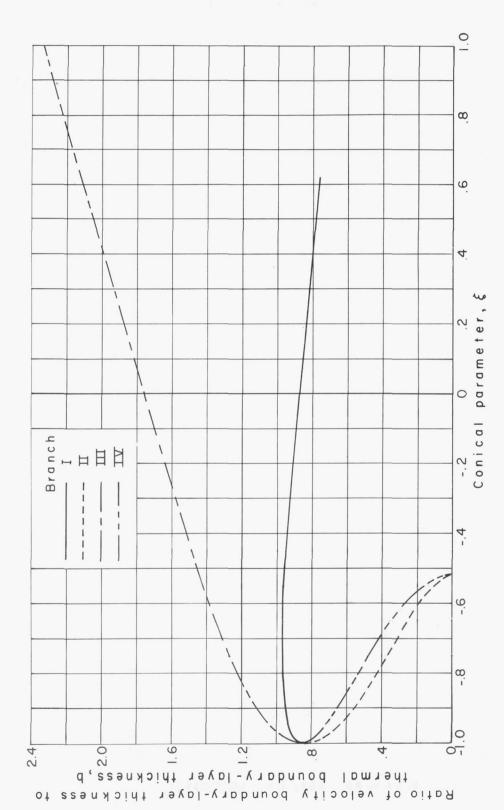


Figure 13.- Variation of b inside expansion fan.

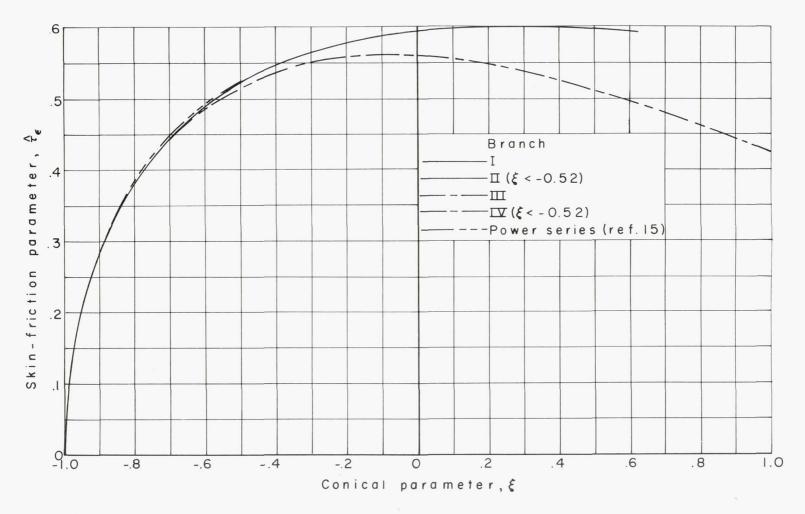


Figure 14.- Variation of  $\; \hat{\tau}_{\varepsilon} \;$  inside expansion fan.

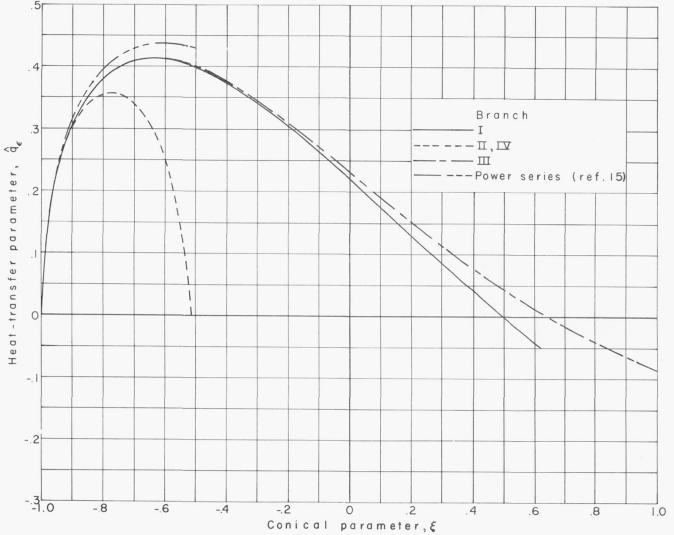


Figure 15.- Variation of  $~~\hat{\mathbf{q}}_{\varepsilon}~$  inside expansion fan.

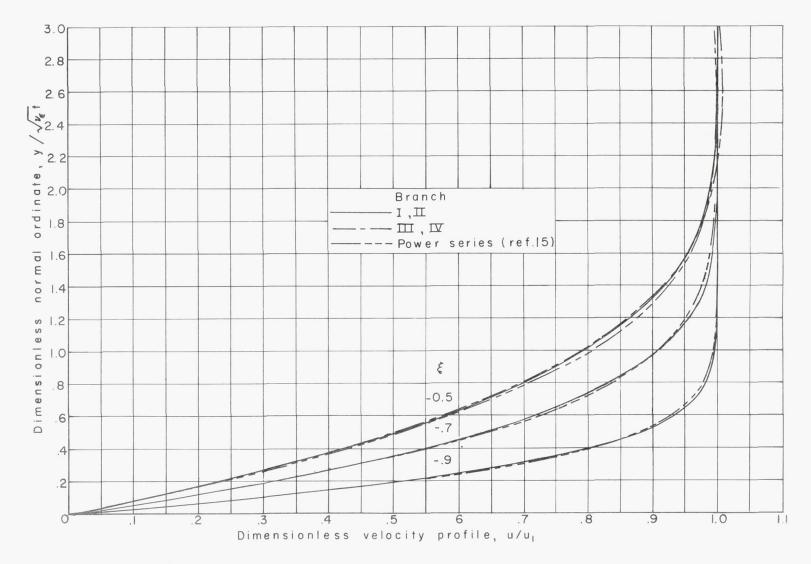


Figure 16.- Comparative velocity profiles near leading edge of expansion fan.

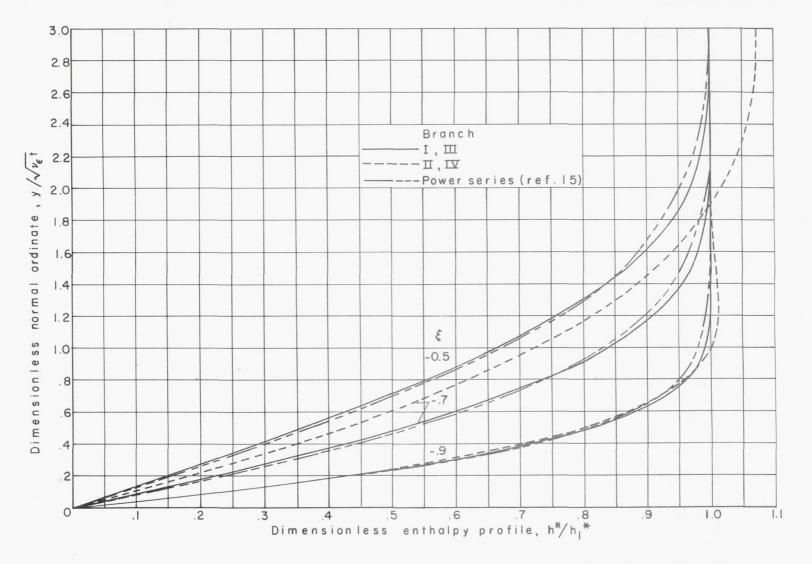


Figure 17.- Comparative enthalpy profiles near leading edge of expansion fan.

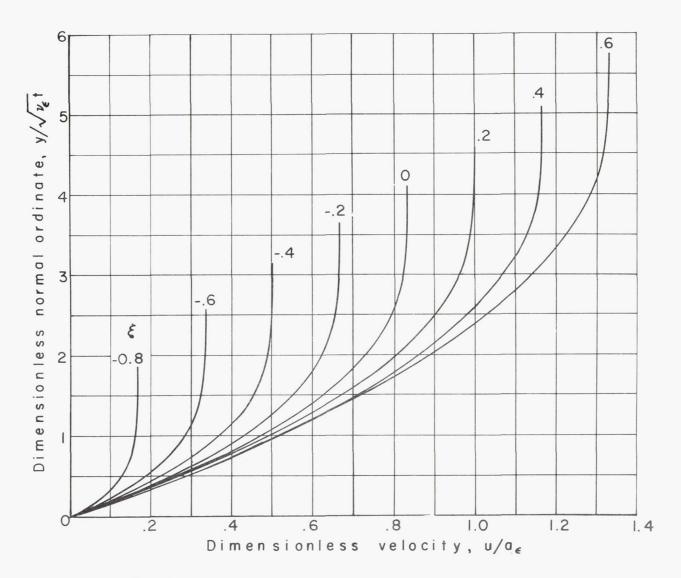


Figure 18.- Velocity profiles inside expansion fan. Branch I solution.

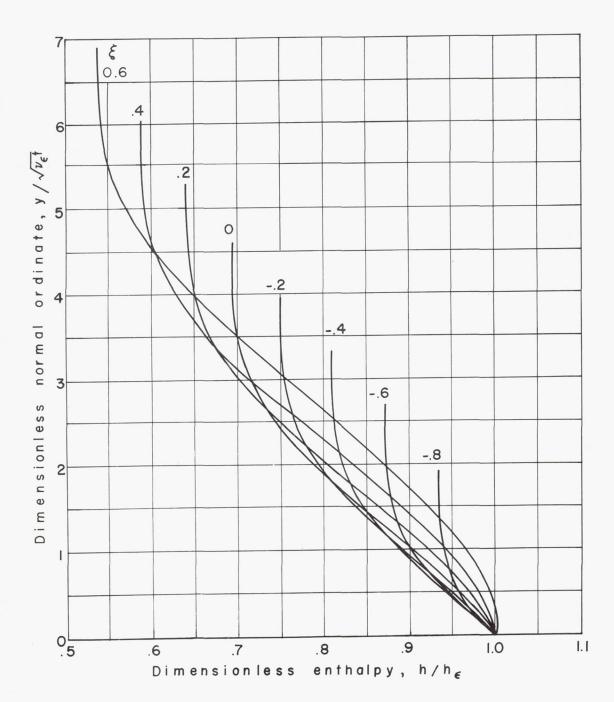


Figure 19.- Enthalpy profiles inside expansion fan. Branch I solution.

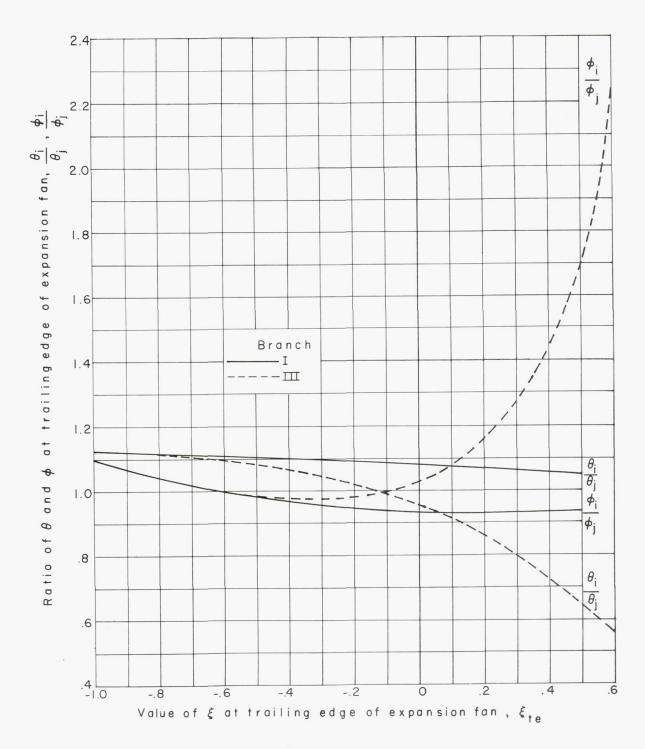


Figure 20.- Ratios of  $\theta$  and  $\phi$  at expansion-fan trailing-edge discontinuity. (Subscript i denotes inside expansion fan at trailing edge; subscript j denotes outside expansion fan at trailing edge.)

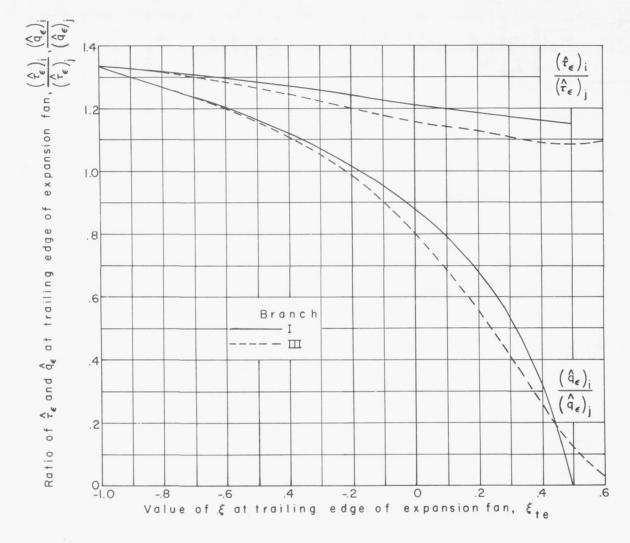


Figure 21.- Ratios of  $\hat{\tau}_{\varepsilon}$  and  $\hat{q}_{\varepsilon}$  at expansion-fan trailing-edge discontinuity. (Subscript i denotes inside expansion fan at trailing edge; subscript j denotes outside expansion fan at trailing edge.)

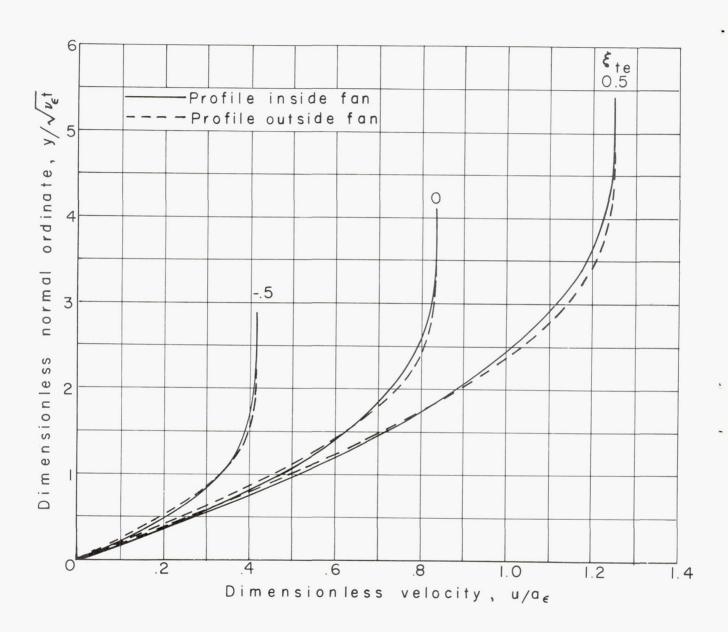


Figure 22.- Velocity profiles on opposite sides of expansion-fan trailing-edge discontinuity. Branch I solution.

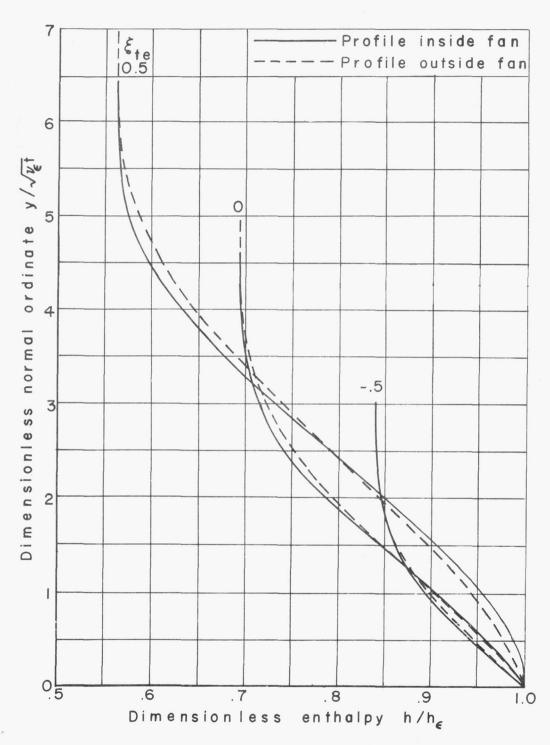


Figure 23.- Enthalpy profiles on opposite sides of expansion-fan trailingedge discontinuity. Branch I solution.

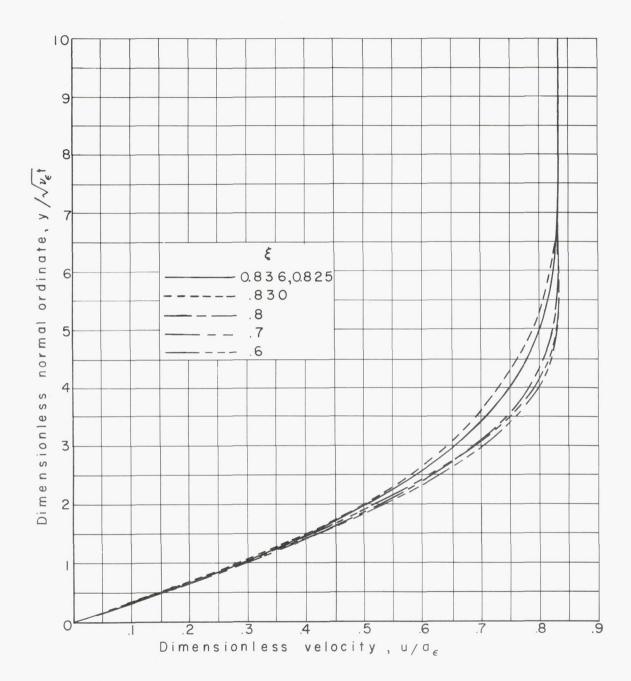


Figure 24.- Velocity profiles near the entropy discontinuity.  $\xi_{te} = 0$ ;  $\xi_{d} = 0.833$ .

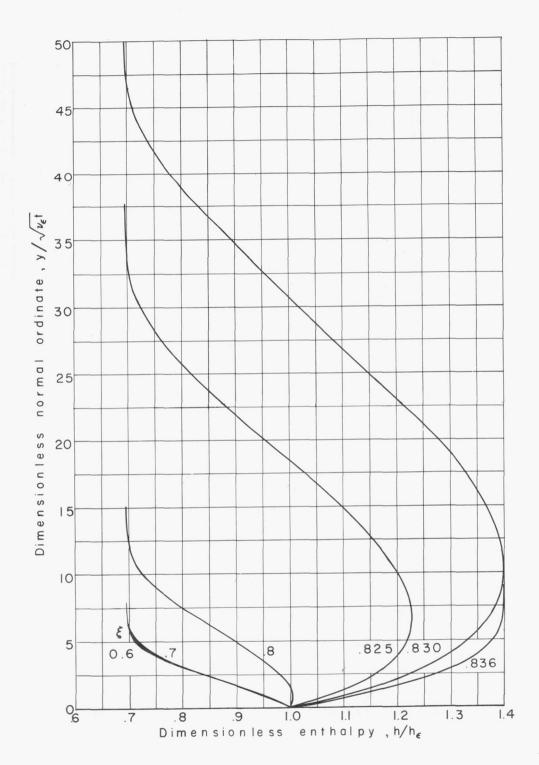


Figure 25.- Local enthalpy profiles near the entropy discontinuity.  $\xi_{\text{te}} = 0$ ;  $\xi_{\text{d}} = 0.833$ .

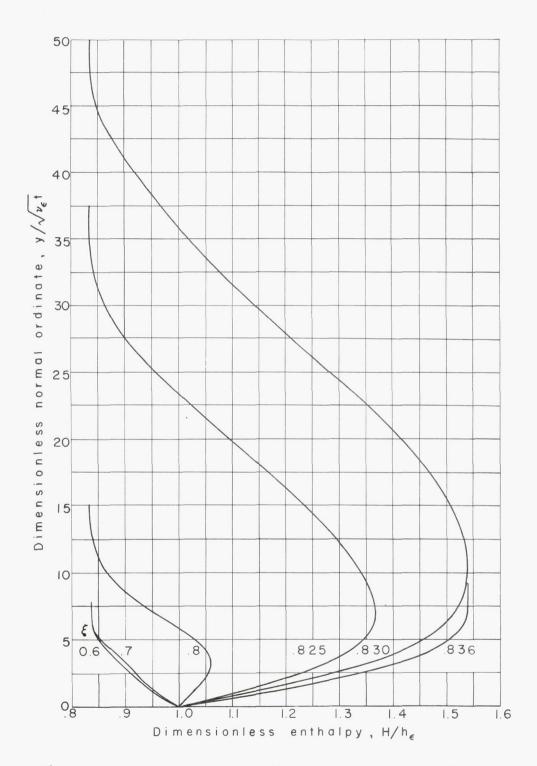


Figure 26.- Stagnation enthalpy profiles near the entropy discontinuity.  $\xi_{\text{te}} = 0$ ;  $\xi_{\text{d}} = 0.833$ .

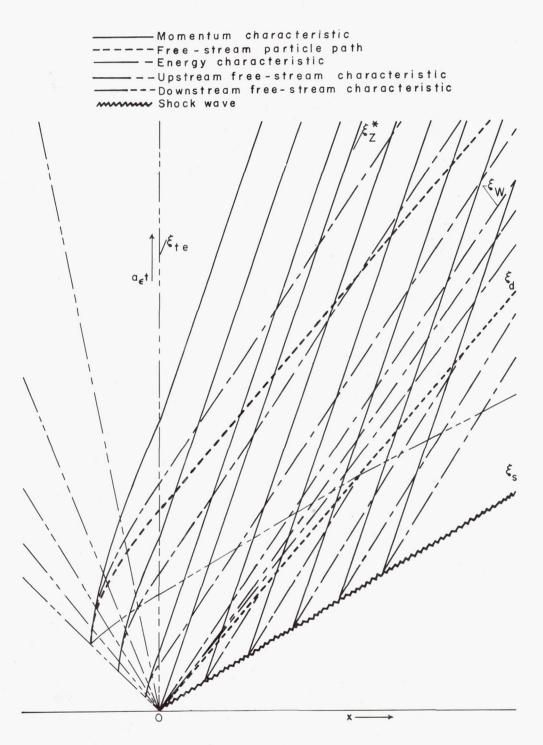


Figure 27.- Boundary-layer characteristic diagram for air-air shock tube.  $\xi_{\text{te}}$  = 0;  $\xi_{\text{s}}$  = 1.62.

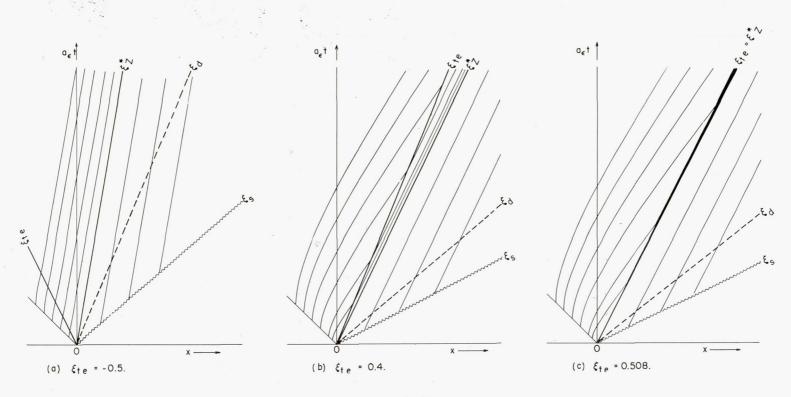
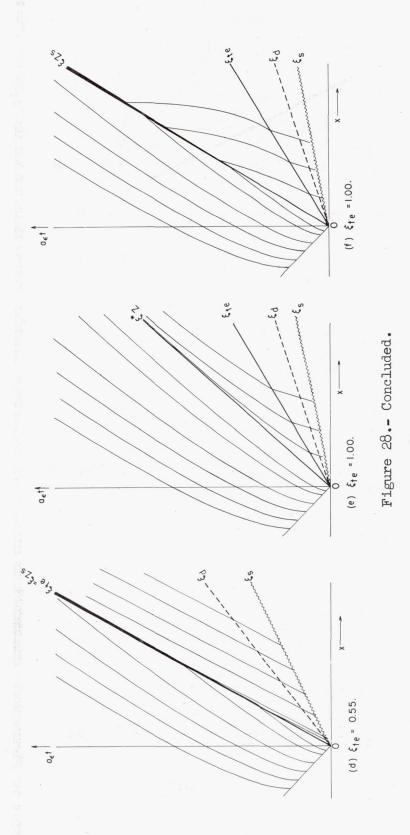


Figure 28.- Boundary-layer momentum characteristic sketches for various values of  $\xi_{\text{te}}$ .



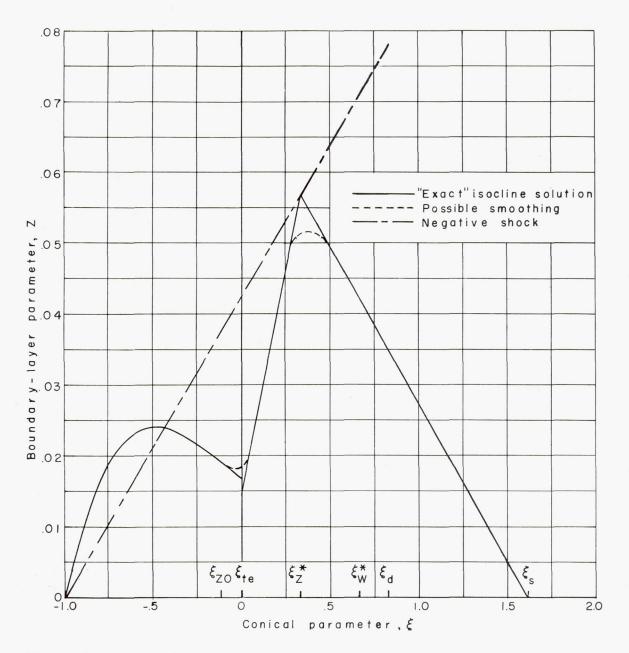


Figure 29.- Variation of Z with  $\xi$  in air-air shock tube.  $\xi_{\text{te}} = 0$ ;  $N_{\text{Pr}} = 0.72$ .

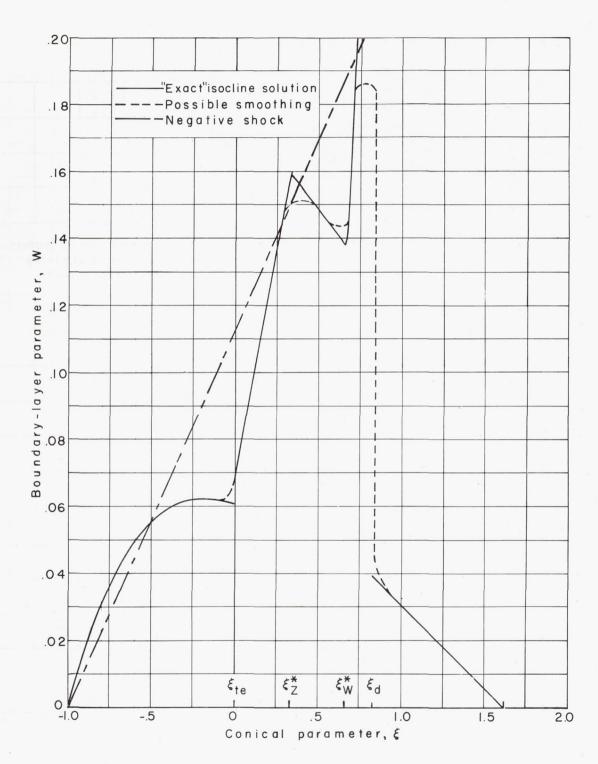


Figure 30.- Variation of W with  $\xi$  in air-air shock tube.  $\xi_{\text{te}} = 0$ ;  $N_{\text{Pr}} = 0.72$ .

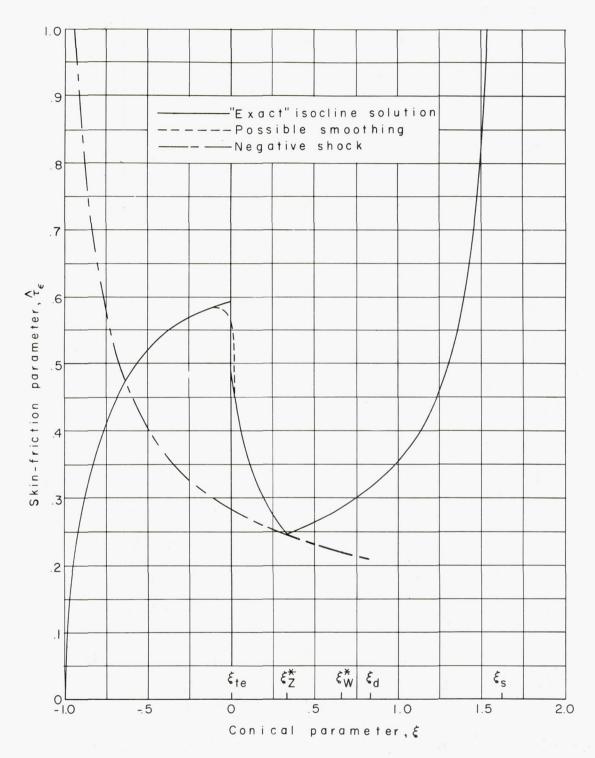


Figure 31.- Variation of  $\,\,\widehat{\tau}_{\varepsilon}\,\,$  with  $\,\,\xi\,\,$  in air-air shock tube.  $\,\,\xi_{\text{te}}$  = 0;  $\,\,N_{\text{Pr}}$  = 0.72.

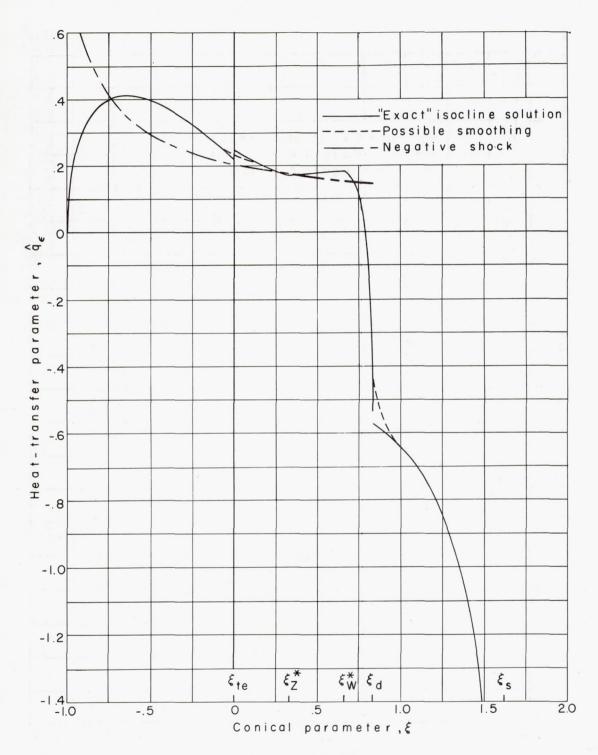
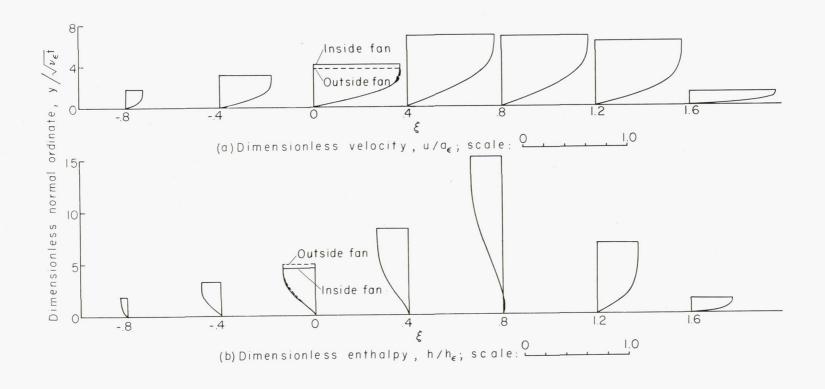


Figure 32.- Variation of  $\hat{q}_{\epsilon}$  with  $\xi$  in air-air shock tube.  $\xi_{te}$  = 0;  $N_{Pr}$  = 0.72.



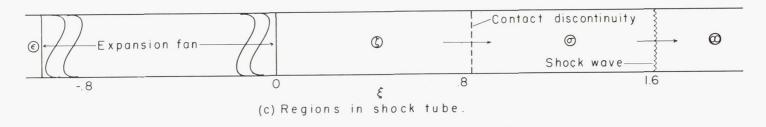


Figure 33.- Composite sketch showing boundary-layer velocity and enthalpy profiles as well as free-stream flow regions in air-air shock tube for  $\xi_{\text{te}}=0$ .  $N_{\text{Pr}}=0.72$ . Circled symbols indicate region.

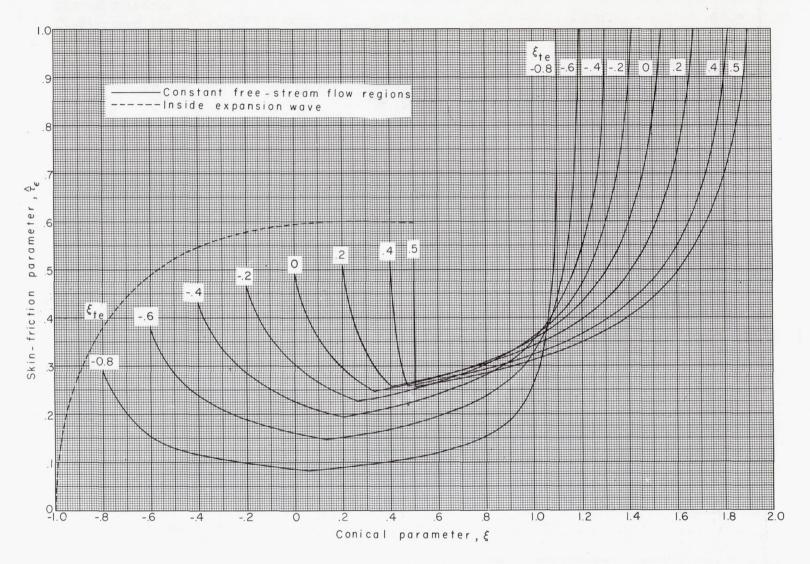


Figure 34 - Distribution of skin-friction parameter in air-air shock tubes.  $\gamma = 1.4$ ;  $N_{Pr} = 0.72$ .

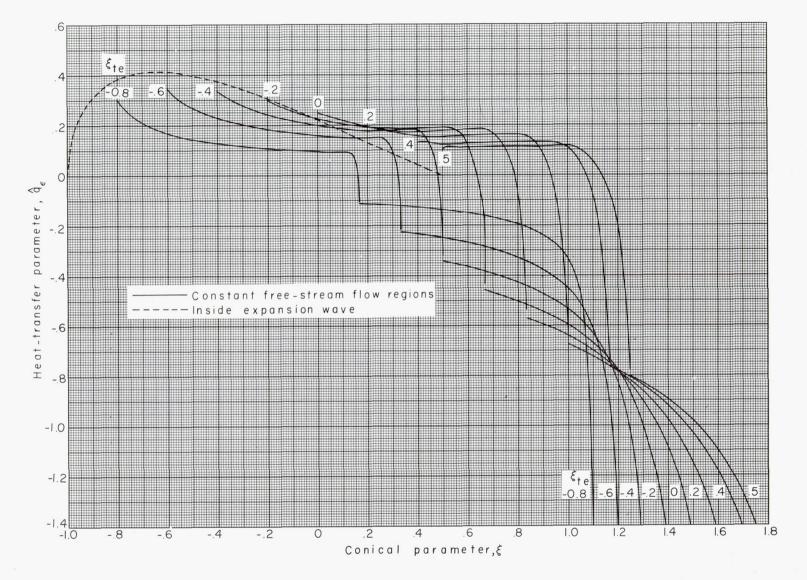


Figure 35.- Distribution of heat-transfer parameter in air-air shock tubes.  $\gamma = 1.4$ ;  $N_{Pr} = 0.72$ .

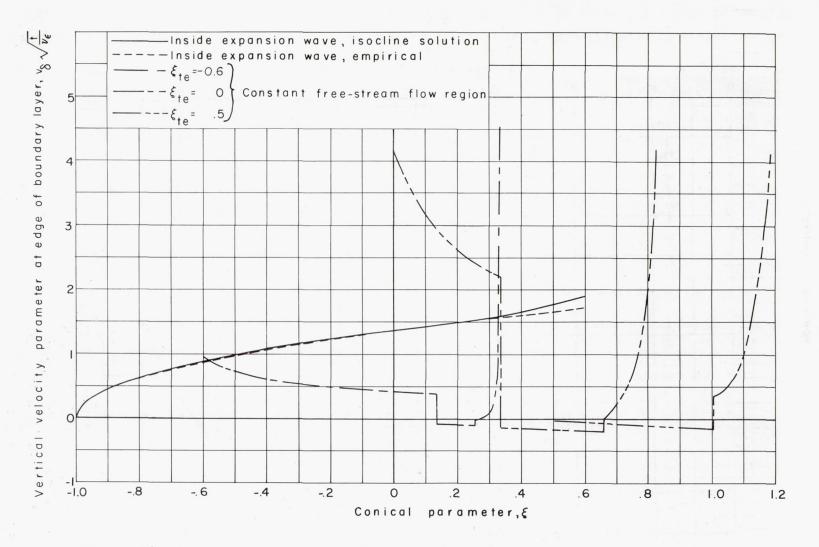


Figure 36.- Distribution of vertical velocity in gas accelerated by expansion wave.

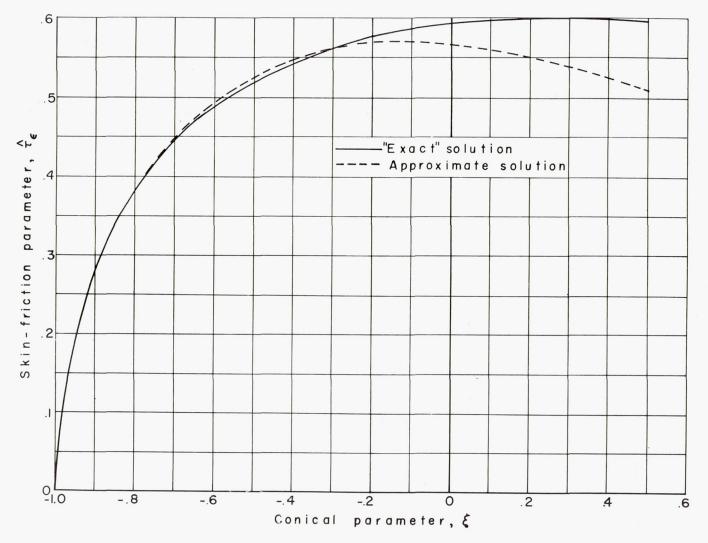


Figure 37.- Comparison of "exact" and approximate distribution of skin-friction parameter inside expansion fan.

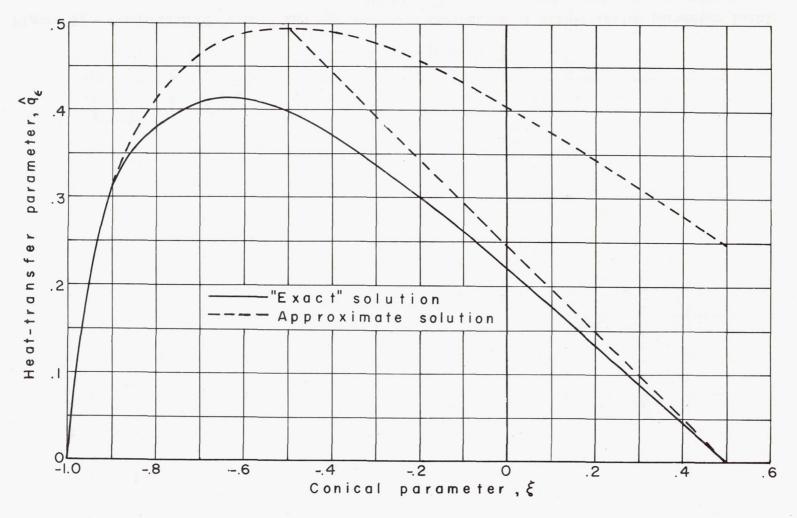


Figure 38.- Comparison of "exact" and approximate distribution of heat-transfer parameter inside expansion fan.

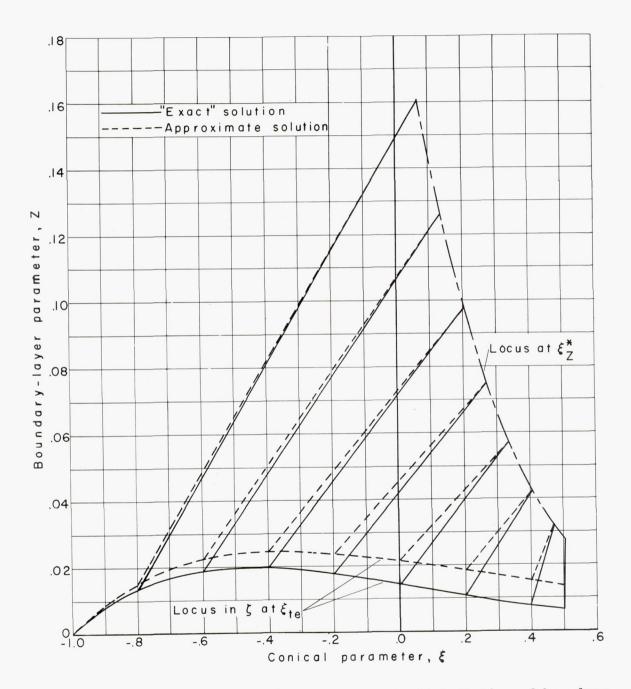


Figure 39.- Comparison of "exact" and approximate distribution of boundary-layer parameter Z in region  $\zeta$  for  $\xi \leq \xi_Z^*$ .

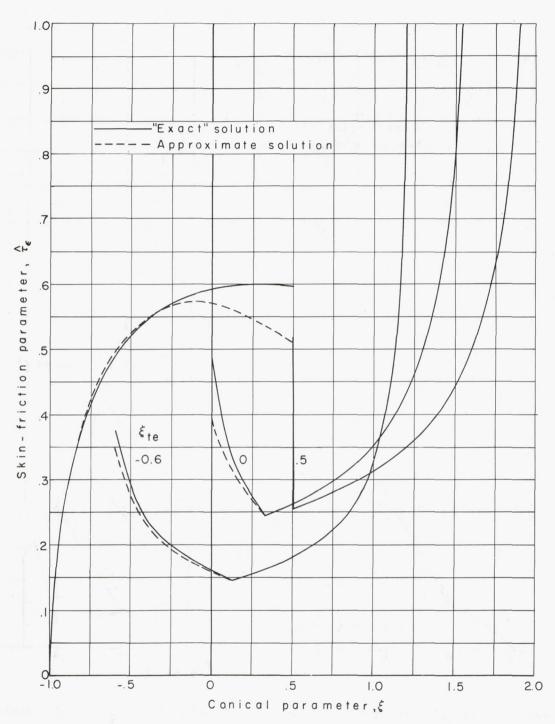


Figure 40.- Comparison of "exact" and approximate distribution of skin-friction parameter in an air-air shock tube.  $\gamma=1.4$ ; Npr = 0.72.

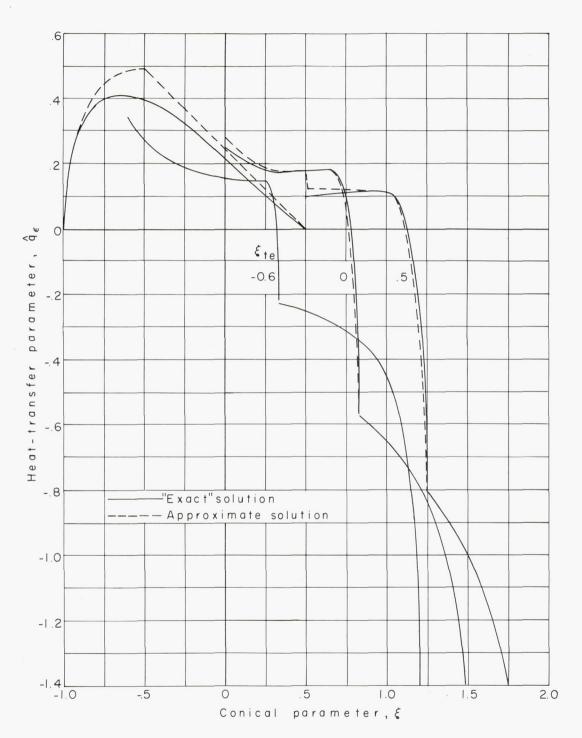


Figure 41.- Comparison of "exact" and approximate distribution of heat-transfer parameter in an air-air shock tube.  $\gamma = 1.4$ ; Npr = 0.72.

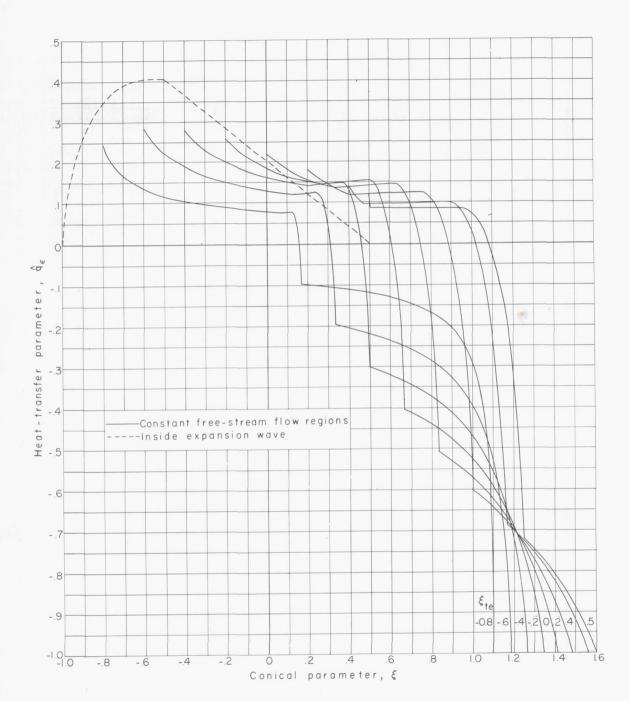


Figure 42.- Approximate distribution of heat-transfer parameter in airair shock tube.  $\gamma$  = 1.4; Npr = 1.0.

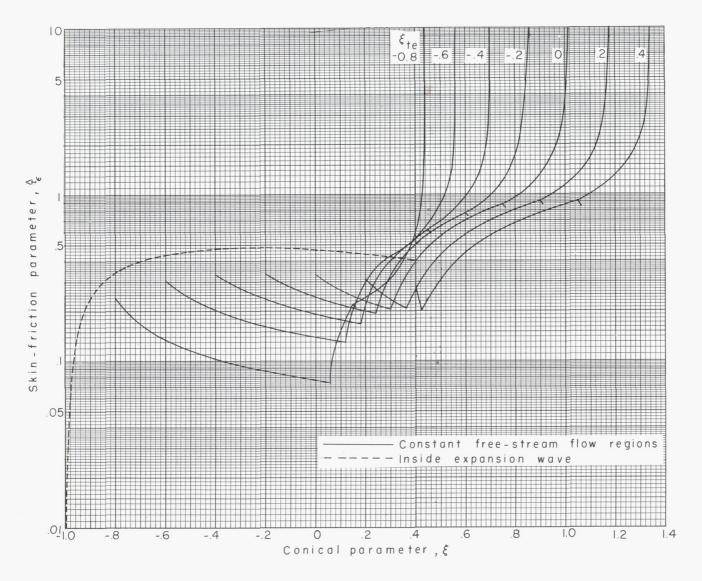


Figure 43.- Approximate distribution of skin-friction parameter in a helium-air shock tube.

.

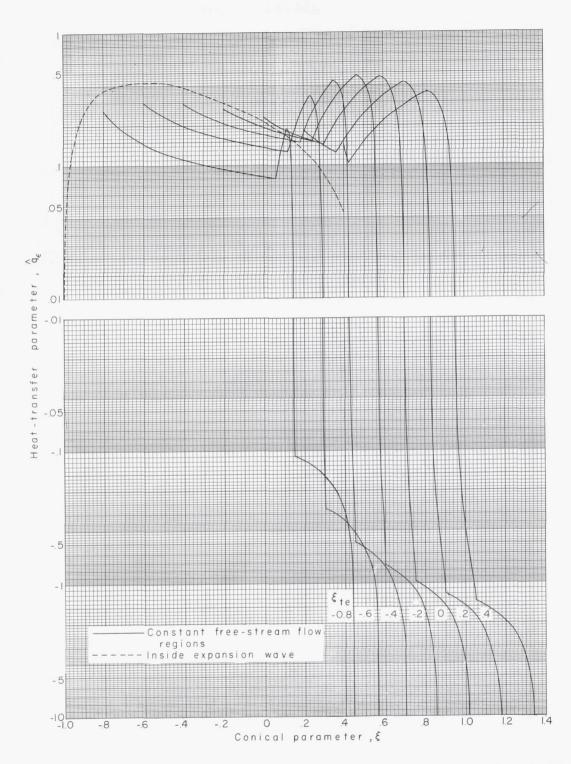


Figure 44.- Approximate distribution of heat-transfer parameter in a helium-air shock tube.

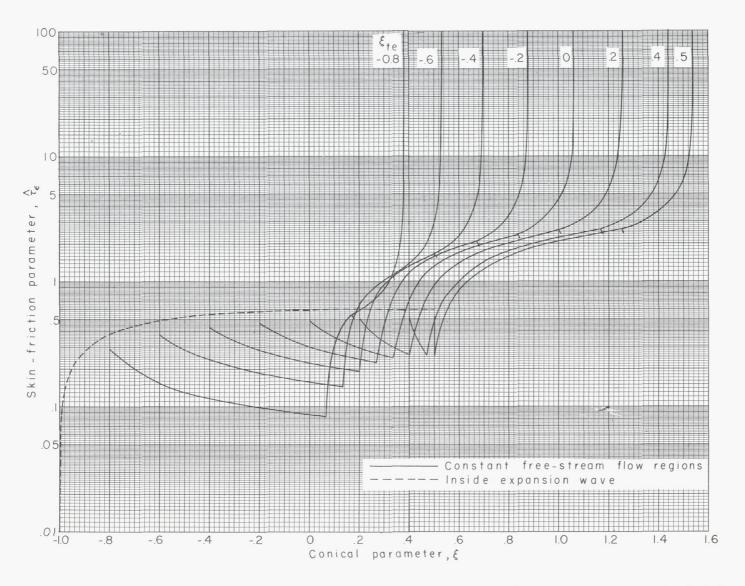


Figure 45.- Approximate distribution of skin-friction parameter in a hydrogen-air shock tube.

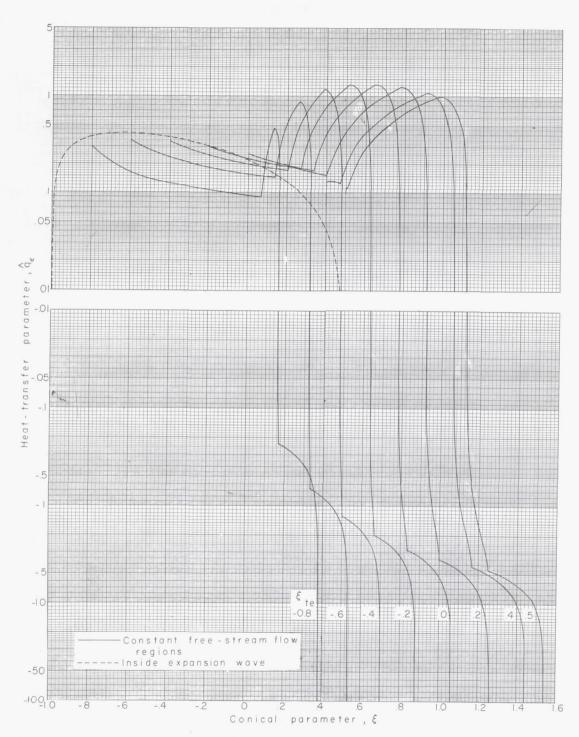


Figure 46.- Approximate distribution of heat-transfer parameter in a hydrogen-air shock tube.

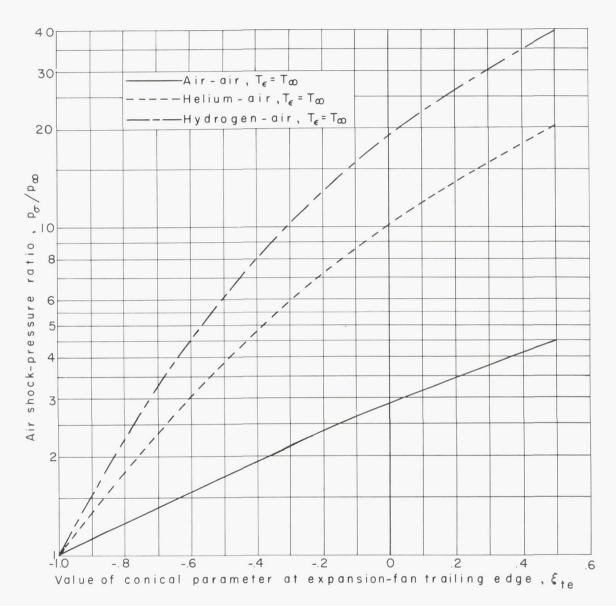


Figure 47.- Air shock-pressure ratio as a function of  $\xi_{\text{te}}$  for various gases in region  $\varepsilon$  of shock tube.